TRANSDUCTION AND AUDIBLE DISPLAYS FOR BROAD BAND SONAR SYSTEMS

By

R.P. Smith, B.E.(Hons)

1972

Thesis presented for the degree of Doctor of Philosophy in Electrical Engineering at the University of Canterbury, Christchurch, New Zealand.

ABSTRACT

This thesis describes an investigation into the feasibility of using a purely audible display in conjunction with a wide bandwidth frequency modulated sonar for the detection and tracking of underwater targets.

Special techniques are devised for the construction of transducer elements and arrays to operate over an extremely wide bandwidth and to allow the generation of an audible display which is self-sufficient and effective.

Certain psycho-acoustic aspects of the display are investigated with particular reference to the detection and tracking of large distributed targets, such as shoals of fish.

It is shown that a wide arc of illumination in the horizontal plane may be used while an accurate tracking capability is retained. This permits the use of a fixed transducer array, thus eliminating an expensive scanning mechanism which is common in more conventional forward-looking sonars for fish detection.

The results of sea trials with a prototype version of the system are described. The sea trials have shown that, although arrays of low directivity are used, a useful operational range may be achieved with the system. A large number of fish shoals were detected and successfully tracked during the trials.

ACKNOWLEDGEMENTS

I gratefully acknowledge the help of Professor L. Kay, Head of the Electrical Engineering Department, University of Canterbury who has supervised the research, and on whose original idea the research is based.

Thanks are also due to Mr A.H. Barth, Senior Lecturer in Electrical Engineering, who acted as supervisor in the early stages of the project, and who has assisted during sea trials.

The assistance of Messrs A.N. Vernon and M.J. Cusdin, senior technicians of the Electrical Engineering Department, who built all the experimental equipment and who assisted during sea trials is gratefully acknowledged.

I would like to thank Mr E. Johnson, Skipper of the "ONAWE", the vessel which was used for experimentation at Lyttelton Harbour, for his patience and assistance.

The project has been supported financially by the Inventions Development Authority, the Marine Department and the National Electronics Development Association (N.Z.) Inc.

Finally, I am grateful to my wife for her support and understanding during the research.

PREFACE

The thesis is organized largely in a sequence corresponding to the chronological order in which the various areas of research were undertaken. Due to the comparatively diverse nature of the various topics discussed, references are given at the end of each chapter, rather than at the end of the thesis.

The most important chapters, with regard to original contribution are chapters 3, 4, 6 and 7, while chapters 8 and 9 present the results of significant experiments and trials with the device at sea.

Key points in discussions and important results are indicated by a vertical bar in the margin or by underlining of the relevant portion of the text.

The following papers were presented and/or published during the period of the research, and certain diagrams in the thesis have been drawn from these papers.

(i) A.H. Barth and R.P. Smith, "Sonar Systems for Detection and Classification of Fish", presented by the second author at the Marine Sciences Conference, Wellington, New Zealand, August 1968.

(ii) R.P. Smith, "Constant Beamwidth Receiving Arrays for Broad Band Sonar Systems", Acustica, 23 : 21 (1970).

(iii) R.P. Smith and L. Kay, "A Fishfinding Sonar Utilizing an Audio Information Display", presented by the first author at the 1970 IEEE Int. Conf. on Eng. in the Ocean Environment, Panama City, Florida, September 1970, and published in the Digest of Technical Papers, IEEE Cat. No. 70C 38-OCC. Also published subsequently in N.Z. Electronics Rev., Nov., 1971.

CONTENTS

CHAPTER 1
INTRODUCTION

CHAPTER 1

INTRODUCTION

1.1 Project History

In 1964, Kay[1] showed that a suitably designed narrow beam linear FM sonar system operating in air could provide an audible display which conveyed considerable useful information to aid the mobility of a blind person. Subsequently, Kay proposed a wide beam binaural version of the device[2] with transducers built into a pair of spectacles and thus fixed in relation to the user's head. The primary source of information enabling the user to estimate the azimuthal position of a target, with this device, is the interaural intensity difference (more commonly referred to as interaural amplitude difference (IAD)) of the audible signals derived from the signals scattered from the target. The IAD is produced by the use of two separate receiving transducers splayed left and right in a manner similar to the antennae of a monopulse radar[3]. Further development work[4] and research into the psychoacoustics of the display[5] led to an improved form of the spectacles which is now being used by more than 100 blind persons in USA, England, Australia and New Zealand.

The obvious effectiveness of the audible display used in the blind mobility aid led to the proposal by Kay of the application of this type of display to an underwater sonar. Although audible displays have played an important part in the development of sonar systems, particularly in the early years, the increasing requirement for high spatial resolution has led to the almost exclusive use of visual presentation. There

remain, however, certain underwater sonar applications for which high resolution is unnecessary and a lower resolution would, in fact, be desirable if this would reduce the system cost or increase its effectiveness. A sonar for fishfinding is such an application.

The aim of the research reported in this thesis has been to investigate the feasibility of the effective use of a binaural audible presentation for an underwater sonar. Due to a variety of reasons discussed in section 1.2, a fishfinding sonar was considered the most suitable vehicle for the investigation.

1.2 The Use of Sonar in Fishing

Although forward-looking fishfinding sonars have been available for more than 20 years, much of the world's annual fish catch is made without the direct assistance of these devices. In countries such as New Zealand and Great Britain, where most of the fishing is carried out by large numbers of small vessels acting independently, the main reason for the rejection of sonar devices would appear to be their high cost, in relation to the vessel cost. A second reason, applicable in the above-mentioned countries, arises due to the fact that the greater part of the annual fish catch is made up of demersal species (fish living near the sea bed). Forward-looking sonars are very much less effective in detecting such species than detecting mid-water or surface species, due to masking reverberation from the sea bottom. The problem of detecting fish close to the bottom has been solved to some extent for vertical-looking sonars[6,7] but these devices cannot be used to search for fish as they only examine the

region directly beneath the vessel.

There would appear to be a definite need for an effective, low cost forward-looking fishfinding sonar with improved detection capability for demersal species.

The use of a wide beam FM sonar with a binaural audio display presents the possibility of cost reduction in two ways, namely,

(i) The cost of display equipment would be negligible in comparison with the cost of conventional display devices (graphic recorders, oscilloscopes).

(ii) Since the binaural display allows a wide arc of illumination, but provides facility to center a target within that arc (see section 1.5), scanning of the transducer array becomes unnecessary. (i.e. the ship itself is directed towards the target by the continual efforts of the operator to center the audible image of the target). The mechanical transducer scanning mechanism of conventional fishfinding sonars is, in itself expensive, but also contributes to the high installation cost of the system.

The problem of increasing the detection capability of a sonar system for demersal fish species is not directly related to the type of sonar system, but is more dependent on the geometry of the sonar beam, the fish, and the sea bottom. A high range resolution capability will not improve the target detectability beyond the point where the resolution cell width becomes less than the extent of the target in range. Similarly, improving the angular resolution in the horizontal plane increases target detectability only up to the point where the beam angle is equal to the angular extent of the target. Furthermore, increasing the angular resolution makes

the system much more susceptible to motion of the vessel in choppy seas.

A possible solution to the problem of demersal fish detection using a sonar of the type described in this thesis is discussed in Ch. 10 section 10.4. The proposed method uses a wide horizontal beamwidth FM sonar with towed transducers.

Although a towed version of the sonar may offer distinct advantages for the local fishing conditions, it was considered preferable to design a ship-mounted version for the feasibility study of the system.

1.3 The Linear FM Waveform and Methods of Signal Processing

The linear FM sonar transmission exhibits a linear decrease (or increase) of frequency with time, throughout each transmitted pulse. The complex representation of the waveform, $s(t)$, thus has the form,

$$s(t) = \text{rect}(t/T - \tfrac{1}{2})\ e^{j2\pi(f_2 t - \frac{1}{2}\mu t^2)} \qquad 1.1$$

where the rectangular envelope of the pulse is defined by the Woodward[8] rect function, T being the duration of the pulse. f_2 is the initial frequency and μ is the sweep rate given by

$$\mu = (f_2 - f_1)/T$$

where f_1 is the final frequency. For a decreasing frequency/time characteristic, $f_2 > f_1$. The frequency/time variation of the transmitted waveform and an echo received from a target at range R, are shown in Fig. 1.1.

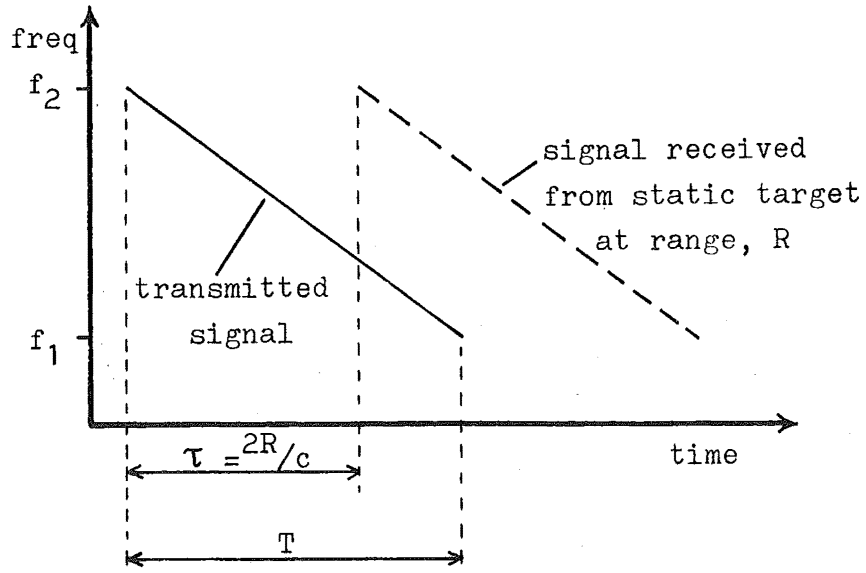

Figure 1.1. Transmitted and Received Waveforms in the Frequency/Time Plane

In processing received signals in an active sonar, one aims to achieve the best possible S/N (peak signal to mean noise level) ratio at the display, within the various limitations of the system. To achieve this, the receiver is generally designed to approximate to an optimum receiver, which may be one of two basic types:

(i) Matched filter receiver, or

(ii) Correlation receiver.

These receivers, although considerably different in implementation, are equivalent in that both produce the maximum possible S/N ratio at their outputs. Matched filters are generally more simply implemented and for this reason have been the basis for receiver design (knowingly or unknowingly) since the earliest sonars. In more recent years, with the advent of shipboard data processing systems, correlation

reception has become at least equally prominent.

The matched filter was shown by North[9] to be described by the following equivalent time domain and frequency domain relationships:

$$H(\omega) = S^*(\omega)\ e^{-j\omega T_d} \qquad 1.2$$

$$h(t) = s(T_d - t) \qquad 1.3$$

where $H(\omega)$ is the frequency response function of the filter, $h(t)$ its impulse response, $S(\omega)$ is the spectrum of the transmitted signal, $S^*(\omega)$ its complex conjugate, and $s(t)$ the signal waveform. T_d is a delay constant needed to make the filter realizable.

For the linear FM transmission, probably the best approximation to the matched filter is the pulse compression receiver[10,11,12]. This comprises essentially, a band pass filter with corner frequencies at f_1 and f_2, followed by a network with a flat frequency response over the operating band and a frequency dispersive delay characteristic in which time delay is a linear function of frequency, the slope in the frequency-delay plane being the negative of the slope of the time-frequency characteristic of the transmitted waveform. It can be demonstrated that such a network is a matched filter by considering the application of an impulse to the band pass filter input. From the assumed characteristics this impulse will give rise to a linearly frequency modulated pulse which is identical to the transmitted pulse except that the direction of the frequency sweep is reversed. The network, thus satisfies the relationship given by eqn. 1.3. In practice, a perfectly linear frequency/delay characteristic will not be achieved, but excellent approximations to matched filters of

this type have been achieved[13].

The output waveform of the matched filter is given by:

$$y(t) = \int_{-\infty}^{\infty} h(\tau)\ v(t-\tau)\ d\tau$$

where v(t) is the received signal waveform. Using eqn. 1.3 for h(t) and assuming that the received signal is a replica of the transmitted signal, having been diminished by a factor k, and delayed by the propagation delay, ΔT, we obtain,

$$y(t) = k \int_{-\infty}^{\infty} s(T_d - \tau)\ s(t - \tau - \Delta T)\ d\tau \qquad 1.4$$

Cook[10] has shown that for a transmitted signal of unit magnitude, and of the form of eqn 1.1, y(t) is given by:

$$y(t) = kT\sqrt{\mu}\ \frac{\sin(\pi\mu tT)}{\pi\mu tT}\ e^{j2\pi(f_2 t + \frac{1}{2}\mu t^2 + 1/8)} \qquad 1.5$$

The envelope of the output pulse is seen to have a sinx/x form and the effective pulse width (measured at -4dB points) is $1/\mu T = 1/\Delta f$, where $\Delta f = f_2 - f_1$. Also, the peak power of the output pulse is $k^2 T\Delta f$ compared with the peak input power which was only k^2.

The pulse compression filter has thus compressed the received pulse by a factor $T\Delta f$ and increased its peak power by a similar factor. The sinx/x envelope is to be expected from the Fourier transform relationship if the spectrum of the transmitted waveform is approximately rectangular, although no such approximation is made in the derivation of eqn. 1.5. The important dimensions of the received pulse and the compressed pulse for a time-bandwidth ($T\Delta f$) product of 100 are summarized in Fig. 1.2. The spectrum of a transmitted waveform having this value of $T\Delta f$ is also shown.

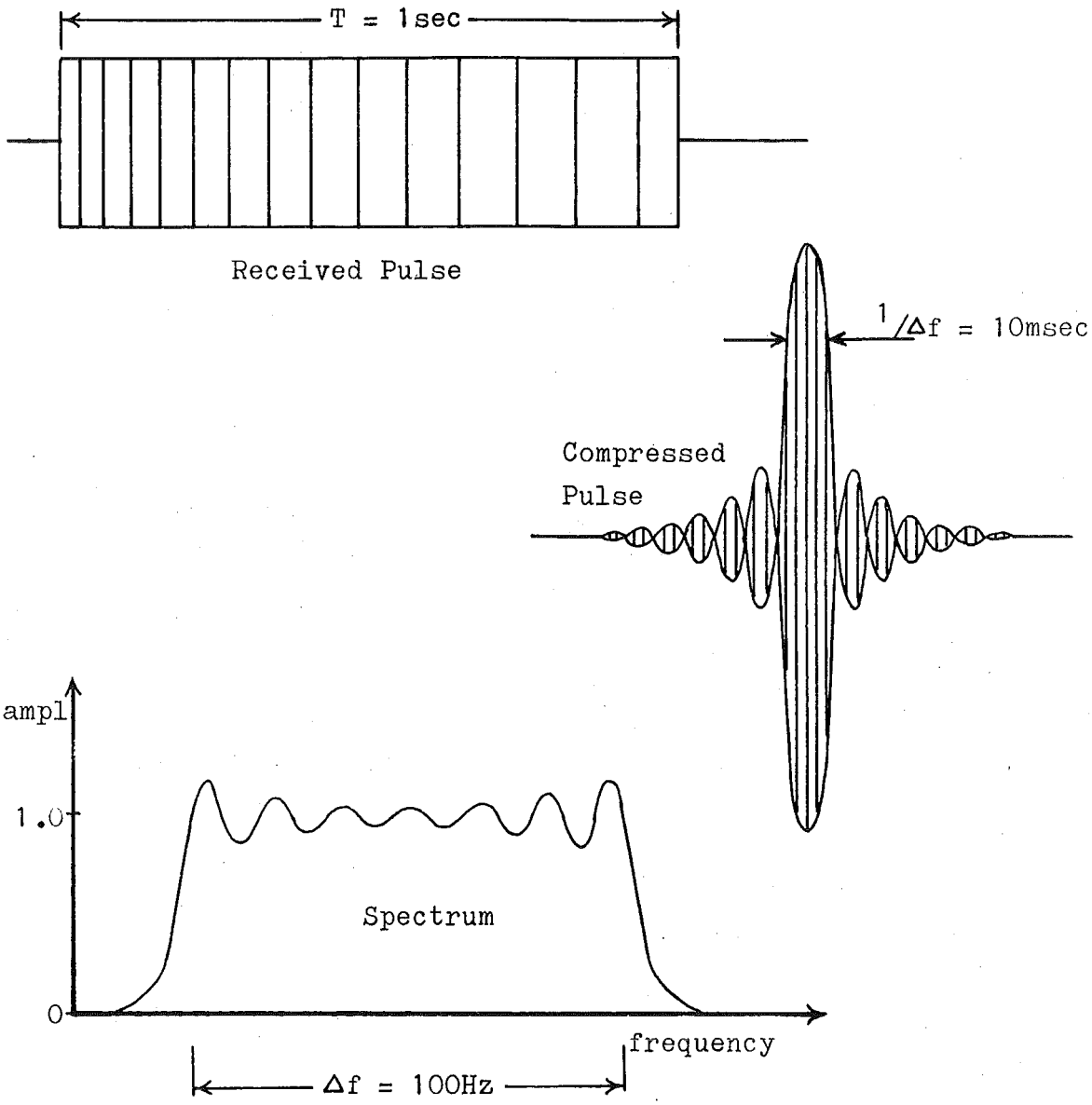

Figure 1.2. Dimensions of received and compressed pulses and spectrum of the transmitted pulse for a time-bandwidth product of 100.

In the preceding analysis, it was assumed that the received signal waveform was a delayed and diminished replica of the transmitted pulse. In practice, the target may be in motion with respect to the sonar arrays, and even if the

velocity of the target in the radial direction were constant the received signal would be a slightly compressed, or expanded version of the transmitted pulse, and thus would not be correctly compressed. The effects of target motion on detection and resolution of targets are discussed in section 1.4.

The correlation receiver[14,15] attempts to determine the cross correlation function of transmitted and received signals, $c_{tr}(\tau)$, given by

$$c_{tr}(\tau) = \int_{-\infty}^{\infty} v(t)\ s(t-\tau)\ dt$$

Assuming a particular received signal may be represented, as before, in the form,

$$v(t) = ks(t - \Delta T)$$

we have

$$c_{tr}(\tau) = k \int_{-\infty}^{\infty} s(t - \Delta T)\ s(t-\tau)\ dt \qquad 1.6$$

This expression is seen to be of equivalent form to that of eqn. 1.4, showing the equivalence of matched filtering and correlation processing.

The correlation receiver may be implemented in at least two distinct ways. The most general approach is to multiply the received signal separately by a number of delayed replicas of the transmitted waveform and to integrate (low pass filter) the outputs. Only a finite number of such replicas is required since c_{tr} will have significant width in the τ domain. The output of the low pass filter following the multiplier, whose replica is coincident with the received signal, will be a waveform equivalent to the envelope described by eqn 1.5 if a linear FM signal is being processed. With this method, it

is clear that, even if it is known that all targets will be static, a delayed replica of the transmitted signal, a multiplier, and a low pass filter will be required for each resolution cell. The implementation of the method in hardware is thus much more complex than the matched filter implementation. The completely general nature of the cross correlation approach, however, makes it well suited to digital processing techniques. Apart from the reduction in hardware in the receiver offered by computer processing, a wide variety of transmitted waveforms may be handled by manipulating the software only.

An alternative, less cumbersome, hardware correlation receiver may be used if a substantial overlap between transmitted and received signals may be arranged. This method, which will be referred to as heterodyne correlation, involves the direct multiplication of transmitted and received signals.

The method is indicated diagrammatically in Fig. 1.3. During the period of overlap, a constant difference frequency, $\mu\Delta T$, may be extracted from the multiplier output for a target at fixed range, R, where,

$$\Delta T = \frac{2R}{c}$$

The output frequency is seen to be a linear function of the range of the target. The desired output waveform is given by:

$$y(t) = s^*(t)\ v(t)$$

where s(t) is the transmitted FM waveform as given by eqn 1.1 and $s^*(t)$ is its complex conjugate. As previously, then,

$$y(t) = k\ s^*(t)\ s(t - \Delta T) \qquad 1.7$$

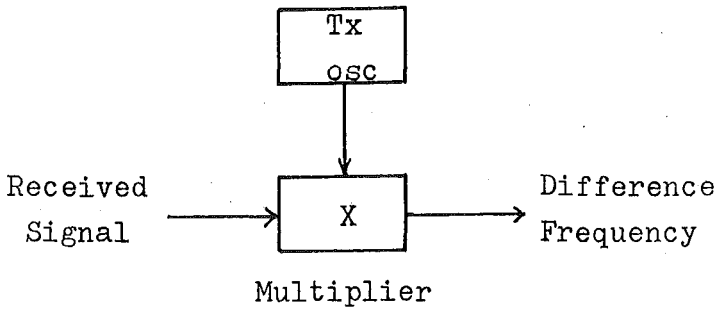

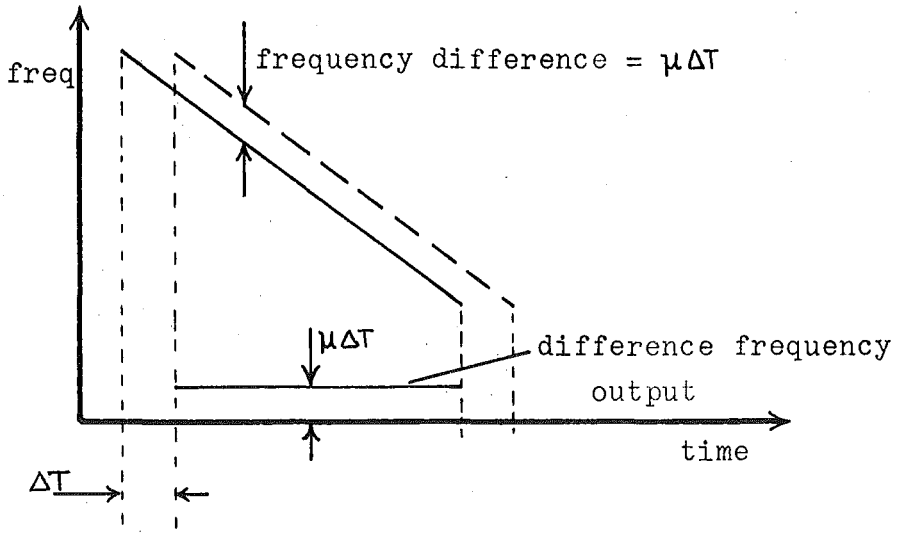

Figure 1.3. The heterodyne correlation process.

Substitution from eqn 1.1 gives

$$y(t) = \text{krect}\left(\frac{t - \frac{1}{2}(T + \Delta T)}{T - \Delta T}\right) e^{j2\pi\mu\Delta T t} e^{-j2\pi(f_2\Delta T - \frac{1}{2}\mu(\Delta T)^2)} \qquad 1.8$$

Here, the rect function defines the overlap period, the first exponent is the constant frequency term, and the second exponent is a phase term which is of no real significance to the correlation process.

If the overlap loss is small, the duration of the fixed frequency signal is approximately T and so the spectrum of

this signal has a sinx/x envelope with a maximum at $f = \mu\Delta T$, and an effective width (at -4dB level) of 1/T Hz. The bandwidth of the received signal has thus been compressed by a factor $T\Delta f$. This demonstrates the close analogy between matched filter and correlation processing, as pointed out by Rihaczek[16]. In the pulse compression filter, the signal bandwidth remains unchanged but the signal duration is reduced by a factor, $T\Delta f$, whereas with the heterodyne correlation receiver, the signal duration remains unchanged but the bandwidth is reduced by the factor $T\Delta f$. Providing their outputs are correctly detected, both lead to the same improvement in S/N ratio since they both compress the signal into the smallest possible resolution cell. Whereas in the pulse compression receiver the output pulse occupies a certain interval in the time domain, whose position corresponds to the propagation delay, in the correlation receiver, the output pulse occupies a certain band in the frequency domain, which is also directly related to the propagation delay.

To achieve the full resolution capability of the transmitted waveform, the multiplier in the heterodyne correlator must be followed by a bank of band pass filters, each of bandwidth, 1/T, and of sufficient number to span the desired operating range. Although it would appear that such a system is almost as cumbersome as the replica correlator, in practice, scanning filter techniques[17] may be employed and the method does not involve the use of time delays which for sonar applications (where long time delays are required) are difficult to achieve.

The heterodyne correlator in the form described will not perform correctly if the target is in motion. The compression or expansion of the received pulse with respect to the transmitted pulse, due to radial motion of the target, causes the heterodyne output signal to contain residual frequency modulation. This means that it will produce a small response at a number of band pass filter outputs, rather than a large response at a single filter output. The effects of target motion on linear FM transmissions are discussed in section 1.4.

The most important characteristic of the heterodyne correlator which leads to its use in the present application, is that the multiplier output comprises a multitude of narrow band signals of considerable duration. This signal format is ideally suited to processing by the human auditory system. Providing the transmitted waveform may be designed so that the heterodyne output contains frequencies within the audible range and of durations of several hundred milli-seconds, this signal may be applied directly to the auditory system. The resulting system is extremely simple in implementation, since it comprises only a single multiplier and amplifiers necessary to raise the level of the received signal to usable magnitude. The auditory presentation of the heterodyned signal is discussed further in section 1.6.

1.4 The Effects of Target Motion on Linear FM Signal Processing

It has been shown, in the previous section, that optimum processing of an undistorted, received linear FM waveform gives rise to an output function which is equivalent to the autocorrelation function of the transmitted waveform. We next

consider the effect of target motion on the performance of receivers such as those described.

Radial motion of a target with respect to the sonar arrays causes frequency shifts due to the Doppler effect. Constant velocities only, will be considered. A constant target velocity towards the sonar arrays causes the frequency/time characteristic of the received waveform, to be displaced upwards, in the direction of increasing frequency and, since higher frequencies undergo a larger Doppler shift than lower frequencies, the slope of this characteristic is steepened. In most radar applications this slope change may be neglected[18,19] but in sonar applications, where fractional bandwidths and time bandwidth products tend to be high, the slope change has a very pronounced effect on receiver performance.

The effects of target velocity on receiver performance will be discussed with reference to a heterodyne correlator receiver since this type of processor is employed in the present application, although exactly analogous effects occur with other processing techniques.

Consider a static target at range, R. This gives rise to a high signal level at the output of the band pass filter whose center frequency is $2\mu R/c$, and whose bandwidth is $1/T$ but very small outputs at other filters in the bank. (Note: a significant response will be produced in some filters by the 'side lobes' of the sinx/x spectrum but various methods may be employed to suppress these lobes[20,21].) If now, the target moves towards the sonar arrays with velocity v, since the signal produced at the output of the multiplier will contain a residual frequency modulation, weak outputs will be produced

at a number of adjacent filters. Furthermore, since all frequencies have been translated upwards by the Doppler effect, the true range of the target will be less than that indicated by the midpoint of the responding filters. This shows the strong coupling between range and velocity measurement, which is a characteristic of the linear FM waveform.

The interaction between range and velocity measurement may be best described by the ambiguity function[8,22] of the waveform. This function is a generalized autocorrelation function which describes the loss in correlation between transmitted and received waveforms, under a generalized mismatch in both time (range) and frequency (velocity). The ambiguity function is given by[22]:

$$|\chi(\tau,\phi)| = \left|\int_{-\infty}^{\infty} s(t)\ s^*(t-\tau)\ e^{j2\pi\phi t}dt\right| \qquad 1.9$$

where ϕ is the frequency mismatch, τ is the time delay mismatch.

The function $\chi(\tau,\phi)$ is the generalized matched filter response in both delay and Doppler and $|\chi(\tau,\phi)|$ is its magnitude. The ambiguity function is conveniently represented, diagrammatically, by a contour of fixed correlation loss in the τ-ϕ plane. Such a contour corresponding to a level of response equal to 0.5 of the maximum response is shown in Fig. 1.4. In this example, for simplicity, no account has been taken of the slope change in the f-t plane produced by the compression or expansion of the received signal. i.e. a simple frequency translation has been assumed. (The 'radar' case.)

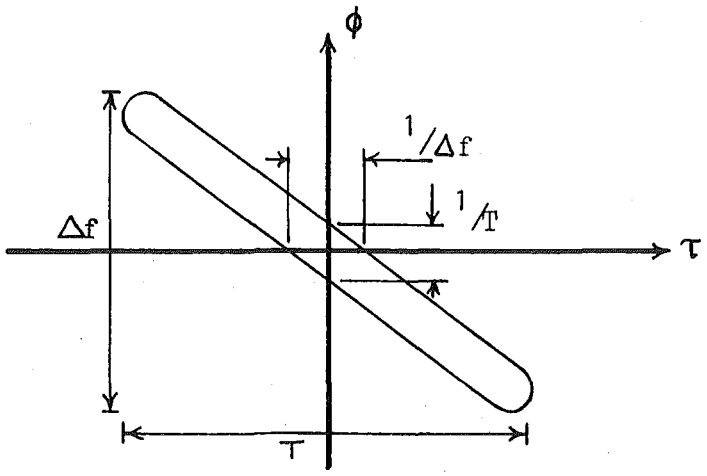

Figure 1.4. Ambiguity contour given by $|\chi(\tau,\phi)| = 0.5|\chi(0,0)|$ for a linear FM transmission of bandwidth, Δf, and duration, T. ('Radar' case)

The slope of the 'backbone' of the ambiguity contour, in this case, is equal to the sweep rate of the transmitted signal and is of the same sign. This is to be expected since an increase in range will cause an increase in frequency at the heterodyne output and a reduction in frequency due to Doppler (outwards velocity) will bring the response back into an ambiguous position. The maximum limits of ambiguity are $\pm\Delta f/2$ in the ϕ direction and $\pm T/2$ in the τ direction. This implies that if a static target at range, R, produces a response of unit magnitude in the band pass filter corresponding to that range, any similar target in the range, $R - cT/4 \leqslant R \leqslant R + cT/4$ can produce a response of at least 0.5 in that filter if its velocity is appropriate.

The dimensions of the ambiguity contour at the origin are approximately $1/\Delta f$ and $1/T$, in the τ and ϕ directions

respectively. In fact a cross section at $\phi = 0$ yields the sinx/x envelope discussed in the previous section (see eqn. 1.5).

In a practical situation, it is usually possible to reduce the effective area of the ambiguity contour on the basis of a priori knowledge of maximum target velocities. In sonar applications, this area is also drastically reduced by the change in slope of the f-t characteristic of the received signal when the target is moving. Since a change in slope constitutes additional information to enable the effects of range and velocity to be distinguished, a reduction in ambiguity is to be expected.

Russo and Bartberger[19] have derived an expression for determining the length of the 'backbone' of the ambiguity contour, which accounts for the effects of time compression or expansion due to Doppler. Using their method, the approximate ambiguity contour for the waveform used in the present application will be determined, for purposes of comparison with the actual performance achieved with auditory processing.

The important characteristics of the linear FM waveform used in the sonar, under discussion in this thesis, are as follows:

Bandwidth, $\Delta f = 40$ kHz

Typical duration, $T = 2$ secs (selected to suit operating range)

Center frequency, $f_o = 60$ kHz.

These figures are derived in Ch. 2. With a waveform of such large bandwidth and such long duration, the sweep rate, μ, bandwidth, Δf, and duration, T, are simply related as follows:

$$\mu \doteq \Delta f/T$$

The relationship between τ_{max}, the maximum limit of the ambiguity contour, and the above parameters is[91]:

$$f_o = \mu^2|\tau_{max}|(T - |\tau_{max}|)^2/z^2 - \mu(T - \tau_{max}) \qquad 1.10$$

where z is defined by,

$$1/z(C^2(z) + S^2(z))^{\frac{1}{2}} = 0.5/(1 - \tau_{max}/T) \qquad 1.11$$

where C and S are the cosine and sine Fresnel integrals.

Manipulation of eqns. 1.10 and 1.11 yields the desired result, namely,

$$\tau_{max} = 0.15 \text{ msec.}$$

This indicates that provided the signal is processed in an optimum fashion, two point targets which are separated by at least 0.74 feet, may be resolved in range, whatever their velocities. It is also noteworthy that since $\tau_{max} << T$, Eqn. 1.10 effectively contains the term μT, wherever μ or T occur. Thus if the bandwidth is fixed, τ_{max} is independent of the signal duration. Ambiguity contours for durations of 1, 2, and 4 secs are sketched in Fig. 1.5.

The increasing ambiguity in frequency (Doppler) with reducing duration is to be expected since the shorter the pulse, the less discernable will be the compression or expansion produced by a given target velocity.

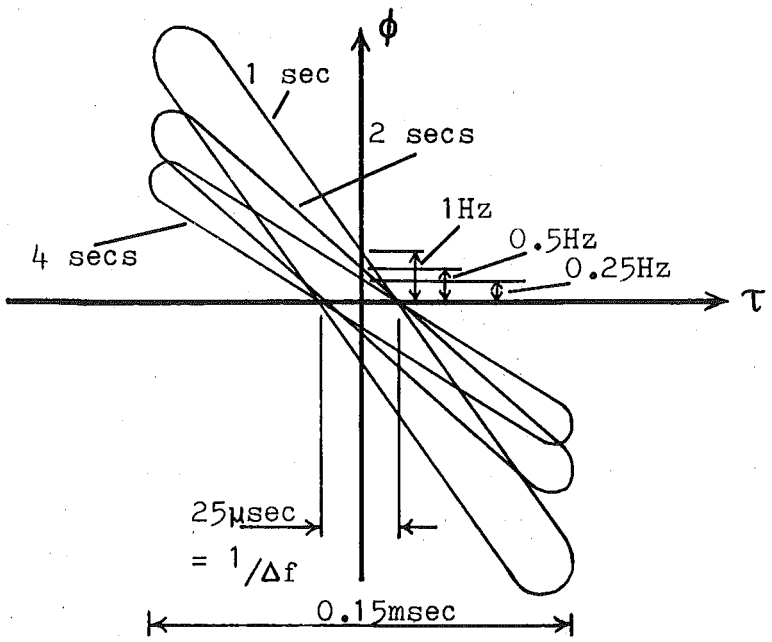

Figure 1.5. Ambiguity contours for the waveform used in the present application for signal durations of 1, 2, and 4 secs. (constant bandwidth of 40 kHz)

It is meaningful at this stage to consider the hardware which would be required to achieve the full potential resolution capability of this waveform. Assume that a heterodyne correlator receiver is to perform the processing, and that the following limits are placed on allowable range and velocity of the target: R_{max} = 100 ft, v_{max} = ±10 ft/sec. To accept signals from targets with a correlation loss of at most 6 dB over this velocity range requires that 20 different compressed versions and 20 different expanded versions of the transmitted waveform be provided to feed 40 different multipliers (modulators). This is necessary since the extent

of the ambiguity contour in the ϕ direction is 1/20th the displacement corresponding to the maximum velocity. Then to achieve a 25 μsec resolution in delay over a total delay of $\frac{2.100\text{ft}}{5000\text{ft/s}}$ = 40 msec requires 1600 band pass filters for each modulator.

The total hardware requirement is thus:

40 compressed or expanded replica generators,

40 modulators,

64,000 band pass filters.

It is clear that even in examining a comparatively small range with substantial restrictions on target velocity, an enormous volume of hardware is necessary to achieve optimum processing of the received signals. Even if time-sharing methods were employed to reduce the number of filters required, the implementation would still be formidable.

If a processing system with coarser resolution than that described above is employed in the receiver, S/N performance will be less than optimum, since each resolution cell will contain more reverberant scatterers than necessary. In the case of detection of fish shoals, however, S/N degradation will continue with increasing resolution cell size, only up until the point at which each cell begins to contain more targets. If, by doubling the width of the resolution cell, the number of reverberant scatterers and the number of targets (fish) are doubled, no change in S/N ratio is produced. Resolving of the targets within a single cell is not possible in this case, of course, but this may not be necessary.

The resolution achieved with auditory processing of the heterodyne output signals is discussed in section 1.6.

1.5 Directional Determination by Amplitude Comparison between Two Arrays

In addition to resolving a target in range, and if necessary in velocity, resolution in direction is required in most sonar or radar systems.

Acoustic or electromagnetic direction finding devices generally make use of the difference in arrival time of signals at various points of the receiving array aperture, to derive information pertaining to the angular position of the scatterer. Arrival time information may be used directly, as in interferometer type systems[23,24], or indirectly as in lobe comparison systems[3,25] which utilize arrival time differences to form directional patterns, but then use consecutive or simultaneous amplitude comparison techniques to resolve the angular position.

A notable exception to the use of arrival time information to determine the direction of a sound source, is the localization of high frequency sounds in the human auditory system, (see Ch. 7 section 7.2). Apparently the binaural auditory system completely ignores time or phase differences between the two ears in determining the direction of sources whose frequency components lie above about 1500 Hz, relying solely on intensity differences caused by the shadowing effect of the head. Incoherent processing of this nature does not appear to have found favour with sonar or radar system designers, presumably due to its poor performance in multiple target situations, or noisy situations, and due to the difficulty in obtaining a simple relationship between intensity difference and scatterer position.

In the present application, a simultaneous lobe comparison method is used. In this technique[3,25,26], two directional receiving arrays are employed, having their normal axes splayed outwards, to provide a variation of relative amplitude with target azimuth angle. The method is ideally suited to presentation to the human auditory system since amplitude comparison, as was mentioned above, is a natural cue in the normal localization process, at least for high frequency sources.

This method is indicated diagrammatically in Fig. 1.6, in which sin x/x directivity patterns are assumed for each array.

It is seen from Fig. 1.6 that unique determination of target azimuth from the relative intensity characteristic is possible only over a limited range of angle, denoted A. If a wider angular range is required, the resulting ambiguity could be resolved to some extent by scanning the arrays slightly to determine, effectively, the gradient of the relative intensity/angle characteristic.

If we consider this method in a target tracking context, rather than in an azimuth estimation role, (i.e. we wish to center a target within the beam, rather than estimate the target position with fixed arrays) the unambiguous region is increased, to that denoted B. Over the entire range, B, correct information is available as to which direction the arrays should be rotated to center the target. Thus over the entire main lobe of the combined sensitivity characteristic, for the case shown in Fig. 1.6 unambiguous information is available.

Since, in a fishfinding situation, one is inevitably concerned with target tracking (approaching) rather than

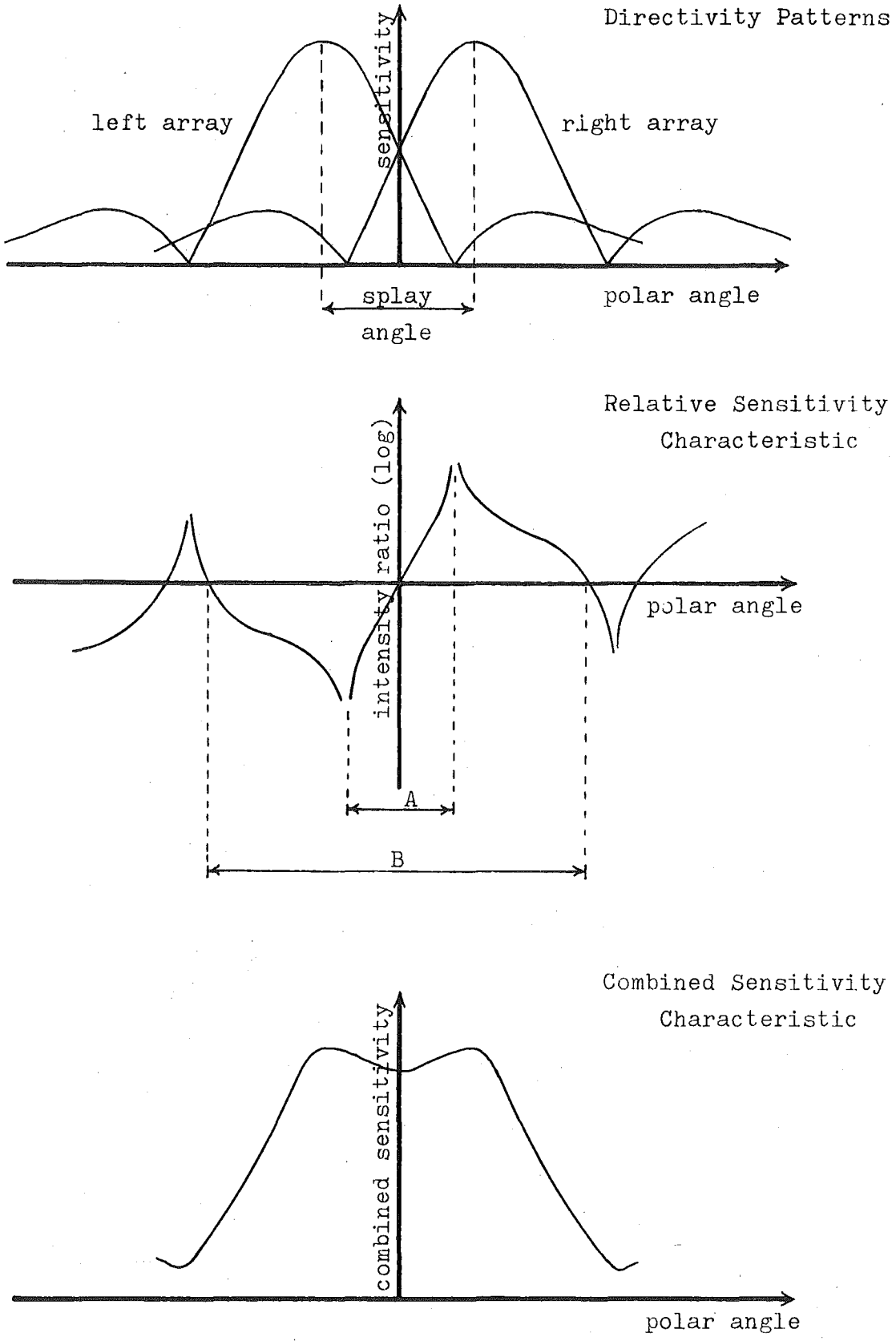

Figure 1.6. Directional determination by lobe amplitude comparison.

estimating the relative positions of a multitude of targets, this system would appear to be viable.

Under noise and reverberation free conditions, the system described above would allow the determination of the azimuthal position of a target, to any desired accuracy, if appropriate detectors were used. In realistic conditions, however, where S/N ratios are far from infinite, the accuracy is related to the slope of the relative intensity characteristic at the origin.

Inspection of Fig. 1.6 shows that any attempt to increase the accuracy (slope) by increasing the angle of splay between the two receiving arrays will also result in a reduction of the sensitivity in the central region of the beam. Instability of the tracking process may also result if the gradient at the origin is too steep.

The design of the beam configuration to achieve a suitable relative intensity vs angle characteristic for audible presentation is discussed in detail in Ch. 7.

1.6 The Auditory System as a Sonar Signal Processor

The human auditory system, in its role of detecting sound sources against a noise background, bears considerable resemblance to certain electronic detectors. It is thus possible to explain various characteristics of auditory detection by analogy with their electronic counterparts.

The simplest, and probably the most universal model of the auditory system, comprises a bank of band pass filters, the width of any one being referred to as the critical bandwidth[27]. The exact manner in which the signals at the outputs of these filters provoke corresponding neural responses,

is of no consequence in the present context. Suffice it to say that experiments in auditory detection suggest that in most cases the detection function may be reasonably represented by simple rectifier followed by a low pass filter[28].

Assuming that such a model of auditory detection is valid, it is clearly apparent why an audio presentation, which contains a number of tonal signals presented simultaneously, will be effective, whereas the presentation of a sequence of short transient signals will be ineffective. In the case of the tonal signals, of different frequencies, the detectors following certain band pass filters will produce strong responses while others will show no response. If a sequence of short transients is presented, however, a large number of filters will respond simultaneously at the application of the first pulse and no further response will be discernable until after a period at least equal to the time constant of the filters. The inability of the human auditory system to recognize two close transients as being different from one larger transient is known as the 'precedence effect'[29].

In a static target situation, the linear FM sonar transmission, with direct heterodyning of the transmitted and received signals, can produce an audio display which comprises a number of tonal signals whose frequencies are directly proportional to the target ranges, all present simultaneously, and for an appreciable period. Such a display is inherently suitable for processing by the human auditory system.

The range resolution which can be expected with the FM transmission used in the present application can be determined directly from the sonar parameters and knowledge of the

critical bandwidths. Over the range of frequency from 1 kHz to 10 kHz, the critical bandwidth is typically from 4% to 6% of the center frequency. (see Ch.2, Fig. 2.4) Below 1 kHz the fractional width of the critical band begins to increase rapidly.

Assuming an FM sweep of 4 secs duration, the resolution at a range of 200 yds will be 6 yds (4%), at a range of 60 yds, it will be 3 yds (5%), and at a range of 20 yds, it will be 3.5 yds (17%). Although this resolution cell width is considerably greater than the theoretical unambiguous limit for the waveform, of 0.74 ft, when considered in relation to the detection problem, it does not seem unreasonable. i.e. the degradation of S/N ratio will be considerably less than the ratio of cell width for auditory detection to theoretical minimum cell width, for targets such as fish shoals, since this cell will presumably contain more fish. The fact that individual fish will not be resolvable is, in itself, unimportant.

In determining the effect of target motion on the auditory display, for the case of a fish shoal target, the effects of both

(i) Translational motion of the entire shoal, and

(ii) Oscillatory motion of individual fish within the shoal,

must be considered.

Translational motion of the 'centre of gravity' of the shoal causes a compression, or expansion, of the scattered signal, as mentioned previously, with the result that at the heterodyne output, a residual FM component (linear if the radial velocity is constant) exists.

In a realistic fishing situation, the highest expected radial velocity would be about 20 ft/sec and this would probably only be achieved if vessel and shoal motions were diametrically opposed. Such a velocity would produce a frequency deviation of the heterodyne output signal of 320 Hz over a single transmitted pulse, or a maximum deviation rate of 160 Hz/sec for a sweep duration of 2 secs.

Many workers (see Ch.6, section 6.2) have shown that the integration time of the auditory system is at most 300 msec. (This integration time is associated with the detector, rather than the critical band filter). The maximum deviation which could occur within this integration time is thus, 50 Hz.

Since the critical bandwidth is never less than about 50 Hz, it may be concluded from the above figures that the detection process will not be significantly degraded by translational target motion, since over a single integration period, the audio signal will remain within a single critical bandwidth.

Since the frequency deviation over the entire sweep period will span several critical bandwidths, the FM component will be recognizable, nevertheless.

Oscillatory motion of individual fish within a shoal has been studied by several workers (see Ch. 6, section 6.5), and rapid frequency deviations of up to 200 Hz have been observed due to the swimming motion of the fish.

Quite apart from the frequency spread at the heterodyne output, due to the spatial distribution of the shoal then an additional frequency spread of up to 200 Hz may be expected due to the swimming motion of individuals within the shoal. Since a large portion of the scattered energy is spread in

frequency by this effect, a reduction in S/N ratio (comparative to a static target situation) is inevitable, since the audio signal energy will be spread over several critical bands.

It is interesting to consider the effect this Doppler spread would have on an electronic processor of the type described in section 1.4. The total energy of the received signal would be spread over a very large number of resolution cells and the correlation loss for each of these cells would be extremely high. The result would be that the detection performance of the electronic processor would be little better than the auditory system, assuming similar detection efficiency. There is no way in which the correlation loss could be lessened, since it is obviously not feasible to store sufficient distorted versions of the transmitted signal to cope with the number of possible signal variations.

The use of interaural amplitude difference (IAD) as an auditory cue to enable the centering of a target within a wide beam is discussed in detail in Ch. 7. Psycho-acoustic measurements and experiments with a model of the system indicate that with the IAD characteristic achieved with the underwater sonar discussed in this thesis, an operator should be capable of centering a target (whether it is specular or diffuse), to within an accuracy of about $\pm 5^{o}$.

Subsequent sea trials have shown that the configuration used provides sufficient information, in an easily interpretable form, to allow extremely accurate target tracking (see Ch. 9).

1.7 References

1. L. Kay, "An Ultrasonic Sensing Probe as a Mobility Aid for the Blind", Ultrasonics, 2 : 53 (1964).
2. L. Kay, "Ultrasonic Spectacles for the Blind", Proc. Int. Cong. on Sensory Devices for the Blind, St Dunstans, 1966.
3. R.M. Page, "Monopulse Radar", IRE Natl. Conv. Rec. Vol 3, Pt 8, p132 (1955).
4. G. Martin, "Electronics and Transducers for an Ultrasonic Blind Mobility Aid", M.E. Thesis, University of Canterbury (1969).
5. D. Rowell, "Auditory Display of Spatial Information", Ph.D. Thesis, University of Canterbury (1970).
6. P.R. Hopkin, "Cathode-Ray Tube Displays for Fish Detection on Trawlers", J. Brit. I.R.E., 25 : 73 (1963).
7. R.W.G. Haslett, "A High-Speed Echo-Sounder Recorder having Seabed Lock", J. Brit. I.R.E., 24 : 441 (1962).
8. P.M. Woodward, "Probability and Information Theory with Applications to Radar", 2nd ed., Pergamon : London (1964).
9. D.O. North, "An Analysis of the Factors which Determine Signal-to-Noise Discrimination in Pulsed Carrier Systems", RCA Tech. Rept, PTR-6C, June 25 (1943).
10. C.E. Cook, "Pulse Compression - Key to More Efficient Radar Transmission", Proc. IRE, 48 : 310 (1960).
11. J.R. Klauder, A.C. Price, S. Darlington and W.J. Albersheim, "The Theory and Design of Chirp Radars", Bell System Tech. J. 39 : 745 (1960).
12. G.P. Ohman, "Getting High Range Resolution with Pulse Compression Radar", Electronics, 33 : no. 41, p53 (1960).

13. C.E. Cook and M. Bernfield, Radar Signals, Ch. 6, Academic Press, New York (1967).

14. T.H. Glisson and A.P. Sage, "On Sonar Signal Analysis", IEEE Trans. Aerospace and Electronic Systems, AES-6 no. 1 : 37 (1970).

15. H.R. Raemer and A.B. Reich, "Correlation Devices Detect Weak Signals", Electronics, Vol 32, no. 21, p58 (1959).

16. A.W. Rihaczek, Principles of High Resolution Radar, McGraw-Hill, New York, Section 3.2 (1969).

17. V.C. Anderson, "DELTIC Correlator", Harvard Acoust. Lab. Tech. Memo No. 37, Jan 5, 1956.

18. S.A. Kramer, "Doppler and Acceleration Tolerances of High-Gain Wideband, linear FM Correlation Sonars", Proc. IEEE, 55 : 627 (1967).

19. D.M. Russo and C.L. Bartberger, "Ambiguity Diagram for Linear FM Sonar", J. Acoust. Soc. Am., 39 : 183 (1965).

20. R.E. Millet, "A Matched-Filter Pulse Compression System Using a Nonlinear FM Waveform", IEEE Trans. Aerospace and Electronic Systems, AES-6, no. 1 : 73 (1970).

21. C.E. Cook and M. Bernfield, Radar Signals, Ch. 7, Academic Press, New York (1967).

22. C.E. Cook and M. Bernfield, op. cit., Ch 4.

23. R.N. Bracewell, "Radio Interferometry of Discrete Sources", Proc. IRE, Jan., 97 (1958).

24. J.V. Lee, "Underwater Acoustic Interferometer", Digest of Tech. Papers, 1970 IEEE Int. Conf. on Eng. in the Ocean Env., 70C 38-OCC, p63.

25. M.I. Skolnik, Radar Systems, McGraw-Hill, New York, Ch. 5 (1962).

26. V.M. Albers, Underwater Acoustics Handbook, Penn. State Univ., Ch. 17, (1960).

27. H. Fletcher, "Auditory Patterns", Rev. Mod. Phys., 12 : 47 (1940).

28. C.W. Sherwin, F. Kodman, J.J. Kovaly, W.C. Prothe and J. Melrose, "Detection of Signals in Noise : A Comparison between the Human Detector and an Electronic Detector", J. Acoust. Soc. Am., 28 : 617 (1956).

29. M.B. Gardner, "Historical Background of the Haas or Precedence Effect", J. Acoust. Soc. Am., 43 : 1243 (1968).

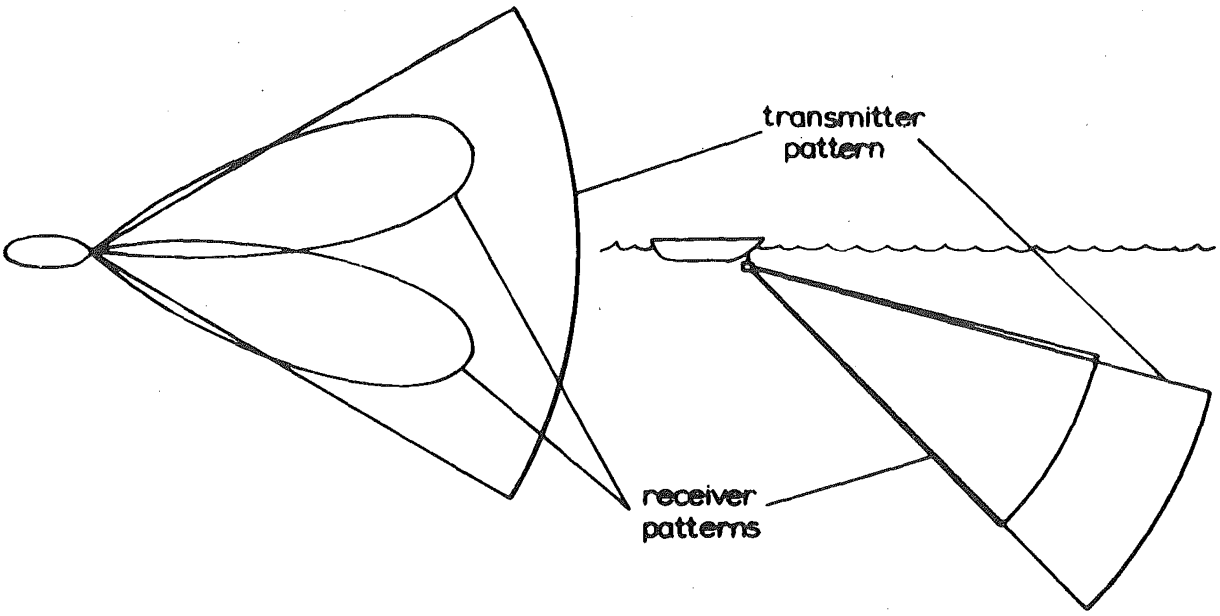

CHAPTER 2

DEVELOPMENT OF SPECIFICATION

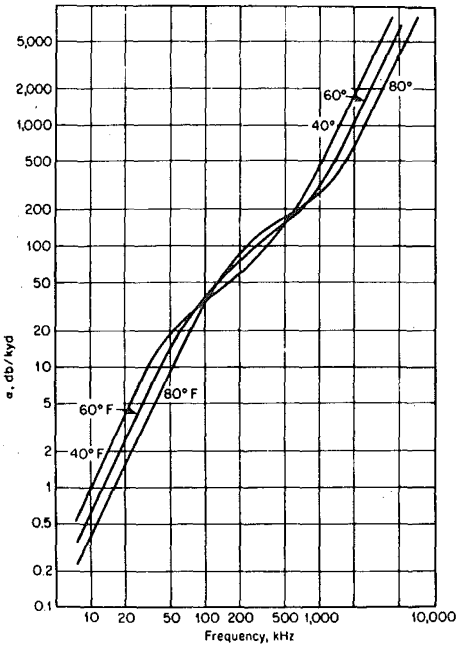

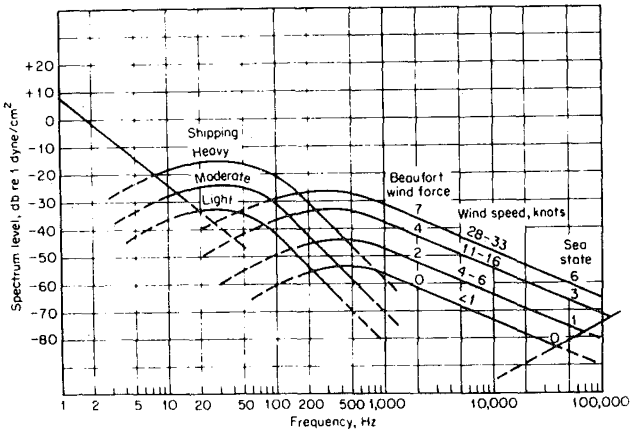

CHAPTER 2

DEVELOPMENT OF SPECIFICATION

2.1 Aims of the Design

The basic philosophy behind the development of the system described in this thesis has been to determine the feasibility of a particular sonar system configuration, namely a wide beam FM sonar using a binaural, audio display. A fishfinding sonar has been the vehicle for this investigation, and results to date indicate a considerable future for this type of device in the fishing industry. However, the author has been more concerned with the system capability than with the particular requirements of a device for fish detection. For this reason, parameters of the system are chosen without too much regard for any particular fishing technique. Once the system has been shown to be a viable proposition, re-design, to meet specific fishing requirements, will be necessary. The prototype system must, however, be a realistic target detection device in order to obtain a meaningful evaluation of the system. A ship mounted forward looking sonar is most suitable for an experimental system, although other configurations may better serve the requirements of the fishing industry.

Considerable flexibility is desirable in the design of an experimental system to enable the effects of changes in parameters to be gauged. This is particularly important in the case of the present device, where the interface between sonar and operator is a very important feature of the system, and unfortunately one which may only be examined experimentally.

2.2 Choice of Overall Beam Dimensions

The binaural lateralization process offers a means of centering a target within a wide sector of illumination, and to take full advantage of this display format, it is desirable to use a beam which is sufficiently wide to obviate the necessity to scan the array. In this way the cost of the sonar installation may be greatly reduced.

Consider the idealized search sector shown in Fig. 2.1, where the region in which a given target will be detectable has been approximated by a sector of a circle subtending an angle, θ, (the nominal beam angle) at the transducer arrays. If R is the maximum range of the sonar with beam angle, θ, the width, W, of the path searched, as the vessel proceeds along an approximately straight course will be,

$$W = 2R \sin \theta/2 \qquad 2.1$$

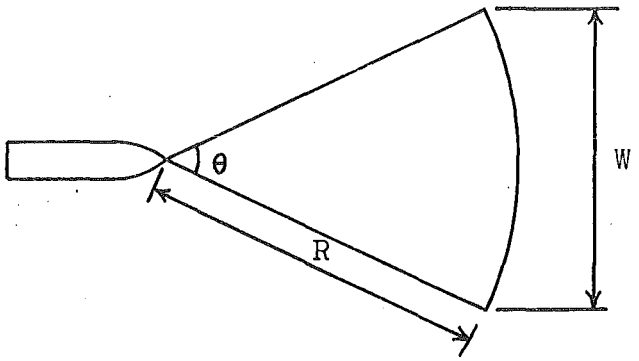

Figure 2.1. Idealized sector of detection.

Let the resolution cell width of the sonar be δR, and the beamwidth in the vertical plane be γ. Assuming, arbitrarily, that a target is just detectable when the signal level it returns is equal to the total signal level returned by scatterers in the resolution cell which it occupies, then

in all cases, regardless of beamwidths, the target will become just detectable when it enters a resolution cell of a certain volume related only to the strength of the target. This volume, V, is given by,

$$V = \text{constant} = \theta\gamma R^2 \delta R$$

Assuming the vertical beamwidth is constant and substituting in equation 2.1, we obtain an expression for the width of the path searched, as a function of θ,

$$W = k\ \theta^{-\frac{1}{2}} \sin \theta/2, \quad \text{where k is a constant.}$$

This function is sketched in Fig. 2.2 with a normalized axis for W.

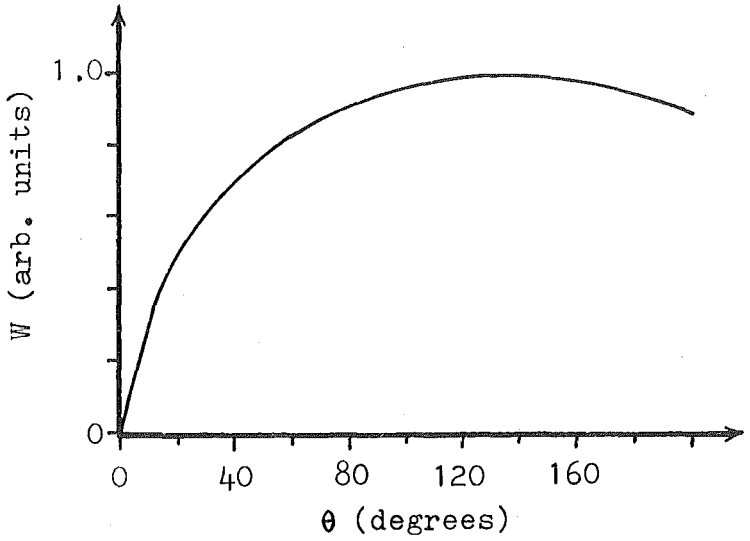

Figure 2.2. Variation of search path width (normalized) with horizontal beamwidth, θ.

Fig. 2.2 shows that the search path width increases rapidly when θ is small, but the variation is slow beyond $\theta = 60^{\circ}$. The magnitude of the maximum range of the sonar varies as $\theta^{-\frac{1}{2}}$ so that it is undesirable to make θ any larger

than is necessary. A value of 60^{o} was chosen since this gives a search path width approximately 80% of the maximum possible.

The preceding analysis holds strictly, only in a situation in which the reverberation level from a particular range increment increases directly with increasing horizontal beamwidth. This condition is satisfied in the case of volume reverberation, but not necessarily in the case of boundary reverberation, in which an increase in beamwidth may not cause an increase in scattering area in a given increment. However, since in the sonar under discussion, the resolution cell width is comparatively coarse due to the appreciable width of the critical band of the auditory system, the condition would be satisfied in many boundary reverberation situations.

The choice of vertical beamwidth must be based on a compromise between achievable range, and the necessity that a target remain detectable down to short ranges to enable accurate tracking. To optimize the beamwidth mathematically would require knowledge of the directivity pattern in the vertical plane, the reverberation conditions, and for a boundary reverberation case, knowledge of the position of target and boundary with respect to the sonar. Since the answer would, no doubt, be critically dependant on the particular situation, no such analysis was attempted. A value for the vertical beamwidth of 20^{o} was chosen, quite arbitrarily. Subsequent sea trials with the sonar, however, have shown this choice to be realistic, allowing fish shoals at greatly varying depths to be tracked accurately (see Ch. 9).

The transmitting array thus has a beam which is $60^{o} \times 20^{o}$. This corresponds to a directivity factor of 34.4 (assuming wedge shaped beams) and a directivity index of 15.4 dB.

2.3 Beam Configuration of the Receiving Arrays

The binaural display proposed for this sonar relies solely on the shape and relative angular positions of the receiving array directivity patterns to produce an intensity difference between audio signals (derived from the two arrays), which is some suitable function of the azimuthal position of the target. For this reason, more stringent restraints must be placed on these directivity patterns than are normally required for more conventional sonars.

A detailed discussion of the requirements for the binaural-display/auditory-system interface is contained in Ch. 7 and only the essential points as they affect the receiving array beams will be stated here. Two main restraints, as follows, are necessary:

(i) The shapes and widths of the directivity patterns in the horizontal plane must be designed to enable a suitable interaural-intensity-difference (IAD) vs target-azimuth characteristic to be produced.

(ii) The receiving array beamwidths and beamshapes must remain approximately constant over the full working bandwidth of the system so that the IAD vs azimuth characteristic does not vary within each transmission.

This latter requirement poses considerable problems in the design of the receiving arrays (see Ch. 4, section 4.3), since normally the beamwidth of an array will approximately halve as the frequency doubles.

The choice of receiving array beamwidths is based on requirements (i) above, and is discussed in detail in Ch. 7. It will be merely stated, here, that beamwidths of approximately 30^{o}, splayed left and right by 13.5^{o} will be employed.

The receiving arrays thus have directivity factors of 68.6 (assuming wedge shaped beams) and directivity indices of 18.4 dB.

2.4 Design of Transmission Waveform

Choice of the center frequency and bandwidth of the linear FM transmission, involves the consideration of many factors. The most important of these are listed below:

(i) Array size for specified beamwidths

(ii) Fractional bandwidth requirements of transducer elements

(iii) Factors influencing the range of the sonar, viz. ambient noise, reverberation, frequency dependence of target cross section, transmitted power, and frequency dependence of seawater attenuation.

(iv) Bandwidth requirements of the display

Horton[1] showed the existence of optimum frequencies for noise limited sonars. Stewart, Westerfield and Brandon[2] state that in the case of a reverberation limited sonar with constant array dimensions, no optimum frequency exists, since the echo/reverberation ratio continues to increase with increasing frequency due to the increasing array directivity. Thus, the maximum range of the sonar increases without limit as the frequency increases. This result is of little practical significance since the transmitted power required to make the sonar reverberation limited (i.e. to ensure that the reverberation level at the receiver exceeds the noise level) may severely restrict the maximum frequency of operation. If the array directivities, rather than their dimensions, are held constant (as in the present case) a reverberation limited

sonar will again have no optimum frequency unless the target itself exhibits a peak in its scattering cross section. If both target and reverberation have flat frequency characteristics, all frequencies will be equally suitable in this case, and the choice will be dependent only on external factors such as (i), (ii) and (iv) above.

As was stated above, the assumption of a reverberation limited sonar is, in itself, unrealistic since in all cases, a certain minimum transmitted power level is required to make the sonar reverberation-limited. It is more meaningful to specify a reverberation/noise ratio required at the maximum range as suggested by Stewart et al.[2].

Ref. (2) derives the following expression for curves of optimum frequency vs maximum range:

$$f^a = \frac{((t - b - \phi + i)(R/N) + (s + t - v - w - \phi - \psi))}{2\alpha_0 ra} \qquad 2.2$$

where the variation of parameters with frequency is accounted for by powers defined as follows:

$k_1 f^t$ = target back scattering cross section,

$k_2 f^b$ = backscattering coefficient of boundary reverberation,

$k_3 f^\phi$ = horizontal beamwidth,

$k_4 f^\psi$ = vertical beamwidth,

$k_5 f^i$ = input bandwidth,

$k_6 f^w$ = output bandwidth,

$k_7 f^s$ = axial source intensity,

$k_8 f^v$ = noise power spectrum density,

$\alpha = \alpha_0 f^a$ = intensity attenuation,

k_1-k_8 constants, r is the range (kyds), f is the frequency (kHz), and α_0 is the coefficient of intensity attenuation at

1 kHz. (R/N) is the ratio of reverberation power to noise power used to define the 'reverberation-limited' condition.

For the present sonar we have $\phi = \psi = 0$ since we require to maintain the specified beam dimensions regardless of frequency. Also, since the transmitter and receiver bandwidths are to be determined by requirements of the audio display (see below) we have $i = w = 0$. The frequency dependence of the target cross section is expected to show a linear increase at moderately high frequencies[3]. The characteristics of fish and fish shoals as targets is discussed further in chapter 6. A linear increase corresponds to a frequency power of unity, thus $t = 1$. The backscattering characteristics of boundary reverberation tend to be independent of frequency when the acoustic wavelength is smaller than the scale of surface roughness. Since this is the most likely situation, $b = 0$.

Since the sonar has a very wide beam in both vertical and horizontal planes, in most situations the transmitted power level required to achieve reverberation limiting will be well below the cavitation limit so a stipulation of constant transmitted power is most meaningful, thus $s = 0$. Assuming operation at frequencies at which the ambient sea noise will exceed the thermal limit, a square law reduction of noise power per unit bandwidth, with increasing frequency may be expected[4]. Thus, $v = -2$. The attenuation due to volume absorption at frequencies above about 10 kHz may be represented[5] as follows:

$$\alpha = 0.033 f^{3/2}$$

this implies $\alpha_0 = 0.033$, $a = 3/2$.

Defining the reverberation limited condition as R/N = 1, and using the above figures, the following expression for optimum frequency as a function of maximum range is obtained:

$$f^{3/2} = 174\ r^{-1}.$$

This function is sketched in Fig. 2.3. It is perhaps worthwhile to state the meaning of this function: If a particular target, whose cross section satisfies the conditions stated previously, is just detectable at range, R, when the sonar frequency is f_o, (the optimum frequency for maximum range, R) then the target will be undetectable at higher or lower frequencies, if the stipulated conditions are maintained as the frequency is changed.

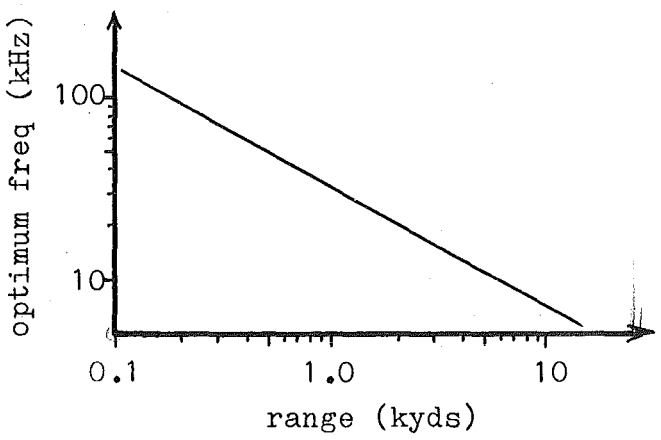

Figure 2.3. Optimum frequency vs maximum range characteristic.

The optimum frequency is not sharply defined due to the comparatively slow variation of the relevant parameters with frequency. Peaks of width greater than one octave are typical.

In order to select an operating frequency from Fig. 2.3, it is necessary to determine the approximate maximum range of the sonar when reverberation limited. This depends on the range resolution as well as the beam dimensions specified previously. The range resolution will be taken as 5% of the target range since this is a typical value for the width of the critical band of the auditory system[6,7] (see Ch. 6 for a discussion of the critical band concept).

Assuming a boundary reverberation situation we may assume that the reference backscattering strength of the seabed for shallow grazing angles will lie in the range -20dB to -35dB[8,9] depending on whether the bottom is sand, sand and rock, or silt. The axial dimension of the scattering area will be approximately equal to the range resolution cell-width (5% of R_{max}) and the transverse dimension will be θR_{max}, where θ is the horizontal beamwidth. The reverberation strength at the maximum range, R_{max} will then be,

$$RS = -20 \text{ (to } -35) + 10 \log \frac{\theta R_{max}^2}{20}$$

The target strength of a fish shoal is a difficult quantity to obtain since it depends on the size and species of the fish, the dimensions and density of the shoal, as well as a multitude of other factors such as aspect angles of individuals, frequency, interaction among scattered signals etc. Reference (10) quotes a figure of approximately 15 dB for a shoal 20 yds across and 16 yds deep. (Target cross section of an individual fish taken to be 0.04 yds^2 and the shoal density taken to be $1/yd^3$). A figure of 5 dB is assumed here as a conservative estimate.

Assuming that a target is just detectable when its target strength is equal to the reverberation strength of that area of the sea bed which occupies the same resolution cell (see Ch. 8, section 8.2.1), the maximum range is given by:

$$TS = RS$$

$$5dB = -20 \text{ (to } -35) + 10 \log \frac{\theta R_{max}^2}{20}$$

This gives an expected maximum range of between 110 and 880 yds for this target, depending on the nature of the bottom. (θ taken as 30° (see Section 2.3.))

Since the sea bottom tends to be irregular in good fishing areas and since this target represents a comparatively large fish shoal, a nominal maximum range of 200 yds will be assumed for the sonar.

Referring to figure 2.3 the optimum frequency for a 'just reverberation limited sonar' with a maximum range of 200 yds is approximately 90 kHz.

The other consideration affecting choice of operating frequency is the bandwidth requirement. The choice of bandwidth is based on two aspects of the system, namely, (i) the audio display characteristics and (ii) the expected target characteristics.

The factors which influence the detection of signals against a background of noise (produced by reverberation) are discussed fully in Ch. 6. The most pertinent feature characterizing auditory detection, and affecting choice of bandwidth is the integration time. The signal/noise ratio required for detection reduces as the signal duration increases, reaching a minimum value at approximately 300 msec (see Ch. 6).

Further increase does not affect the threshold level. In order to achieve this duration for a target at the nominal maximum range of 200 yds, a bandwidth of at least 6 kHz is required. To achieve this for a target, which becomes just detectable at a range of 100 yds, a bandwidth of approximately 12 kHz is required. This is considered to be the minimum acceptable system bandwidth on the basis of auditory detection requirements.

From the point of view of detecting, and possibly recognizing, fish shoal targets, the wider the bandwidth, the better. This is because the backscattering cross sections of fish vary considerably with frequency, variation by up to 30 dB over an octave being common (see Ch. 6, Fig. 6.10). A narrow band sonar could at times have a very restricted range on a particular shoal due to the reduced target strength of individual fish in the shoal, at the operating frequency. A wide bandwidth ensures that the target cross section will be large, at least for part of the transmission. A possible added advantage of choosing a wide bandwidth is that when a shoal is approached and the signal/noise ratio becomes good, an estimation of the size of the fish may be feasible on the basis of signal level fluctuations due to variations in scattering strength (see section 6.5).

On the basis of the various factors mentioned above, a system bandwidth of one octave extending from 40 kHz to 80 kHz was chosen. This bandwidth was considered feasible from the point of view of hardware limitations (i.e. transducer elements and arrays). Increasing the bandwidth beyond one

octave, in addition to placing greater demands on the transducer design, could introduce problems from harmonic components in the transmitted waveform which could not be eliminated by filtering.

2.5 Acoustic Power Requirements

In order to achieve the greatest possible range from a sonar under all environmental conditions, it is necessary to transmit sufficient power to produce a reverberation limited condition at all ranges. The transmitter source strength required for each of two background situations will be evaluated here to provide a basis for electronic design. In these examples, reverberation limitation will be defined as the condition at which the audio signal level due to reverberation, within a critical bandwidth (corresponding to the maximum range of 200 yds), is 10 dB above the noise level in that band, due to ambient noise in the sea. The maximum audio frequency, corresponding to maximum range is taken as 3 kHz (see section 2.6), and the receiving array beamwidths are taken as 30^{o} (see section 2.3).

case (i) Shallow water, sea bottom reverberation predominant. The critical bandwidth corresponding to the resolution cell width at maximum range will be approximately 5% of 3 kHz, i.e. 150 Hz. We require to find the reverberation level and noise level in this band, under the above conditions, and the transmitter level required to make the ratio 10 dB.

The reverberation level is

$$RL = SL - 2.TL + 10 \log A + S_b \text{ dB re 1 } \mu\text{bar} \qquad 2.3$$

where SL is the transmitter source level, TL is the one way transmission loss, S_b is the sea bottom scattering strength for one yd^2 (shallow grazing angle assumed) and A is the area of sea bottom occupying the resolution cell at maximum range.

TL is 50 dB (spreading loss of 46 dB and attenuation at the rate of 22 dB per kyd[11])

S_b is at least -35 dB[8]

A is 1050 yd^2 (based on a 10 yd resolution cell width and a 30^o receiving array beamwidth in the horizontal plane.)

This gives,

$$RL = SL - 105 \text{ dB re 1 } \mu\text{bar.} \qquad 2.4$$

The effective bandwidth of sea noise, which will give rise to audio noise, is twice the critical bandwidth since noise above and below the transmitted frequency is involved. The bandwidth of sea noise is thus 300 Hz. The noise level is then,

$$NL = N - DI + 10 \log 300 \text{ dB re 1 } \mu\text{bar} \qquad 2.5$$

where N is the spectrum level of ambient noise and DI is the directivity index of a receiving array.

The maximum expected spectrum pressure level of noise in the bandwidth of interest is approximately -50 dB[4] (wind speed 22 knots).

The directivity index of each receiving array is approximately 18 dB. The noise level is thus,

$$NL = -43.2 \text{ dB} \qquad 2.6$$

To give a 10 dB reverberation/noise ratio, a source strength of 71.8 dB is required. This corresponds to a transmitted power level of only about 0.1 watts.

case (ii) Deep water, volume reverberation predominant.

For this case, as before,

$$NL = -43.2 \text{ dB re 1 } \mu\text{bar} \qquad 2.7$$

but the reverberation level is given by,

$$RL = SL - 2.TL + S_V + 10 \log V \text{ dB re 1 } \mu\text{bar} \qquad 2.8$$

where S_V is the scattering strength per unit volume and V is the volume of the resolution cell at the maximum range.

In comparatively shallow water (approx. 250 ft), S_V is typically -78 dB [11], although lower values have occasionally been reported.

V is 73,000 yd^3 (based on a cell width of 10 yds and receiving array beams 30^o wide and 20^o deep).

The source level required to give a 10 dB reverberation/noise ratio is thus 97 dB corresponding to a transmitted power level of about 12 watts.

The electronics must thus be capable of driving the transmitting array to produce an acoustic power output of up to 12 watts.

2.6 System Gain Requirements

From section 2.5 the effective sound pressure level of noise, which will give rise to audio noise in the critical band corresponding to the resolution cell at maximum range, is approximately -43.2 dB re 1 μbar. In the reverberation limited condition defined previously, the reverberation level in the same critical band will be 10 dB above this, i.e. -33.2 dB re 1 μbar. The average sensitivity of a single

receiving array element is approximately -89.3 dB re 1v/μbar (see Ch. 3, section 3.6), so that electrical signal level at the transducer terminals contributed by the most distant resolution cell will be -122.5 dB re 1v.

Suppose a target is present at the maximum range. Assuming that it will produce a tonal signal at the audio display, this signal will be detectable if its level is approximately equal to the noise level occupying the same critical band (see Ch. 8, section 8.2.1). i.e. if a target at the maximum range is to be just detectable in the background due to reverberation, it must produce a voltage of approximately -122.5 dB re 1v at the terminals of the receiving array elements.

To produce a comfortable listening level in the headphones used with the sonar, the voltage at the earphone terminals must be approximately 0.1v. This implies that the overall system gain for signals from the maximum range must be 102.5 dB if the transmitter level is to be minimal. Compensation for the variation of signal level with range may be affected by using frequency shaping networks in the audio stages. These circuits are discussed in section 5.3.5.

2.7 Choice of Audio Bandwidth

The audio bandwidth is chosen to enable best utilization of the human auditory system in its role of detecting and recognizing signals. Figure 2.4 shows a plot of the width of the critical bandwidth of the auditory system (expressed as a percentage of the center frequency) against frequency. The fractional width of the critical band is seen to be minimal in the frequency range from 2 kHz to 5 kHz. It is logical to

choose the maximum audio frequency within this range in order to obtain maximum resolution, and hence maximum signal detectability, at the maximum range of the system.

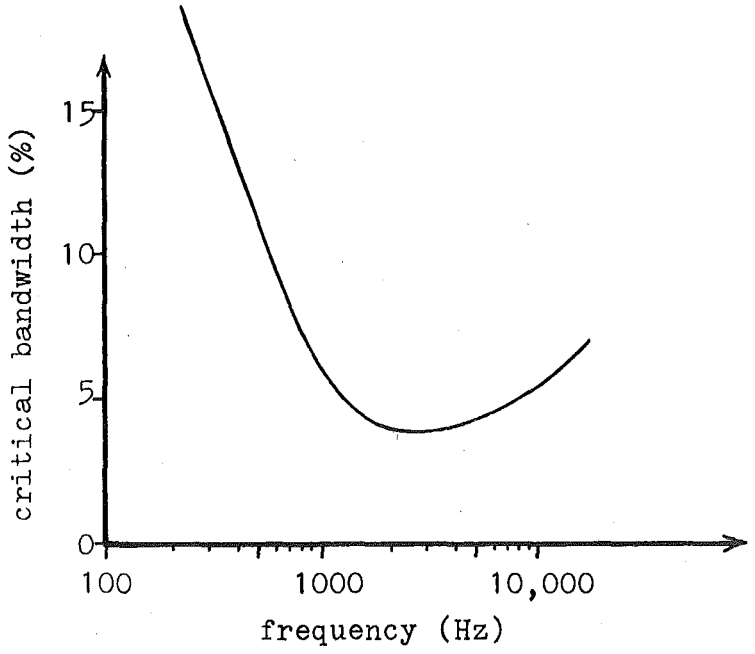

Figure 2.4. Fractional width of the critical band of the auditory system as a function of frequency (from refs 6,7).

Since the frequency sweep rate of the FM transmission may be increased, step-wise as a target is approached, there is no need for the audio bandwidth to extend down to very low frequencies. In fact it is undesirable to use frequencies below about 300 Hz due to the very poor resolution, resulting from the widening critical bandwidth.

The audio bandwidth is thus specified as the decade from 300 Hz to 3 kHz.

2.8 Conclusions

The basic parameters of the sonar have been determined in this chapter. More detailed specifications are evolved throughout the thesis. It should be stressed that some of the assumptions used in determining the broad specification of the sonar are justifiable only for the purposes of determining the magnitudes of various parameters and many significant problems are obscured by these assumptions. For instance, the assumption of wedge shaped beams in the vertical plane implies that reverberation from the surface will not affect the operation of the sonar. In practice, side lobes in the directivity patterns are inevitable and surface reverberation cannot be ignored. Problems, such as this, are discussed in various chapters of the thesis as they appear relevant.

2.9 References

1. J.W. Horton, Fundamentals of Sonar, United States Naval Institute, Annapolis, Md, 1957. pp317-352.
2. J.L. Stewart, E.C. Westerfield and M.K. Brandon, 'Optimum Frequencies for Active Sonar Detection', J. Acoust. Soc. Am., 33 : 1216 (1961).
3. R.W.G. Haslett, "Determination of the Acoustic Back-scattering Patterns and Cross sections of Fish", Brit. J. Appl. Phys., 13 : 349 (1962). (See diagram reproduced in section 6.5.)
4. V.O. Knudsen, R.S. Alford and J.W. Emling, "Underwater Ambient Noise", J. Mar. Res., 7 : 410 (1948).
5. M.J. Sheehy and R. Halley, "Measurement of the Attenuation of Low-Frequency Underwater Sound", J. Acoust. Soc. Am., 29 : 566 (1953).

6. J.E. Hawkins and S.S. Stevens, "Masking of Pure Tones of Speech by White Noise", J. Acoust. Soc. Am., 22 : 6 (1950).

7. T.H. Schafer, R.S. Gales, C.A. Shewmaker and P.O. Thompson, "Frequency Selectivity of the Ear as Determined by Masking Experiments", J. Acoust. Soc. Am., 22 : 490 (1950).

8. R.J. Urick, "Backscattering of Sound from a Harbour Bottom", J. Acoust. Soc. Am., 26 : 231 (1954).

9. C.M. McKinney and C.D. Anderson, "Measurements of Back-scattering of Sound from the Ocean Bottom", J. Acoust. Soc. Am., 36 : 158 (1964).

10. A.D. Gomez and H.W. Volberg, Final Report for Feasibility Study of Fish Echoes in Relation to Sonar Detection, US Dept Int., Fish and Wildlife Service, Bureau Comm. Fisheries, Contract No. 14-17-0007-211 (1964).

11. R.J. Urick, Principles of Underwater Sound for Engineers, McGraw-Hill, N.Y., 1967, Chapters 7 and 8.

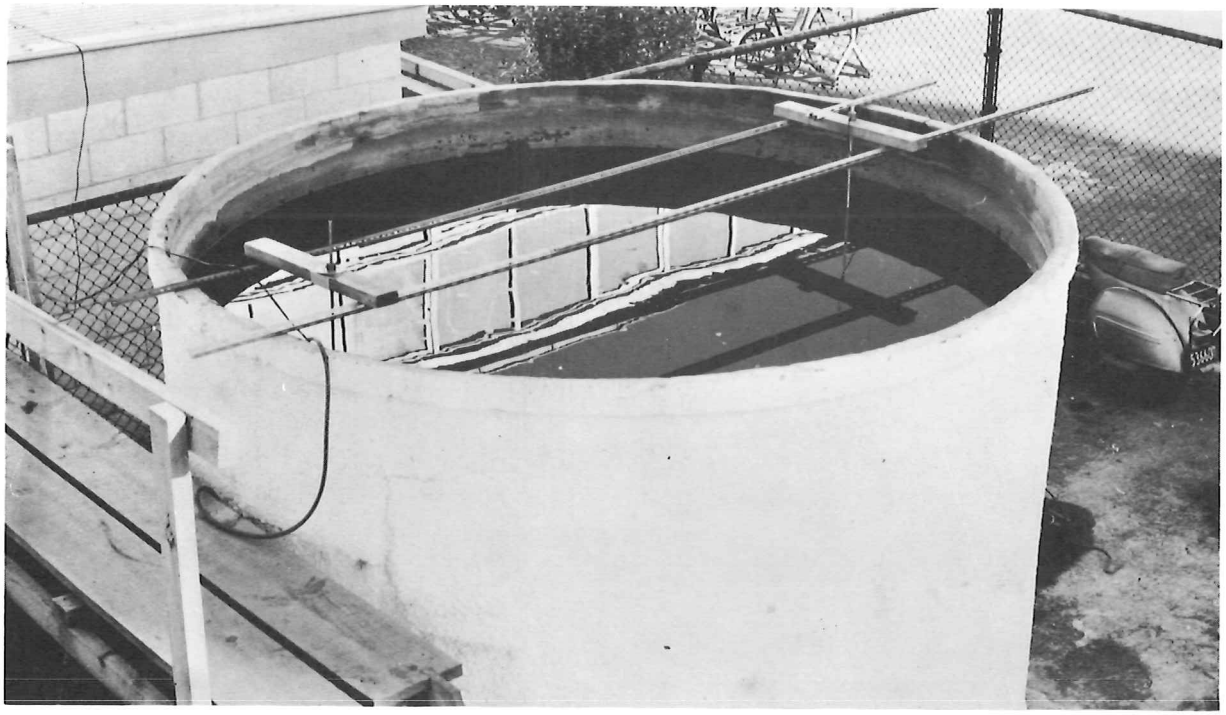

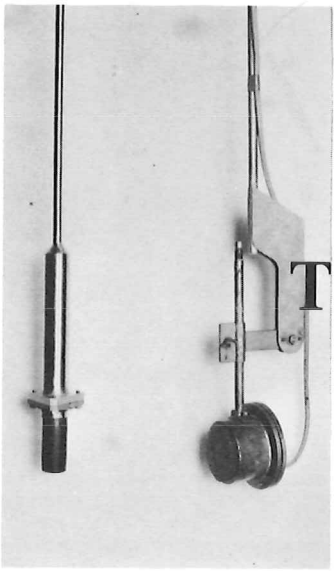

CHAPTER 3

DESIGN OF TRANSDUCER ELEMENTS

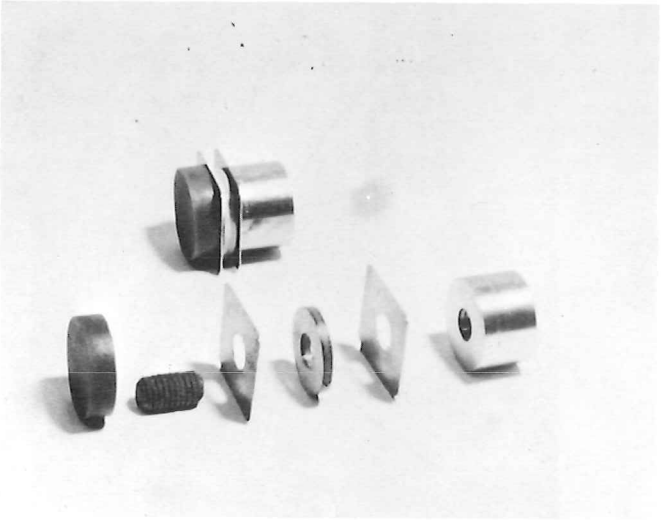

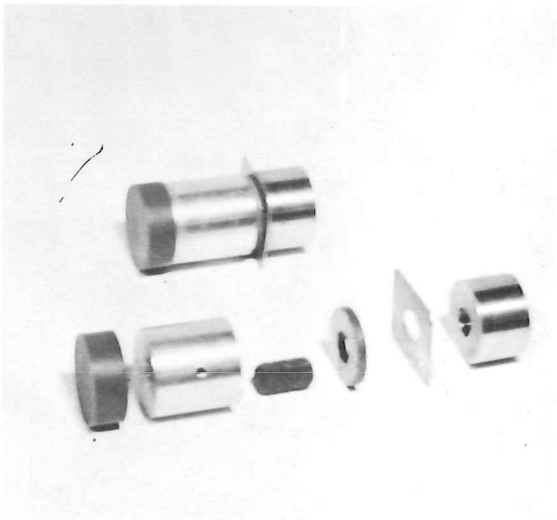

CHAPTER 3

DESIGN OF TRANSDUCER ELEMENTS

3.1 Introduction

The requirement of a frequency bandwidth of one octave (see Ch.2, Section 2.4) poses severe problems on the design of transducer elements. Transducers commonly used for sonar applications[1,2] have bandwidths typically 10%-20% of the center frequency. Wider bandwidths have been reported for free flooding cylindrical transducer elements[3], but this type of element is considered unsuitable for the present application, for the following reasons:

(i) These elements are omni-directional, so in a free flooding arrangement, radiation in the reverse direction is difficult to suppress, and

(ii) Strong interaction among such elements is inevitable in a free flooding array, and this makes array directivity patterns difficult to control.

The comparatively narrow bandwidth of thickness, or longitudinally expanding elements, results from the considerable mismatch between the acoustic impedances of transducer materials and the seawater medium. (The acoustic impedance ratio is typically 20:1.)

Two possible approaches to the problem of achieving broadband characteristics are:

(i) to use elements which have no resonance within or near the operating band, or

(ii) to improve the acoustic match to seawater by interposing matching sections.

In the case of the transmitting elements, approach (i) is unacceptable since it leads to low transmitting efficiency and extreme limitations on the maximum power output. Approach (ii) is clearly preferable.

For the receiving elements, signal/noise ratio provides the criterion for choosing between the two approaches. The performance of a receiving element is adequate if the lowest expected ambient noise level of the medium may be detected at its terminals. Kendig[4] has shown that the equivalent thermal noise pressure of an electroacoustic transducer, P_t, is given by:

$$P_t = (4kT\pi\rho c/\lambda^2\eta D)^{\frac{1}{2}} \quad \text{in a 1 Hz band,}$$

where k = Boltzman's constant, T = absolute temperature (deg. K), η is the receiving efficiency, and D is the directivity factor. Assuming a directivity factor of 68.6 (see Ch. 2, Section 2.3), the noise pressure at 60 kHz is

$$P_t = \frac{1.4}{\sqrt{\eta}} \cdot 10^{-5} \text{ μbar in a 1 Hz band}$$

$$= -99.1 - 10\log \eta \text{ dB re 1 μbar (1 Hz band)} \qquad 3.1$$

According to Mellen's[5] extrapolations of Knudsen's[6] measured sea noise characteristics, the ambient sea noise level at 60 kHz in a sea state ½, is -79 dB re 1 μbar (1 Hz band). From equation 3.1, then, the receiving efficiency of an element can be as low as 1% before thermal noise becomes significant in comparison with ambient noise, even in a very quiet sea. The above analysis suggests that there is no need to use matching sections for the receiving elements, providing preamplifier noise is not significant.

Although unnecessary, it was considered convenient to use similar matched elements in both transmitting and receiving arrays.

The physical dimensions of the active faces of the transducer elements are determined solely by the requirements of the array designs. These requirements are discussed in Ch. 4 and it will be merely stated here that circular active faces 1.7 cm in diameter were considered suitable.

3.2 Choice of Active Material

Ferroelectric ceramic material was chosen as the active material for the transducer elements. Some of the important advantages of ferroelectrics over piezoelectric crystals and magnetostrictive materials are summarized in Table 3.1. The high electromechanical coupling coefficient and the availability of ferroelectric material in a wide variety of shapes and sizes has led to the almost exclusive use of this material in modern high frequency sonar applications.

	ferroelectric		piezoelectric		magnetostrictive	
	barium titanate	PZT-4	quartz	ADP	annealed nickel	ferrox-cube 7A
electro-mechanical coupling factor	0.38	0.52	0.1	0.3	0.25	0.2
polarization	pre-polarized		inherent polarization		require external polarization	
Curie point (^{o}C)	115	328	575	120	530	358
shapes available	unlimited		very restricted		limited	
mechanical strength	high		low		high	

Table 3.1 Comparison of transducer material properties[7-11].

PZT-4[9], a lead zirconate - lead titanate ceramic material manufactured by the Clevite Corporation was considered suitable for both the transmitting and receiving elements due to its high coupling coefficient and low dielectric loss.

3.3 Matching Techniques

Langevin[12] was the first to consider the possibility of using composite, or 'sandwich' structures, in order to change the characteristics of a piezoelectric element. Various forms of composite construction have been used since that time[13], but usually the aim has been to control the fundamental resonant frequency of the structure while retaining a comparatively high Q factor.

Cady[14] developed a rigorous theory to explain the performance of three section sandwich transducers of arbitrary dimensions. He predicted an increase of bandwidth of approximately three times by the insertion of a suitable quarter wave diaphragm between an ADP crystal and a seawater medium.

McSkimin[15] and others[16], concerned with the design of broadband ultrasonic delay lines, showed the considerable advantages of the use of matching sections between transducer and delay medium.

Kossof[17] showed that if, in addition to matching the element to the water load, its other active face is matched to an absorbent backing material, further increase in bandwidth is possible. In this case, however, efficiency clearly suffers.

References (14-17) describe the use of matching sections to improve the bandwidth of resonant piezoelectric elements.

In a sense, however, this is a contradiction in terms since perfect matching prohibits a true mechanical resonance. In a practical situation, matching will not be perfect even at the center frequency, but it is clear that the pressure amplification achieved by using a half-wavelength piezoelectric section will be small if matching is employed. This argument leads to the proposal of the use of a thin, non-resonant active section. The use of non-resonant matched transducers has not been reported in the literature, possibly because most of the research on matching techniques has been oriented towards high frequency (Megahertz) applications. In such applications the thickness of resonant piezoelectric discs is very small and for mechanical reasons it is undesirable to reduce it.

In the present application, the use of a thin active section is desirable since it greatly reduces the size and cost of the transducer elements.

Rings of PZT-4 2 mm ($\lambda/26$) in thickness and 15 mm ($\lambda/3.8$) O.D. were chosen. The specification of these elements is contained in appendix I.

3.4 Equivalent Circuit Development

In order to proceed with the detailed design of a matched transducer element, it is necessary to develop a mathematical model to describe the electrical and mechanical performance of a composite structure. The equivalent electrical circuit approach[18] seems most convenient for this analysis.

Consider the transducer element shown in Fig. 3.1, comprising an active element, a matching section, and a backing section which is unloaded.

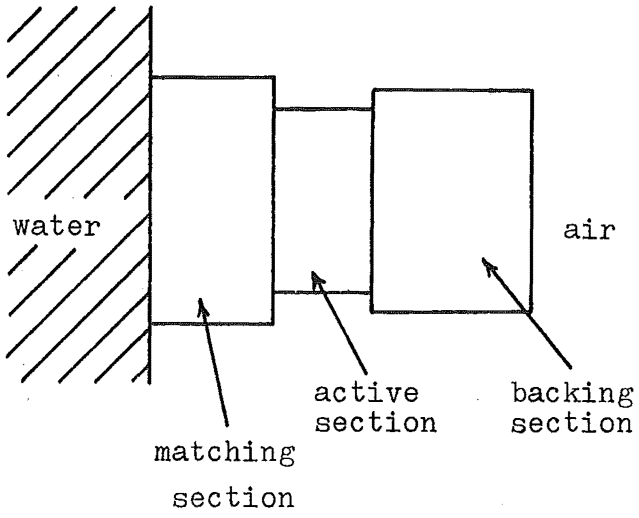

Figure 3.1. Transducer element comprising a matching section radiating into water, an active electrostrictive element, and an unloaded backing section.

The equivalent electrical circuit describing the performance of the active element may be obtained from the piezoelectric equations and the wave equation[19]. Its form is shown in Fig. 3.2. The values of C_o, v, and N depend on the material properties, and on the mechanical and electrical boundary conditions which apply in this particular situation. Since the lateral dimension of the element cannot be considered to be either acoustically very large or very small, the boundary conditions are intermediate between those of the thickness expander mode (laterally clamped) and the length expander mode (constant lateral stress). The difference between the equivalent circuits applicable at these two extreme conditions is quite small so that either may be used as a good approximation to the above case. The assumption made here is

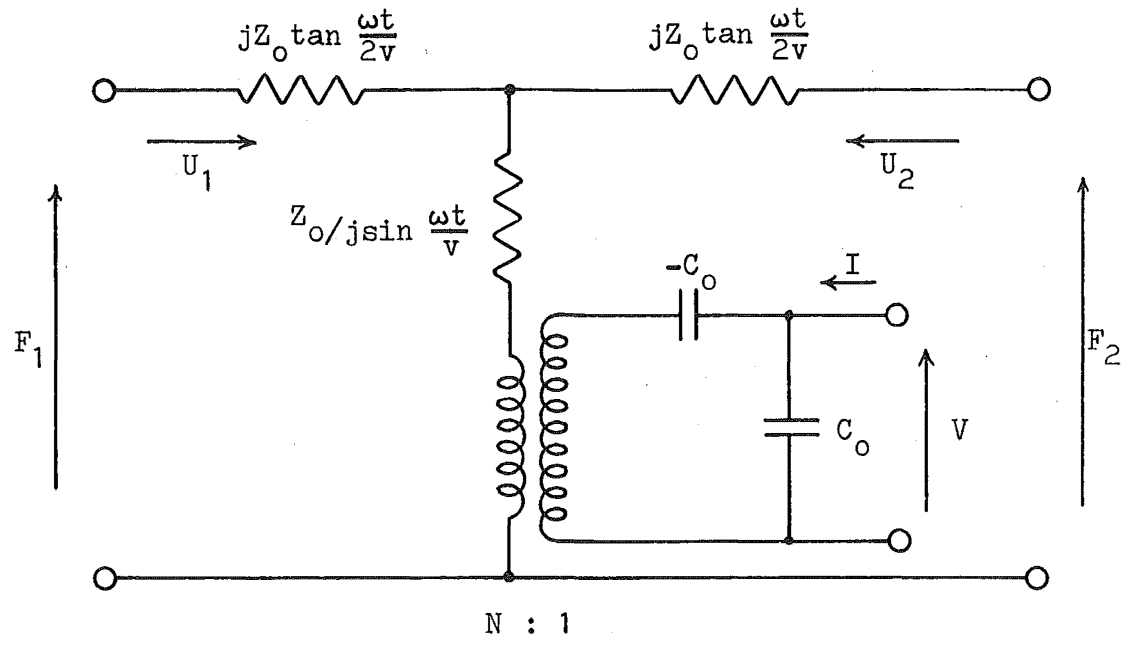

The nomenclature used in the above equivalent circuit is as follows:

F_1, F_2 : forces at faces 1 and 2, respectively

U_1, U_2 : velocities at faces 1 and 2

N : electrical/mechanical transformation ratio (force/voltage)

$Z_o = \rho v A$: mechanical impedance of the element (axial)

v : propagation velocity in the axial direction

C_o : clamped capacitance of the element

t : axial thickness of the element

V : applied driving voltage

I : input current

ω : operating frequency (radians/sec)

Figure 3.2. Equivalent circuit for the active element.

that thickness expander mode boundary conditions apply. This leads to the following expressions for the various circuit quantities:

$C_o = \frac{\pi d^2}{4t} \cdot \frac{1}{\beta_{33}^S}$ where d is the element diameter, β_{33}^S is the dielectric impermeability in the axial direction under laterally clamped conditions.

$v = v_t^D = \sqrt{\frac{c_{33}^D}{\rho}}$ where ρ = density, c_{33}^D is the elastic stiffness constant in the axial direction for constant charge density conditions.

$Z_o = \rho v_t^D A = \rho v_t^D \cdot \frac{\pi d^2}{4}$

$N = C_o h_{33} = \frac{\pi d^2}{4t} \cdot \sqrt{\frac{c_{33}^D}{\beta_{33}^S}} \cdot k_t$, where k_t is the effective coupling factor for the thickness mode, and h_{33} is the piezoelectric stress constant for the thickness mode.

By allowing k_t to tend to zero, we obtain the equivalent circuit for a piezoelectrically inactive section, such as the matching and backing sections (see Fig. 3.3).

The complete equivalent circuit for the three sectioned element with water load follows immediately from the preceding circuits, and is shown in Fig. 3.4.

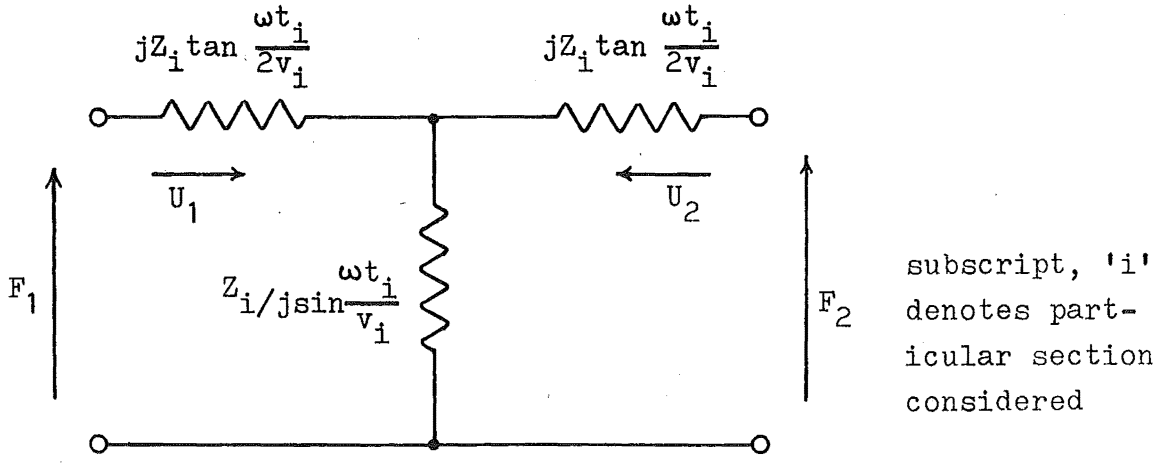

Figure 3.3. Equivalent circuit for a piezoelectrically inactive section.

In the development of the complete equivalent circuit, no account has been taken for losses in the individual sections or in the bonds between sections. Although mathematically it is quite straight forward to account for such loss, it is difficult to predict even the order of magnitude of the bonding losses. The assumption is made here that the losses will be small enough to allow a reasonably accurate prediction of the transducer performance. This assumption was found to be justified.

3.5 Theoretical Performance of the Matched Element

Having established the equivalent circuit of the complete structure (Fig. 3.4), the required materials and their dimensions may be determined, and the theoretical electroacoustic performance of the element predicted.

From the theory of lossless transmission lines, if the thickness of the matching section, t_m, is $\lambda/4$ at some

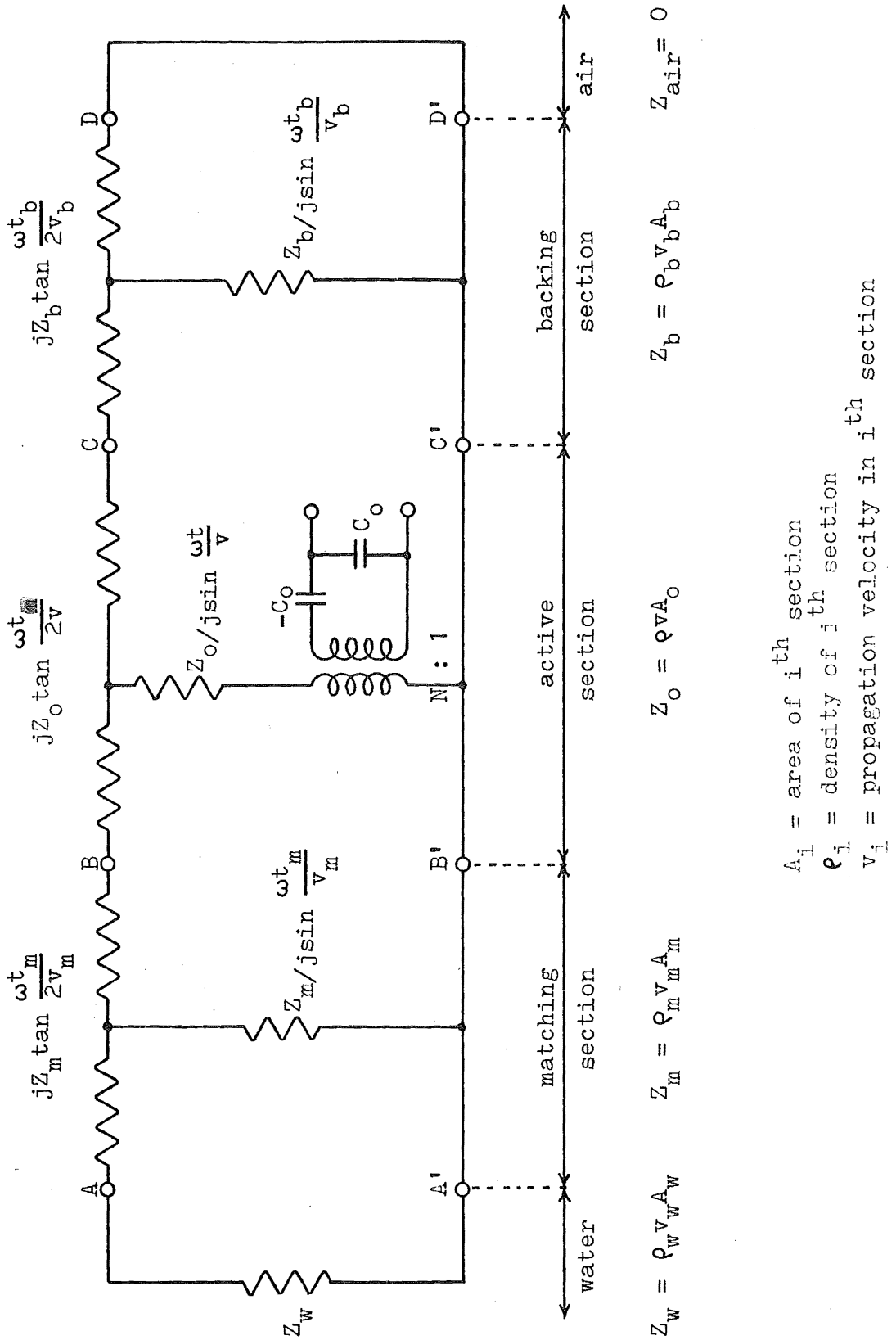

Figure 3.4. Equivalent circuit for the complete three-section structure with water load.

particular design frequency, f_o, the impedance, looking into the matching section from BB' at this frequency, is real and given by:

$$Z_{in_{BB'}} = \frac{Z_m^2}{Z_w}$$

For perfect mechanical matching at the face of the active element, we require that

$$Z_{in_{BB'}} = Z_o, \quad \text{at center frequency, } f_o.$$

To achieve this condition, we require that,

$$Z_m = \sqrt{Z_o Z_w}$$

or

$$\rho_m v_m A_m = \sqrt{\rho_o v A_o \cdot \rho_w v_w A_m}$$

From the relevant data contained in appendix I, this yields:

$$\rho_m v_m = 7.2 \sqrt{\frac{A_o}{A_m}} \cdot 10^6 \quad \text{MKS Rayls.} \qquad 3.2$$

Note: It is not necessary that A_o equal A_m although clearly A_m cannot be much larger than A_o if a longitudinal mode of vibration is to be maintained in the composite structure. It is convenient to be able to vary A_m (and hence Z_m) slightly to avoid the need to produce a matching material with a precise predetermined characteristic impedance.

A nominal diameter of 1.7 cm was chosen for the matching section giving,

$$A_m = 1.53\ A_o$$

thus from eqn 3.2,

$$\rho_m v_m = 5.82 \cdot 10^6 \text{ Rayls.} \qquad 3.3$$

The matching section thickness is chosen so that at the system center frequency, f_o, (60 kHz) it is equal to $\lambda/4$.

The primary purpose of the backing section is to present a comparatively high mechanical impedance to the rear face of the active element. This has the effect of reducing the vibrational amplitude at CC' (Fig. 3.4), making it a suitable point to support the element without unnecessary energy loss. The thickness of the backing element is chosen to be $\lambda/4$ at the center frequency, f_o, so that true clamped conditions exist at this frequency. The characteristic mechanical impedance of the backing material should ideally be much higher than that of the active element although this is not essential. Brass, of characteristic acoustic impedance $29.8 \cdot 10^6$ Rayls was chosen for convenience of fabrication.

A digital computer program was used to determine the theoretical performance of the matched element from the equivalent circuit. Fig. 3.5 shows the theoretical variation of the total acoustic power output as a function of frequency over the frequency band of interest. Also shown in this figure is the corresponding characteristic for the active section alone, radiating directly into water.

The characteristics of Fig. 3.5 show that although the matching section causes a substantial increase in transmitting sensitivity ($\approx$ 20 dB), the bandwidth over which it is effective is too narrow for the system requirements. The experimental results of section 3.5 confirm this.

The bandwidth over which matching is effective is primarily determined by the impedance transformation ratio, Z_w/Z_o. The larger this ratio, the narrower will be the effective bandwidth.

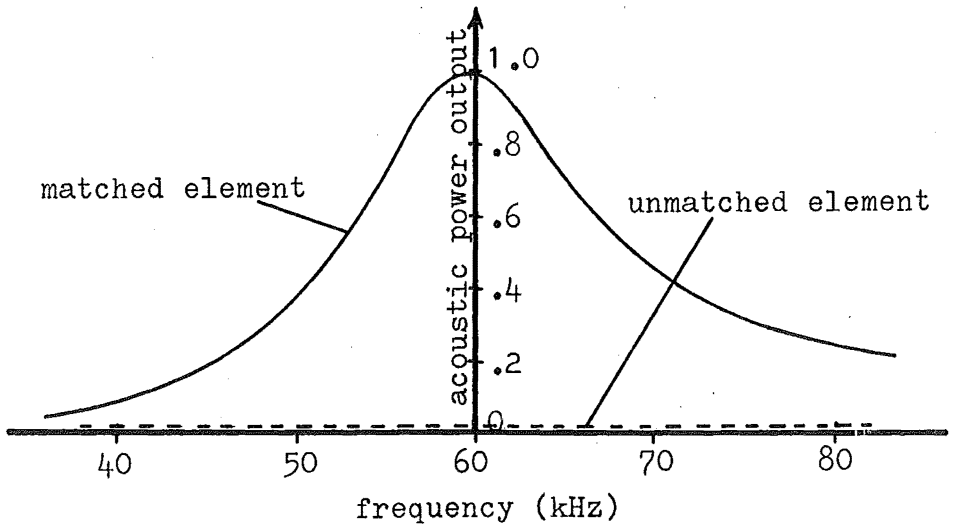

Figure 3.5. Theoretical performance of matched and unmatched transducers, for constant driving voltage.

If two matching sections are employed, the transformation ratio required for each section is the square root of the overall transformation ratio and a significant increase in bandwidth may be expected.

Theoretical results for the performance of an element comprising two quarter-wavelength matching sections are shown in Fig. 3.6. These results indicate that a suitable operational bandwidth may be achieved with this configuration. Experimental results confirmed this.

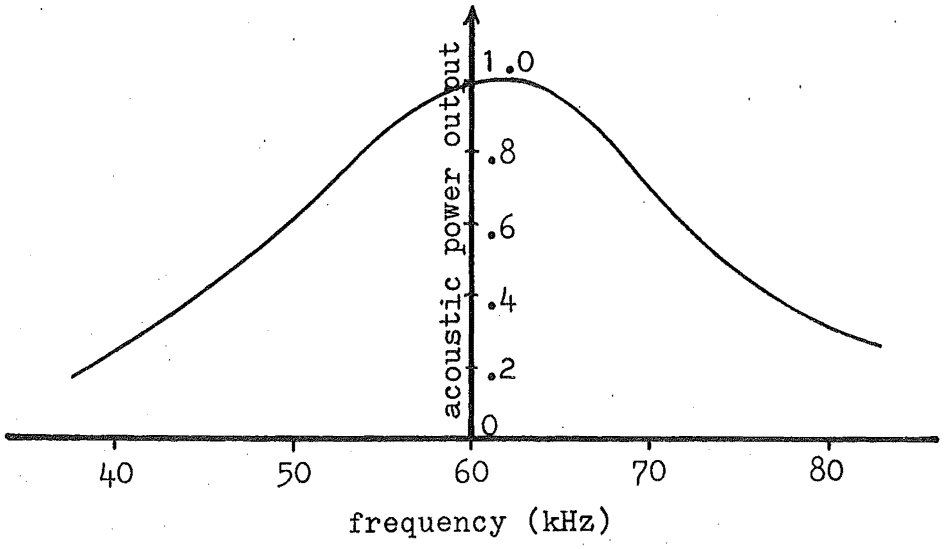

Figure 3.6. Theoretical performance of a transducer element with two matching sections (to same normalization as Fig. 3.5).

3.6 Measured Performance of Matched Elements

For an element with one matching section, a matching material of characteristic impedance approximately $5.8 \cdot 10^6$ Rayls is required (see eqn. 3.3). For the double-march element, materials having characteristic impedances of approximately $11.5 \cdot 10^6$ Rayls and $2.95 \cdot 10^6$ Rayls are required for the inner and outer matching sections respectively.

Since there are no suitable materials available with characteristic impedances near $5.8 \cdot 10^6$ or $2.95 \cdot 10^6$, it was necessary to develop such materials. Merkulova[20] has tabulated the acoustic properties of certain loaded epoxy resin compounds at ultrasonic frequencies. His work provided a guide for the development of the required materials. Araldite (Ciba Co. Pty Ltd) epoxy resin D (CY230) with

hardener HY951 was used as the base medium and powdered garnet (Barton Mines Corporation) of approximately 14μ" particle size was used as the filler. Characteristic impedances over the range 2.5 $.10^6$-10^7 Rayls could be obtained by varying the filler concentration. Velocities of propagation in these materials were measured by producing a standing wave in a cylindrical specimen and probing for velocity nulls.

Aluminium, which has a characteristic impedance of 13.9 $.10^6$ Rayls, was used for the innermost matching section of the double-match element. Although this impedance is rather higher than the desired value this may be compensated for in the garnet matching section and the performance is not significantly affected.

Brass was used for the backing sections and a brass shim was interposed between the active section and the backing element, to enable the element to be supported. The photographs on the title page of this chapter, and diagrams of Fig. 3.7 show the constructional details and the points at which electrical contact is made.

The elements were tested in a large concrete water tank, using a long-pulse technique to eliminate the effect of reflections from surface and walls. This technique is described in appendix III. The total acoustic power radiated from an element was determined from measurements of the far-field axial pressure and the directivity pattern at 5 kHz intervals over the frequency range from 35-85 kHz. The driving voltage was maintained constant.

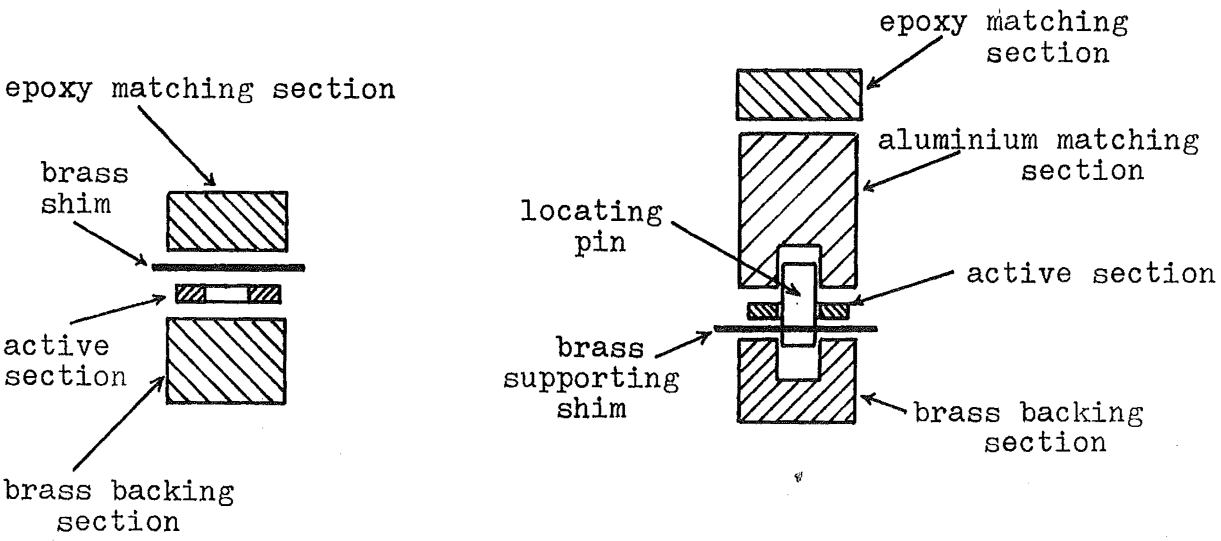

Figure 3.7 Constructional details of matched elements. (See appendix II for characteristics and dimensions of the individual sections.)

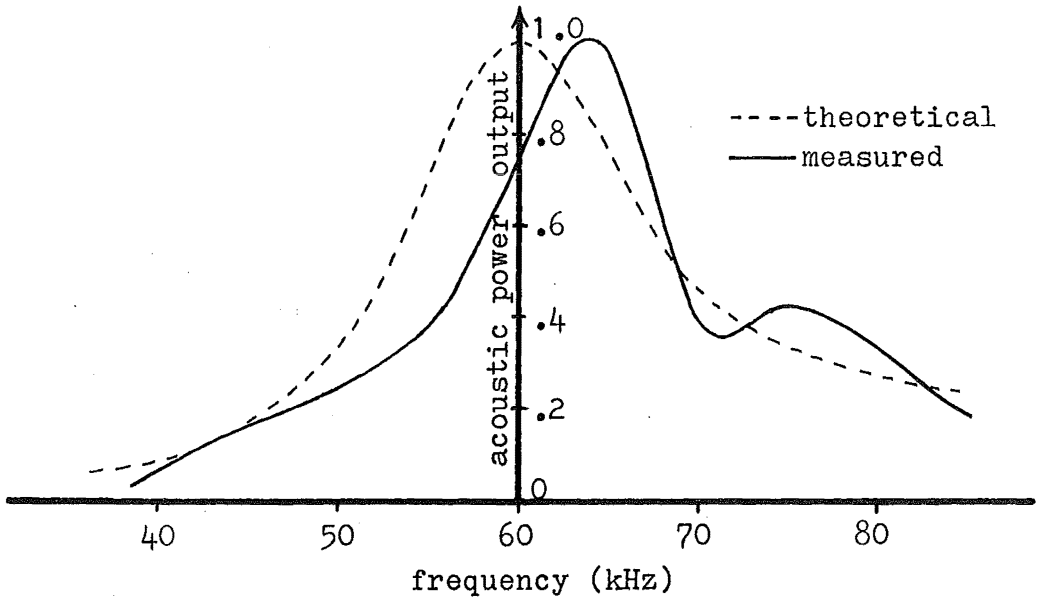

Figure 3.8. Experimental and theoretical characteristics for an element with one matching section.

3.6.1 Acoustic Power Output Characteristics

Fig. 3.8 shows a typical result for an element with one matching section. The theoretical curve is also shown.

The corresponding results for an element with two matching sections are shown in Fig. 3.9.

The agreement between experimental and theoretical results is excellent, considering no account was taken for losses in the equivalent circuit. It is clear that the element of Fig. 3.9 will yield a suitable bandwidth for the system requirements.

3.6.2 Efficiency Measurements

Measurements of input admittance of the element of Fig. 3.9 were made in both air and water media.

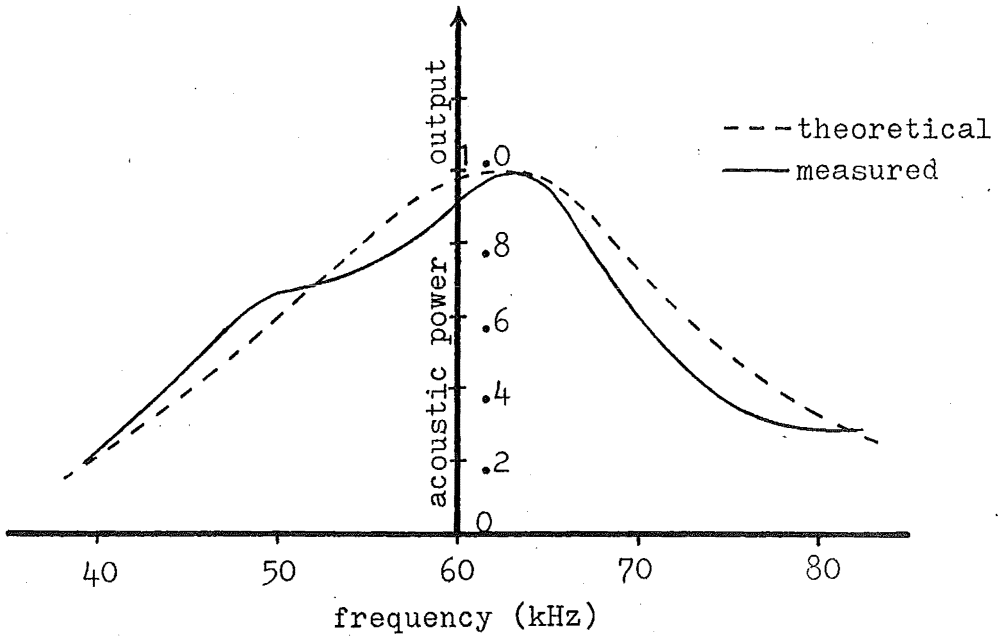

Figure 3.9. Experimental and theoretical characteristics for an element with two matching sections.

The values of total susceptance and total conductance obtained are shown in Fig. 3.10.

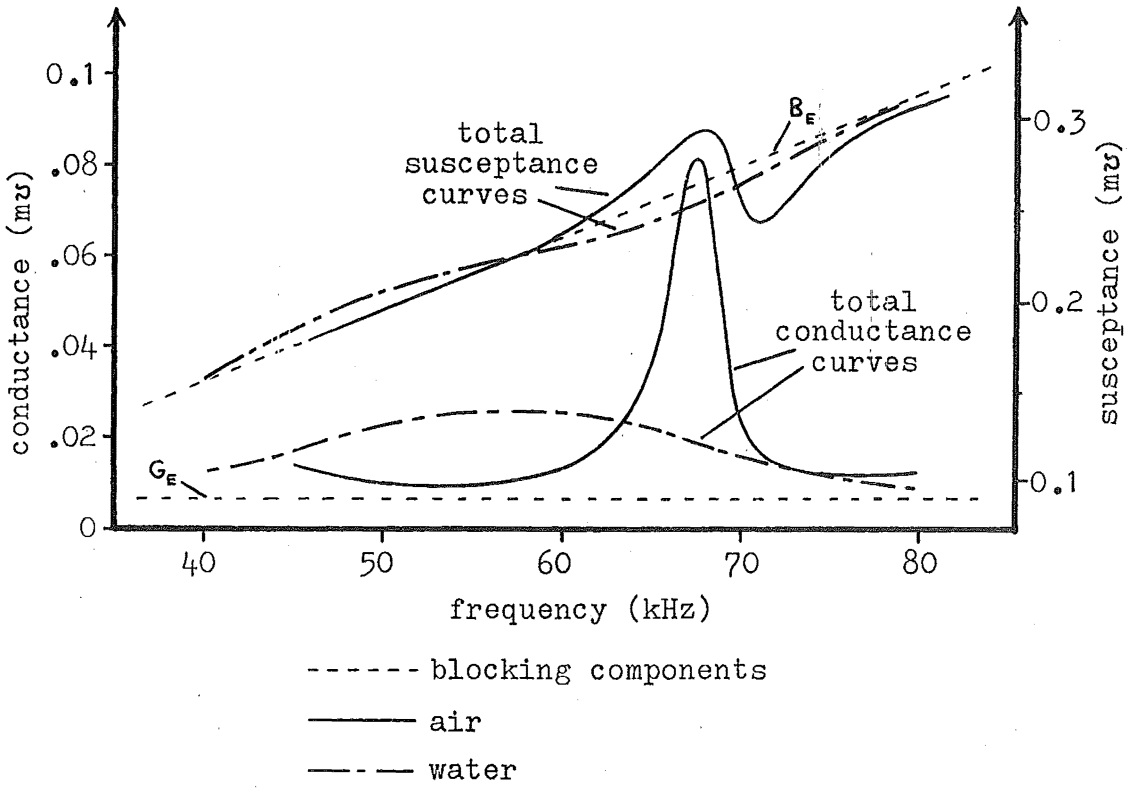

Figure 3.10. Results of admittance measurements in air and water.

From these values, the motional components of conductance and susceptance were obtained by subtraction of the blocking conductance, G_E and the blocking susceptance, B_E. These quantities are plotted in Fig. 3.11. The circle diagrams of Fig. 3.12 are obtained from the results of Fig. 3.11 by plotting these values in the admittance plane.

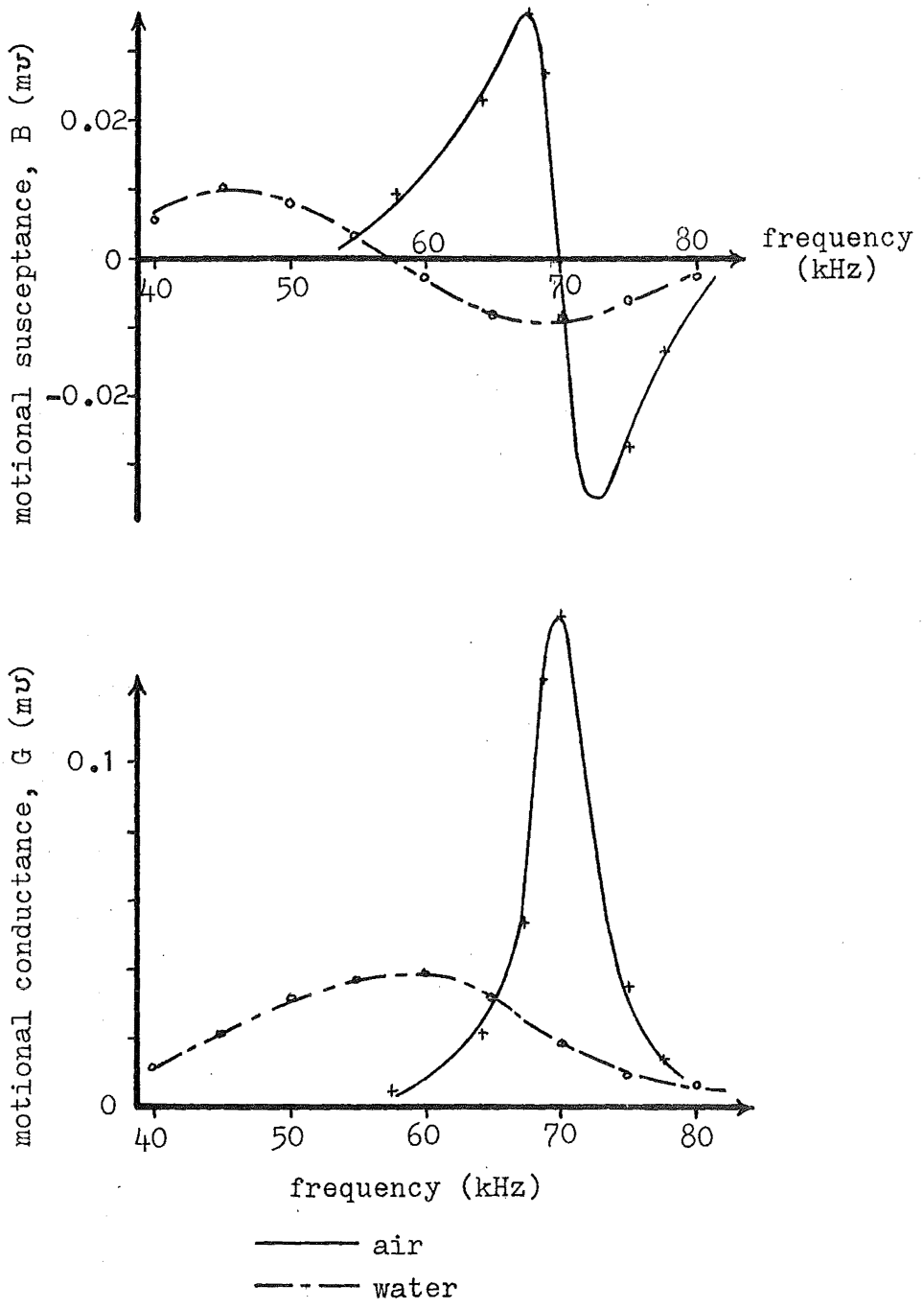

Figure 3.11. Motional admittance characteristics derived from Fig. 3.10.

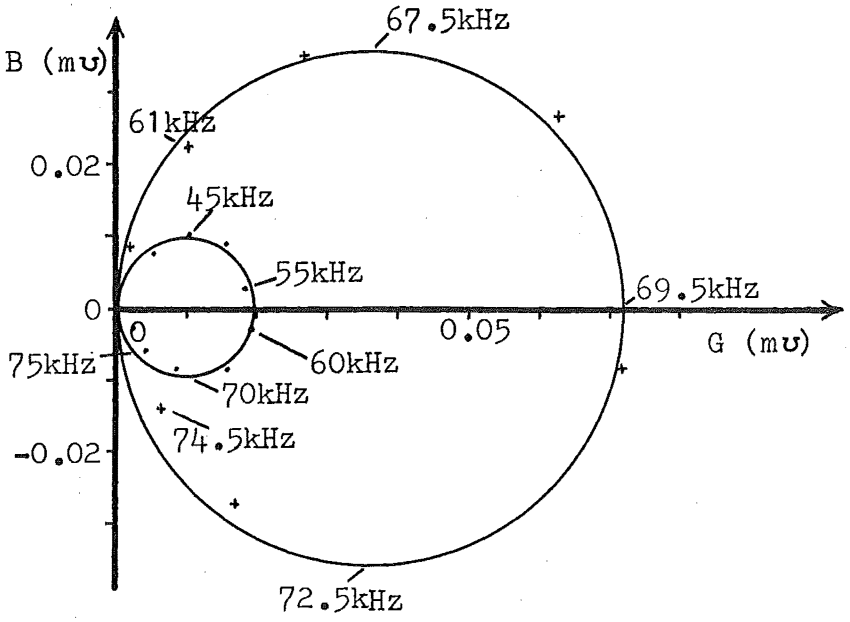

Figure 3.12. Motional admittance circles for water and air operation.

The efficiency of an electroacoustic transducer at the point of maximum sensitivity (i.e. where the motional susceptance passes through zero) may be determined[21] from the circle diameters and the blocking conductance, G_e. (See Fig. 3.10). The efficiency at other points within the operating band may be obtained by comparison of the acoustic power output characteristic (Fig. 3.9) and the total conductance characteristic for operation in water (Fig. 3.10). The resulting efficiency as a function of frequency is plotted in Fig. 3.13.

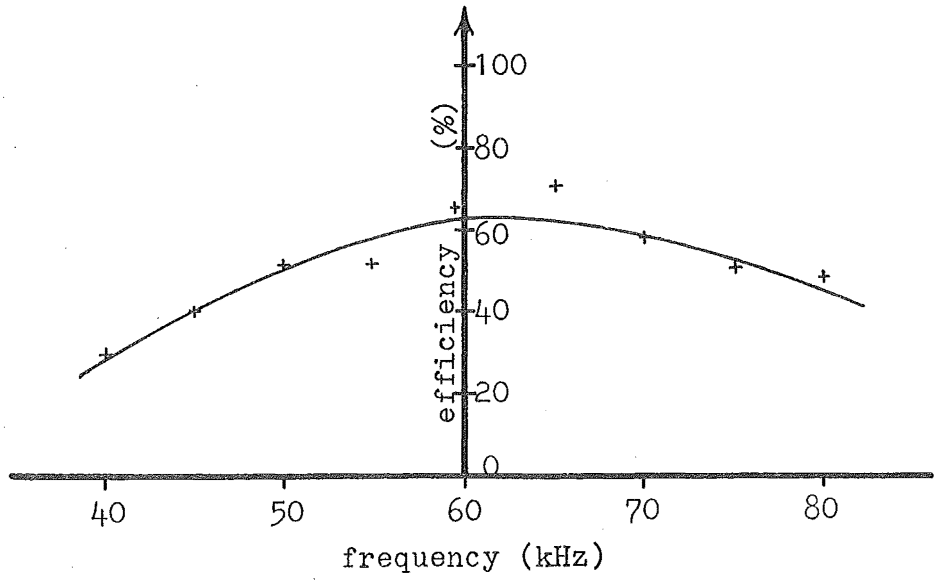

Figure 3.13. Variation of efficiency with frequency.

The average efficiency over the octave band from 40 kHz to 80 kHz, as determined from Fig. 3.13 is 51%. Due to the large number of measurements involved in the determination of this figure the associated accuracy will not be high. It is estimated that the average efficiency will lie in the range from 40% to 60%. This is a particularly high efficiency for such broad band transducers.

3.6.3 Sensitivity Characteristics

Using a reciprocity calibration technique[22], normal transmitting and receiving sensitivities were determined for the 'double-matched' element, and the results of these measurements are presented in Fig. 3.14.

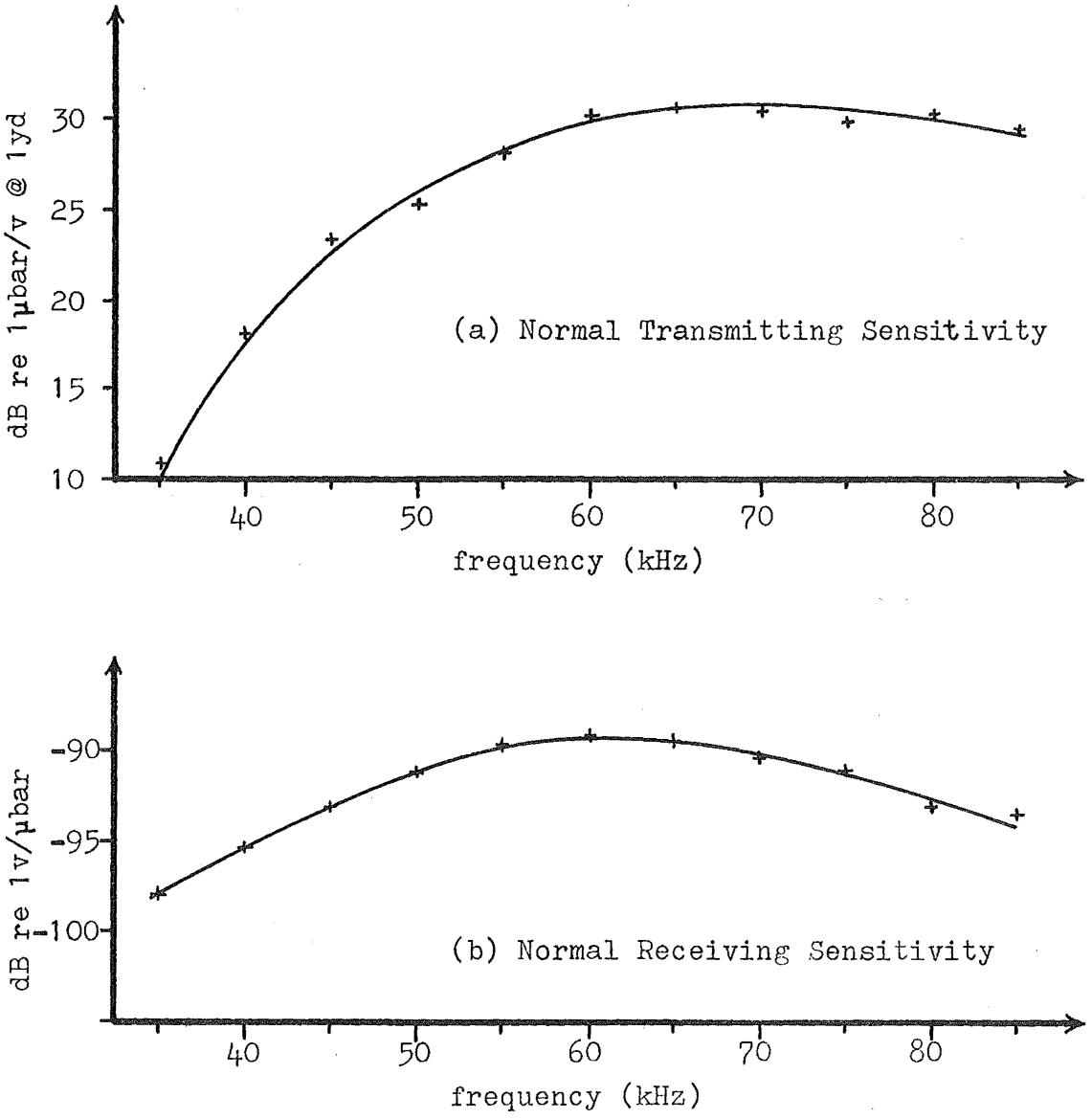

Figure 3.14. (a) Normal transmitting sensitivity, (b) normal receiving sensitivity, of the 'double-matched' element.

3.7 The Effects of Variation of Element Dimensions

A theoretical and experimental study of the effects of varying the thickness of each of the three passive sections of the double-match element was conducted. The purpose of this study was to determine whether an improvement in performance could be achieved by such variations and to assess the effect

of errors in thicknesses or velocities. Small variations in material properties or dimensions are unavoidable during the production of elements in large quantities, and it is essential that the element performance should not be seriously affected by such errors.

3.7.1 Variation of Thickness of the Epoxy Matching Section

A number of elements were constructed with the aluminium and brass sections of the required quarter wavelength thickness, but with the epoxy section thickness varying over the range 0.15λ to 0.35λ. Fig. 3.15 shows typical theoretical and experimental results obtained under these conditions.

It is seen from the characteristics of Fig. 3.15 that if the thickness of the epoxy matching section is either greater than or less than $\lambda/4$, the frequency of maximum sensitivity reduces. A slight increase in 3 dB bandwidth results if the epoxy thickness is slightly less than $\lambda/4$ but the response becomes more peaked. Neither 3 dB bandwidth, nor frequency of maximum response, change significantly for small variations in the epoxy thickness, suggesting that close tolerance on this dimension will be unnecessary.

The results obtained for variation of the thickness of the aluminium matching section show similar trends to those of Fig. 3.15 and will not be included here.

3.7.2 Variation of Backing Section Thickness

A set of elements was constructed with the two matching sections having the required quarter wavelength thickness, but with the backing section thickness varying over the range 0.17λ to 0.32λ. Fig. 3.16 shows typical theoretical and experimental results obtained under these conditions.

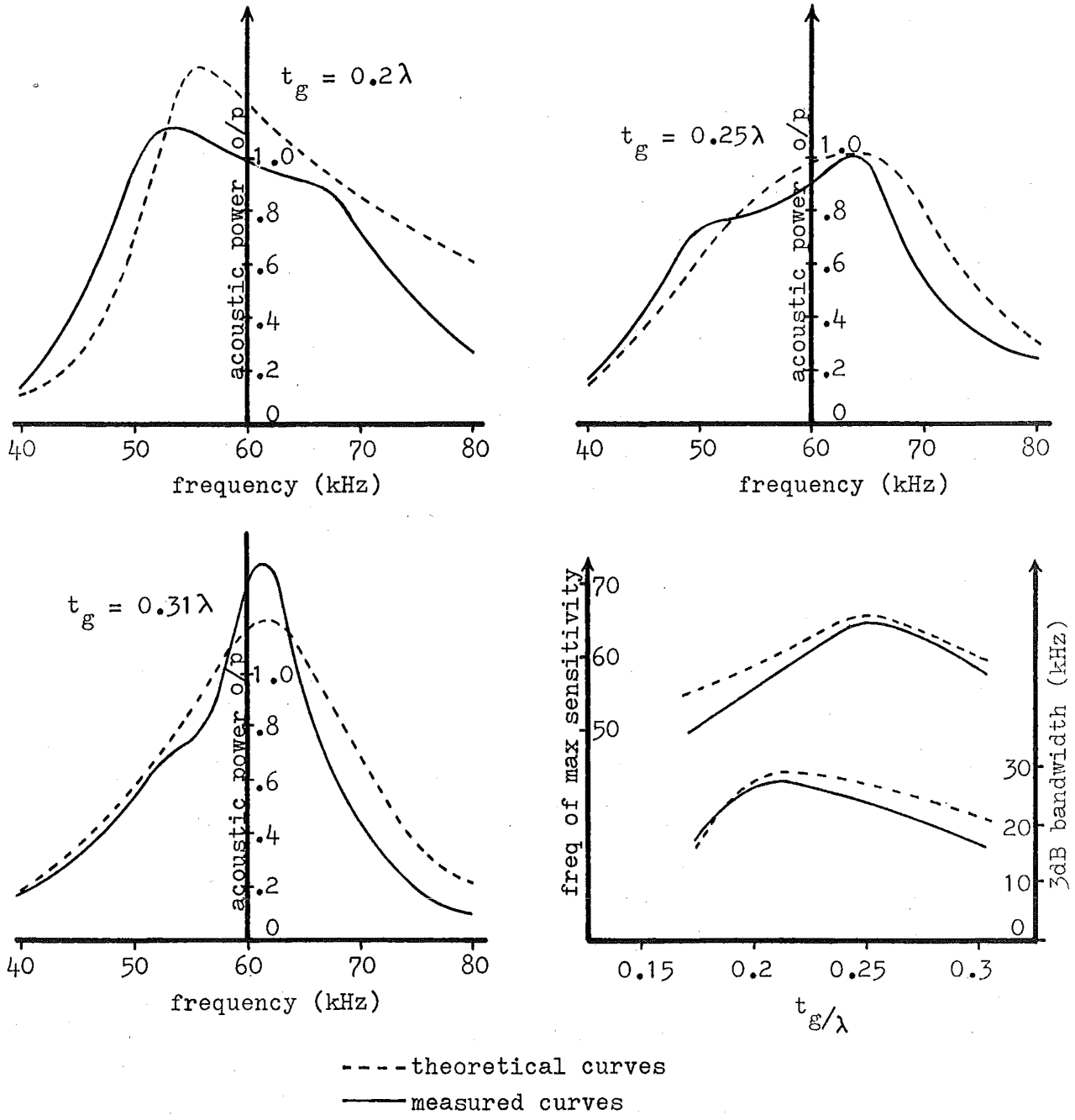

Figure 3.15. The effect of variation of thickness of the epoxy matching section, t_g.

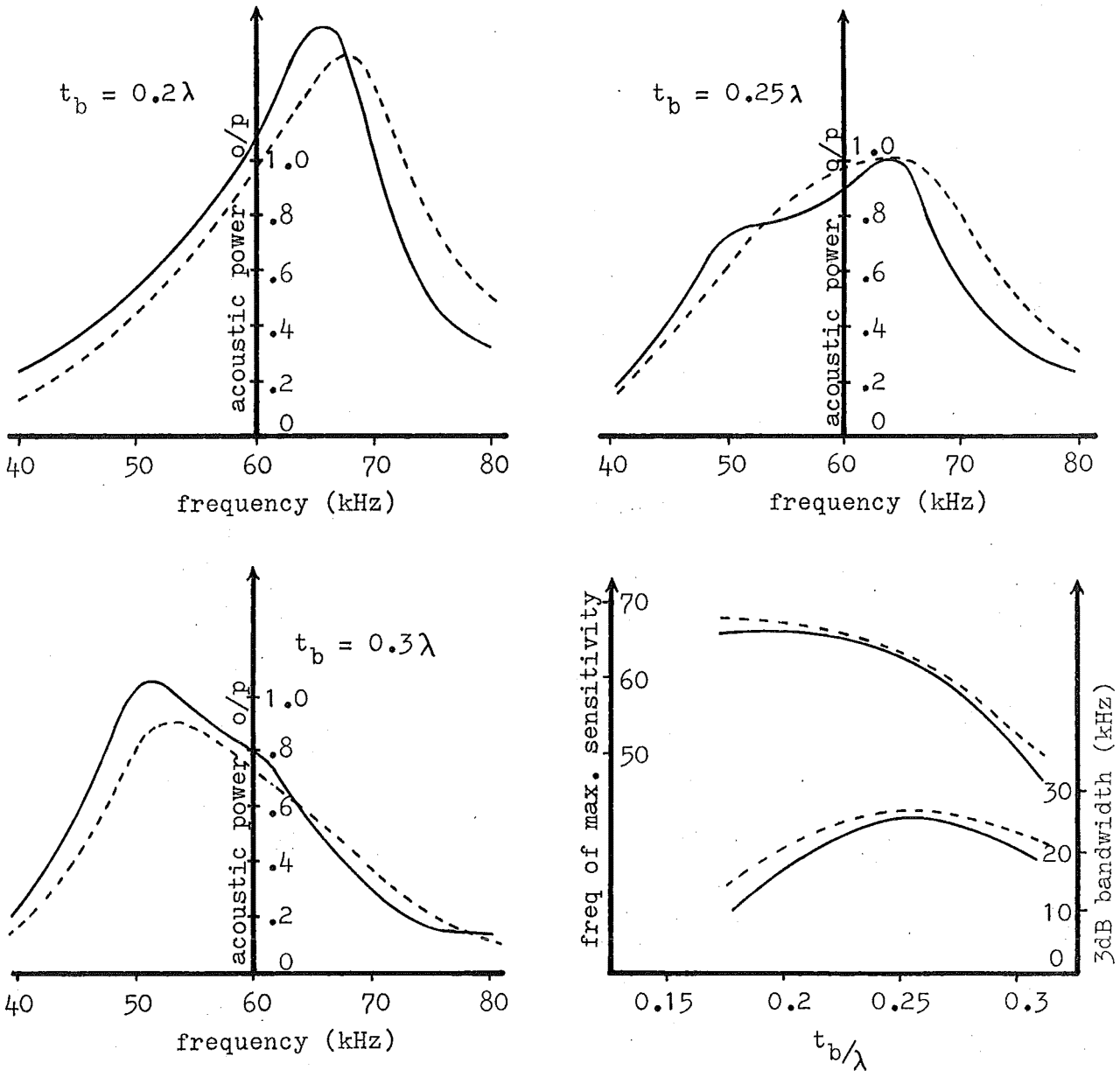

Figure 3.16. The effect of variation of thickness of the backing section, t.

These characteristics show that reduction of the thickness of the backing section causes an upward shift of the peak frequency, whereas increase in thickness lowers the peak frequency. The bandwidth reduces as the thickness deviates from $\lambda/4$ but the transmitting sensitivity increases. The output characteristics are comparatively insensitive to small variations of backing section thickness.

3.8 Conclusions

It has been shown that an efficient wideband transducer element may be constructed using a thin piezoelectric section and two quarter-wave matching sections. The use of a thin active section, rather than the conventional half-wavelength thickness greatly reduces the cost and size of the transducer element.

The performance of such an element is comparatively insensitive to small errors in the dimensions, making it suitable for production in large quantities.

Although approximations were made in the development of an equivalent circuit to predict the performance of the element, good agreement between theoretical and experimental results was achieved.

3.9 References

1. D. Schofield, "Transducers", Underwater Acoustics, ed. V.M. Albers, Plenum Press, New York (1963).
2. R.S. Woollet, "Trends and Problems in Sonar Transducer Design", IRE Int. Conv. Rec. 1962, p49.
3. G.W. McMahon, "Performance of Open Ferroelectric Ceramic Cylinders in Underwater Transducers", J. Acoust. Soc. Am., 36 : 528 (1964).

4. P.M. Kendig, "Broad Band Thermally Generated Noise of a Resonant Electroacoustic Transducer", J. Acoust. Soc. Am. 37 : 847 (1965).

5. R.H. Mellen, "The Thermal Noise Limit in the Detection of Underwater Acoustic Signals", J. Acoust. Soc. Am., 24 : 478 (1952).

6. V.O. Knudsen, R.S. Alford, and J.W. Emling, "Underwater Ambient Noise", J. Marine Res., 7 : 410 (1948).

7. R.W.B. Stephens and A.E. Bate, Acoustics and Vibrational Physics, Arnold, London, 1966.

8. D.G. Tucker and B.K. Gazey, Applied Underwater Acoustics, Pergamon Press, London, 1966.

9. H. Jaffe and D.A. Berlincourt, "Piezoelectric Transducer Materials", Proc. IEEE, 53 : 1372 (1965).

10. T.F. Hueter and R.H. Bolt, Sonics, Wiley, New York, 1955.

11. D. Berlincourt and H.H.A. Krueger, "Properties of Clevite Ceramics", Technical Paper, TP-226, Clevite Corporation.

12. P. Langevin, Brit. Pat. 145, 691 (1921).

13. W.J. Fry, J.M. Taylor and B.W. Henvis, Design of Crystal Vibrating Systems, Dover Publications, New York, 1948.

14. W.G. Cady, "A Theory of the Crystal Transducer for Plane Waves", J. Acoust. Soc. Am., 21 : 65 (1949).

15. H.J. McSkimin, "Transducer Design for Ultrasonic Delay Lines", J. Acoust. Soc. Am., 27 : 302 (1955).

16. W.F. Konig, L.B. Lambert, and D.L. Schilling, "The Bandwidth, Insertion Loss and Reflection Coefficient of Ultrasonic Delay Lines for Backing Materials and Finite Thickness Bonds", IRE Int. Conv. Rec. Vol. 9, Pt 6, 285 (1961).

17. G. Kossof, "The Effects of Backing and Matching on the Performance of Piezoelectric Ceramic Transducers", IEEE Trans. on Sonics and Ultrasonics, SU-13, No. 1 : 20 (1966).

18. W.P. Mason, Electromechanical Transducers and Wave Filters, 2nd Ed., Van Nostrand, New Jersey, 1948.

19. H.W. Katz, Solid State Magnetic and Dielectric Devices, Wiley, New York, 1959.

20. V.M. Merkulova, "Acoustical Properties of some Solid Heterogeneous Media at Ultrasonic Frequencies", Soviet Physics - Acoustics, 11 : 55 (1965).

21. D.G. Tucker and B.K. Gazey, Applied Underwater Acoustics, Ch. 5, Pergamon Press, London, 1966.

22. V.M. Albers, Underwater Acoustics Handbook, Pennsylvania State University Press, 1960.

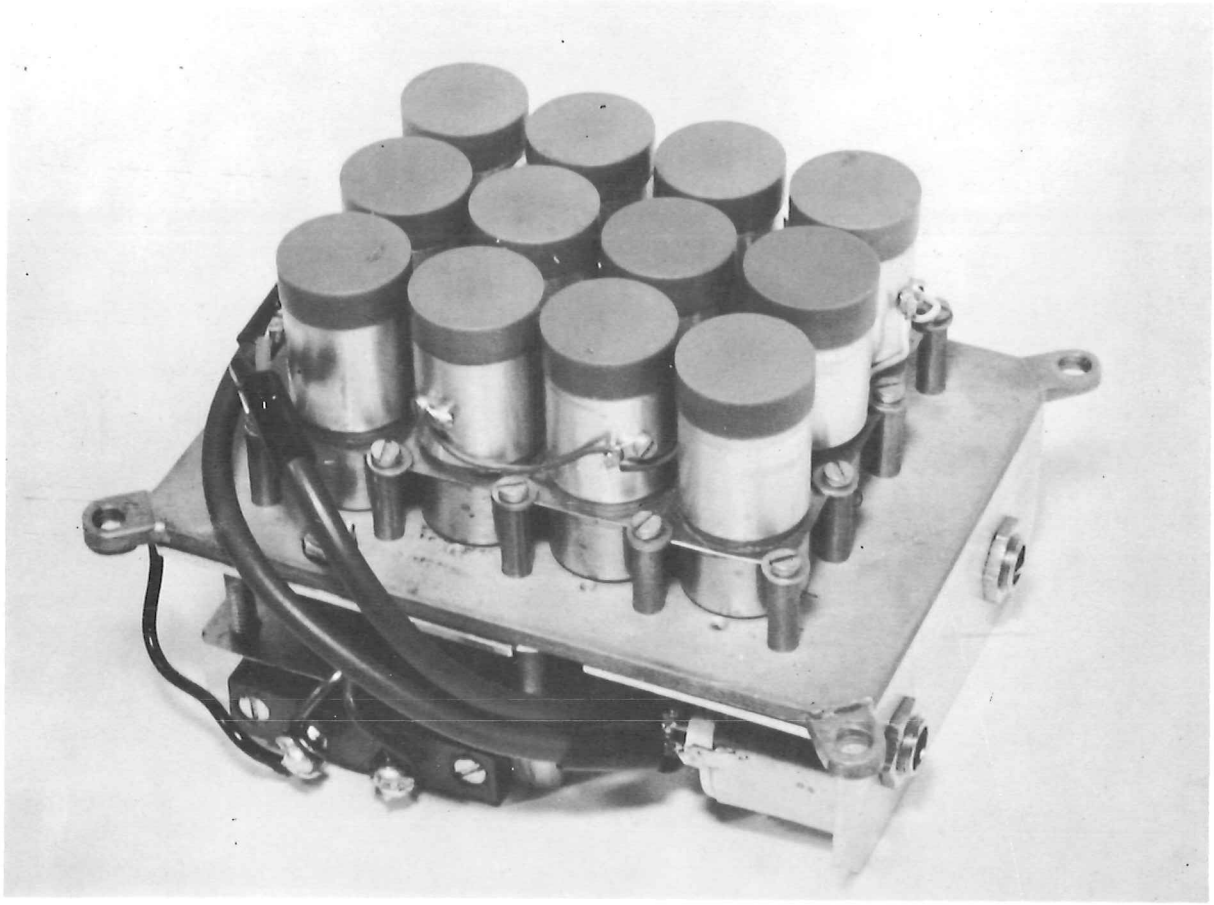

CHAPTER 4

DESIGN OF TRANSDUCER ARRAYS

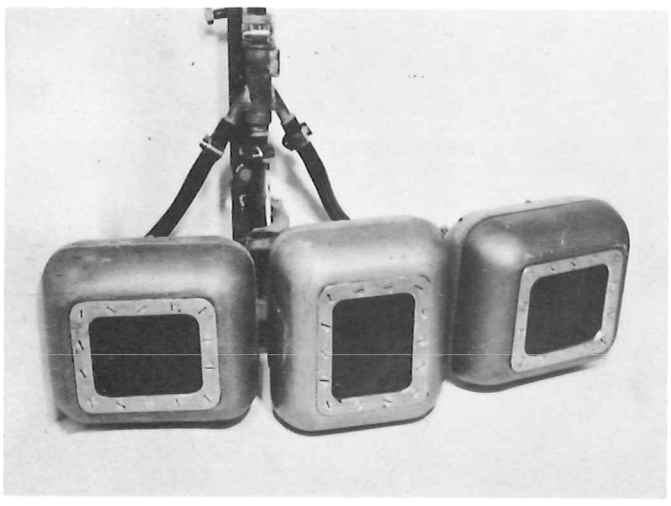

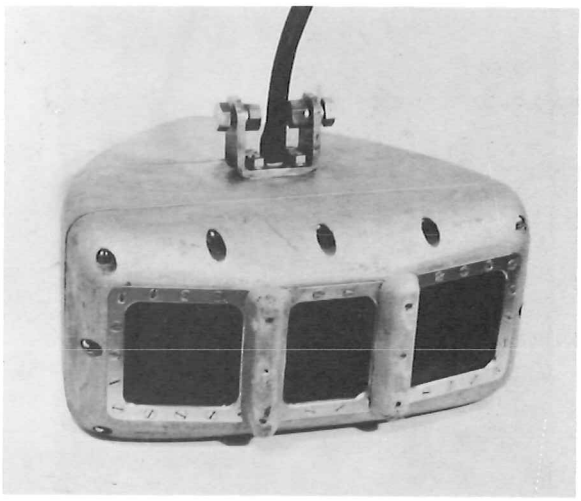

CHAPTER 4

DESIGN OF TRANSDUCER ARRAYS

4.1 Introduction

The design of a transducer array is generally based on two primary requirements, namely (i) the specified angular dimensions of the main lobe of the directivity pattern, and (ii) the allowable side lobe response levels. In narrow band sonar applications, the designer aims to meet these two requirements with a minimal number of array elements. In wide fractional bandwidth applications, it is often desirable to maintain the width of the main lobe constant over the operating band. This ensures that the basic sonar parameters, such as signal detectability and angular resolution, are not frequency dependent.

The array design for the present application is based on the above factors and one additional factor, namely the shape of main lobe patterns in the horizontal plane. It is shown in section 7.4 that variation of the shape or width of the main lobe of the receiver directivity patterns in the horizontal plane may seriously affect the binaural lateralization process. It is thus essential that the receiving arrays should have directivity patterns of constant width and shape. It is also essential that the main lobes of these patterns should be approximately cardiodal in shape. This ensures that the IAD characteristic (see section 7.1) varies smoothly in the center section of the beam.

Variations in shape or width of the transmitter directivity pattern in the horizontal plane do not affect the IAD characteristic. It is nevertheless desirable to maintain this width approximately constant to achieve high transmitting efficiency. If width variation is allowed, the transmitter beamwidth must be unnecessarily large causing poor utilization of the radiated energy.

In the vertical plane it is much more important to have low side lobe response levels than to have constant beamwidth. This is because of the close proximity of the sea surface, and in shallow waters, the sea bottom. Both these boundaries are excellent acoustic reflectors and it is essential that the reverberation level from these boundaries due to non-zero side lobe response should be small compared to the reverberation level due to the main lobe. Section 4.7 discusses the requirements of the directivity patterns in the vertical plane.

The effects of non-zero side lobe response in the horizontal plane are discussed in section 7.3.

Table 4.1 summarizes the broad specification of the directivity patterns.

Array	Plane	Beamwidth (6 dB level)
Transmitter	horiz.	60 deg. constant if possible
	vert.	25 deg. need not be constant
Receiver	horiz.	30 deg. constant width and constant cardiodal shape
	vert.	25 deg. need not be constant

Table 4.1. Directivity pattern specifications.

4.2 Review of Present Constant Beamwidth Array Techniques

Five techniques for maintaining the beamwidth of an array constant over wide frequency bands have appeared in the literature. These techniques will be briefly described here, in order that their suitability for the present application may be discussed.

The use of an array surface which is a section of a cylinder or sphere has been shown [1] to produce constant beamwidths over frequency bands several octaves in width under certain circumstances, namely, (i) that the radius of curvature is large compared to the wavelength, and (ii) that the number of elements comprising the radiating surface is large.

The beam shape resulting from this technique is quite unsuitable for the receiving arrays due to the high ripple content of the main lobe, but it would appear suitable for the transmitting array. The results of a theoretical and experimental study of such curved arrays is contained in section 4.5.

Tucker[2] has described a constant beamwidth technique based on the synthesis of a desired beam pattern from a large number of deflected sin x/x patterns, derived from a single linear array. Although very wide bandwidths may be achieved using this technique[3], the beamshape varies considerably over quite small frequency bands and is flat topped making it unsuitable for the receiving arrays. The difficulty and cost of constructing the time delay sections (required for beam deflection) for high level signals renders the technique unsuitable for the transmitting array.

Morris[1] developed a twisted surface array, based on the method of Tucker[2], but which uses a series of physically deflected linear arrays in place of the artificially deflected ones. Although the technique may be used equally well for either transmitting or receiving arrays and can maintain constant beamwidth in both vertical and horizontal planes, the cost and complexity of construction make it an unrealistic solution to the present problem.

The use of non-linear acoustic interaction[4] between two high frequency acoustic signals to produce the desired sonar transmission signal yields a constant beamwidth[5] provided the generating frequencies are much higher than the system center frequency. A form of parametric amplification produces similar results in the reception mode. While this technique offers some interesting possibilities for wide band sonar systems, it is still in the research stage and practical systems employing this technique have not been evaluated. It was thus considered unwise to attempt to use the technique in the present application.

Another method[12], which is becoming widely used in modern high resolution sonars uses digital processing of the signals received from the elements of plane or cylindrical arrays to achieve the desired beam pattern. The complexity and expense involved in this technique is prohibitive for the present application.

None of the above mentioned techniques offers a realistic solution to the problem of receiving array design. It was thus necessary to develop an inexpensive technique to achieve constant beamwidth and an acceptable beam shape.

4.3 Development of a Constant Beamwidth Receiving Array

It is well known (see for example Karbo[6]) that any attempt to reduce side lobe levels of a linear array by sensitivity shading of the constituent elements results also in an increase in main lobe width. Sensitivity shading, then, provides a means of varying array beamwidth. The 3 dB beamwidth, B, of a uniform linear array of length, ℓ, is given by:

$$B = 2 \arcsin \left(\frac{1.39c}{\ell \pi f}\right) \qquad 4.1$$

Thus for beamwidths less than about 45 deg., there is an approximately inverse variation of beamwidth with frequency.

It was argued that the narrowing of beamwidth with increasing frequency could be compensated for by frequency dependent sensitivity shading.

Consider the generalized linear array of Fig. 4.1, having overall length ℓ, and sensitivity variation p(x), along its length.

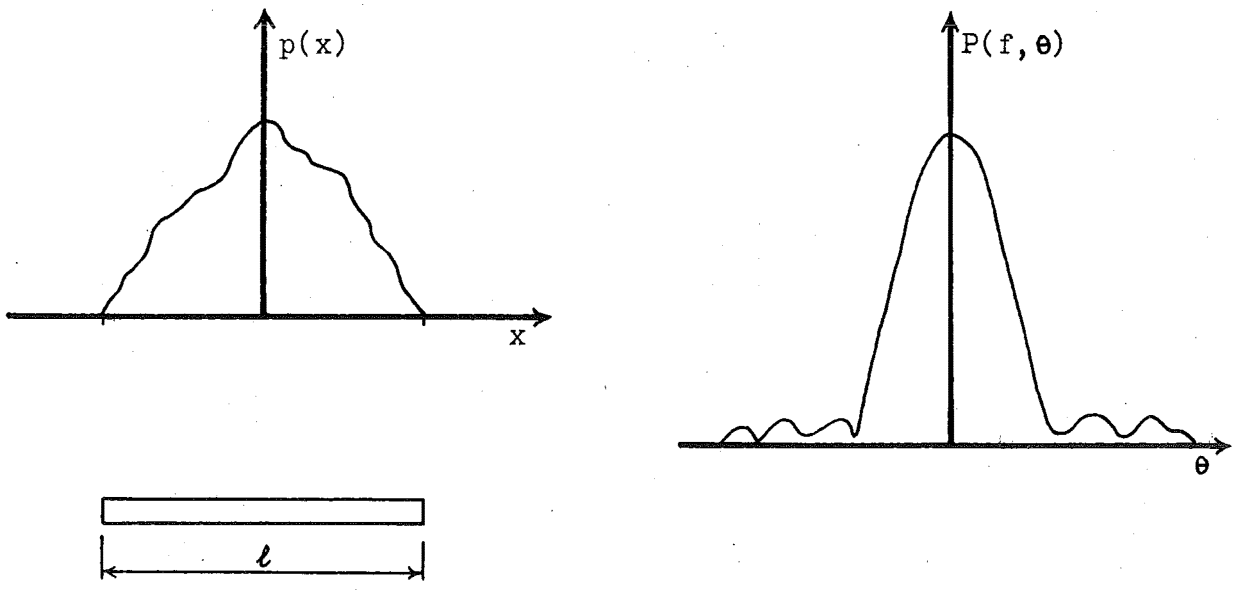

Figure 4.1. Generalized linear array and its directivity pattern.

The variation of array sensitivity, P, with frequency, f, and polar angle, θ, is given by the Fourier transform relationship,

$$P(f,\theta) = \int_{-\infty}^{\infty} p(x)\ \exp(-j2\pi\ \frac{xf}{c}\ \sin\ \theta)\ dx$$

If p(x) is also a function of frequency, on substituting the limits for x, we obtain

$$P(f,\theta) = \int_{-\ell/2}^{\ell/2} p(x,f)\ \exp(-2\pi\ \frac{xf}{c}\ \sin\ \theta)\ dx \qquad 4.2$$

To achieve constant beamwidth and beamshape, we require that the right hand side of Eqn 4.2 be independent of f in the range $f_1 \leqslant f \leqslant 2f_1$, where f_1 is the lower limit of the octave band. While there are, no doubt, many functions p(x,f) which will yield this condition, few if any will be realizable in hardware. We thus postulate a realizable array and attempt to find function p(x,f) which will closely approximate the desired beam properties.

The array of Fig. 4.2, comprising four rectangular sections of similar dimensions, the inner two sections of constant sensitivity, p_o, and the outer two sensitivity, $p_1(f)$, was proposed. This array can clearly satisfy the beamwidth and beam shape requirements at the two extremes, f_1 and $2f_1$ of the octave band if we make $p_1(f) = p_o$ at $f = f_1$ and $p_1(f) = 0$ at $f = 2f_1$ since the array would be acoustically the same at these two frequencies. We now determine whether the function $p_1(f)$ exists and is realisable over the range, $f_1 \leqslant f \leqslant 2f_1$.

For the array of Fig. 4.2, from Eqn 4.2, we have

$$P(f,\theta) = \int_{-\ell/2}^{\ell/2} p_1(f)\exp(-2\pi\ \frac{xf}{c}\ \sin\ \theta)dx$$

$$+ \int_{-\ell/4}^{\ell/4} (p_o - p_1(f))\ \exp(-2\pi\ \frac{xf}{c}\ \sin\ \theta)dx$$

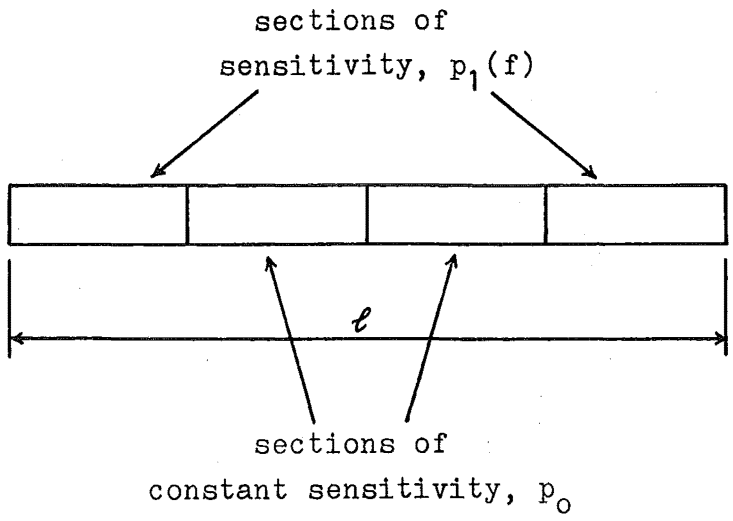

Figure 4.2. Proposed constant beamwidth array

Thus

$$P(f,\theta) = p_1(f) \frac{\ell \sin(\frac{\pi \ell f}{c} \sin\theta)}{\frac{\pi \ell f}{c} \sin\theta} + (p_o - p_1(f)) \frac{\frac{\ell}{2} \sin(\frac{\ell \pi f}{2c} \sin\theta)}{\frac{\ell \pi f}{2c} \sin\theta} \quad 4.3$$

On the normal axis to the array,

$$P(f,0) = (p_1(f) + p_o) \frac{\ell}{2} \quad 4.4$$

At the 3 dB beam angle, θ', by definition,

$$P(f,\theta') = P(f,0)/\sqrt{2} \quad 4.5$$

Substitution of Eqns 4.3 and 4.4 into 4.5 yields

$$p_1(f) \frac{\ell \sin(\frac{\ell \pi f}{c} \sin\theta')}{\frac{\ell \pi f}{c} \sin\theta'} + (p_o - p_1(f)) \frac{\frac{\ell}{2} \sin(\frac{\ell \pi f}{2c} \sin\theta')}{\frac{\ell \pi f}{c} \sin\theta'}$$

$$= (p_1(f) + p_o) \frac{\ell}{2\sqrt{2}} \quad 4.6$$

Now, from Eqn 4.1, at frequency f_1, since the array is uniform,

$$\theta' = \theta_{f_1}' = \arcsin\left(\frac{1.39c}{\ell\pi f_1}\right) \qquad 4.7$$

and if constant 3 dB beamwidth is to be maintained, θ' must have this value for all f in the range $f_1 < f < 2f_1$. Thus substituting this expression for θ' in Eqn 4.6 we obtain the required sensitivity function, $p_1(f)$ necessary to maintain constant beamwidth.

$$p_1(f) = \frac{H - 1}{H + 1 - 2H\cos(0.695f/f_1)} \cdot p_o \qquad 4.8$$

where

$$H = \frac{\sqrt{2}\ \sin\ (0.695(f/f_1))}{0.695f/f_1}$$

Equation 4.8 holds strictly, only for the case of an array of four rectangular sections. For ease of element manufacture, it is desirable to have circular, rather than rectangular active faces. For the case of an array of four circular elements, a similar analysis to the above yields the corresponding sensitivity function, $p_2(f)$, given by

$$p_2(f) = \frac{H' - 1}{H' + 1 - 2H'\cos(0.7(f/f_1))} \cdot p_o \qquad 4.9$$

where

$$H' = \frac{2\sqrt{2}\ J_1(0.35(f/f_1))}{0.35(f/f_1)} \cdot \cos(0.35(f/f_1))$$

It is shown in a paper by the present author[7] (reproduced as appendix IV) that sensitivity functions $p_1(f)$ and $p_2(f)$ are almost identical in the range $f_1 \leqslant f \leqslant 2f_1$ so that $p_1(f)$ may be used in both situations. Figure 4.3 shows the variation of $\frac{p_1(f)}{p_0}$ with frequency in the range of interest.

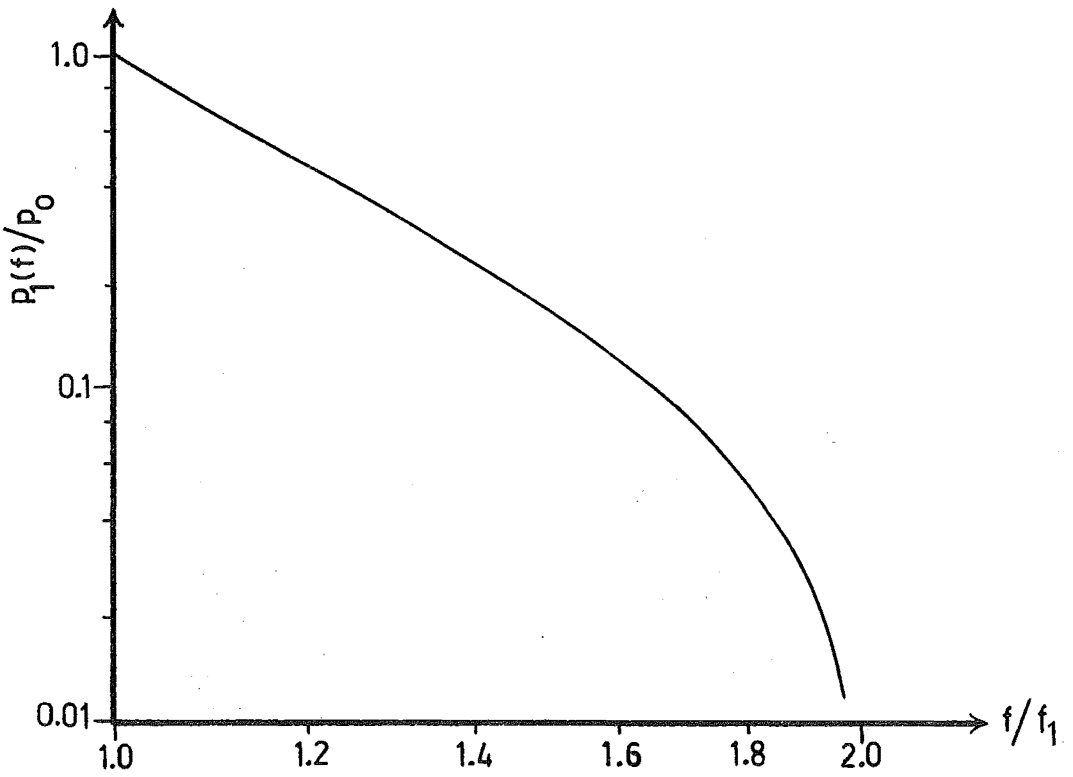

Figure 4.3. Sensitivity function $\frac{p_1(f)}{p_0}$ (Eqn 4.8).

The theoretical directivity patterns for an array of four circular elements with 19 mm between centers, and with the sensitivity of the outer elements reduced according to the curve of Fig. 4.3 are shown in Fig. 4.4.

The patterns of Fig. 4.4 show that, in addition to maintaining a constant 3 dB beamwidth, this technique yields a main lobe shape which is constant to within 1 dB down to the -10 dB level of sensitivity. Also, since the main lobe has an approximately sin(x)/x shape, it meets the requirements of the binaural lateralization process. This technique, then appears to offer an excellent solution to the problem of receiving array design. Appendix IV contains theoretical results for other array configurations.

The length of the array of Fig. 4.4 was chosen in order to meet the system beamwidth requirements. The diameter of the active face of each array element was thus chosen to be 1.7 cm.

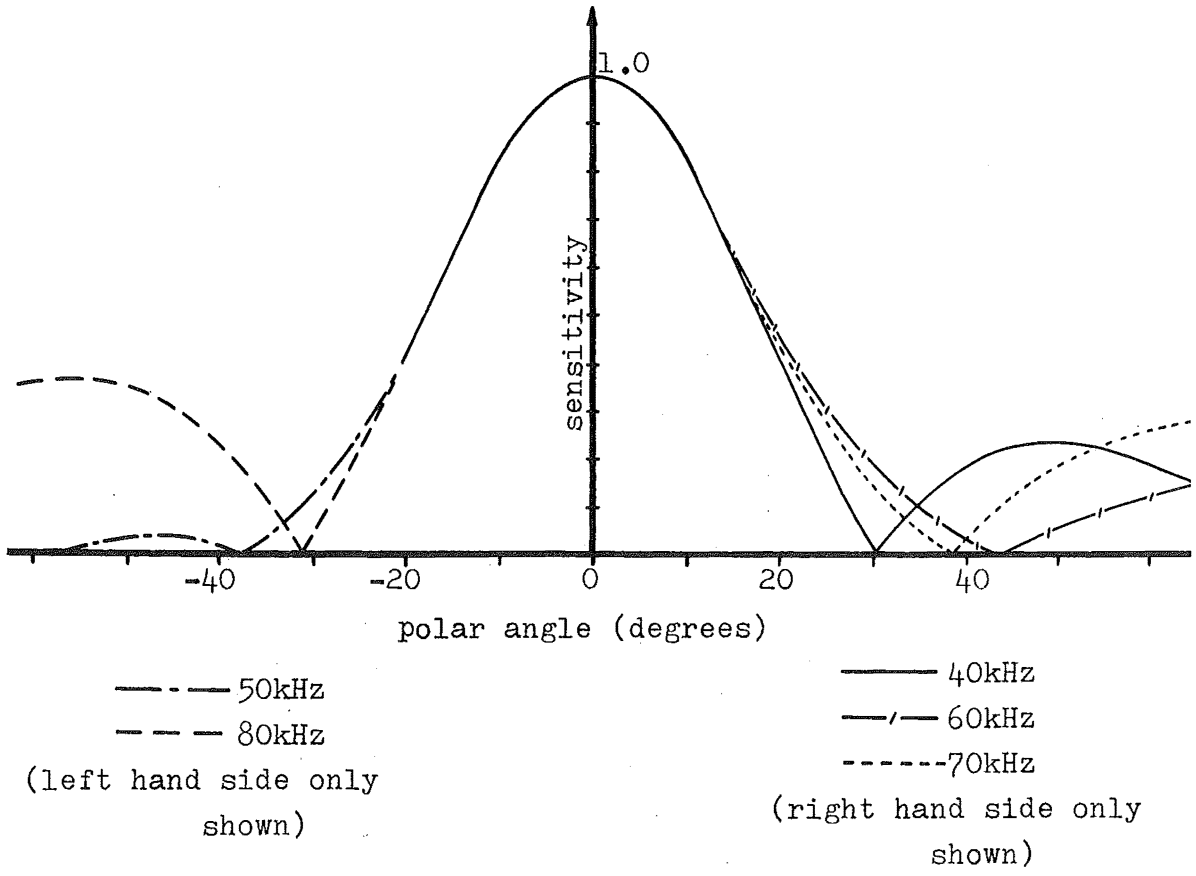

Figure 4.4. Theoretical directivity for an array of four circular piston radiators at 19 mm centers.

4.4 Measured Performance of the Constant Beamwidth Array

The simple passive network of Fig. 4.5, having the transfer function,

$$G(s) = \frac{1 + s^2LC_1}{1 + s^2L(C + C_1)}$$

can provide a close approximation to the sensitivity function, $p_1(f)/p_0$ over the band $f_1 \leqslant f \leqslant 2f_1$ if the pole is positioned at approximately 0.73 f_1 and the zero positioned at approximately 2.2 f_1. The phase and amplitude characteristics measured for this network are shown in Fig. 4.6 along with the ideal characteristics as prescribed by the curve of Fig. 4.3.

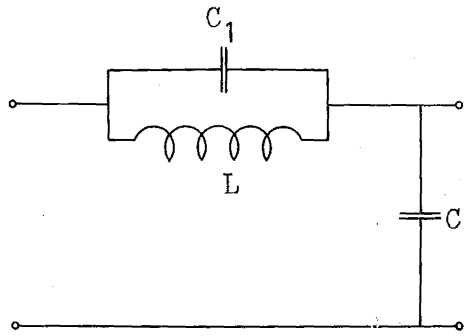

Figure 4.5. Network to control outer element sensitivity.

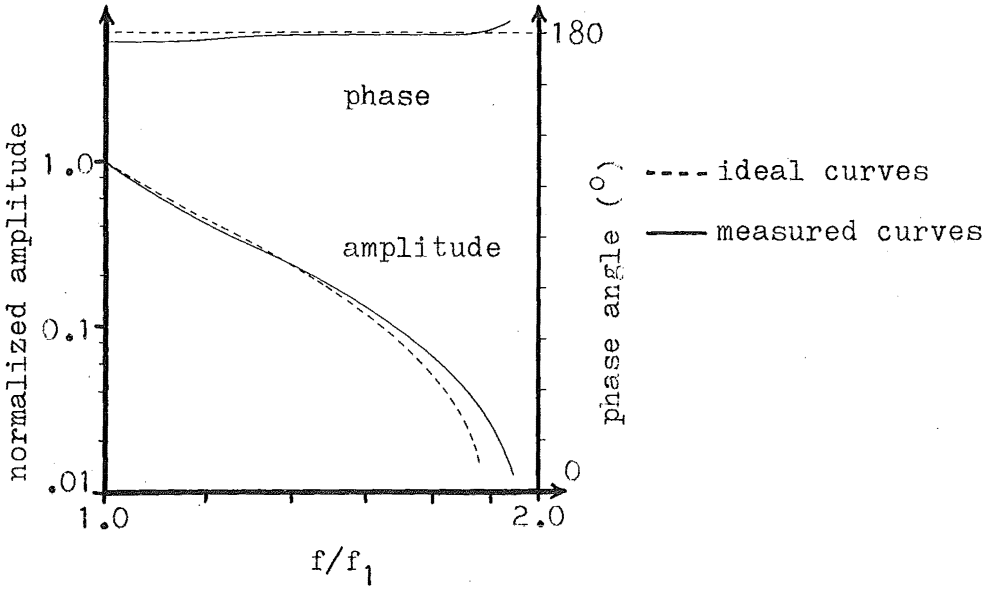

Figure 4.6. Phase and amplitude response of the network of Fig. 4.5.

Over the frequency band from 40 kHz to 80 kHz the network amplitude response departs from the ideal response by at most 0.24 dB, and the phase shift remains within 3.2 deg. of 180 deg.

An array of four circular elements, each of 17 mm diameter, was constructed. The network of Fig. 4.5 was used to control the sensitivity of the outer elements with respect to the inner elements. Directivity patterns were measured using the technique described in appendix III. These patterns are shown in Fig. 4.7. Fig. 4.8 shows the measured variation of 3 dB and 6 dB beamwidth for the constant beamwidth array and for the four element array with uniform sensitivity.

Measured 3 dB beamwidth variation, over the frequency range 40-80 kHz, for the constant beamwidth array is ±1.8%, as compared with ±24% measured for the uniform array. The corresponding figures for measured 6 dB beamwidth variation are ±2% and ±19% for the constant beamwidth array and uniform array, respectively.

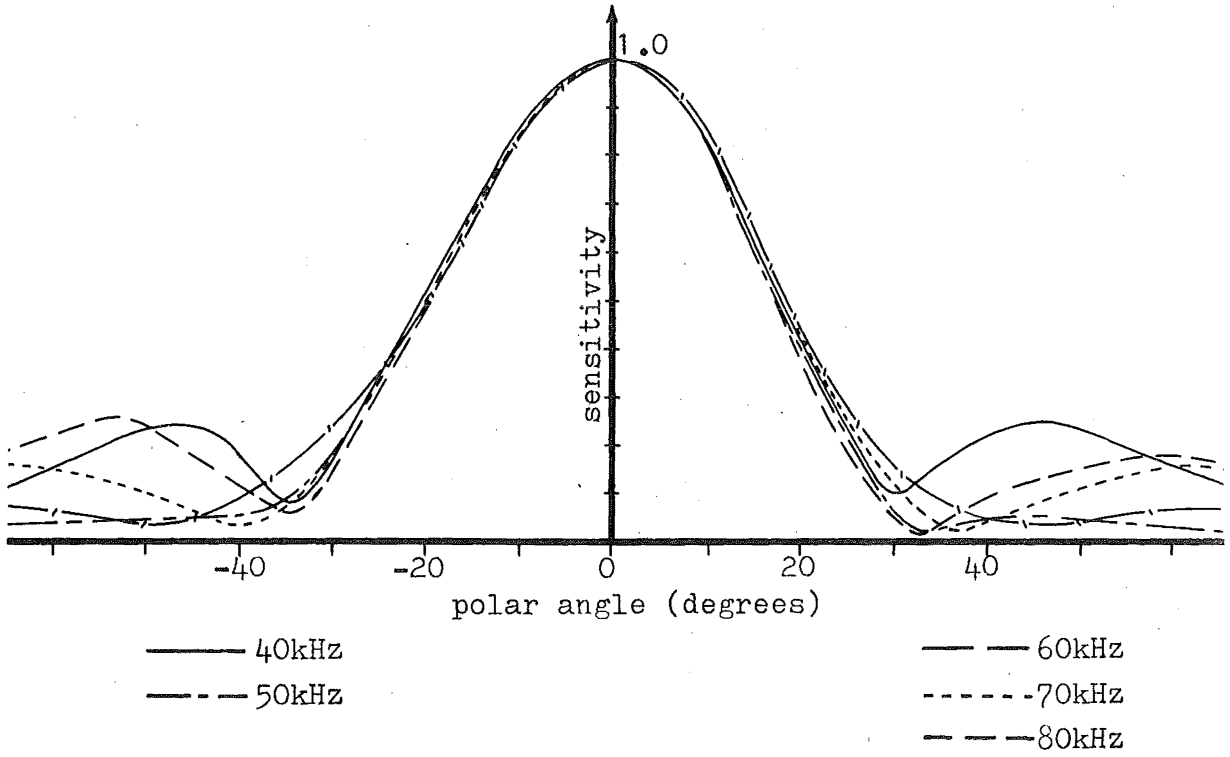

Figure 4.7. Measured directivity patterns.

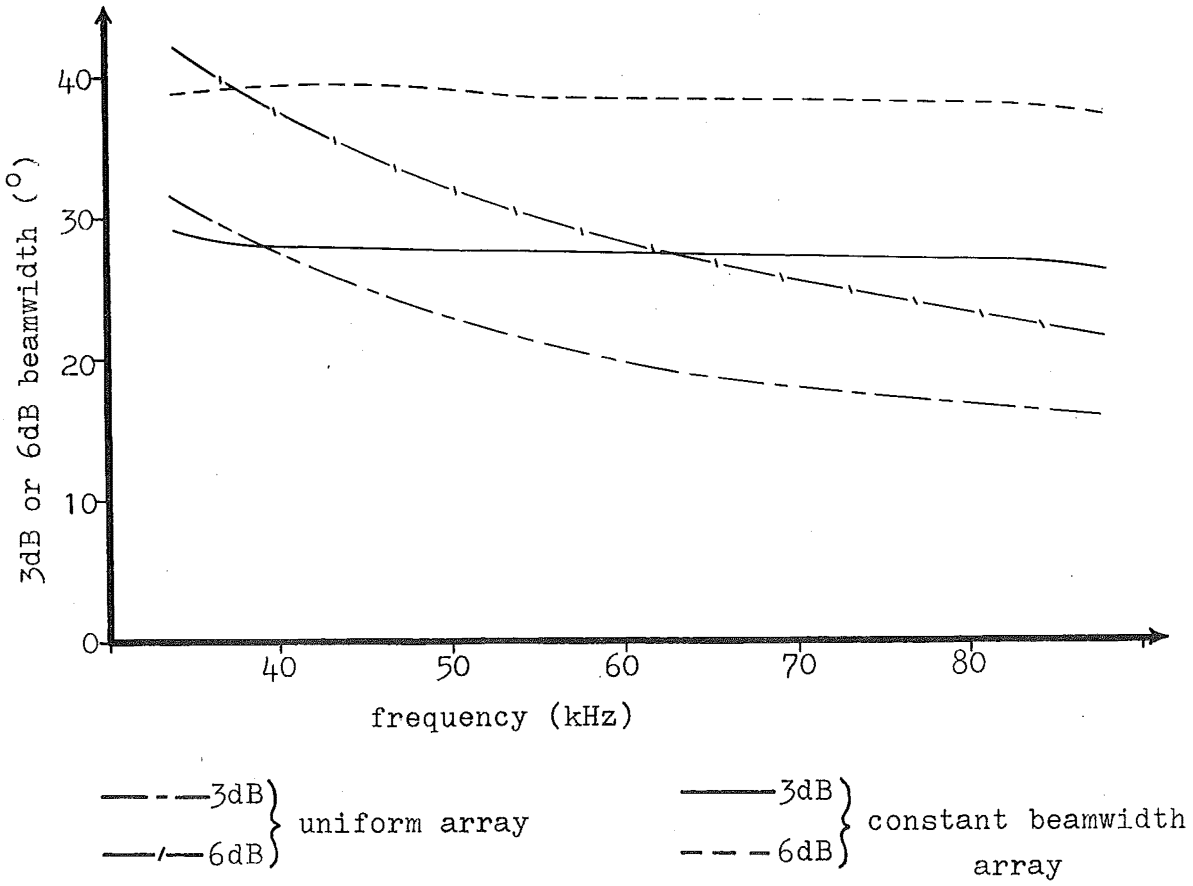

Figure 4.8. Measured beamwidth variation for the constant beamwidth array and for the four element array uniformly illuminated.

The experimental results of Figs 4.7 and 4.8 show a close agreement with the theoretical results of Fig. 4.4 indicating that the constant beamwidth technique may be simply implemented to achieve suitable directivity patterns for the receiving arrays in the horizontal plane. Receiving array design for directivity in the vertical plane is discussed in section 4.6.

4.5 Development of Constant Beamwidth Transmitting Array

As was mentioned in section 4.2, the use of cylindrical array surfaces appears to offer a convenient solution to the problem of achieving a constant, wide beamwidth for the transmitting array in the horizontal plane. The theoretical and experimental results of Morris[1] apply only for the case of a true cylindrical radiating face. Since such a surface is impractical, theoretical results were obtained for arrays of piston radiators with their centers lying on a circular arc. Typical directivity patterns for various arc radii and numbers of elements are shown in Fig. 4.9. The arc subtends a 60^{o} angle in each case.

It is seen from these patterns that to avoid pronounced dips in the main lobe, it is necessary to use a large radius and a large number of array elements.

An array was built using 10 elements on an arc of radius 16 cm. These dimensions were chosen as they appeared to offer a fair compromise between performance and size. The theoretical and measured results for this array are shown in Fig. 4.10. Although the elements were matched to within 1 dB and extreme care was taken in the positioning of the elements, the measured patterns depart considerably from the theoretical patterns and are less satisfactory. This suggests that an array of this type is extremely sensitive to small differences in element sensitivities. These rather unsatisfactory performance results led to the rejection of this technique for the transmitting array.

It was decided to adapt the constant beamwidth technique, developed for the receiving arrays, for application to the transmitting array.

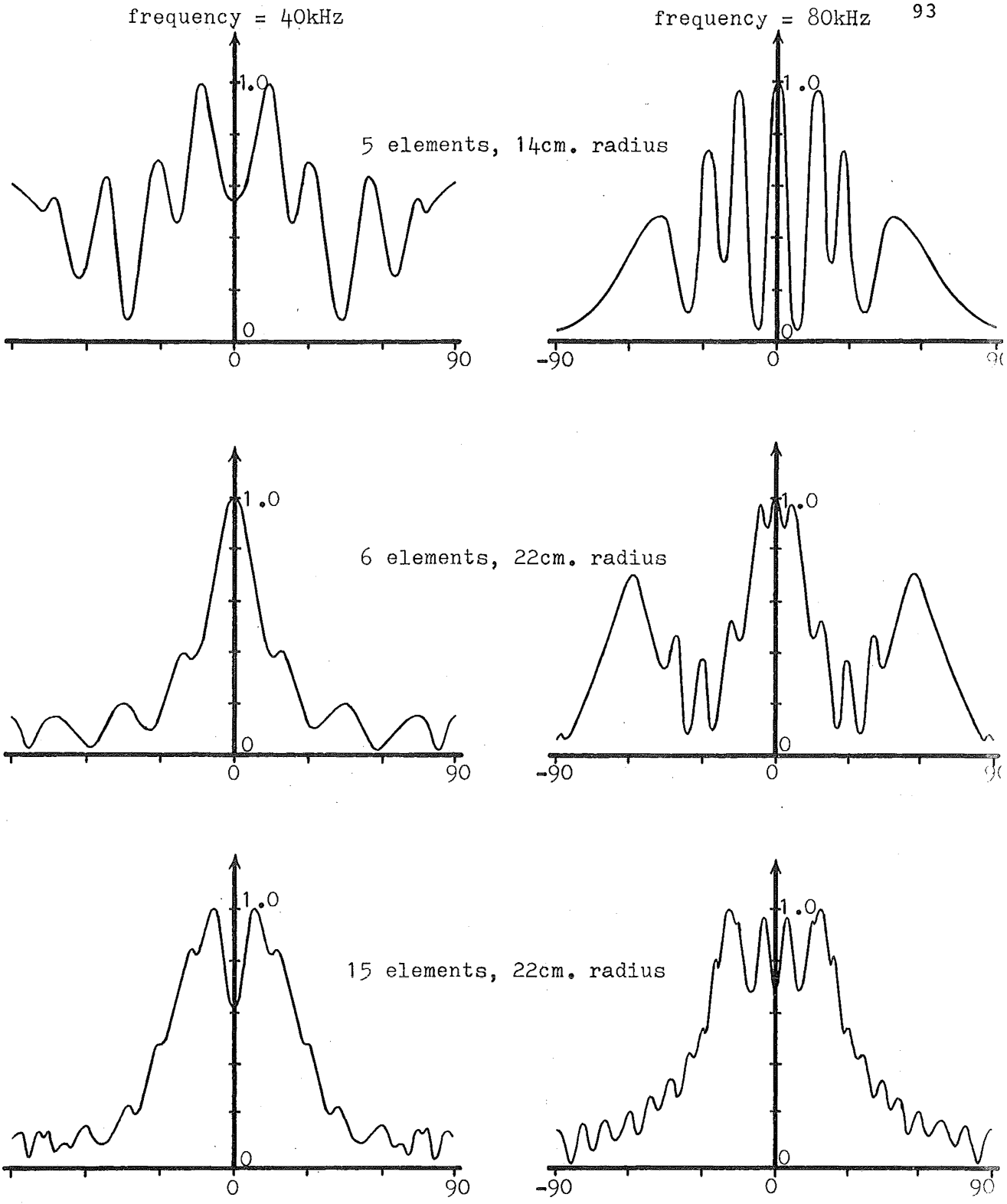

horizontal axis : polar angle in degrees

vertical axis : sensitivity (linear scale)

Figure 4.9. Theoretical performance of arrays having the elements located on a circular arc.

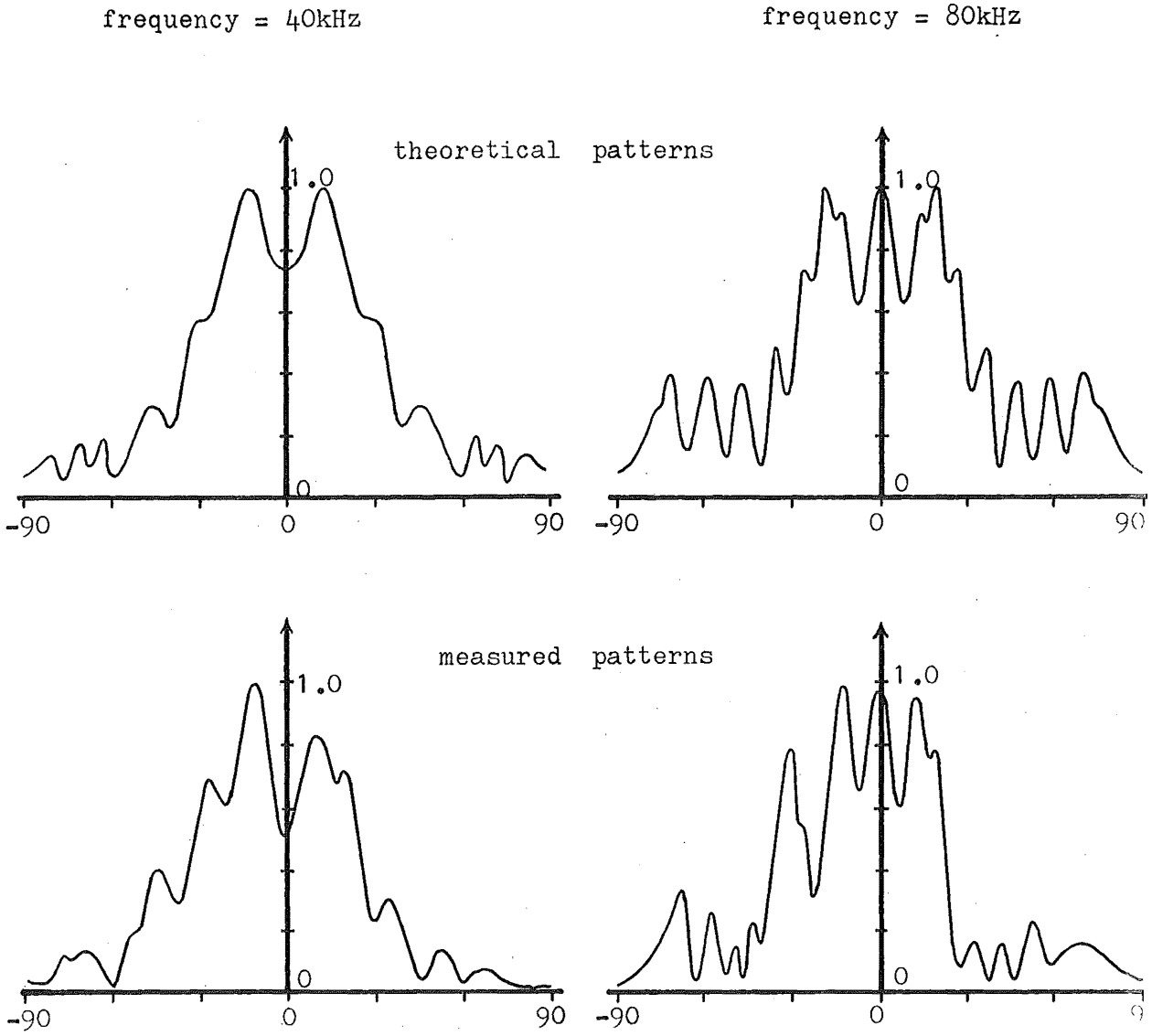

horizontal axis : polar angle in degrees

vertical axis : sensitivity (linear scale)

Figure 4.10. Theoretical and measured performance of a circular array of 10 elements at a radius of 16 cm.

Since a wider beamwidth is required in the case of the transmitting array, a 3 element array was proposed. Measurements were made at 40 kHz on such an array, with the sensitivity of the outer elements being a variable fraction k, of the inner element sensitivity. Figure 4.11 shows the directivity patterns obtained with this array for various values of k. It is seen from Fig. 4.11 that a 6 dB array beamwidth of 55 deg. may be achieved at 40 kHz, if the outer element sensitivity is 12 dB below that of the inner element.

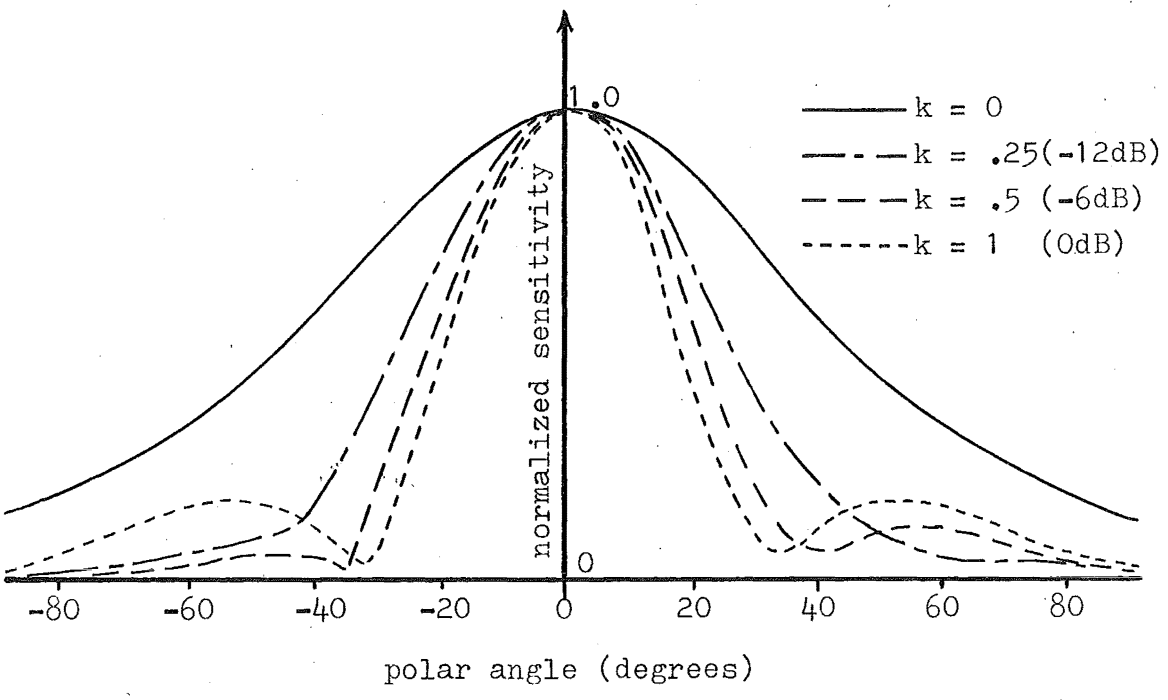

Figure 4.11. Directivity patterns for 3 element array at 40 kHz, with various outer element sensitivities.

Similar measurements were made at 80 kHz for the three element array and Fig. 4.12 shows the patterns obtained for various values of k. These patterns show that an array beamwidth of 55 deg. may be achieved at 80 kHz if the outer element sensitivity is 34 dB below that of the inner element.

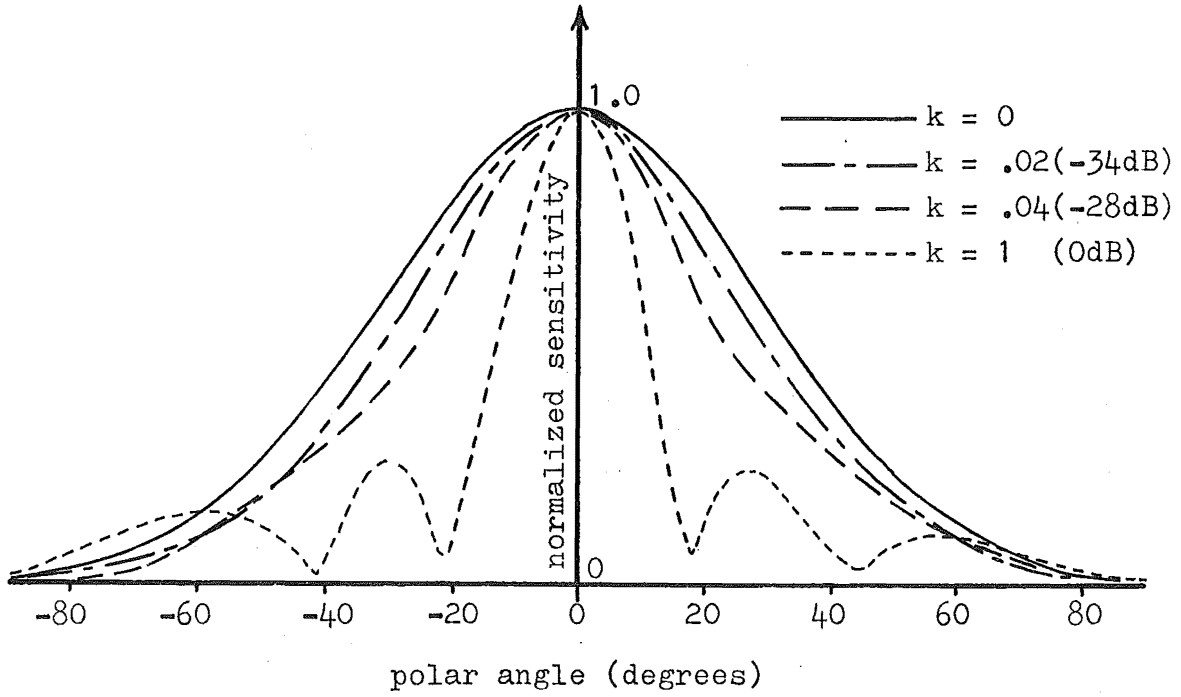

Figure 4.12. Directivity patterns for 3 element array at 80 kHz with various element sensitivities.

Fig. 4.13 shows the directivity patterns obtained at 40 kHz, 60 kHz, and 80 kHz when the outer element sensitivity $p_3(f)$ is reduced at a rate of 22 dB/octave starting from an initial sensitivity of -12 dB (at 40 kHz) with respect to the inner element sensitivity, p_0'. These results show that a constant beamwidth of approximately the specified value may be achieved in this manner. The implementation of this technique is discussed in section 5.3.9.

An experimental, rather than a theoretical approach to the design of this array was used here, for two reasons. Firstly, since small variation in beamwidth is of no consequence for this array, an accurate determination of the required sensitivity variation with frequency is not necessary, and

secondly since there is effectively only one element providing almost all the radiated energy at the higher frequencies, the presence of the rubber diaphragm between element and the water has a considerable effect on the directivity patterns obtained so that an accurate theoretical analysis would be extremely difficult.

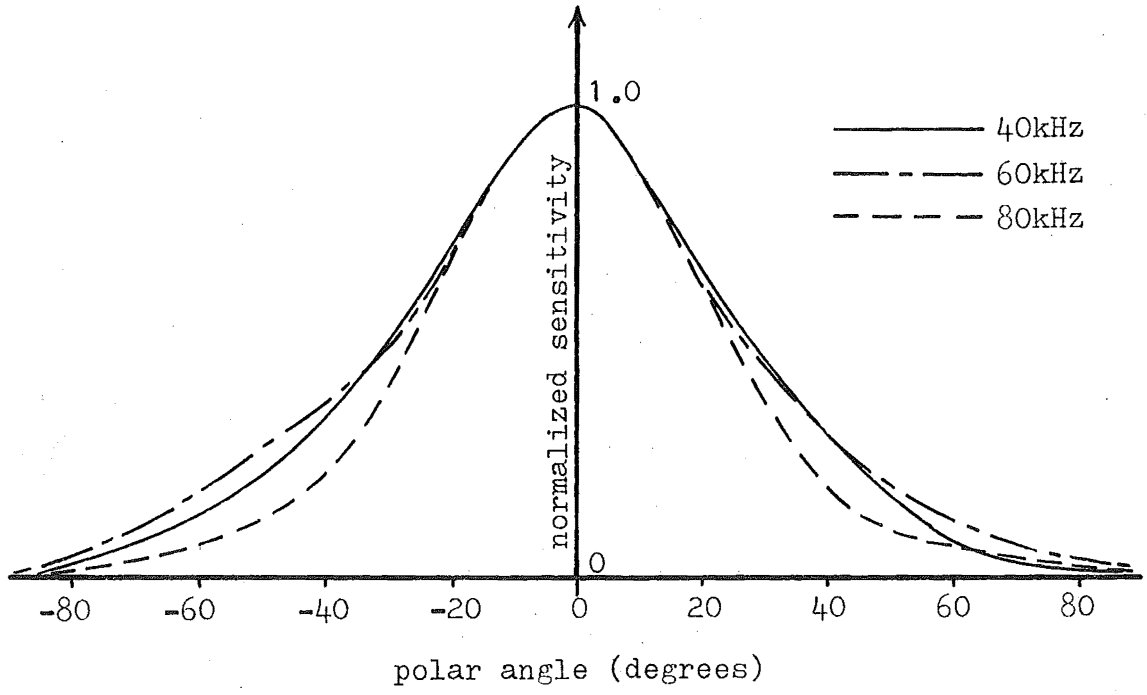

Figure 4.13. Directivity patterns for the constant beamwidth transmitting array.

4.6 Array Designs for Vertical Directivity Patterns

The dimensions of the radiating faces of the transducer elements were chosen to suit the requirements of the constant beamwidth receiving array design, with a minimum number of elements being used. This led to the choice of a radiating face diameter of 1.7 cm. This comparatively large diameter and the correspondingly large element spacing required, restricts the extent to which side lobes in the vertical plane

may be suppressed at the high frequency end of the operating frequency band, due to the appearance of part of the second major lobe of the directivity pattern within the range of real angles. It was not envisaged that significant lobe levels at extreme angles in the vertical plane would pose a problem in practice, since the distance from the array to the surface would be small enough to allow scattered signals from the surface immediately above the arrays to be suppressed by filtering in the audio stages. (Problems did, however, arise due to surface scattering from these extreme angles, and two methods for improving the situation were investigated. See Ch.8, section 8.4.)

Initially, it was felt that satisfactory performance would be achieved without the use of sensitivity shading for the receiving arrays in the vertical plane, but with vertical shading in the transmitting array. Due to the beam-broadening effect of sensitivity shading, 4 rows of elements are required for the transmitting array, as compared with only 3 for the receiving arrays. The vertical directivity patterns for one receiving array, comprising 3 rows of equal sensitivity are shown in Fig. 4.14.

Many researchers[8-10] have reported techniques for array design based on specified beamwidth and side lobe levels. The Dolph-Chebychev technique[10] appears to be the most easily applied in the present situation. The Dolph characteristics for an array of four elements (11) show that a 25 deg. beam-width may be obtained at 60 kHz if the elements are at 19 mm centers.

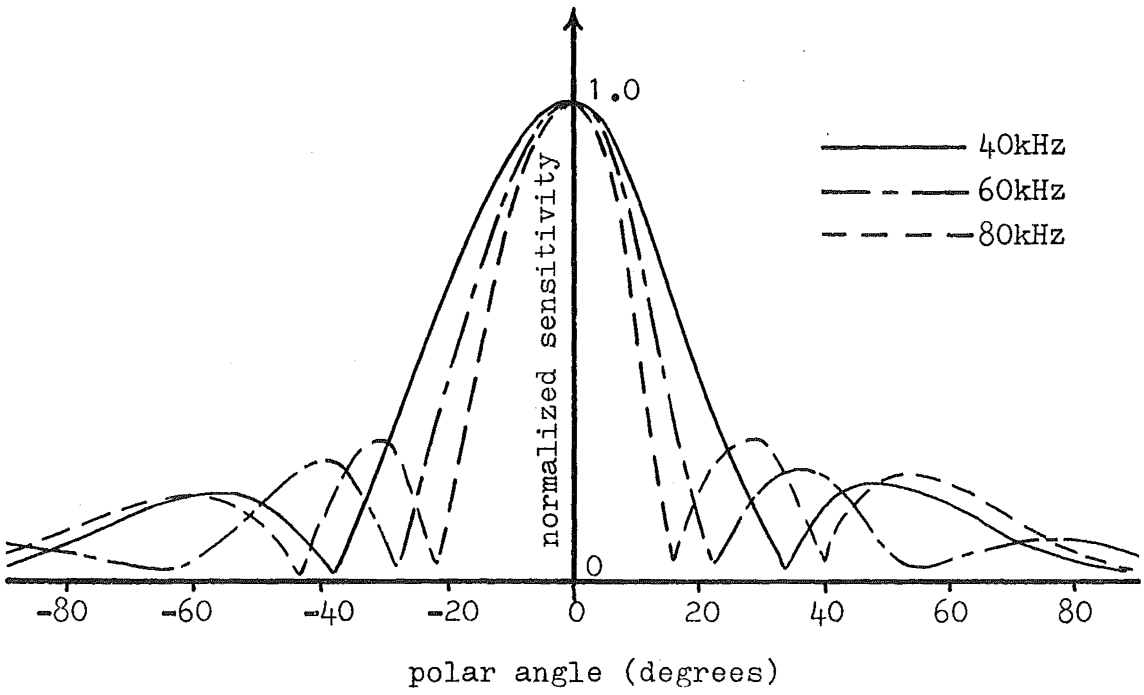

Figure 4.14. Directivity patterns for the receiving arrays in the vertical plane.

The element sensitivities in this case are 0.38, 1, 1, 0.38, and the maximum side lobe level, excluding the second major lobe, is 30 dB below the axial sensitivity. Since the maximum side lobe level of the receiving arrays in the vertical plane, again excluding the second major lobe, is -13 dB, a total side lobe suppression of 43 dB is achieved when the arrays are operated together.

The directivity patterns obtained for the four element array with Dolph shading are shown in Fig. 4.15.

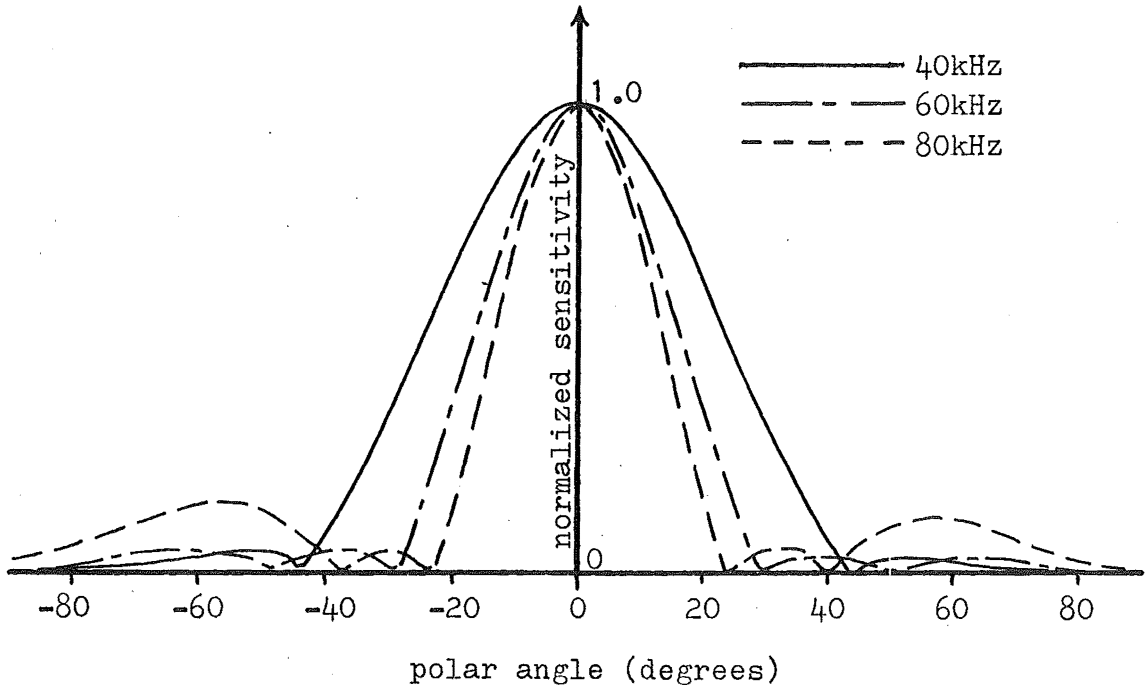

Figure 4.15. Directivity patterns for 4 element array with Dolph shading.

4.7 Two-dimensional Array Configurations

The diagrams of Fig. 4.16 show the element configurations for the transmitting array and one receiving array. The numbers within the elements show the transmitting or receiving sensitivities as determined in the preceding sections.

4.8 Conclusions

A technique which uses simple passive network has been developed to maintain the horizontal beamwidths of transmitting and receiving arrays constant over the full frequency bandwidth of one octave. The directivity patterns which result from this technique show very little variation of shape over a large portion of the main lobe, and the patterns exhibit smooth

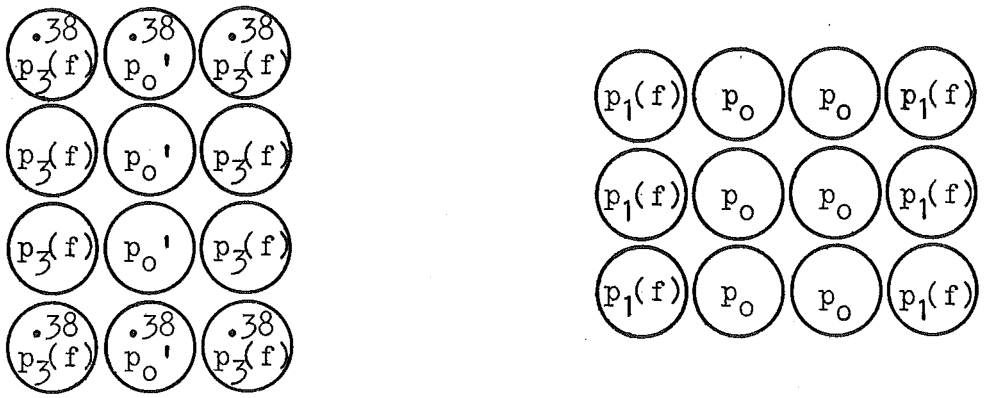

transmitting array receiving array

Figure 4.16. Transmitting and receiving array configurations.

variation within the main lobe. The patterns are thus ideally suited to the lobe-amplitude comparison method of directional determination, which is the method employed in the present application.

The constant beamwidth technique is extremely simple in implementation and requires only a very small number of separate array elements.

Using amplitude tapering in the transmitting array only, a side lobe suppression (ignoring the second major lobe) of approximately 40 dB has been achieved.

4.9 References

1. J.C. Morris, "Broad Band Constant Beamwidth Transducers", J. Sound Vib. 1 : 28 (1964).
2. D.G. Tucker, "Arrays with Constant Beamwidth over a Wide Frequency Range", Nature, 180 : 496 (1957).
3. J.C. Morris and E. Hands, "Constant Beamwidth Arrays for Wide Frequency Bands", Acustica, 11 : 341 (1961).
4. H.O. Berktay, "Possible Exploitation of Non-linear Acoustics in Underwater Transmitting Applications", J. Sound Vib., 2 : 435 (1965).
5. H.O. Berktay, J.R. Dunn and B.K. Gazey, "Constant Beamwidth Transducers for use in Sonar with very Wide Frequency Bandwidths", Appl. Acoustics, 1 : (1968).
6. D.J. Karbo, "Effects of Shading on Minor-lobe Level and Beamwidth in Symmetrical Uniformly Spaced 6- and 4-Element Arrays", J. Acoust. Soc. Am., 35 : 838 (1964).
7. R.P. Smith, "Constant Beamwidth Receiving Arrays for Broad Band Sonar Systems", Acustica, 23 : 21 (1970) (reproduced as Appendix IV).
8. R.L. Pritchard, "Optimum Directivity Patterns for Linear Point Arrays", J. Acoust. Soc. Am., 25 : 879 (1953).
9. D.J. Karbo, op. cit.
10. C.L. Dolph, "A Current Distribution of Broadside Arrays which Optimizes the Relationship between Beamwidth and Side-lobe Level", Proc. IRE, 34 : 335 (June 1946).
11. V.M. Albers, Underwater Acoustics Handbook, Pennsylvania State University Press, 1960, Ch. 11.
12. V.C. Anderson, "Digital Array Phasing", J. Acoust. Soc. Am., 32 : 867 (1960).

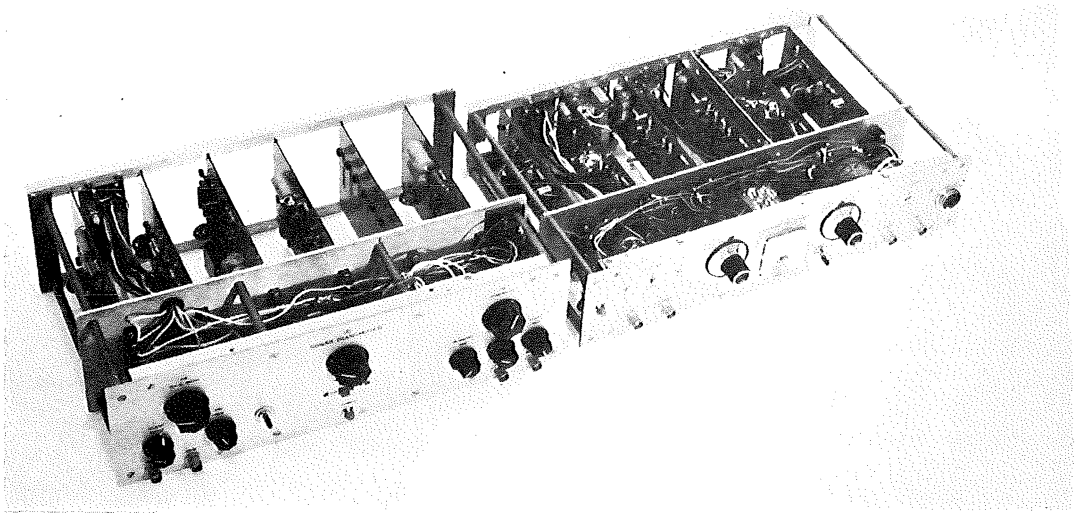

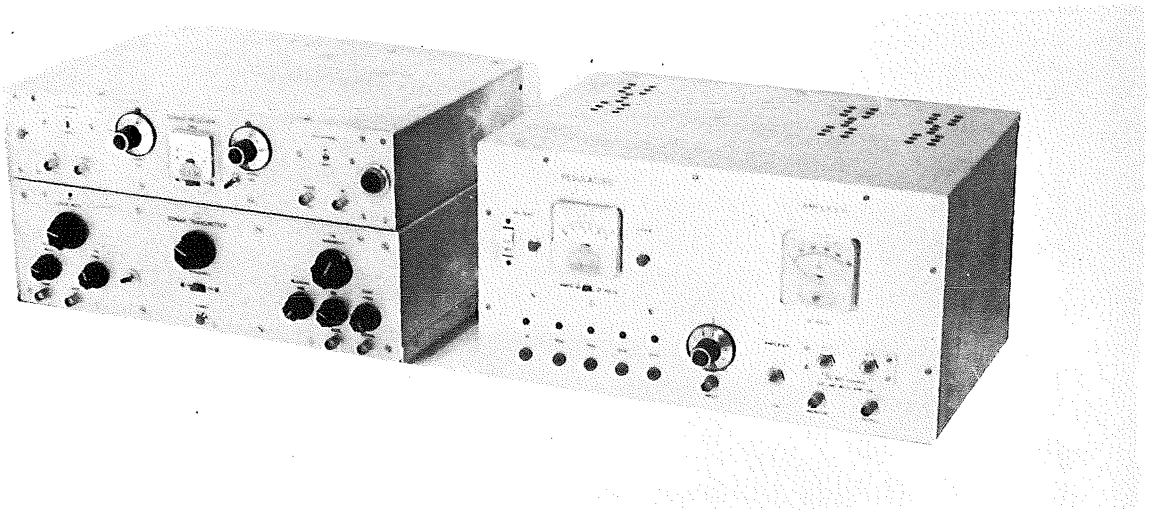

CHAPTER 5

DESIGN OF ELECTRONIC EQUIPMENT

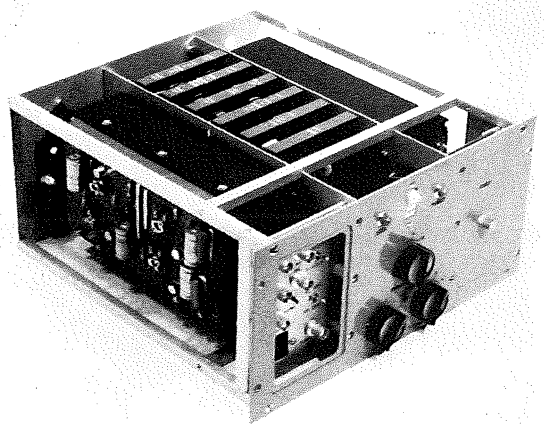

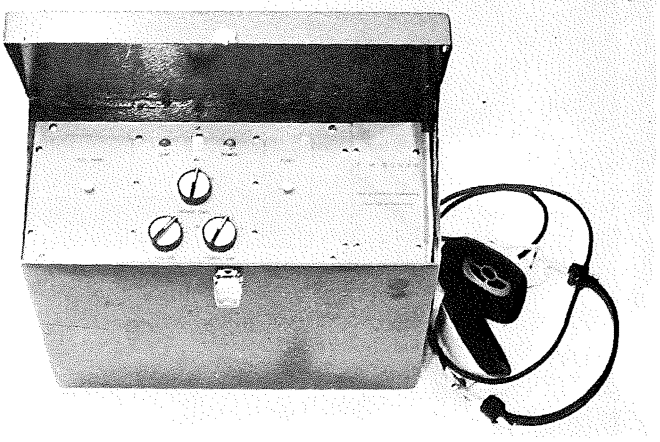

CHAPTER 5

DESIGN OF ELECTRONIC EQUIPMENT

5.1 Introduction

The electronic equipment was designed to perform three main roles, namely,

(i) to generate suitable transmissions to allow the testing of transducer elements and arrays in a water tank of limited size,

(ii) to meet the system requirements for transmission, reception, and display in operation at sea, and

(iii) to be capable of producing suitable transmissions for operation in air (using electrostatic transducers) to facilitate system testing, and model studies.

The techniques used for the testing of transducer elements and arrays in the water tank are described in appendix III. A pulsed CW transmission is necessary to suppress echoes from the water surface and from the tank wells. The carrier frequency must be variable over the operating band of the system (40-80 kHz).

The basic requirements of the sonar system for operation at sea were discussed in Ch. 2. In order to examine the effects of variations in the basic system parameters it was considered desirable that such quantities as bandwidth, center frequency, and repetition frequency could be easily altered, in a known fashion, at sea.

The only additional requirement for operation of the sonar in air is an extension to the range of repetition frequencies available, in view of the five times reduction of

propagation velocity in air, as compared to water.

The following broad specification for the electronic equipment was proposed to meet the requirements of the three operational roles mentioned above.

Repetition frequencies

1/8 Hz to 8 Hz in octave steps

Bandwidths for FM operation

5 kHz, 10 kHz, 20 kHz, 40 kHz

Upper frequency limit for FM operation

80 kHz, 70 kHz, 60 kHz, 50 kHz

Pulse lengths for pulsed CW operation

0.2 msec. to 10 msec. continuously variable

Carrier frequencies for pulsed CW operation

35 kHz to 85 kHz, continuously variable.

A more detailed specification is developed throughout the chapter.

5.2 Development of System Block Diagram

The essential elements of the FM binaural sonar[1] and the pulsed CW (PCW) sonar[2] are shown in Figs 5.1 and 5.2 respectively. The shaping networks in the diagram of Fig. 5.1 are necessary to compensate for the reduction of echo strength from a target as range increases, due to increasing transmission loss. These networks increase the audio gain as frequency (range) increases so that, within the working range of the system, a target produces an audio response of approximately constant intensity.

The other blocks of Fig. 5.1 and 5.2 are considered self-explanatory.

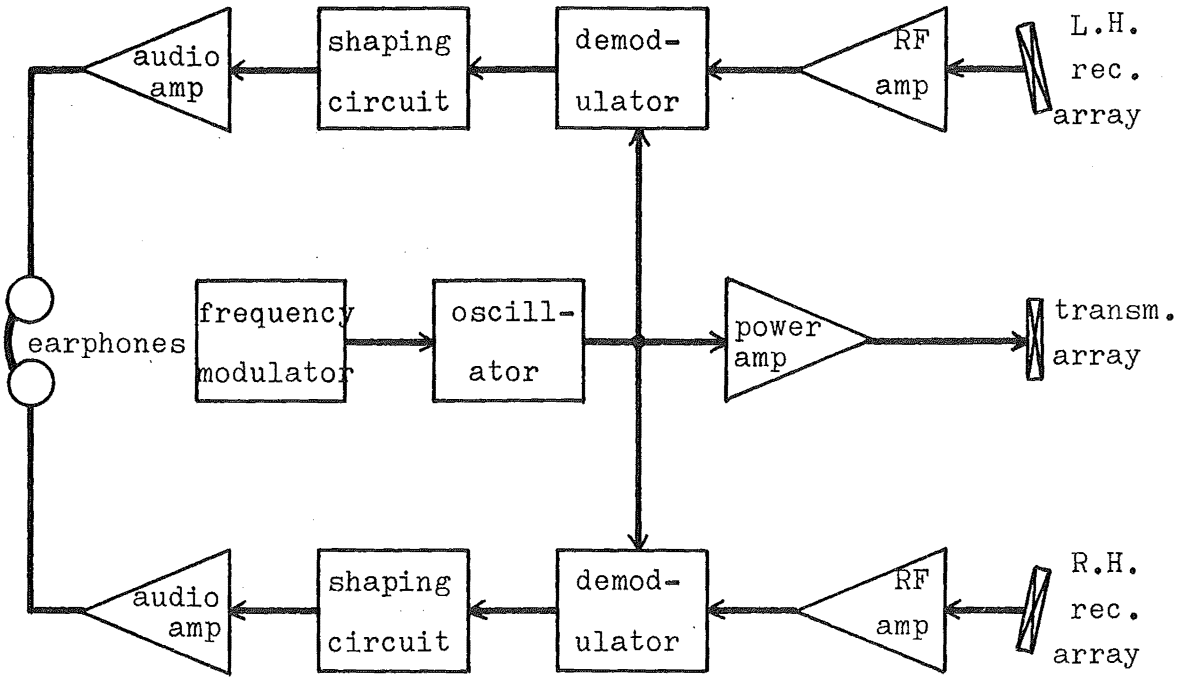

Figure 5.1. Elements of FM binaural sonar

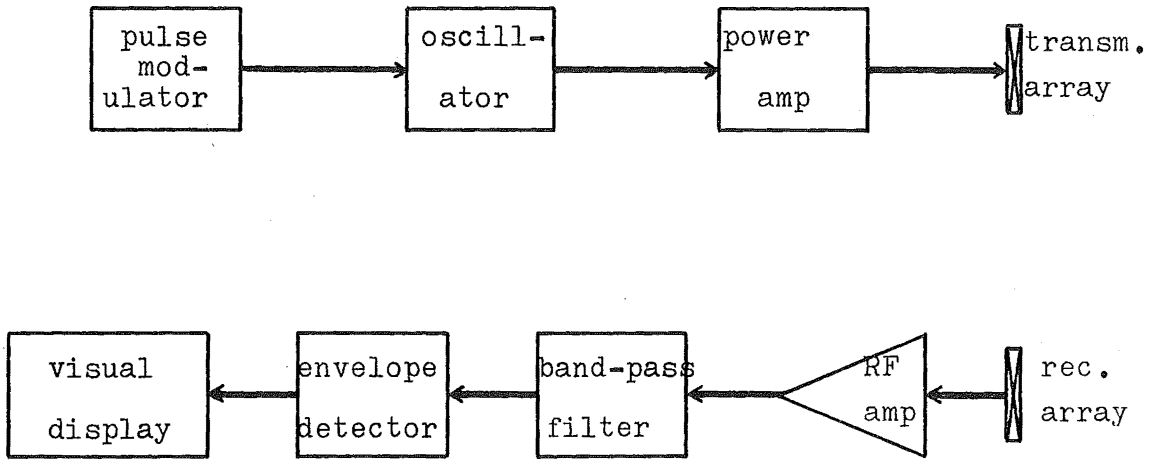

Figure 5.2. Elements of PCW sonar

It will be shown in section 5.4 that the PCW sonar may be formed from the elements of the FM sonar with very little additional hardware. The discussion for the moment will be limited to the FM case.

Certain additions to the block diagram of Fig. 5.1 are necessary due to limitations of the electronic circuitry, characteristics of the medium, array requirements, and audio display considerations. These are

(i) High pass filters are necessary between the receiver RF amplifiers and the demodulators to reduce the level of low frequency noise at the demodulator inputs. Although the design of the demodulators is such that signal feedthrough is severely suppressed, since the low frequency ambient noise level in the sea is very much higher than the noise level in the operating band, additional suppression is warranted.

(ii) A gate is necessary between the transmitter oscillator and the power amplifier to cut the transmission during the flyback period of the oscillator. Although a flyback period whose duration is less than one cycle is possible, its implementation is difficult and there is nothing gained by it, since the audio signal from a particular target is interrupted for a period at least as long as the propagation delay. Also, it is desirable that each frequency sweep should commence with a comparatively slow build-up of signal level, to prevent a large transient at the commencement of the audio signal from each target. A gate which cuts the transmitter signal sharply and allows it to build up slowly again after a short delay is employed.

Gates are also employed in the receiver circuits between the demodulators and the shaping circuits, to fade out and fade in the audio signals between consecutive sweeps. This arrangement is found to produce less disturbance in the audio presentation than any other arrangement tried. The time characteristics of the transmitter and receiver gates are shown in Fig. 5.3.

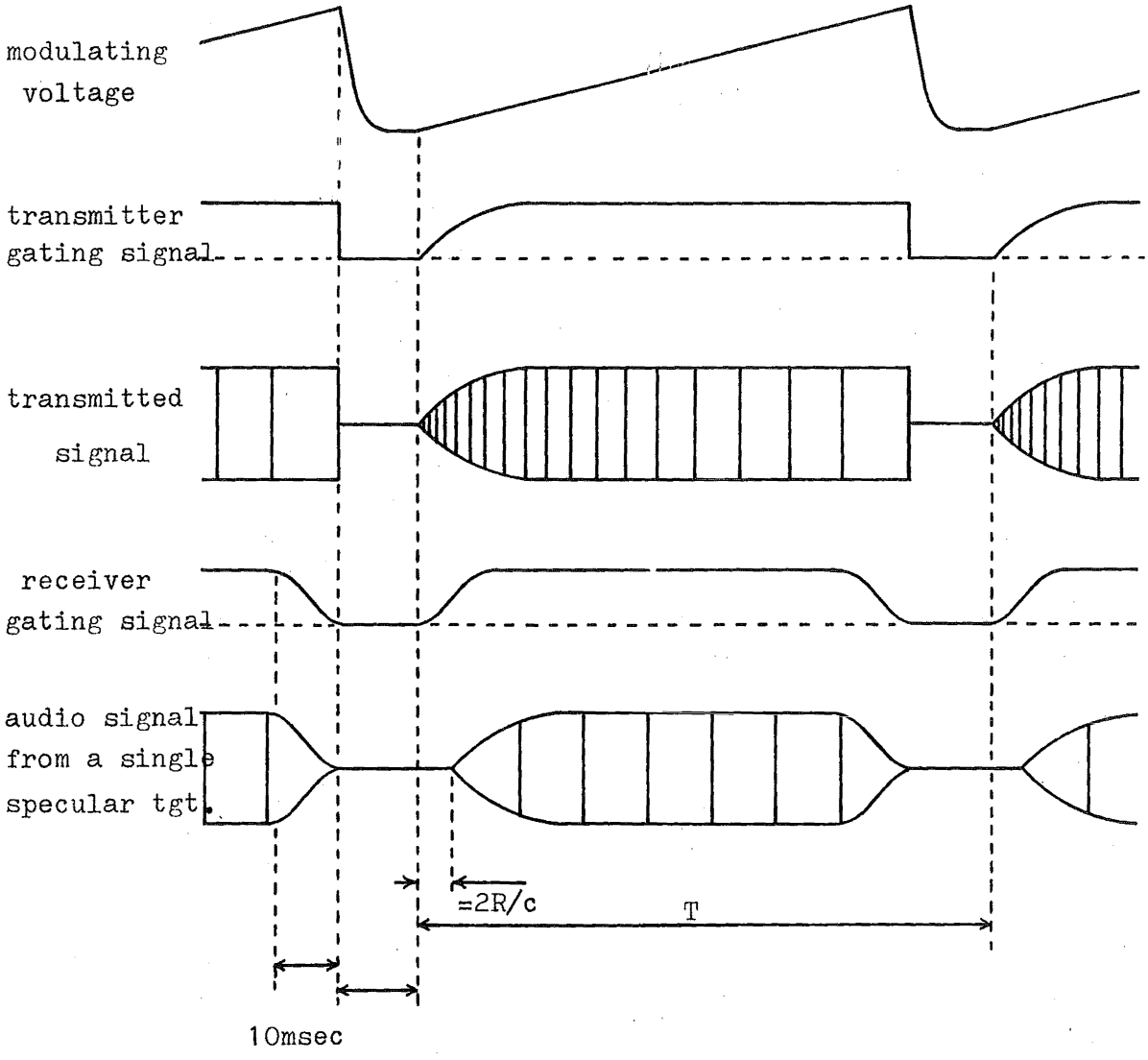

Figure 5.3. Transmitter and receiver gate characteristics.

The receiver gates anticipate the sharp cut-off of the trans-

mission so that the audio signal is reduced to zero at this point. These gates turn on again slowly, as the transmission signal begins to rise again. The slow turn-on characteristic of the transmitter gate ensures that the audio signal from a target at range R (delayed by time, 2R/c) commences without a sharp transient.

This gating procedure appears rather cumbersome, since the transients which would otherwise be introduced would not affect the theoretical performance of the sonar. These measures are taken, however, because it has been found that such disturbances are extremely distracting and irritating to the operator, and his performance would undoubtedly suffer in consequence.

(iii) To provide the necessary gating signals mentioned in (ii) and to synchronise the frequency modulation with these signals, a timing unit is required.

(iv) It was shown in chapter 4 that additional circuitry is required at the electronics/arrays interfaces to meet the peculiar beamwidth and beamshape requirements in the horizontal plane and the sidelobe suppression requirements in the vertical plane.

(v) The frequency modulator/oscillator combination, which comprises a sawtooth generator and voltage controlled oscillator (VCO), necessarily produces a non-sinusoidal waveform. Due to the wide bandwidth of the transducer elements, harmonic components, at least when the fundamental frequency is near 40 kHz, will be transmitted and subsequently received. Since a switching type of demodulator is employed, these harmonics can give rise to spurious audio signals. A low pass filter with a sharp cut-off at 80 kHz is employed to

produce a sinusoidal FM signal, from the VCO output signal.

Fig. 5.4 shows a modified version of the block diagram of the FM binaural sonar, which incorporates the additions mentioned above. One receiving channel only is shown. A block diagram which incorporates the additional elements required for PCW operation is discussed in section 5.4.

5.3 Design of Individual Circuits for the FM Sonar

A description of the individual circuits comprising the blocks of Fig. 5.4 will now be given. Where particularly stringent performance requirements are imposed on the performance of a circuit, or where novel techniques have been employed, the description will be detailed. Where the circuit design is conventional, the description will be very brief. The final circuits used in each block are shown in appendix V.

5.3.1 The frequency modulated oscillator

Extremely high linearity of the frequency sweep of the FM transmission is necessary, if the audio tone produced from a stationary target is to be constant, within a small tolerance.

Figure 5.5 shows an FM transmission with exaggerated non-linearity and the echo which is received from a target at range R. Let the departure from the ideal linear transmission (dotted) be $\delta(t)$, where $\delta(0) = \delta(T) = 0$ (T is the duration of the frequency sweep). Let the instantaneous frequency of the ideal linear transmission be f, given by the relationship,

$$f = 2f_1 - \mu t \qquad 0 \leqslant t \leqslant T$$

where f_1 is the lower frequency limit of the octave
is the frequency sweep rate, given by $\mu = f_1/T$, s
bandwidth is one octave.

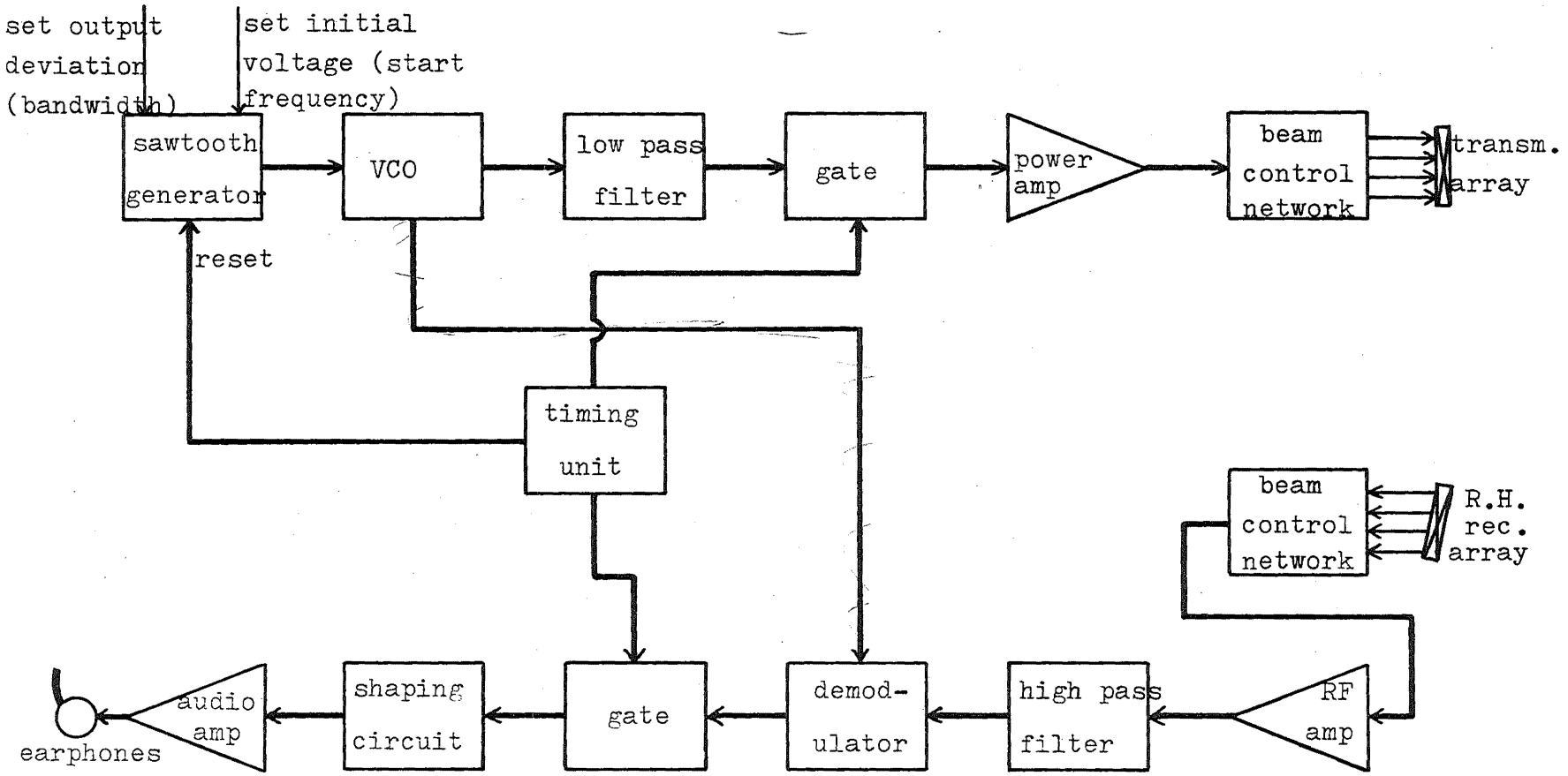

Figure 5.4. Modified FM system block diagram (one receiving channel only shown).

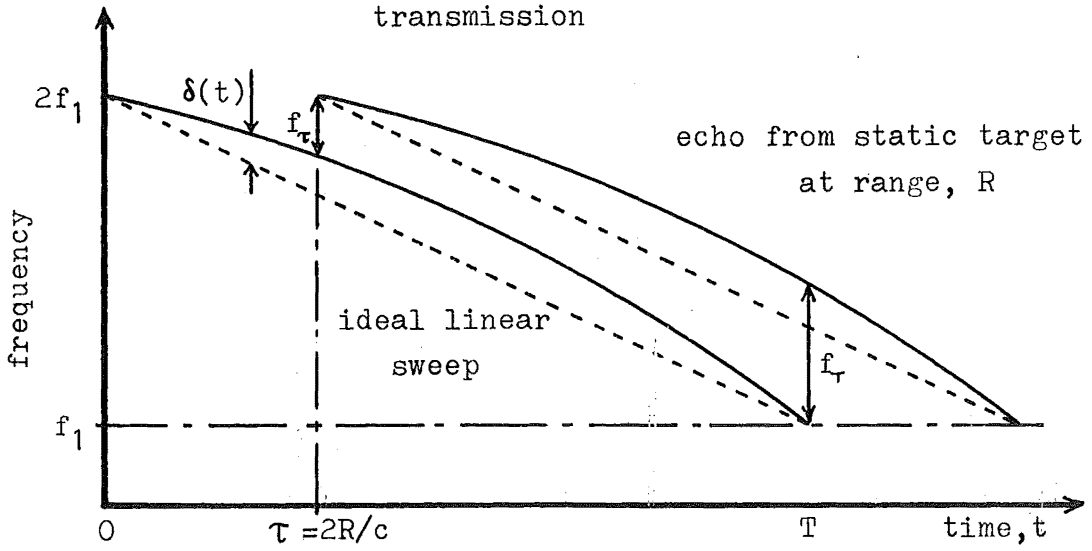

Figure 5.5. Non-linear FM transmission and echo.

At time $t = \tau = 2R/c$, the audio frequency produced at the output of the demodulator due to the target at range R is

$$f_\tau = \mu\tau - \delta(\tau)$$

and at $t = T$

$$f_T = \mu\tau + \delta(T-\tau)$$

It is clear from Fig. 5.5 that if the departure from linearity, $\delta(t)$ is a simple curve of constant or smoothly varying curvature, and if the maximum departure is small, the points $t = \tau$ and $t = T$ will correspond to the minima and maxima, respectively, of the audio frequency. The total fractional change in the pitch of the audio tone, then, is

$$\frac{\Delta f}{f} = \frac{f_T - f_\tau}{\mu\tau} = \frac{\delta(T-\tau) + \delta(\tau)}{\mu\tau} \qquad 5.1$$

To proceed further we need to know the manner in which $\delta(t)$ varies over the sweep period. Since this variation is difficult to predict or measure we will take a particular example to determine at least the order of magnitude of $\Delta f/f$. The precise form of $\delta(t)$ does not greatly affect the magnitude of $\Delta f/f$ and for convenience a ½ cycle sinusoidal variation will be assumed. Thus,

$$\delta(t) = \hat{\delta} \sin \frac{\pi t}{T} , \qquad \theta \leqslant t \leqslant T$$

Then, from eqn 5.1

$$\Delta f/f = \frac{2\hat{\delta} \sin \frac{\pi\tau}{T}}{\mu\tau} \qquad 5.2$$

Since, in practice, $\tau << T$

$$\Delta f/f \doteq \frac{2\pi\hat{\delta}}{\mu T}$$

$$= \frac{2\pi\hat{\delta}}{B} , \text{ where B is the bandwidth.}$$

For a 40 kHz bandwidth, then,

$$\Delta f/f \doteq 1.6\hat{\delta}.10^{-3}\%.$$

If $\hat{\delta}$ is 1 kHz, say, which represents a deviation of 2.5% of the total bandwidth, the variation in the audio frequency is

$$\Delta f/f = 16\%.$$

Any error in linearity of the FM transmission, then, is magnified approximately six times in the audio signal.

It would be extremely difficult to assess, quantitatively, the effect of sweep non-linearity on the performance of the sonar/human operator combination. The human auditory system can certainly detect pitch variation of the order of 0.3%[3]

under certain circumstances. The effects of non-linearity on the performance of electronic processors, which assume a linear transmission, have been examined by Cook[4,5] and Hunter[6]. Cook shows that non-linearity produces significant side-lobes in the time (range) domain if the signal is processed by pulse compression.

Hunter shows the equivalent result for frequency domain matched filtering, i.e. the formation of side-lobes in the frequency domain.

A design figure of 2% for the allowable fractional change in pitch of the audio signal was chosen to reduce the effect of non-linearity to negligible proportions. This requires that the maximum deviation of the FM transmission from the ideal linear from be < 0.3% of the transmission bandwidth.

An integrator, using a high gain operational amplifier, was considered the most suitable manner to generate the saw-tooth voltage waveform required to modulate the VCO. Junction field effect transistors (FETs) are used to reset the output voltage to a value corresponding to the starting frequency, at the commencement of each sweep. The circuit diagram is shown in Fig. 5.6. Voltages V_1 and V_i determine the initial output voltage and the rate of rise of output voltage, respectively. FETs T_1 and T_2 are in the off condition during each ramp and are switched on for several milliseconds at the completion of each ramp to reset the output voltage.

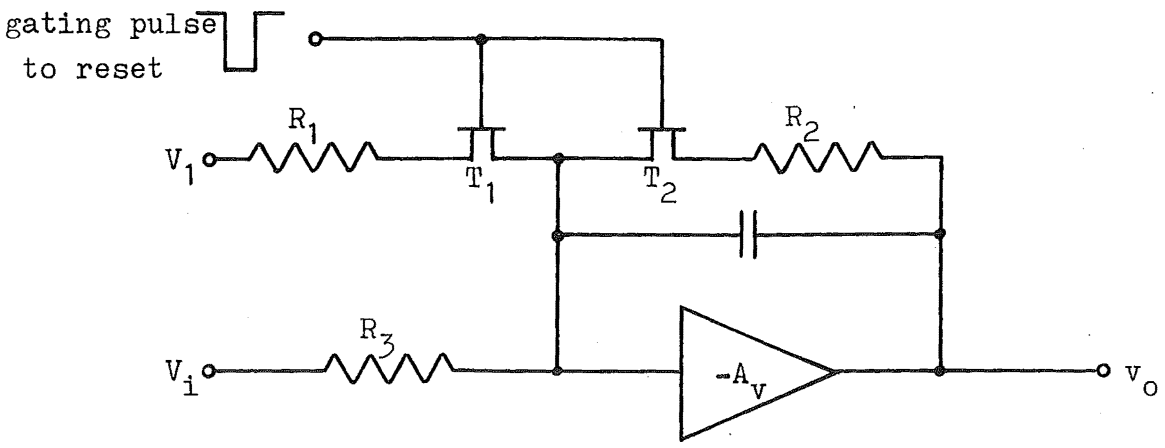

Figure 5.6. Saw-tooth generator circuit

Let the effect of leakage current through the capacitor, C, and through the FET, T_2, be represented by resistance R_o shunting the capacitor. Leakage through T_1 does not affect linearity so the branch comprising R_1, T_1 need not be considered in the analysis. The effective circuit of the integrator, during each ramp, then, is as shown in Fig. 5.7.

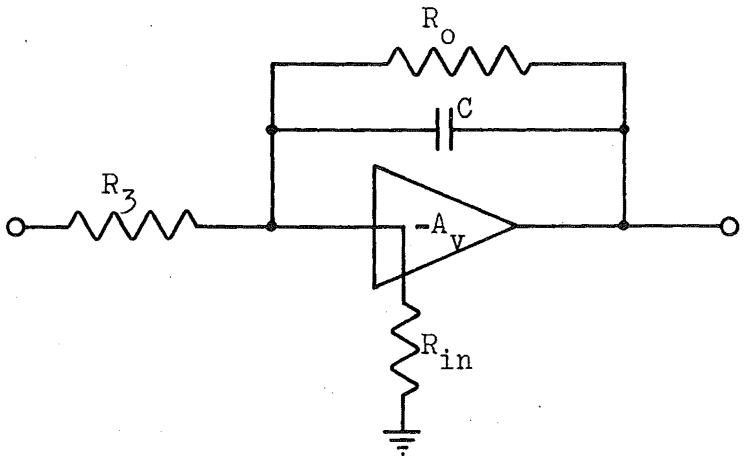

Figure 5.7. Effective integrator circuit during the ramp.

Assuming that at t = 0, $v_0 = 0$, analysis of the circuit of Fig. 5.7, using the Laplace transform technique, gives

$$\frac{\frac{V_i}{s} + \frac{V_0(s)}{A_v}}{R_3} = - V_0(s) \left[\frac{1 + 1/A_v}{1/sC} + \frac{1 + 1/A_v}{R_0} + \frac{1}{A_v R_{in}}\right] \qquad 5.3$$

Since $A_v >> 1$ we obtain, on rearranging eqn 5.3,

$$- \frac{V_i}{s^2 CR_3} = V(x) \left[1 + \frac{1}{sC}\left(\frac{1}{R_0} + \frac{1}{R_{in}A_v} + \frac{1}{R_3 A_v}\right)\right] \qquad 5.4$$

Let $\frac{1}{R_0} + \frac{1}{R_{in}A_v} + \frac{1}{R_3 A_v} = \frac{1}{R}$ then we obtain

$$V_0 = - \frac{V_i}{CR_3} \cdot \frac{1}{s(s + 1/CR)}$$

which gives the time function,

$$v_0(t) = -V_i \frac{R}{R_3} (1 - \exp(-t/RC))$$

Now at t = 0, $v_0 = 0$ and at t = T,

$$v_0(T) = -V_i \frac{R}{R_3} (1 - \exp(-T/RC))$$

The ideal linear voltage ramp, defined in a similar way to the ideal linear frequency sweep of Fig. 5.5, then is

$$v'(t) = -V_i \frac{R}{R_3} (1 - \exp(-T/RC))\, t/T \qquad 0 \leqslant t \leqslant T$$

The maximum fractional deviation of $v_0(t)$ from $v'(t)$ then, is given by

$$\Delta v/v = \frac{v_0(T/2) - v'(T/2)}{v_0(T)} \qquad 5.5$$

Substitution from the above equations into eqn. 5.5 yields the approximate expression for $\Delta v/v$,

$$\Delta v/v \doteq -T/8RC.$$

Since the maximum value of T required is 8 secs, to achieve linearity within 0.1% we require that RC > 1000 secs.

Using the type 2N4360 FET and with R_3 = 100 k, R_{in} = 10 k, C = 1 μF (polycarbonate), $A_v = 10^5$, a value of RC of 1200 secs may be achieved. The required linearity may thus be achieved without the use of special techniques or components.

The principle used in the VCO is the repetitive charging of a capacitor at a rate proportional to the input voltage. Fig. 5.8 demonstrates this principle. If, at any instant, the charging rate, $dv/dt = \tan\alpha$ is directly proportional to the input voltage, $v_0(t)$, the period of oscillation, T, is given by,

$$T = \frac{V_2 - V_1}{\tan\alpha} = \frac{V_2 - V_1}{kv_0}, \quad k \text{ constant.}$$

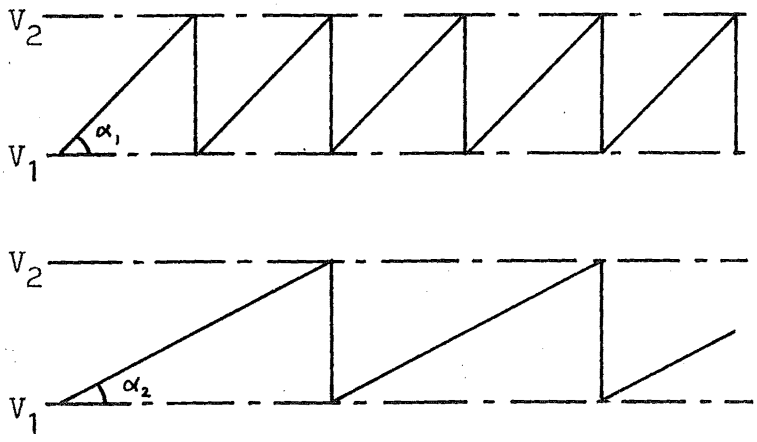

Figure 5.8. Principle of the Voltage Controlled Oscillator.

If V_1 and V_2 are also constant, the frequency of oscillation, f, is

$$f = 1/T = \frac{k}{V_2 - V_1} v_0 = k'v_0$$

This technique is implemented by the electronic circuit of Fig. 5.9, which is based on a low frequency VCO design after Voelker[7].

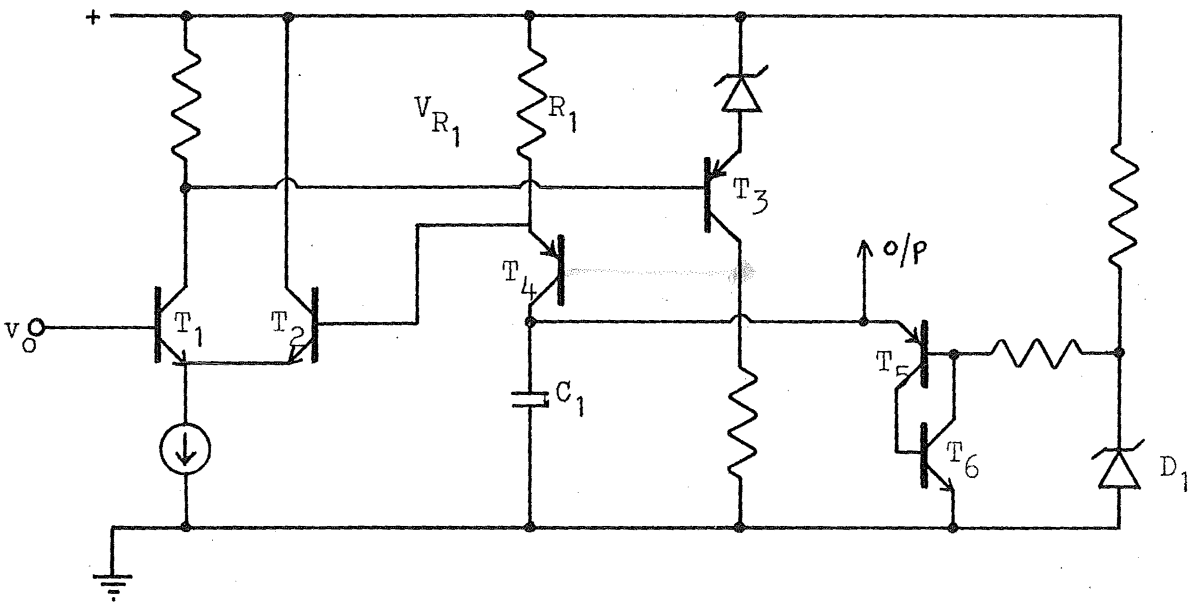

Figure 5.9. Voltage Controlled Oscillator

The high gain differential amplifier comprising transistors T_1, T_2 and T_3 compares the voltage across R_1 with the input voltage and feeds a voltage to the base of transistor T_4 to minimize the difference. Thus, V_{R_1}, the voltage on R_1, and hence the charging current into capacitor, C_1, is forced to follow the input voltage. The fast 'silicon pair' switch comprising transistors T_5, T_6 discharges C_1 when its voltage reaches a fixed level determined by zener diode, D_1.

The principle sources of non-linearity in this circuit configuration are as follows:

(i) The departure of V_{R_1} from v_0 due to the finite open loop gain of the differential amplifier,

(ii) variation of the current into C_1 due mainly to the non-zero emitter-base current in T_4, and

(iii) the finite time taken for the discharge of C_1 by the switch, T_5-T_6.

The overall voltage/frequency conversion accuracy obtained with this circuit is, however, quite adequate for the present application. Measurements with the most accurate instruments available in the E/E Dept. (a 6 digit digital frequency meter and a 4 digit voltmeter) were unable to detect any departure from linearity. From this one may conclude that the departure from linearity is less than 0.1%. The overall FM sweep linearity will clearly be better than the design figure of 0.3%. The actual circuit used for the saw-tooth generator and VCO is contained in appendix V, part (i).

5.3.2 Transmitter and receiver filters

Since the output of the VCO has a saw-tooth waveform, it is desirable to convert this to a square wave before filtering in order to eliminate second harmonic components, thus easing filter design. This conversion is performed by a Schmitt trigger. The low pass filter required for the transmitter, then, must provide rejection of frequencies above 120 kHz (third harmonic of 40 kHz) and must have an approximately flat characteristic over the operating band from 40 kHz to 80 kHz.

An active filter design after Farrer[8] in a two stage configuration was chosen. This filter is particularly versatile, allowing independent control of the positions of

poles and zeros. The attenuation characteristic achieved with this filter is shown in Fig. 5.10.

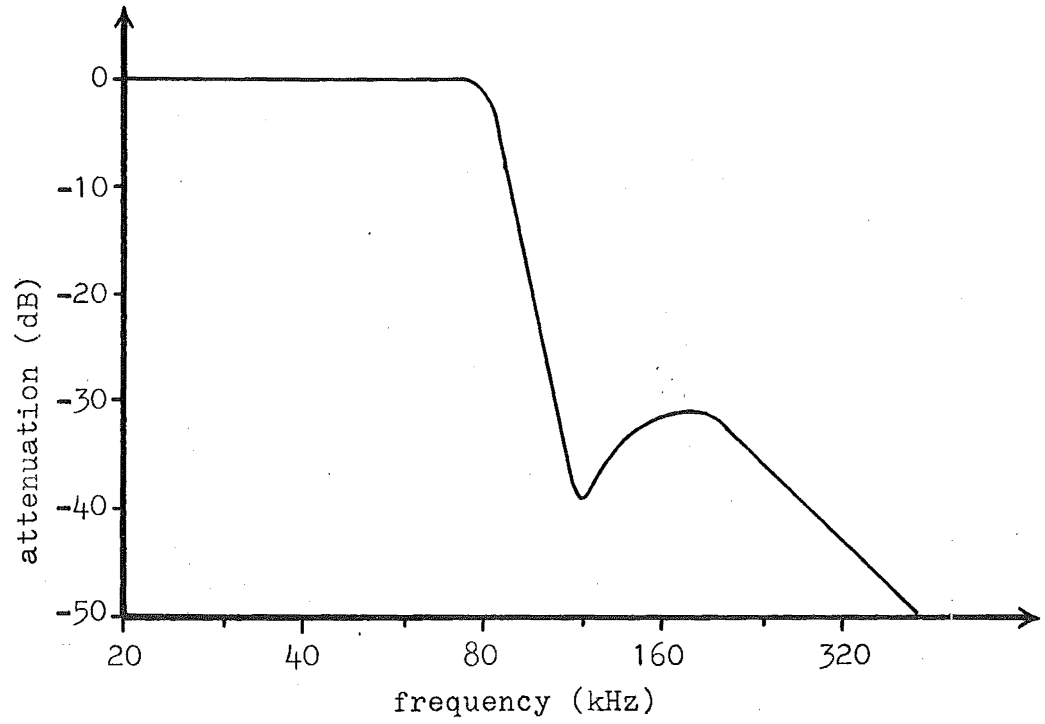

Figure 5.10. Transmitter LP filter characteristic.

The receiver filters are based on a high pass version of the Farrer[8] design. Here, a sharp cut-off is unnecessary, the more important requirement being the very high rejection of low frequency signals. The attenuation characteristic of the filter used in the receivers is shown in Fig. 5.11.

The actual circuit configurations used in the transmitter and receiver filters are shown in appendix V, part (ii).

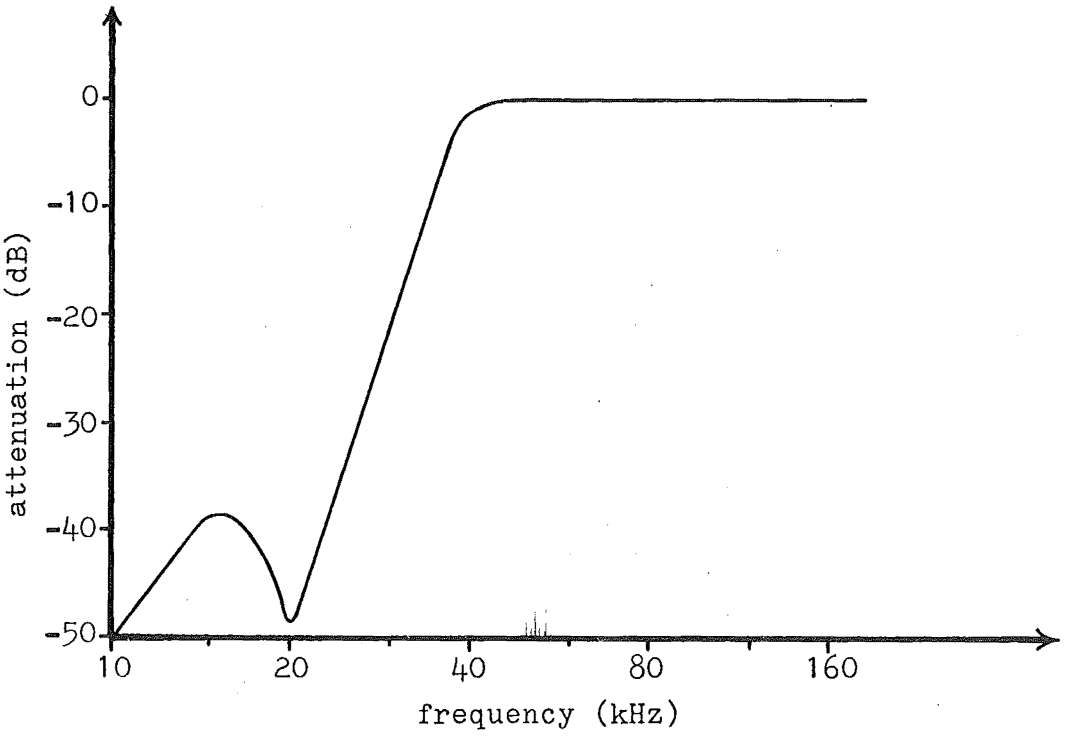

Figure 5.11. Receiver HP filter characteristics.

5.3.3 Transmitter and receiver gates

Series/parallel junction FET gates are used for both audio signal gating in the receivers and RF signal gating in the transmitter. Since FETs have reversible drain characteristics for small bi-directional drain-source voltages, a slowly increased or decreased gate voltage can produce slow turn-on or turn-off switching characteristics, without significant signal distortion. The series/parallel configuration gives extremely high on/off ratios (typically 60 dB).

Figure 5.12 shows the circuit arrangement necessary to produce the slow turn-on and turn-off characteristics, required for the receiver gates.

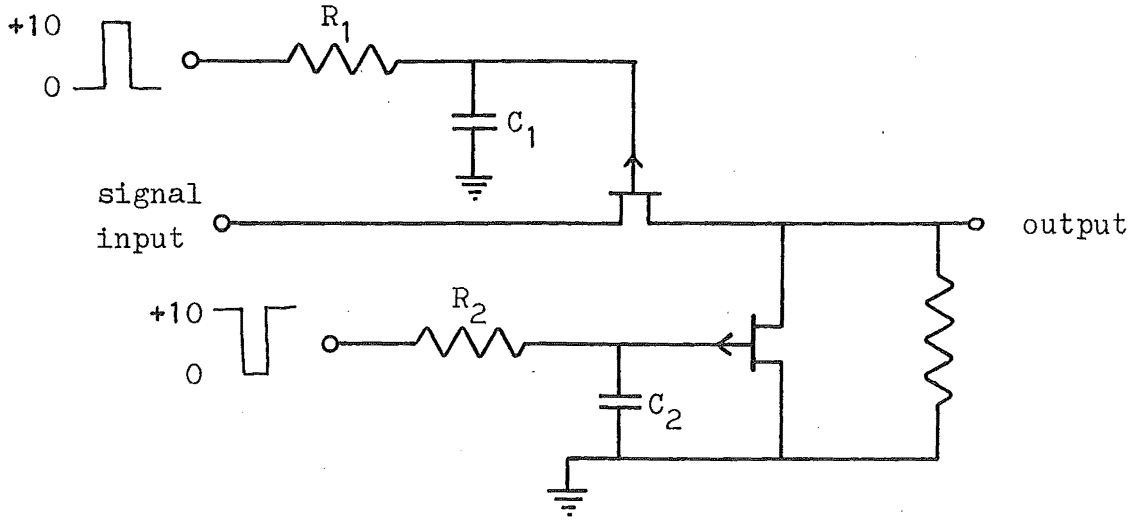

Figure 5.12. Slow turn-on, turn-off FET gate.

The switching signal levels and time constants R_1C_1 and R_2C_2 must be chosen so that T_1 turns on at approximately the same time and at approximately the same rate as T_2 turns off.

Diodes across resistors R_1 and R_2 may be used to achieve fast turn-off, slow turn-on characteristics, as are required by the transmitter gate.

Appendix V part (iii) contains the actual circuits used.

5.3.4 Demodulators

The most important requirement of the demodulator circuits is that they should generate the required audio difference frequencies without introducing spurious audio frequency components of significant magnitude. Spurious frequencies may be introduced by any non-linear effects in the demodulating elements.

To minimize intermodulation and harmonic distortion effects, switching modulators are essential. In order to suppress signal and carrier feedthrough, and hence to simplify

filtering problems in the receivers, double balanced modulators were considered desirable.

The performance of this type of demodulator may be analysed directly by the use of the convolution integral. Let the carrier signal be represented in the form

$$s(t) = -1 + 2\mathrm{rep}_{1/f_c}\,(\mathrm{rect}(2f_c t))$$

where rep and rect are the Woodward functions[9]. Let the input signal be represented in the form

$$u(t) = \cos 2\pi f_s t$$

Note: fixed carrier frequency, f_c, and fixed signal frequency, f_s, are assumed to simplify the analysis. This approximation is justifiable in view of the extremely slow frequency sweep rates involved. (The frequency changes by less than 1% per 100 cycles.)

The spectra of the carrier and signal waveforms are:

$$S(f) = -\delta(f) + \mathrm{comb}_{f_c}\,(\mathrm{sinc}f/2f_c),$$

$$U(f) = \tfrac{1}{2}(\delta(f-f_s) + \delta(f+f_s)).$$

The output spectrum of the demodulator, V(f) is given by the convolution integral of U, V:

$$V(f) = U*V = \int_{-\infty}^{\infty} [\mathrm{comb}_{f_c}\,(\mathrm{sinc}\frac{F}{2f_c}) - \delta(F)]$$

$$\tfrac{1}{2}[\delta(f - F - f_s) + \delta(f - F + f_s)]dF$$

$$= \tfrac{1}{2}\left\{\sum_{-\infty}^{\infty} (\mathrm{sinc}\,\tfrac{n}{2} \cdot \delta(f - f_s - nf_c)) + \sum_{-\infty}^{\infty} (\mathrm{sinc}\,\tfrac{n}{2}(f + f_s - nf_c))\right\}$$

$$- \delta(f - f_s) - \delta(f + f_s)$$

The following frequency components, thus, appear at the output:

$$\tfrac{1}{2}\ \text{sinc}\ \tfrac{1}{2}\ (\delta(f - f_s - f_c) + \delta(f + f_s - f_c) + \delta(f - f_s + f_c) + \delta(f + f_s + f_c))$$

(sum and difference frequencies) $(f_s \pm f_c)$

$$\tfrac{1}{2}\ \text{sinc}\ \tfrac{3}{2}\ (\delta(f - f_s - 3f_c) + \delta(f + f_s - 3f_c) + \delta(f - f_s + 3f_c) + \delta(f + f_s + 3f_c))$$

$(f_s \pm 3f_c)$

$$\tfrac{1}{2}\ \text{sinc}\ \tfrac{5}{2}\ (\delta(f - f_s - 5f_c) + \delta(f + f_s - 5f_c) + \delta(f - f_s + 5f_c) + \delta(f + f_s + 3f_c)$$

$(f_s \pm 5f_c)$

etc.

The above analysis shows that both signal and carrier are suppressed and the only terms which may be audible are terms such as $3f_s - 3f_c$, $5f_s - 5f_c$ which could arise if the input waveform contains harmonics. In the present application, such components will be very small in magnitude since the transmitted waveform is approximately sinusoidal and also since harmonic components will tend to be suppressed due to the higher attenuation of high frequencies in sea water.

Spurious frequency components may be produced by this type of demodulator in the following two ways:

(i) by non-linearity or the switching elements when they are in either the 'on' or 'off' state, or

(ii) by the influence of one or more of the input signal components on the switching time of the elements[9].

The latter of these effects may be minimized by the use of a carrier waveform with very rapid switching characteristics, and fast switching modulating elements. Non-linearity in either of the two operating states of the modulating elements depends mainly on the inherent characteristics of these elements and on the magnitude of the input signal.

The demodulator employed is shown in Fig. 5.13 (the detailed circuit diagram is contained in appendix V, part (iv)). MOS FETs were chosen since they have extremely linear 'on' characteristics and may be switched rapidly from the 'on' to the 'off' state.

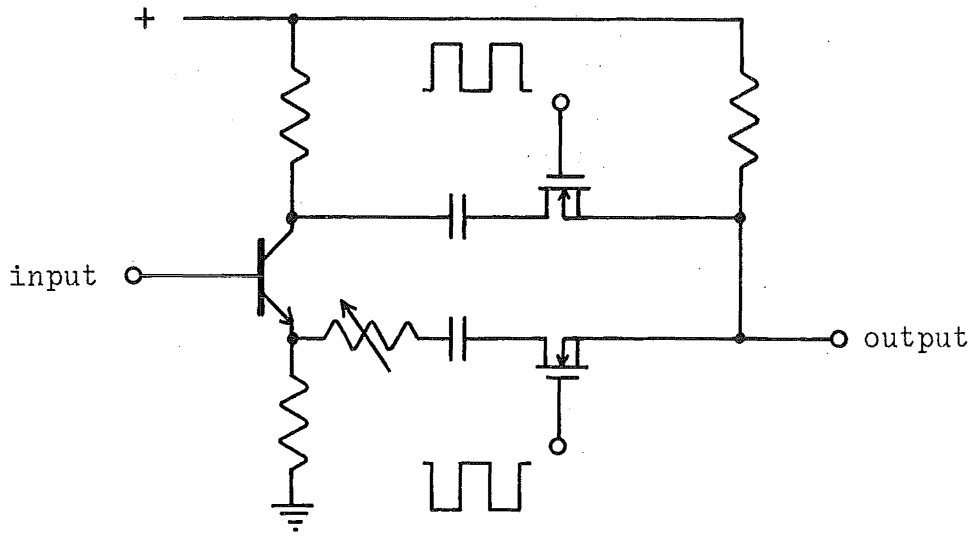

Figure 5.13. Simplified diagram of the demodulator circuit.

Fig. 5.14 shows the voltage-current characteristic measured for the particular MOS FET type (3N142) used in the design, for the 'on' state.

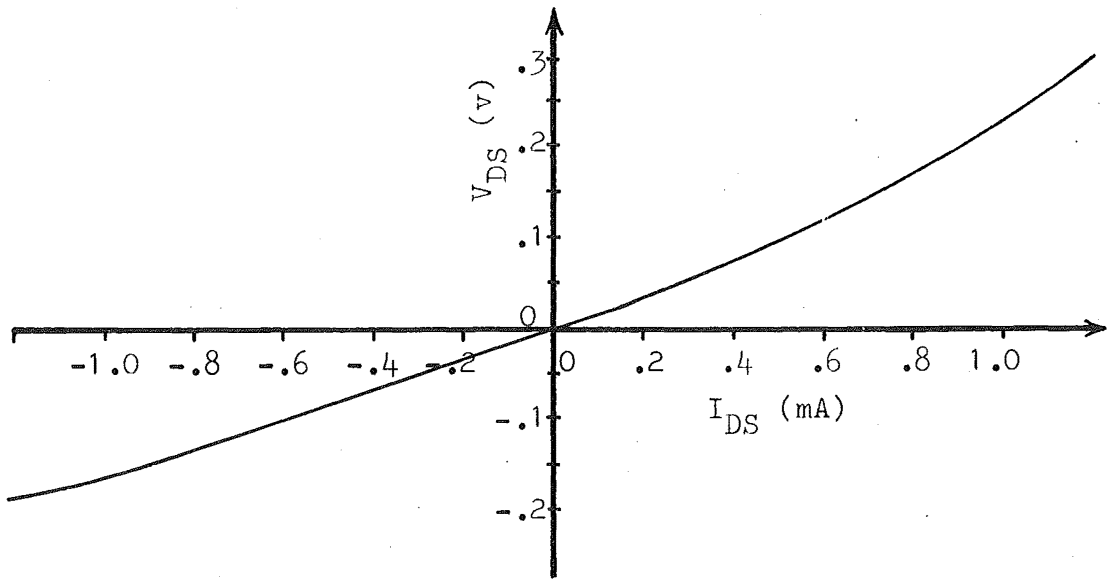

Figure 5.14. Measured voltage/current characteristic for the type 3N142 MOS FET.

The performance of the demodulator of Fig. 5.13 was determined with respect to harmonic and intermodulation distortion in the following manner:

(i) A fixed frequency carrier signal was applied and a single input signal of fixed frequency, but variable level, was injected. The harmonic distortion produced as a function of input level was then determined by spectrum measurements at the output of the shaping network. The results are presented in graphical form in Fig. 5.15. The 3rd harmonic component, as might be expected, was found to be the most significant.

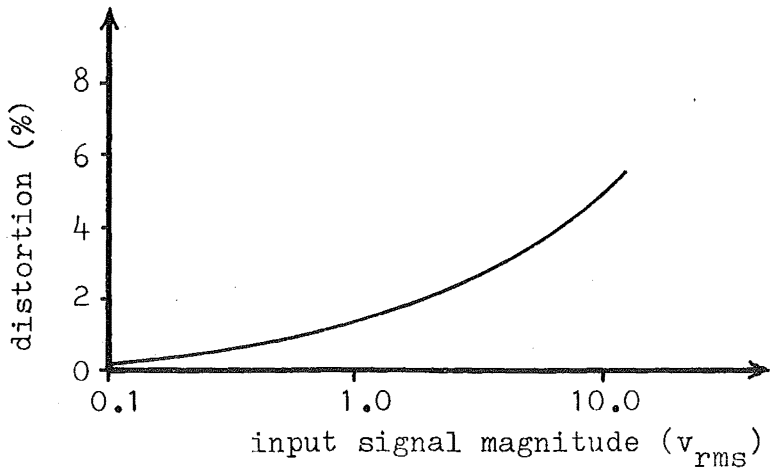

Figure 5.15. Harmonic distortion (%) as a function of input signal level.

(ii) Two input signals of slightly different frequencies were injected, one at a fixed low level, and the other at a variable level. The graph of Fig. 5.16 shows the variation of the total intermodulation distortion content expressed as a percentage of the primary signal magnitude, and as a function of the secondary signal magnitude. The results were obtained from spectrum measurements at the output of the shaping network.

The above measurements were made after the shaping network, since this network aggravates the effect of distortion by increasing the level of higher frequency products (see section 5.3.5).

In practice, the most troublesome signals from the point of view of causing the largest distortion products will be the largest signals present at the input. The largest signals at the input are due to (i) cross-talk between transmitting and receiving arrays and (ii) scattering from the sea surface close

to the arrays.

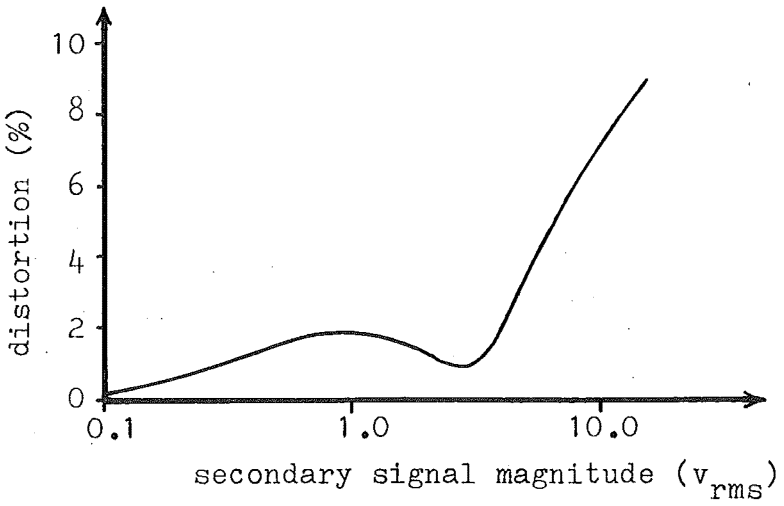

Figure 5.16. Intermodulation distortion expressed as a percentage of the primary signal magnitude, as a function of the secondary signal magnitude.

Since the cross-talk signal is at least 20 dB greater than any other signal received in normal operation, it imposes the greatest limitations on the demodulator performance. Even if the signal magnitude produced by cross-talk is restricted to less than 1 volt rms, intermodulation distortion problems are evident. Methods of reducing the effects of this particular problem are discussed in Ch. 8, section 8.3.

5.3.5 Shaping Networks

The main purpose of the shaping networks in the receivers is to boost the level of the audio signal produced by a given target as the target range increases. Since audio signal frequency is directly proportional to target range and since the propagation loss due to spreading varies as the fourth power of range, the audio gain must increase at a rate of approximately 12 dB per octave to compensate. (Since attenuation

is small over the working range of the system, compensation for attenuation loss is not considered necessary.) The shaping network performs the additional task of eliminating the high frequency signals present at the output of the demodulator. Although these frequencies are well above the audio band, suppression is necessary to prevent restriction of the dynamic range of the audio amplifier.

A transfer characteristic similar to that shown in Fig. 5.17 is required.

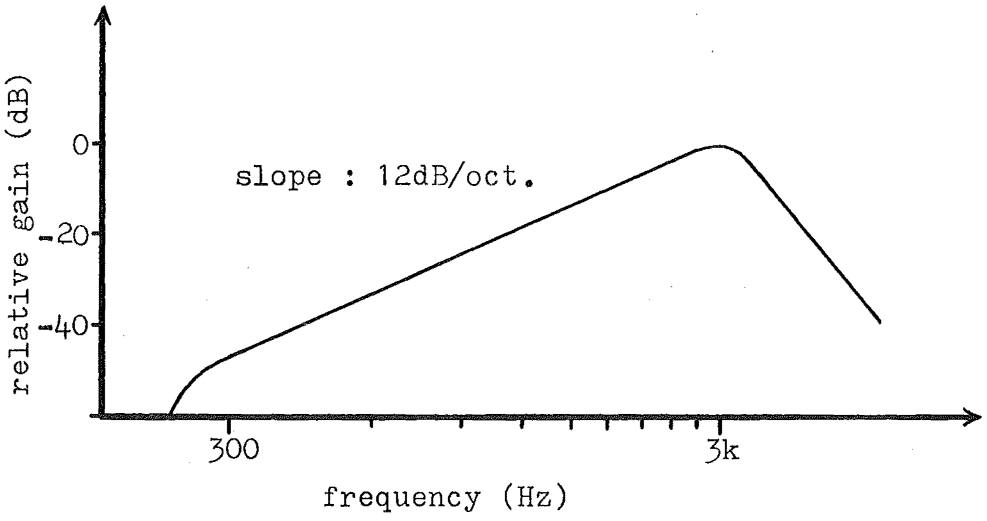

Figure 5.17. Required transfer function for the shaping networks.

Figure 5.17 implies an audio bandwidth of approximately 3 kHz and a dynamic frequency range from 300 Hz - 3 kHz, as was specified in Ch. 2, section 2.7.

A single L-C tuned amplifier with capacitative coupling at the input, as shown in Fig. 5.18, was employed. The overall frequency response characteristic of this shaping network is shown in Fig. 5.19.

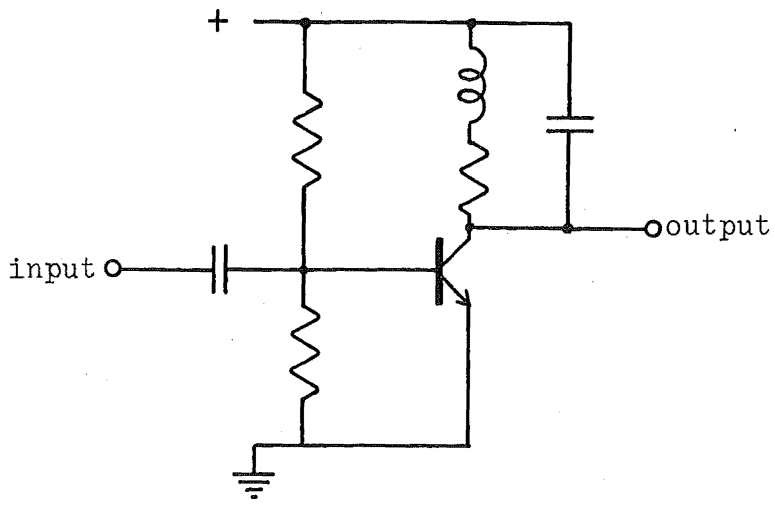

Figure 5.18. Circuit of the shaping network

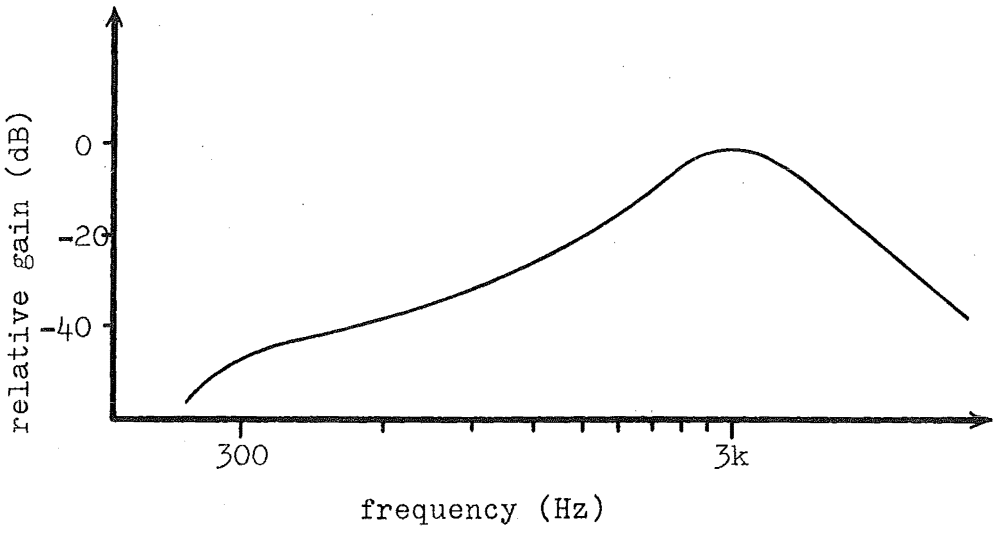

Figure 5.19. Measured overall response characteristic for shaping network.

The details of the circuit used are contained in appendix V, part (v).

5.3.6 Transmitter Power Amplifier

The power amplifier employs a conventional class AB common emitter transformer output stage with class AB common collector drivers. The complete circuit diagram and performance specification are contained in appendix V, part (vi).

Since the impedance of the transducer elements is largely capacitative over the entire operating frequency range, output efficiency is extremely low. In this prototype version of the system, this is of little consequence. In a commercial installation, however, this would be highly undesirable. One possible method for greatly increasing the output efficiency would be to use a controlled saturable reactance in parallel with the transducers, to tune out the capacitance. Since the sweep rate is slow, the effective permeability of the reactor could be controlled to achieve a resonance condition, throughout the entire sweep.

5.3.7 Timing Unit

The timing unit involves the straight-forward application of astable and monostable multivibrators in conjunction with a frequency divider (comprising a chain of jk flip-flops) to provide the required range of repetition periods. Figure 5.20 shows a block diagram of the unit. The 8 Hz astable provides a source of timing pulses to the divider chain, which provides pulse outputs at the seven repetition frequencies required. Monostables provide the gating and reset pulses required for the receiving and transmitting circuits. A delay monostable ensures that the receivers are blanked before the transmitter is blanked, as was discussed in section 5.2. Full circuit diagrams for this unit are contained in appendix V, part (vii).

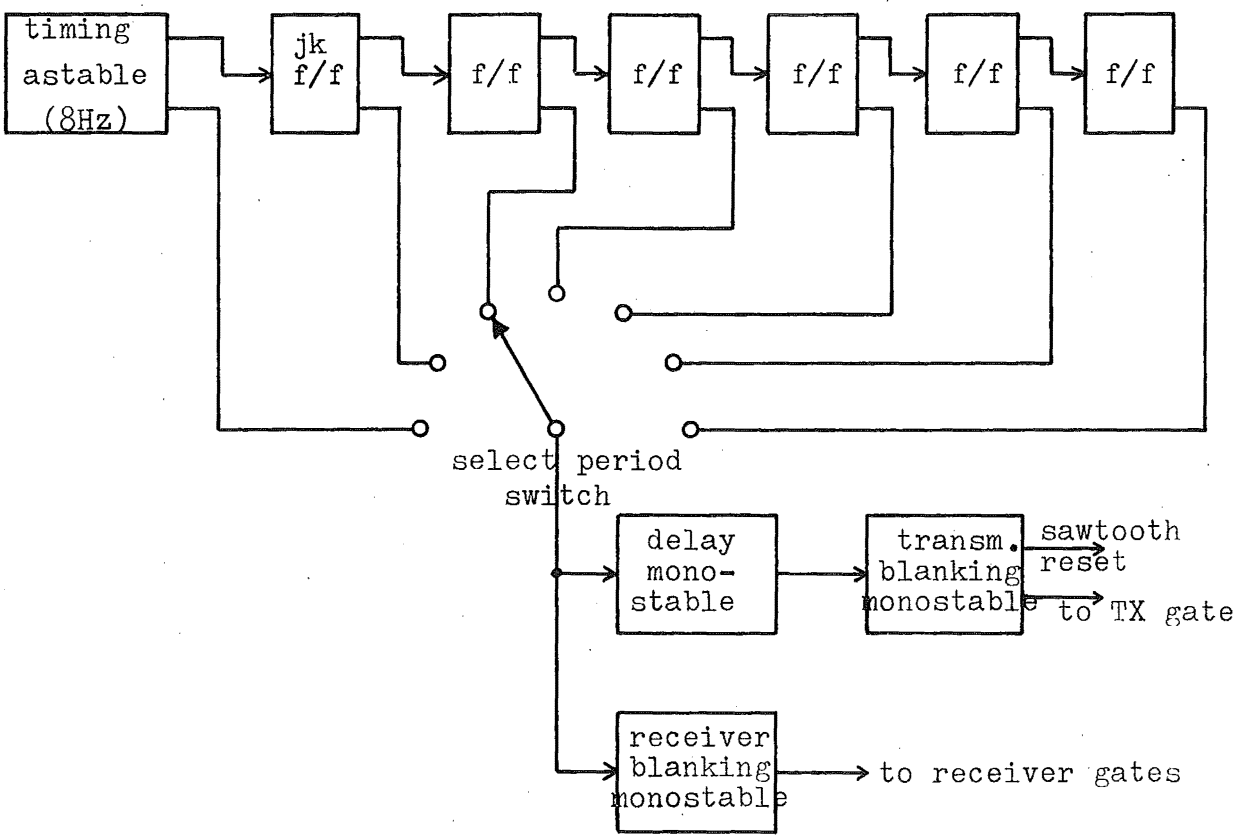

Figure 5.20. Block diagram of the Timing Unit.

5.3.8 Receiver Amplifiers

The designs of RF and audio amplifying stages are largely conventional, the principal requirements being, low input referred noise level, and low harmonic and intermodulation distortion.

The overall RF amplification is set by the maximum allowable input level at the demodulators (see section 5.3.4). The audio amplifier gain (which is variable to suit ambient noise conditions, etc.) must be sufficient to produce an

adequate listening level under all reverberation conditions, (see section 2.6).

The actual circuits used in these amplifiers are contained in appendix V, part (viii).

5.3.9 Beam Control Networks

As was discussed in chapter 4, in order to achieve constant transmitting and receiving array beamwidths in the horizontal plane, special shaping networks must be employed.

For the transmitting array, the sensitivity of the outer rows of elements is reduced using a network similar to that of Fig. 4.5, with the capacitance of the transducer serving as capacitor C. The phase error due to the effective 'loss' resistance of the transducer elements is sufficiently small to yield suitable horizontal beam patterns. The patterns of Fig. 4.12 were, in fact, measured using this arrangement. A tapped transformer at the output of the transmitter power amplifier provides signals for the upper and lower rows of the transmitting array at a lower level, to reduce side lobes in the vertical plane. Fig. 5.21 shows the circuitry used for driving the transmitter array.

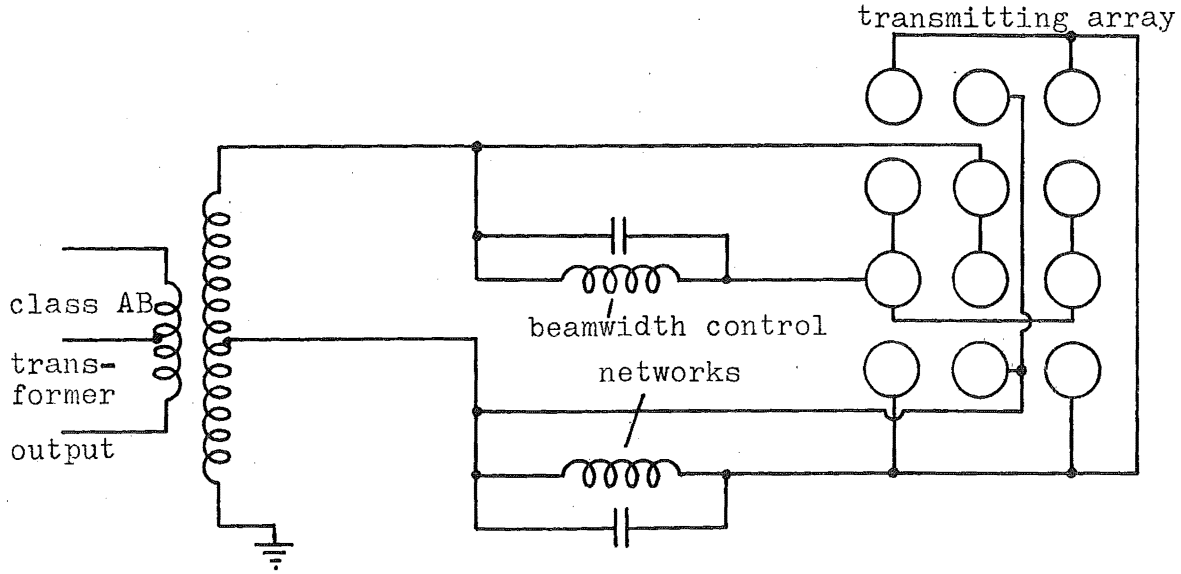

Figure 5.21. Transmitting array driving network.

For the receiving array, preamplification is necessary before the beamwidth control network to minimize noise introduced by this network. As with the transmitting array, two independent channels are required to allow constant beamwidth in the horizontal plane. MOS FETs are employed as the input elements in the preamplifiers to achieve low noise performance. The circuits used are contained in appendix V, part (ix). A schematic diagram showing the manner in which the elements of the array are connected is shown in Fig. 5.22.

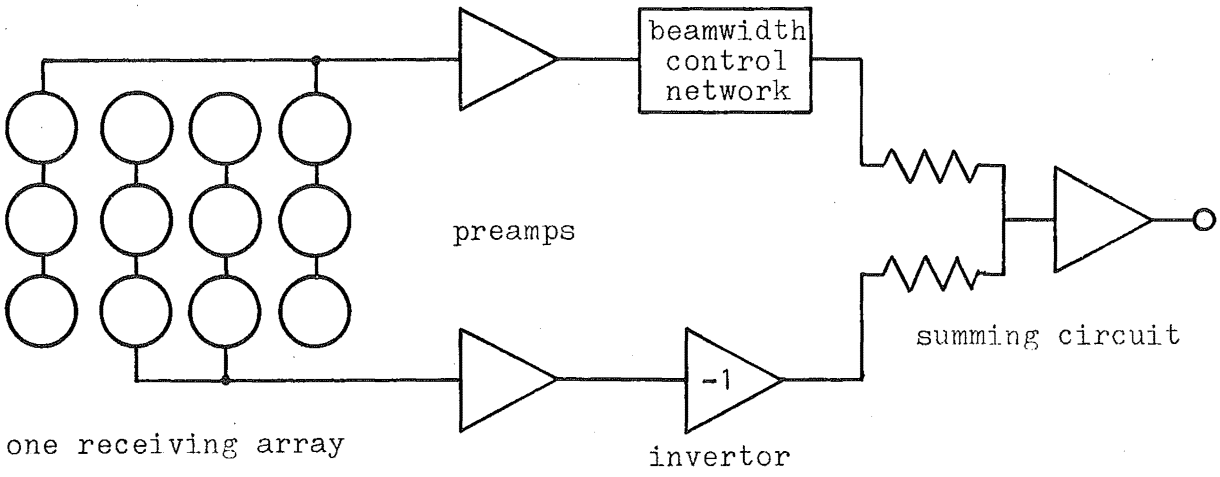

Figure 5.22. Schematic of receiving array electronics.

5.4 Operation in PCW Mode

A variable frequency PCW output for the testing of transducer elements and arrays (see appendix III) may be simply obtained by replacing the saw-tooth voltage feeding into the VCO with a variable DC level and providing an alternative gating circuit. It is desirable to synchronize the timing astable to the high frequency output of the VCO, so that transients produced by the gating are identical in successive pulses. This is achieved by first synchronizing an

intermediate frequency astable with the VCO, then synchronizing the timing astable to this. A block diagram showing the essential units required for operation of the sonar in the PCW mode is shown in Fig. 5.23.

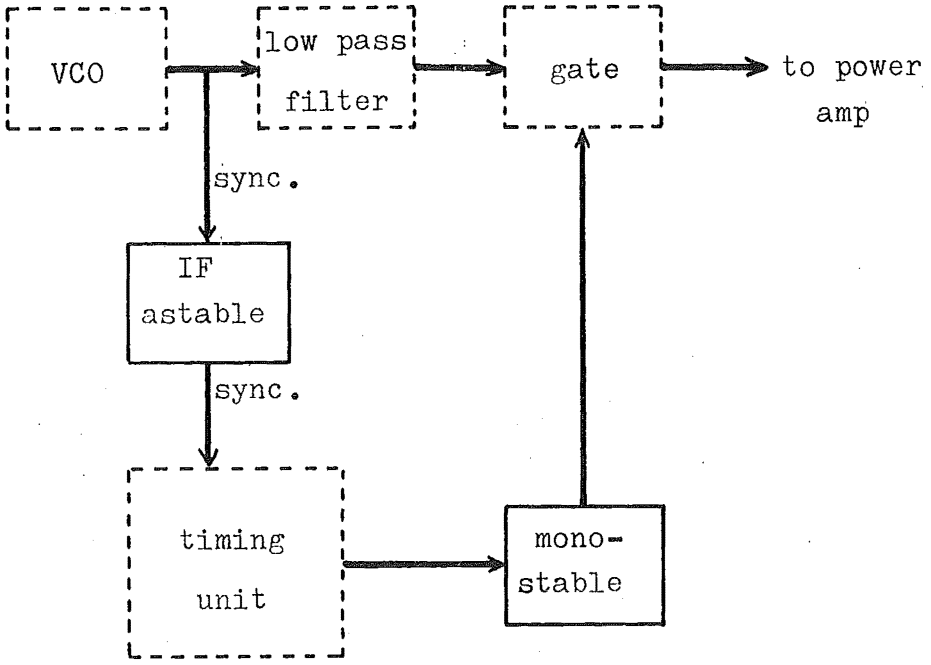

Figure 5.23. Additional elements (solid) required for the generation of a PCW transmission for the testing of transducer elements and arrays.

5.5 Construction Methods

For the prototype version of the electronics, plug-in printed circuit cards were used wherever possible to allow ease of access for servicing. Two separate units were employed, one containing the receivers and the transmitter (excluding the power amplifier), and the other containing the power amplifier and regulator units to provide constant voltage power supplies to the electronics. Two 12 volt lead-acid accumulators provide the power source (24 volts) for

the sonar. The prototype electronic units are shown in the top photograph of the title page to this chapter.

A single splash proof unit was built later to enable the sonar to be ship mounted, for an extended period of time. The lower photograph of the title page shows this unit.

5.6 Conclusions

The electronic circuits described in this chapter have undergone extensive trial periods at sea and have proved to function adequately and reliably. In these circuits expense and complexity have not been spared as they have been designed to best enable a study of the feasibility of the FM binaural sonar system. Whether or not the level of sophistication used in these circuits is necessary, for the satisfactory functioning of the system will not be known until a separate study into the minimum acceptable specification is conducted. Even with the present electronic design, the electronic package is neither bulky nor particularly expensive so that it is unlikely that the electronics will prove any obstacle to the successful development of the system as a commercial instrument.

5.7 References

1. L. Kay, "Ultrasonic Spectacles for the Blind", presented at the International Conference on Sensory Devices for the Blind, St Dunstans, England, 1966.
2. J.W. Horton, Fundamentals of Sonar, United States Naval Institute, Annapolis, Maryland, 1957.
3. von D. Maiwald, "The Calculation of Differential Thresholds by Means of a Functional Model" (in German) Acustica 18: 193 (1967).
4. C.E. Cook, "Effects of Phase Modulation Distortion on Pulse Compression Signals" IRE Int. Conv. Rec., Part 4, 174 (1962).
5. C.E. Cook, "Transmitter Phase Modulation Errors and Pulse-compression Waveform Distortion", Microwave J., 6: 63 (1963).
6. J.D. Hunter, "The Effects of Distortions in Linearly Frequency Modulated Sonar:, Dept. Memo. No. 42, Dept. of Elect. Eng., Univ. of Canterbury (1969).
7. W.H. Voelker, "Transistor Circuit Converts Voltage to Regulated Frequency", Electronics, Nov. 16, (1964), p73.
8. W. Farrer, "A Simple Active Filter with Independent Control over the Pole and Zero Locations", Electronic Eng. April (1961), p219.
9. P.M. Woodward, Probability and Information Theory with Applications to Radar, Pergamon Press, London, 1953, p28.

CHAPTER 6

SIGNAL DETECTION AND RECOGNITION IN THE AUDIBLE DISPLAY

CHAPTER 6

SIGNAL DETECTION AND RECOGNITION IN THE AUDIBLE DISPLAY

6.1 Introduction

In this chapter, the problem of detection and recognition of audio frequency signals in the binaural display, due to the presence of targets, is considered. Detection and recognition are intimately related operations in any sonar display, since in noisy conditions, the process of detection amounts to the process of recognizing the difference between noise, alone, and signal plus noise. Given that such a difference is correctly detected, the additional process of recognizing the target itself is normally necessary to determine whether or not the target is of interest. Considerably higher signal/noise ratios are necessary for this operation than are necessary for detection.

In the present sonar application, we are interested in one type of target only, namely the fish shoal. Unfortunately there is very little information published on the scattering properties of fish shoals although individual fish have received considerable attention. Due to this lack of information, predictions made in this chapter concerning the detection and recognition of fish shoal targets are necessarily based on a purely heuristic approach.

It should be stressed that this chapter represents a preliminary investigation of display characteristics only, and that a great deal of work remains to be done before any detailed specification of the display capability will be

possible. It is felt, however, that the work contained here could provide a basis for future investigation.

Specifically, this chapter reviews various published experimental results in the field of auditory detection of signals and relates these results to the signal and noise conditions at the audio display. Under certain simplifying assumptions, predictions of detection thresholds are made. Possible cues for the recognition of fish shoal targets are examined and an experiment to determine the effect of signal/noise ratio on target recognition is described.

6.2 Binaural Masking Effects

It was shown originally by Licklider[1] (using speech) and by Hirsh[2] (using tones), that the extent to which a signal is masked by white noise, when both signal and noise are presented binaurally, is critically dependent on the interaural phase relationships for both signal and noise. This discovery initiated extensive research programs in the field of binaural masking effects, and some of the most significant results of these studies will be reviewed, here, briefly. Tonal signals have received the most attention, and in addition to interaural phase difference effects, studies have been conducted into the effects of interaural time differences, interaural correlation differences, and interaural intensity differences. Other narrow band signals have been investigated to some extent. We consider firstly, the case of tonal signals.

Suppose that a 500 Hz tonal signal together with white noise is presented to both ears, such that there is no interaural difference in intensity or phase for either component.

(This stimulus condition is referred to as No-So.) The signal will be detected in the noise provided the signal/noise ratio* is at least 17 dB[3] for signal durations of 200 msec. or more.

If now the phase of the noise at one ear, is reversed, giving the Nπ-So condition, the detection threshold is found to drop by about 12 dB[4,5]. The Nπ-So condition, thus gives a masking level difference (MLD) of 12 dB with respect to the No-So condition. If the noise is now returned to the in-phase condition and the signal phase at one ear reversed (No-Sπ condition) an even higher MLD of 14 to 15 dB is observed. Reversal of both signal phase and noise phase, however, gives an approximately zero MLD. i.e. the Nπ-Sπ stimulus gives the same detection threshold as the No-So stimulus.

These results indicate that the binaural auditory system is able to effect cancellation of the noise to some extent, and in cases when the signal is not similarly affected, a release from masking is achieved. The fact that the No-Sπ stimulus gives the largest MLD (this has been confirmed by many workers) suggests that there is a <u>subtraction</u> of the neural signals originating from the two ears, rather than an addition. The results seem more reasonable in the light of the Jeffress[6] neural model of the binaural auditory system. Jeffress proposes that there is a spatially distributed system of neural delays arranged in opposition so that in the central region, nerve impulses originating from the two ears arrive with the same delay, but differential delays of increasing magnitude are achieved at points more remote from the central region. Assuming the subtraction hypothesis, then, the No-Sπ

*The signal/noise ratio, here, is defined as the difference between the signal pressure level (dB re 0.002 μbar) and the spectrum pressure level for the noise, expressed in the same way.

stimulus should produce maximum signal and minimum noise at the central neural region. In fact, if the hearing mechanism was perfect we would expect an infinite signal/noise ratio at this point. Since the release from masking is only 14 dB, we must assume that errors are introduced at some point in the system, possibly in the transduction of acoustic to neural energy. These errors effectively reduce the cross correlation of the neural noise signals so that cancellation during the subtraction process is incomplete. Since the signal is maximum at the central neural region, small errors will not greatly affect it. We may thus determine the effect of the errors on the cross correlation of the neural noise from the fact that there is a 14 dB difference between adding the noise sources ($N\pi$-$S\pi$) and subtracting them (No-$S\pi$).

Let the neural noise from the left hand ear comprise two components, a and b, and that from the right hand ear comprise a and c, so that 'a' represents the portion of the two noise signals which is perfectly correlated, b and c are the uncorrelated portions. (a, b and c: rms signal levels.) Addition thus gives a resultant rms noise level, n_a, of

$$n_a = \sqrt{(2a)^2 + b^2 + c^2}$$

and subtraction gives

$$n_s = \sqrt{b^2 + c^2}$$

Assuming b and c to be of the same magnitude, then and from the fact that $20 \log(n_s/n_a) = -14$ dB, we find that $b = c = a/\sqrt{12}$. The cross correlation coefficient, R_{LR}, is then given by[7]

$$R_{LR} = a^2/(a^2 + b^2) = 0.925$$

i.e. noise which is perfectly correlated at the ears gives rise to neural noise of correlation, 0.925.

The 500 Hz Nπ-So stimulus should give maximum signal/noise, after subtraction, at a neural region at which signals from one ear are delayed by 1 msec. with respect to signals from the other ear. There are thus two possible reasons for the reduction in the MLD observed for the Nπ-So stimulus, namely,

(i) that there is less nerve tissue in remote neural regions than in the central region. This possibility has been suggested[8] as a reason for the improved sensitivity of the auditory system to interaural time differences for sound sources near the median plane[9], or

(ii) that due to the neural time delay difference for signals from the two ears, the cross correlation of the two noise signals has been reduced. We assume that since only noise within the critical bandwidth[10] contributes to masking of the signal, the neural noise signals are band limited. Taking 50 Hz[11] as the value of the critical bandwidth at 500 Hz and using the expression of Rice[13] to evaluate the cross correlation after a one msec delay, we obtain a value of 0.995. This effect, alone would produce a difference in MLD of only 0.32 dB so it appears that reason (i) or some other process must account for most of the 2 dB reduction observed.

Suppose that the tonal signal is presented monaurally but the noise binaurally, in phase (No-Sm condition). We would expect the maximum signal/noise at the same neural region as for the No-Sπ condition but since the signal is now monaural, we would expect a 6 dB reduction in the maximum S/N and hence

the MLD. Egan[14] reports an MLD of 8.4 dB for this stimulus, which is 5.7 dB below his estimate of the MLD for the No-Sπ stimulus (14.1 dB). This appears to support the argument. For the Nπ-Sm stimulus, by applying a similar argument we would expect an MLD 6 dB below that for the Nπ-So stimulus. Egan's value of 5.1 dB for MLD for the Nπ-Sm condition is 6.9 dB below the value of 12 dB for the Nπ-So condition reported by Blodgett et al.[4]

When both signal and noise are presented monaurally, the MLD is observed to be approximately zero[14] as might be expected. This means that unless interaural disparities exist, two ears are no better than one for the detection of signals.

The effect of interaural phase shifts for both signal and noise, at 36^{o} intervals over the full 360^{o} range, has been investigated by Jeffress, Blodgett and Deatherage[5]. They found that the maximum MLD always occurs when the difference between the interaural phase shift for noise, and that for signal is 180^{o}. Another interesting characteristic of their results (on which they do not comment) is the shape of the MLD vs interaural phase shift for tone curves, for various interaural noise phase differences. A typical curve for noise No and varying signal phase difference is reproduced in Fig. 6.1. It is seen from the curve of Fig. 6.1 that the MLD rises rapidly as the signal phase difference shifts from the So position, but the variation in the region of maximum MLD (No-Sπ) is much slower. It appears from this curve that the neural delay network behaves in much the same way as would an electrical delay line, which was fed at opposite ends by the signals present at the two ears.

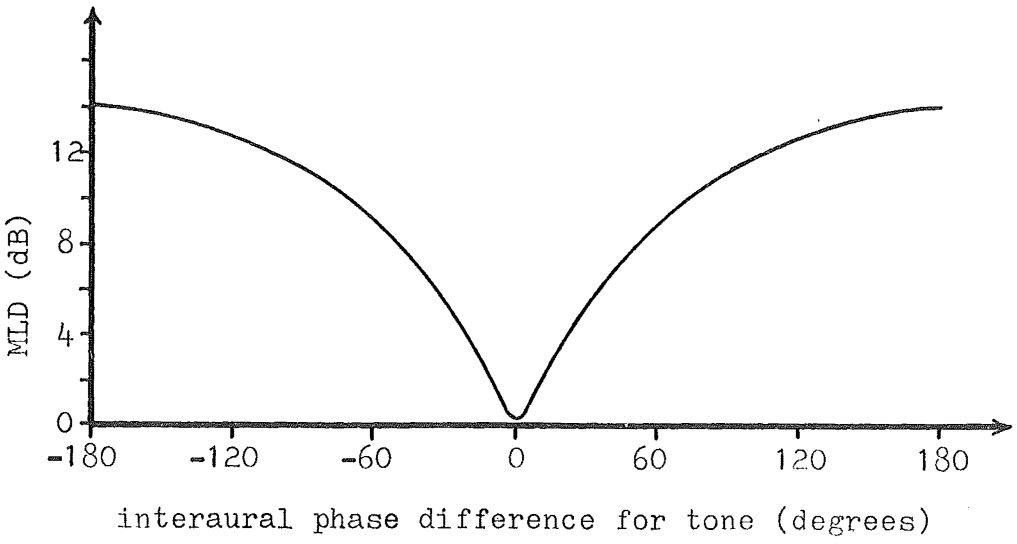

Figure 6.1. Variation of MLD with interaural phase difference for 500 Hz tone with noise in phase (No). After Jeffress et al.[5].

Fig. 6.2 (a) shows a schematic representation of such a model. An invertor has been included in one signal path so that the 'subtraction' process becomes one of addition (at any point along the delay line), which is more acceptable electrically. The signal and noise at each ear are assumed to pass through a critical band filter, centered at the signal frequency. If the tonal signals only were present, a standing wave would be set up with a maximum in the center for the Sπ stimulus and a minimum in the center for the So stimulus. The time averaged standing wave ratio (SWR) would be finite due to errors in the transduction process, but possibly quite high. If the noise signals only were present, a standing wave with a time averaged SWR of 14 dB would be set up with the distance between adjacent nodes being the same as that for the signal alone.

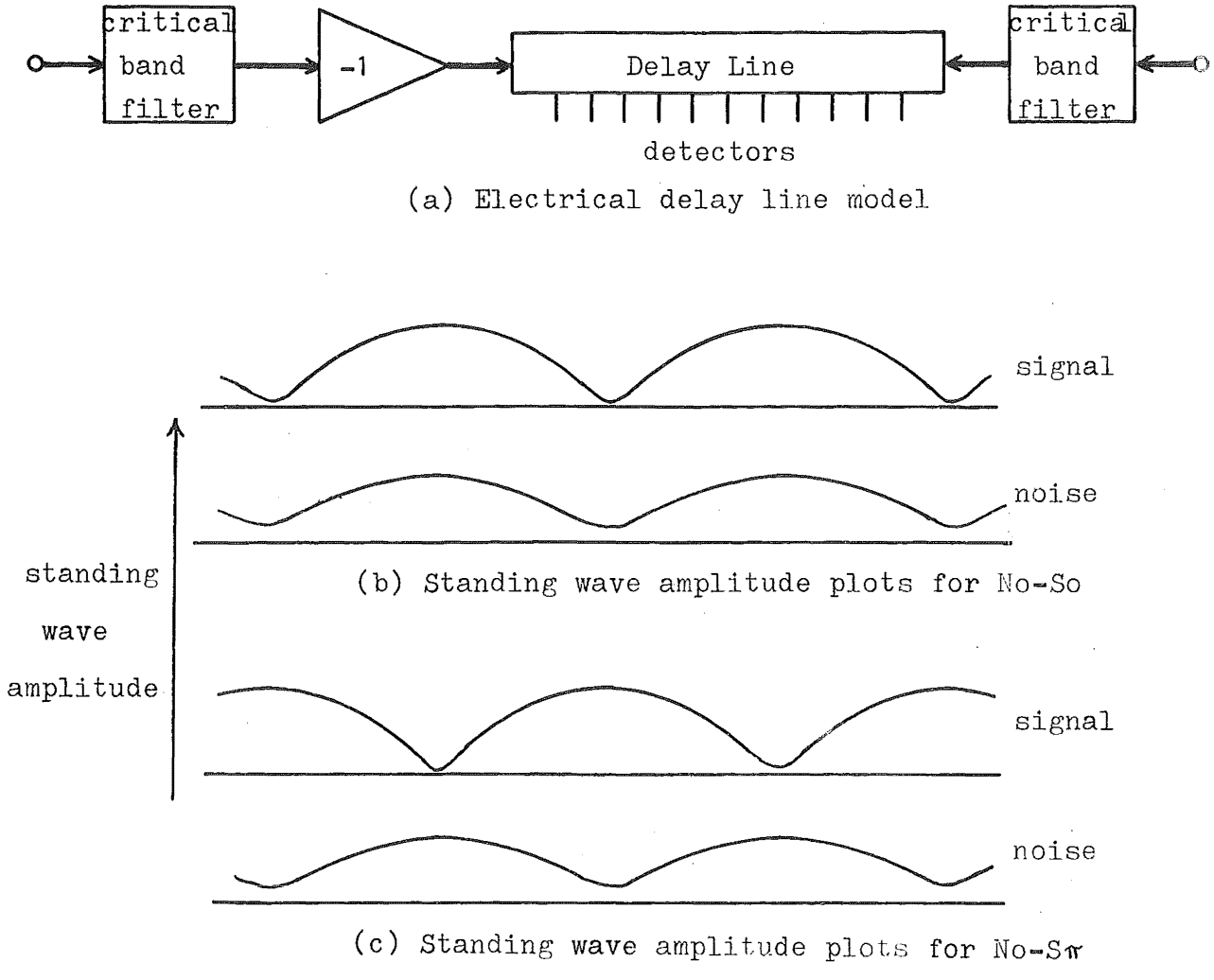

Figure 6.2. Delay line model of the binaural detection mechanism and standing wave plots for two stimulus conditions.

With both signal and noise present the two standing waves are superposed. Figure 6.2(b) shows the time averaged amplitude vs distance plots for the standing waves of signal alone and of noise alone for the No-So stimulus. Corresponding plots for the No-Sπ stimulus are shown in Fig. 6.2(c). From Fig. 6.2(b), assuming that the signal is just detectable for the

signal and noise magnitudes shown, it is clear that a small lateral shift of the standing wave for signal (due to an external phase shift) will produce a rapid rise in S/N at positions near the center. A similar shift for the No-Sπ condition (Fig. 6.2(c)), will not greatly affect the S/N. This is exactly the behaviour observed.

The effect of varying the interaural correlation of the noise at the two ears has been investigated in two ways. Licklider[1] and Robinson and Jeffress[15] reduced the cross correlation by adding uncorrelated noise at the two ears, whereas Jeffress, Blodgett and Deatherage[4,16] and Langford and Jeffress[17] used a single noise generator and delayed the noise to one ear by varying amounts. Fig. 6.3 shows typical results obtained with the two methods for the signal conditions, So and Sπ.

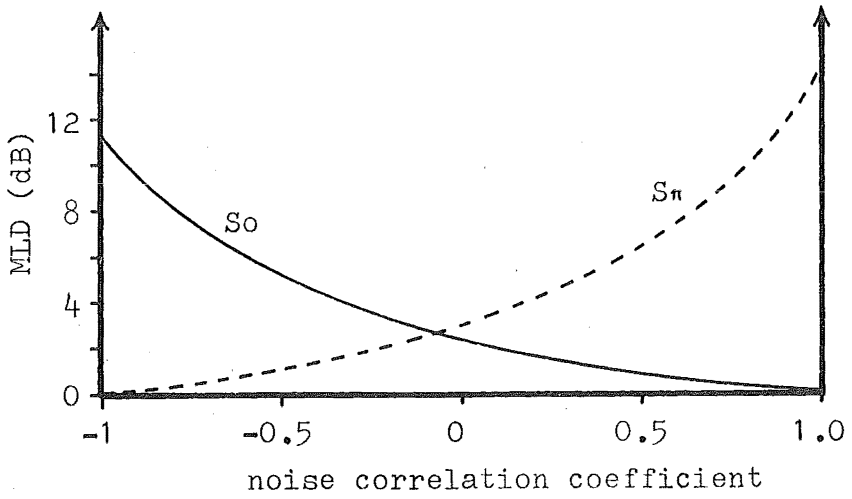

6.3.(a) MLD variation with interaural noise correlation. Correlation reduced by adding uncorrelated noise at the two ears. Data from Robinson and Jeffress[15].

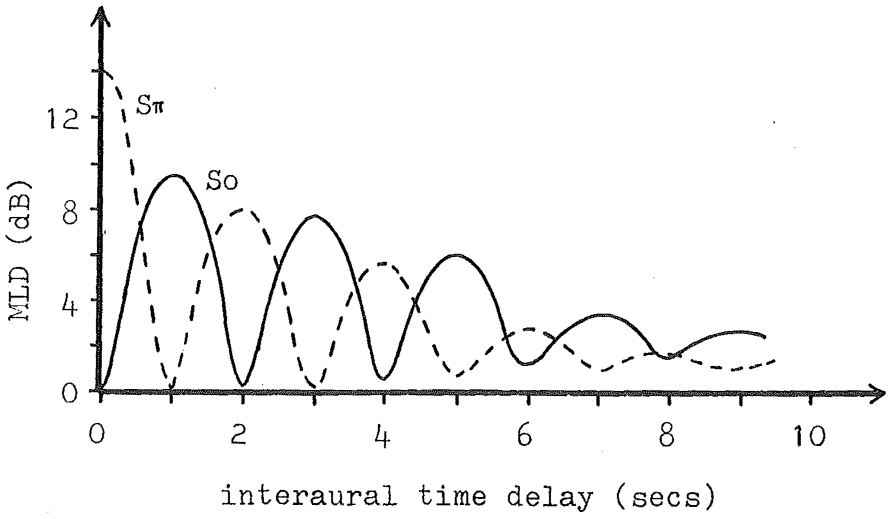

(b) MLD variation with interaural time difference for the noise at the two ears. Data from Langford and Jeffress[15] interpolated on the basis of results of Jeffress, Blodgett and Jeffress[4].

Figure 6.3. Effect of varying interaural noise correlation on MLD's.

Fig. 6.3(a) shows that for the So stimulus, the MLD reduces rapidly as the interaural noise correlation coefficient, R, departs from -1.0 (Nπ), but the variation is much slower as R approaches 0 (Nu). A further gradual reduction of MLD occurs as R is increased from 0 to 1.0 (No). Similar behaviour is observed for the Sπ stimulus condition. The form of variation shown here is consistent with that which would be observed with the delay line model, since a slight reduction in correlation would rapidly reduce the standing wave ratio for

noise but the variation would be much slower as the SWR approached unity (Nu condition). As the correlation is increased again with opposite polarity, the standing wave would again be formed, but this time the nodes would be in the same positions as those of the signal so the variation of MLD would be small. The 3 dB MLD observed when R = 0 is simply the difference between adding two highly correlated noise sources (Nπ) and two uncorrelated noise sources.

The variation of MLD as the time delay of the noise to one ear is varied, is oscillatory due to the fact that the noise is band limited by the critical band filters. According to Rice[13] the cross correlation coefficient of the two noise signals, R, is given by

$$R = \cos(2\pi f_s \tau).\sin(\pi W\tau)/\pi W\tau$$

where W is the critical bandwidth, f_s is the signal frequency, and τ is the time delay. In the delay line model, then, as the interaural time difference for noise is gradually increased, the standing wave for noise moves continuously to the right or left and the SWR progressively reduces due to the $\mathrm{Sin}(\pi W\tau)/\pi W\tau$ term in the expression for R. The results may be compared with those of Fig. 6.3(a) by determining the value of R at each of the maxima and plotting the maximum MLD's as a function of R. Langford and Jeffress[17] found that the agreement is excellent providing they assume a value of 100 Hz for the critical bandwidth at 500 Hz rather than the commonly assumed value of 50 Hz. They claim that this represents substantial evidence that the effective critical bandwidth for binaural listening is greater than that for monaural listening. Durlach[18] finds that the 100 Hz value for the critical

bandwidth, applied to his equalization-cancellation model of binaural masking, gives excellent results, adding support to Langford and Jeffress' argument.

The effect of intensity differences between the two ears for either noise or signal has been investigated by Egan[14]. He found that if the stimulus is initially No-So, and the signal at one ear gradually reduced until the No-Sm condition exists, the MLD rises smoothly to a final value of 8.4 dB. Alternatively, if the signal is initially No-Sπ, which gives, according to his measurements, an MLD of 14.1 dB, and the signal at one ear is progressively reduced, a smooth reduction of MLD occurs until the No-Sm value of 8.4 dB is reached. These results are consistent with the delay line model, but his results for the case of varying the interaural intensity difference for noise certainly are not. He shows that, even when the noise level at one ear is 40 dB below that in the other, but is in phase (No) an MLD of about 2 dB is observed for monaural signal stimulus. Blodgett, Jeffress and Whitworth[19] reported a similar effect, but there does not appear to be any quantitative explanation of this phenomena reported in the literature. There appears to be insufficient evidence for cases of different signal stimuli to even postulate a mechanism.

The effect of signal duration on binaural masking thresholds has been investigated by Blodgett, Jeffress and Taylor[4]. Their results show that the role of signal duration in binaural masking is very similar to that in monaural masking, suggesting that the same detection mechanisms are involved. The behaviour of the auditory system in detecting signals appears to be similar to that of an electronic

detector comprising a narrow band filter (critical bandwidth) followed by a rectifier and lossy integrator[20,21]. The time constant of the lossy integrator is generally accepted to be from 150 to 200 msec[21,22] so that as the signal duration is reduced below about 300 msec, the intensity must be increased to maintain a constant detection performance. For durations less than the integration time down to quite small durations, the signal energy required for a constant detection performance tends to remain constant[23]. For very small durations the signal energy must be increased, presumably since the signal bandwidth then exceeds the critical bandwidth.

Masking level differences have been found to be most pronounced at frequencies in the region of 250 Hz[16,24] and fall off gradually at higher frequencies and quite abruptly at lower frequencies. For the No-Sm stimulus, an MLD of 9.5 dB is observed at 250 Hz, but at 3 kHz this has reduced to about 2 dB and at 150 Hz it is negligible. Wilbanks and Whitmore[24] show that the variation of MLD with frequency may be accounted for by assuming the correlation of the neural noise is frequency dependent. This seems a reasonable explanation for the reduction of MLD with increasing frequency, since we can imagine that the errors introduced in the acoustic/neural transduction may be timing errors in the generation of nerve impulses. If this was so the errors would become more significant as frequency increased. It cannot, however, explain the drastic reduction of MLD below 250 Hz. It appears that a completely different mechanism is involved in this reduction.

Binaural masking effects for cases when the signal is complex, but occupies only a narrow bandwidth have received

little attention. Webster[25] and Rilling and Jeffress[26] used narrow band noise as the signal, and found that the masking level differences observed under various interaural stimulus conditions follow closely those observed for tonal signals. The absolute threshold S/N for detection of a narrow band noise signal occupying a bandwidth less than the critical bandwidth, appears to depend only on the signal power, and for equal power levels narrow band noise and tone appear equally detectable. Creelman[27] used trains of damped sinusoids as signals and observed the variation of listener detection efficiency as a function of signal bandwidth and duration. He found that when the signal bandwidth was large (highly damped condition) detection efficiency decreased with increasing duration, for constant signal energy. This suggests that the ear is incapable of effecting an integration of energy when the signal is intermittant. The results are not very conclusive and it appears that the signal waveform, in addition to the bandwidth, may be important in the detection of complex signals.

6.3 Stimulus Conditions for Reverberation and Signals in the FM Sonar

In the preceding section, it was shown that the auditory detection thresholds for signals in noise may be significantly influenced by the nature of the signals, or by interaural differences for either signals or noise. In this section, we examine the relevant characteristics of the audio signals derived from the FM sonar, due to the presence of targets and reverberation, in order to predict the detection conditions.

We consider, firstly, the stimulus conditions for the AF noise due to reverberation. In any particular detection situation, from the critical band theory[10] of auditory detection, we need only consider reverberant scatterers which contribute masking noise in a critical bandwidth centered on the signal frequency, f_s. Providing the velocity of individual scatterers is small, we may thus restrict interest to an annular region at range R, and of width ΔR, where,

$$\frac{\Delta R}{R} = \frac{\Delta f_s}{f_s}$$ (Δf_s is the width of the critical band at frequency, f_s)

Fig. 6.4 defines this region for boundary and volume reverberation for the case of idealized beam patterns.

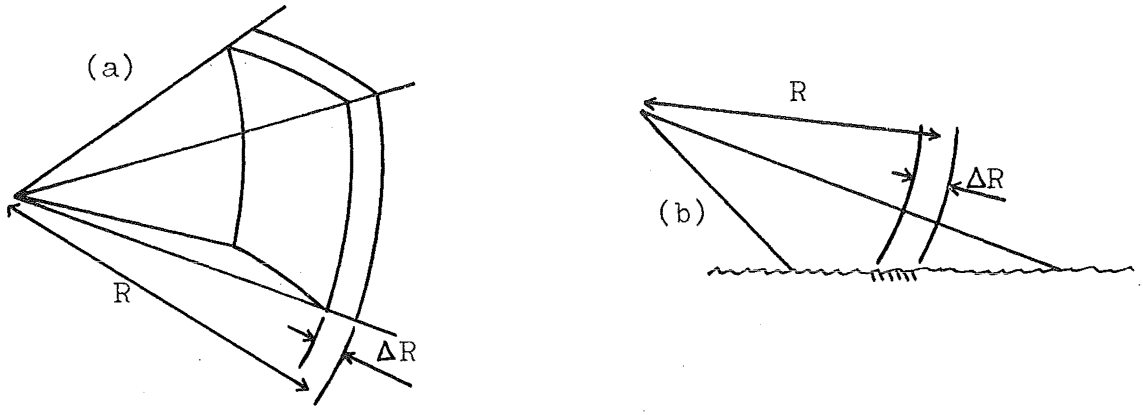

Figure 6.4. Scattering region for (a) volume and (b) boundary reverberation.

Let the scattering region in any given situation contain n scatterers, and assume that the i^{th} scatterer reproduces the transmitted signal, s(t) with amplitude a_i and onset time, t_i. With the idealized beams considered, then we may represent the noise signal V(t), at a receiver as the summation of the n

scattered signals. Thus,

$$V(t) = \sum_{i=1}^{n} a_i \, s(t-t_i) \qquad 6.1$$

where a_i, t_i are the stochastic variables of the process V(t).

We have assumed here that each scatterer reproduces the transmitted signal with constant amplitude and delay. In practice, since the duration of the transmitted signal is several seconds, it is very likely that both the position of the i^{th} scatterer and its scattering strength will vary within a single transmission. However, the representation of V(t) in the form of eqn 6.1 is nevertheless valid if the reverberation process can be considered stationary. The process can, in fact, be considered stationary provided (1) n is very large and that over any small time interval the average number of scattered signals at the receiver is constant, and (2) the average number of scatterers per unit volume is constant over the scattering region considered. These conditions are generally met for volume reverberation and often met for boundary reverberation. The conditions are not met in cases where there exist large individual scatterers.

From the central limit theorem and assumption (1), the probability distribution of V, p(V), is normal, i.e.

$$p(V) = \frac{1}{\sqrt{2\pi}\sigma_v} e^{\left(-\frac{V^2}{2\sigma_v{}^2}\right)}$$

where $\sigma_v{}^2$ is the variance of V.

The transmitted signal, s(t),may be represented in the form (see Ch. 1)

$$s(t) = s_o(t)\ e^{j2\pi(f_2 t - \frac{1}{2}\mu t^2)} = s_o(t)\ e^{j\phi(t)}$$

where $s_o(t)$ is the envelope, assumed to be rectangular and given by:

$s_o(t) = \text{rect}(t/T - \frac{1}{2})$, T is the duration of a single transmitted pulse.

The received signal is, then

$$V(t) = \sum_{i=1}^{n} a_i s_o(t-t_i)\ e^{j2\pi(f_2(t-t_i) - \frac{1}{2}\mu(t-t_i)^2)}$$

$$= \sum_{i=1}^{n} a_i s_o(t-t_i)\ e^{j\phi(t)}\ e^{-j\phi(t_i)}\ e^{j2\pi\mu t_i t}$$

The audio signal produced by the demodulation of V(t) with the transmitted signal is given by

$$V'(t) = s^*(t)V(t) = \sum_{i=1}^{n} a_i \text{rect}\left(\frac{t - \frac{T}{2} - \frac{1}{2}t_i}{\frac{T}{2} - t_i}\right)\ e^{-j\phi(t_i)}\ e^{j2\pi\mu t_i t}$$

Since in the present application, $t_i \ll T$, we may neglect the overlap loss thus

$$V'(t) \doteq s_o(t) \sum_{i=1}^{n} a_i\ e^{-j\phi(t_i)}\ e^{j2\pi\mu t_i t} \qquad 6.2$$

It is clear from eqn 6.2 that the stochastic variables, t_i, a_i of the reverberation process are retained in the demodulation process, so that the statistics of the audio signals are identical to those of the scattered signals at the receiving array. Furthermore, since the frequencies, μt_i, are restricted to lie in the range Δf_s centered at frequency f_s, V'(t) may be represented in quasi-harmonic form,

$$V'(t) = E(t)\ e^{j2\pi f_s t}\ e^{j\theta(t)}$$

where E(t) is the envelope and $\theta(t)$ is the phase. Also since V' is normally distributed, E(t) is Rayleigh distributed and $\theta(t)$ is uniformly distributed, i.e.

$$p(E) = \frac{E}{\sigma_v^2} \cdot e^{-(E^2/2\sigma_v^2)}$$

$$p(\theta) = 1/2\pi \qquad 0 \leq \theta \leq 2\pi$$

From the above analysis we may conclude that provided certain conditions are met, the AF noise within a critical bandwidth due to reverberation, is statistically identical to band limited white noise, and that experiments in auditory detection of signals against white noise will be relevant to the sonar detection problem.

We next consider the relationship between the two audio noise signals derived from the scattered signals incident at two receiving arrays, which are physically separated, and whose beams are splayed. This corresponds to the array configuration used in the FM sonar under discussion. Fig. 6.5 shows the geometry of the two receiving arrays having separation d and splay angle $\Delta\gamma$.

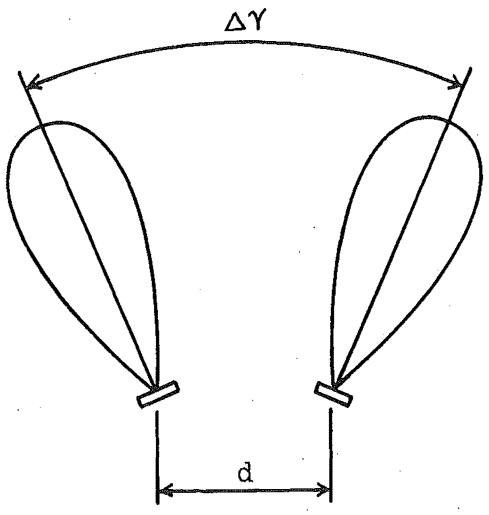

Figure 6.5. Geometry of the two receiving arrays.

The signal from the i^{th} scatterer, which lies at an angle α_i to the normal of the transmitting array has a different onset time at the two receivers (due to their spatial separation) and a different amplitude (due to the splay of the directivity patterns). We shall consider, here, a two dimensional model of the scattering region, assuming that the scatterers lie very near to the plane containing the normals to the three arrays. This approach is justified since we are interested only in differences between the signals at the two arrays and such differences are unaffected by the angular extent of the scattering region in the vertical plane. Also, to further simplify the situation, we shall consider the following two cases separately:

i) The receiving arrays separated by distance, d, but having omnidirectional directivity patterns, and

ii) The receiving arrays coincident, but having the appropriate directivity patterns splayed at angle $\Delta\gamma$.

The analysis used here is based on that used by Ol'shevskii[28] for a narrow band transmission, but extended to the present broad band application.

Case i) Omnidirectional receivers, separation d.

Referring to Fig. 6.6, consider the scattering region to be divided into a number of cells of equal, but small angular width, $\Delta\alpha$. Let the number of such scattering cells be m, and assume that the directivity pattern of the transmitting array in the horizontal plane is given by $D_T(\alpha)$. By summing the signals from each cell with weighting $D_T(\alpha_k)$ over all k, we may obtain expressions for the signals, $V_L(t)$, $V_R(t)$ at the left and right arrays, respectively.

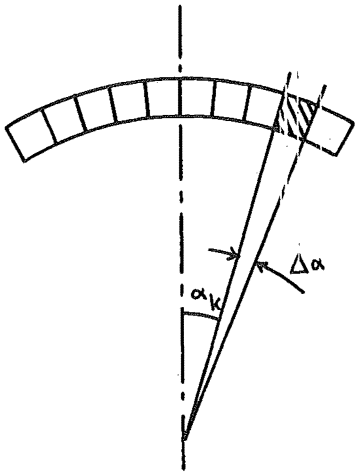

Figure 6.6. Geometry of the scattering cells.

Thus,

$$V_L(t) = \sum_{k=1}^{m} D_T(\alpha_k) \sum_{i=1}^{n} a_i s(t - t_i - \Delta t_k/2)$$

$$V_R(t) = \sum_{q=1}^{m} D_T(\alpha_q) \sum_{j=1}^{n} a_j s(t - t_j + \Delta t_q/2)$$

where m is the average number of scatterers in each cell, Δt_k is the difference in onset time at the two receivers, for signals from scatterers in the k^{th} cell, and is given by:

$$\Delta t_k = d \sin(\alpha_k)/c$$

The audio signals, $V_L'(t)$, $V_R'(t)$, derived from $V_L(t)$, $V_R(t)$ and presented to the left and right ears are:

$$V_L'(t) = s_o(t) \sum_{k=1}^{m} D_T(\alpha_k) \sum_{i=1}^{n} a_i \, e^{-j\phi(t_i+\Delta t_k/2)} \, e^{j2\pi\mu(t_i+\Delta t_k/2)t}$$

$$V_R'(t) = s_o(t) \sum_{q=1}^{m} D_T(\alpha_q) \sum_{j=1}^{n} a_j \, e^{-j\phi(t_j-\Delta t_q/2)} \, e^{j2\pi\mu(t_j-\Delta t_q/2)t}$$

The interaural cross correlation function, $\psi_{LR}(d)$ is given by:

$$\psi_{LR}(d) = \langle V_L'(t).V_R'(t) \rangle$$

Since for $k \neq q$ or $i \neq j$, we have independent random events, there will be no contribution to the cross correlation function, then

$$\psi_{LR}(d) = \langle s_o^2(t) \sum_{k=1}^{m} D_T^2(\alpha_k) \sum_{i=1}^{n} a_i^2 \; e^{-j2\pi(f_2-\mu t)\Delta t_k} \; e^{-j2\pi\mu\Delta t_k t_i} \rangle \qquad 6.3$$

The first exponential term, here, is a phase term dependent on the instantaneous signal frequency, $(f_2 - \mu t)$ and the difference in the arrival times, Δt_k, for signals scattered from the k^{th} cell. The second exponential term defines the phase variation among scatterers of the k^{th} cell as a function of their radial position (determined by t_i). Since equation 6.3 contains the oscillatory time varying term, $e^{+j2\pi\mu\Delta t_k t}$, we would expect that the time averaged cross correlation would be zero. However, the period of oscillation will be very large for cells near the central region and in the case of slow sweep rates (long range settings), even at the extremity of the main lobe of the transmitting array pattern, the period will be greater than one second. The human auditory system is incapable of integrating signals for durations in excess of about 0.2 sec., so we are interested here in a short term averaged cross correlation function only. We thus write:

$$\psi_{LR}(d,t) = \langle s_o^2(t) \sum_{k=1}^{m} D_T^2(\alpha_k) \; e^{-j2\pi(f_2-\mu t)\Delta t_k} \sum_{i=1}^{n} a_i^2 \; e^{-j2\pi\mu\Delta t_k t_i} \rangle \qquad 6.4$$

Since we have assumed the number of scatterers to be very large and their distribution to be uniform, we may approximate the expression of eqn 6.4 by the integral expression:

$$\psi_{LR}(d,t) = \eta c \int_{-\pi/2}^{\pi/2} D_T^2(\alpha)\ e^{-j2\pi(f_2-\mu t)\Delta t(\alpha)} \cdot \langle a^2 \rangle \int_{t_1}^{t_1+\delta t_1} e^{-j2\pi\mu\Delta t(\alpha)t'}\ dt'\ d\alpha$$

where $\langle a^2 \rangle$ is the variance of the process, a_i, t_1 is the onset time of the closest scatterer in the region considered, δt_1 is the total range of onset times for the scattering region, η is the average number of scatterers per unit range per unit angle, c is the velocity of propagation and t' is the continuous variable replacing t_i. Since the critical bandwidth is typically of the order of 5% of the center frequency, $\delta t_1 \approx$ 5% of t_1 so the phase, $2\pi\mu\Delta t(\alpha)t'$ changes by only about 30^o over the range from t_1 to $t_1 + \delta t_1$. We may thus replace the second integral by:

$$\delta t_1\ e^{-j2\pi\mu\Delta t(\alpha)t_1}$$

This yields,

$$\psi_{LR}(d,t) = \eta c \delta t_1 \langle a^2 \rangle \int_{-\pi/2}^{\pi/2} D_T^2(\alpha)\ e^{-j2\pi(f_2 - \mu(t-t_1))\Delta t(\alpha)}\ d\alpha$$

Since $\mu t_1 << f_2 - \mu t$, we may neglect it. The cross correlation coefficient, $R_{LR}(d,t)$ is thus given by:

$$R_{LR}(d,t) = \frac{\int_{-\pi/2}^{\pi/2} D_T^2(\alpha)\ e^{-j2\pi(f_2 - \mu t)\Delta t(\alpha)}\ d\alpha}{\int_{-\pi/2}^{\pi/2} D_T^2(\alpha)\ d\alpha} \qquad 6.5$$

Figure 6.7 shows the variation of $R_{LR}(d,t)$ for case i) as a function of t, the time measured from the commencement of the sweep, and for two values of d : 0.34m and 0.22m, these being

the values for the original array configuration and for the single housing configuration (see Ch.4 title page). The integrals were evaluated numerically using the measured directivity pattern for the transmitting array.

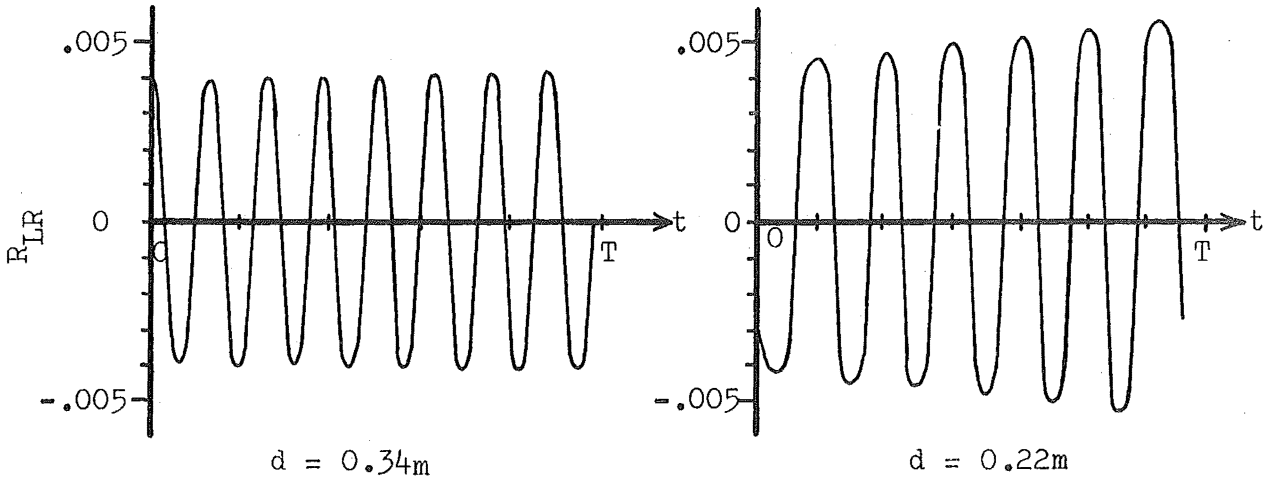

Figure 6.7. Cross correlation coefficient, $R_{LR}(d,t)$ for case i)

<u>case ii) Coincident receivers, directivity patterns splayed by angle $\Delta\gamma$.</u>

Since the directivity patterns of the two receiving arrays are identical, we may represent them in the form:

$$D_L(\alpha) = D(\alpha + \Delta\gamma/2)$$

$$D_R(\alpha) = D(\alpha - \Delta\gamma/2)$$

Setting $t_k = 0$ in eqn 6.3 and taking into account the above directivity patterns, we obtain:

$$\psi_{LR}(\Delta\gamma) = \langle s_o^2(t) \sum_{k=1}^{m} D_T^2(\alpha_k)\, D_L(\alpha_k)\, D_R(\alpha_k) \sum_{i=1}^{n} a_i^2 \rangle$$

This leads to the following integral approximation to $R_{LR}(\Delta\gamma)$.

$$R_{LR}(\Delta\gamma) = \frac{\int_{-\pi/2}^{\pi/2} D_T^2(\alpha)\, D(\alpha+\Delta\gamma/2)\, D(\alpha-\Delta\gamma/2)\, d\alpha}{\int_{-\pi/2}^{\pi/2} D_T^2(\alpha)\, D^2(\alpha)\, d\alpha} \qquad 6.6$$

Figure 6.8 shows the variation of $R_{LR}(\Delta\gamma)$ over the range from 0° to 60°.

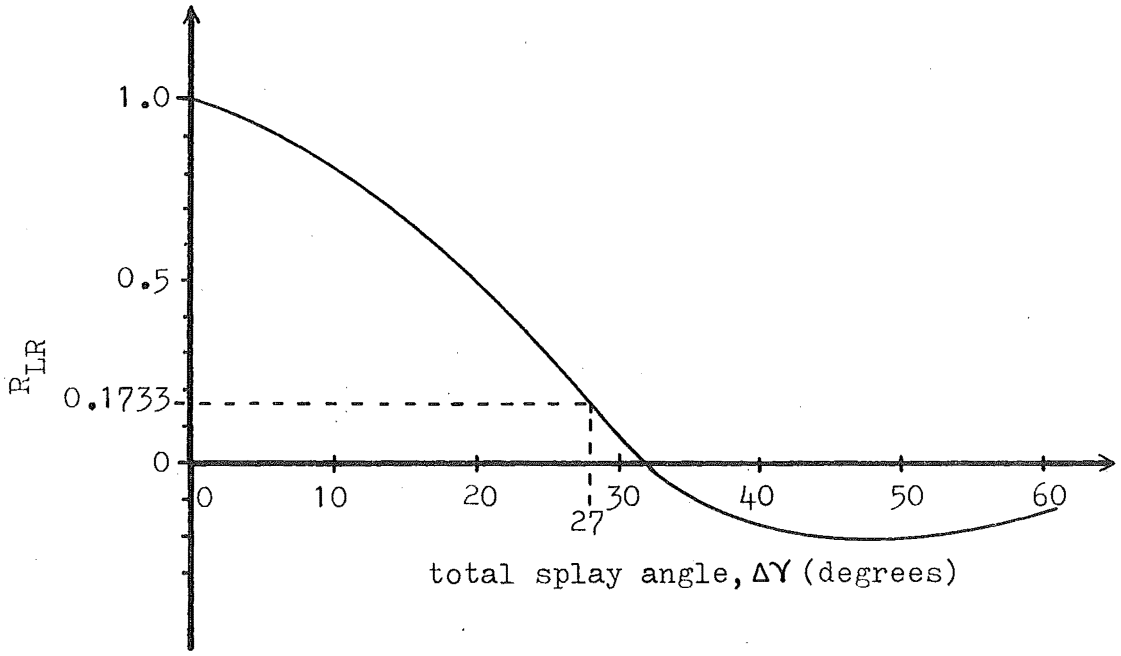

Figure 6.8. Variation of $R_{LR}(\Delta\gamma)$ over the range 0° to 60° for case ii).

It is clear from Fig. 6.7 that with a spatial separation of 0.22 m (9λ at 60 kHz) or 0.34 m (14λ), cross correlation of noise signals derived from the two omni-directional arrays is negligible over the entire sweep period. Figure 6.8 shows that even for coincident arrays, the cross correlation coefficient for noise signals falls rapidly with increasing splay angle. For the 27° splay angle used in the

sonar (see chapter 2) R_{LR} is 0.1783. The combined effect of both splay and spatial separation may be estimated as the product of the cross correlation coefficients for the two individual cases. We may thus assume that the interaural correlation of background noise signals in the sonar display is effectively zero.

We next consider the stimulus conditions for signals due to the presence of targets in the region illuminated by the sonar. Consider a single specular target at constant range, R, and at an angle, α, to the normal of the transmitting array. The signals at the left and right receiving arrays, due to this target will be:

$$V_L(t) = a\ D_T(\alpha)\ D(\alpha + \Delta\gamma/2)\ s(t - t_o - \Delta t(\alpha)/2)$$

$$V_R(t) = a\ D(\alpha)\ \ D(\alpha - \Delta\gamma/2)\ s(t - t_o + \Delta t(\alpha)/2)$$

Where t_o is the onset time of the signal measured at the point midway between the centers of the two receiving arrays, $\Delta t(\alpha)$ is the difference in onset time for signals at the left and right arrays, a is the amplitude of the signal return.

With the same signal notation as previously, the audio signals derived from the signals at the two arrays are:

$$V_L'(t) = s_o(t)\ a\ D_T(\alpha)\ D(\alpha+\Delta\gamma/2)\ e^{-j\phi(t_o+\Delta t(\alpha)/2)} \times e^{j2\pi\mu(t_o+\Delta t(\alpha)/2)t}$$

$$V_R'(t) = s_o(t)\ a\ D_T(\alpha)\ D(\alpha-\Delta\gamma/2)\ e^{-j\phi(t_o-\Delta t(\alpha)/2)} \times e^{j2\pi\mu(t_o-\Delta t(\alpha)/2)t}$$

The short term averaged cross correlation function is then

$$\psi_{LR}(\alpha,t) = a^2 D_T^2(\alpha) D(\alpha+\Delta\gamma/2) D(\alpha-\Delta\gamma/2) e^{-j2\pi(f_2-\mu t)\Delta t(\alpha)} \times e^{-j2\pi\mu\Delta t(\alpha)t_o}$$

Since we are not concerned with the effects of amplitude difference on the cross correlation coefficient, i.e. we consider two signals with identical waveforms to be perfectly correlated, regardless of any difference in magnitude, the cross correlation coefficient, $R_{LR}(\alpha,t)$ is

$$R_{LR}(\alpha,t) = \frac{D(\alpha+\Delta\gamma/2)\ D(\alpha-\Delta\gamma/2)\ e^{-j2\pi(f_2-\mu t)\Delta t(\alpha)}}{|D(\alpha+\Delta\gamma/2)|\,|D(\alpha-\Delta\gamma/2)|} \qquad 6.7$$

where t_o, as previously, has been neglected in comparison with $(f_2 - \mu t)$.

Fig. 6.9 shows plots of R_{LR} from eqn 6.7 as a function of t in the range $0 \leqslant t \leqslant T$ for $\alpha = 0^o$, 5^o, 10^o and 20^o and also plots of R_{LR} as a function of α in the range $0^o \leqslant \alpha \leqslant 30^o$ for $t = 0$, $0.5T$ and T. A splay angle of 27^o and an array separation of 0.22 m was assumed. The only effect of the directivity patterns on R_{LR} is to cause an inversion at each null point.

It is seen from Fig. 6.9 that, in general, the interaural correlation for the signal will oscillate between the limits ±1 within each sweep period at a frequency which increases with increasing azimuth angle of the target. At constant t, R_{LR} oscillates rapidly with increasing azimuth angle.

We have effectively a binaural tonal stimulus at frequency, $2\mu R/c$ with an interaural phase difference which is a function of both time and target azimuth angle. (Since the frequency difference is extremely small the concept of a time variant phase is more meaningful than that of a fixed frequency

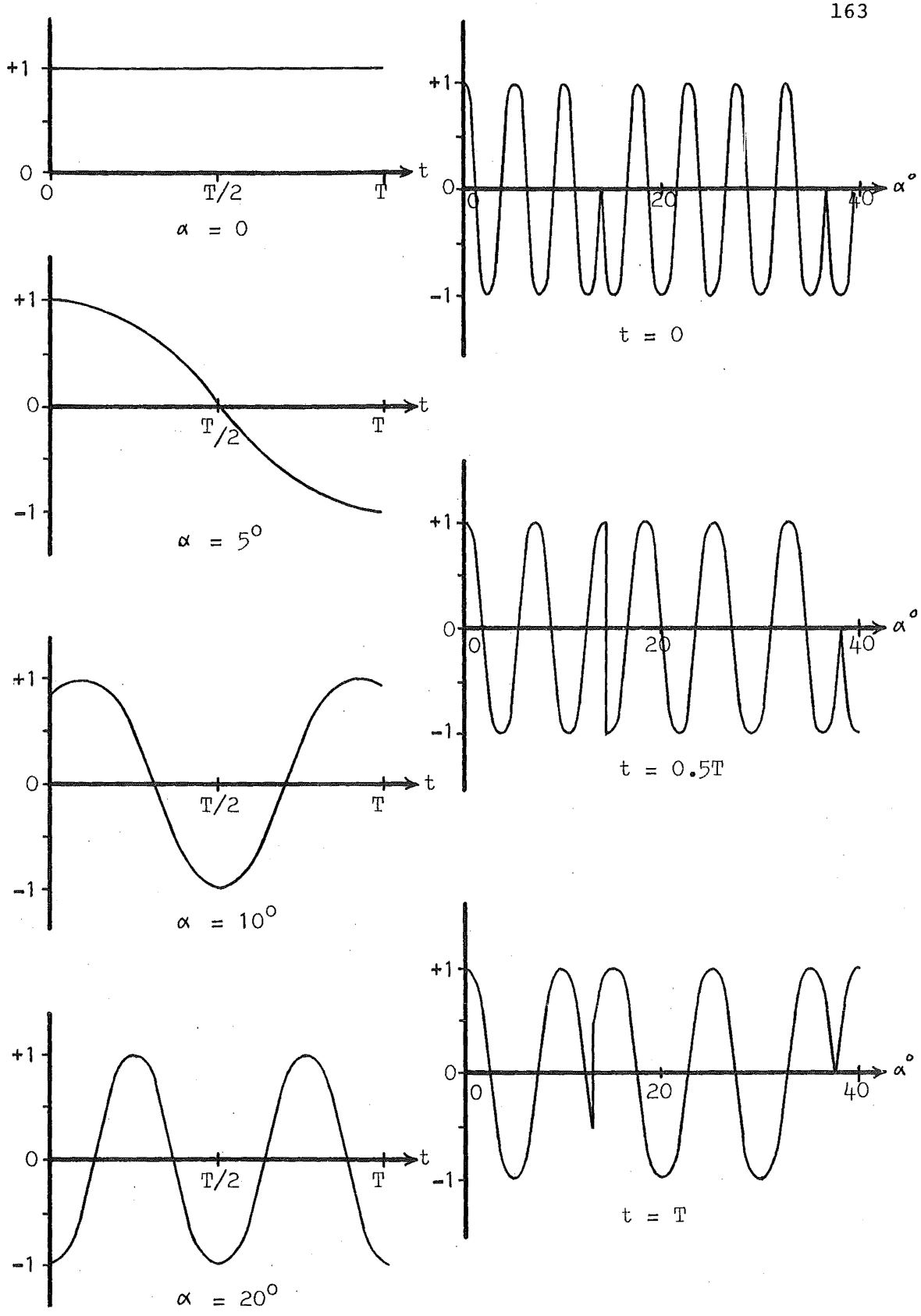

Figure 6.9. Variation of R_{LR} with time, t, and with azimuth angle, α, for a specularly reflecting target.

difference.) In addition there will be an interaural intensity difference which is a function of the directivity patterns and the azimuth angle.

For a target at zero azimuth angle, the signal stimulus is So for all t in the range $0 \leqslant t \leqslant T$. For small azimuth angles, the stimulus condition is S_θ where θ lies in the range $0 < \theta < \pi$ and is time variant between these limits. For large azimuth angles the interaural intensity difference becomes significant and the stimulus condition oscillates between the conditions So' and Sπ' (the prime indicates an interaural intensity difference). The detection thresholds under these various stimulus conditions are discussed in section 6.4.

We next consider a target comprising a large number of scatterers subtending an angle $\Delta\alpha$ at the arrays and lying at an azimuth angle α_1. We assume that the extent of the target in range is less than $R\Delta f_s/f_s$ (i.e. the audio signals derived from the scattered signals at the arrays lie within a single critical bandwidth).

Assume, firstly, that the number of scatterers is very large and that their angular extent, $\Delta\alpha$, is comparatively small compared with the array beamwidths. Under these assumptions, we may apply a similar analysis to determine the cross correlation coefficient as was employed in the case of reverberation (case i)). We thus obtain the following expression for the interaural correlation coefficient, $R_{LR}(\alpha_1,t)$

$$R_{LR}(\alpha_1,t) = \frac{D(\alpha_1+\Delta\gamma/2)\ D(\alpha_1-\Delta\gamma/2) \int_{\alpha_1-\Delta\gamma/2}^{\alpha_1+\Delta\gamma/2} e^{-j2\pi(f_2-\mu t)\Delta t(\alpha)}\ d\alpha}{|D(\alpha_1+\Delta\gamma/2)|\,|D(\alpha_1-\Delta\gamma/2)|\ \Delta\alpha}$$

6.8

Fig. 6.10 shows plots of $R_{LR}(\alpha_1,t)$ as a function of t in the range $0 < t < T$ for target azimuth angles of 0^o, 10^o, 20^o and for target angular extents, $\Delta\alpha$ of 5^o and 10^o. R_{LR} was evaluated numerically from eqn 6.8 for a splay angle, $\Delta\gamma$, of 27^o and an array separation of 0.22 m.

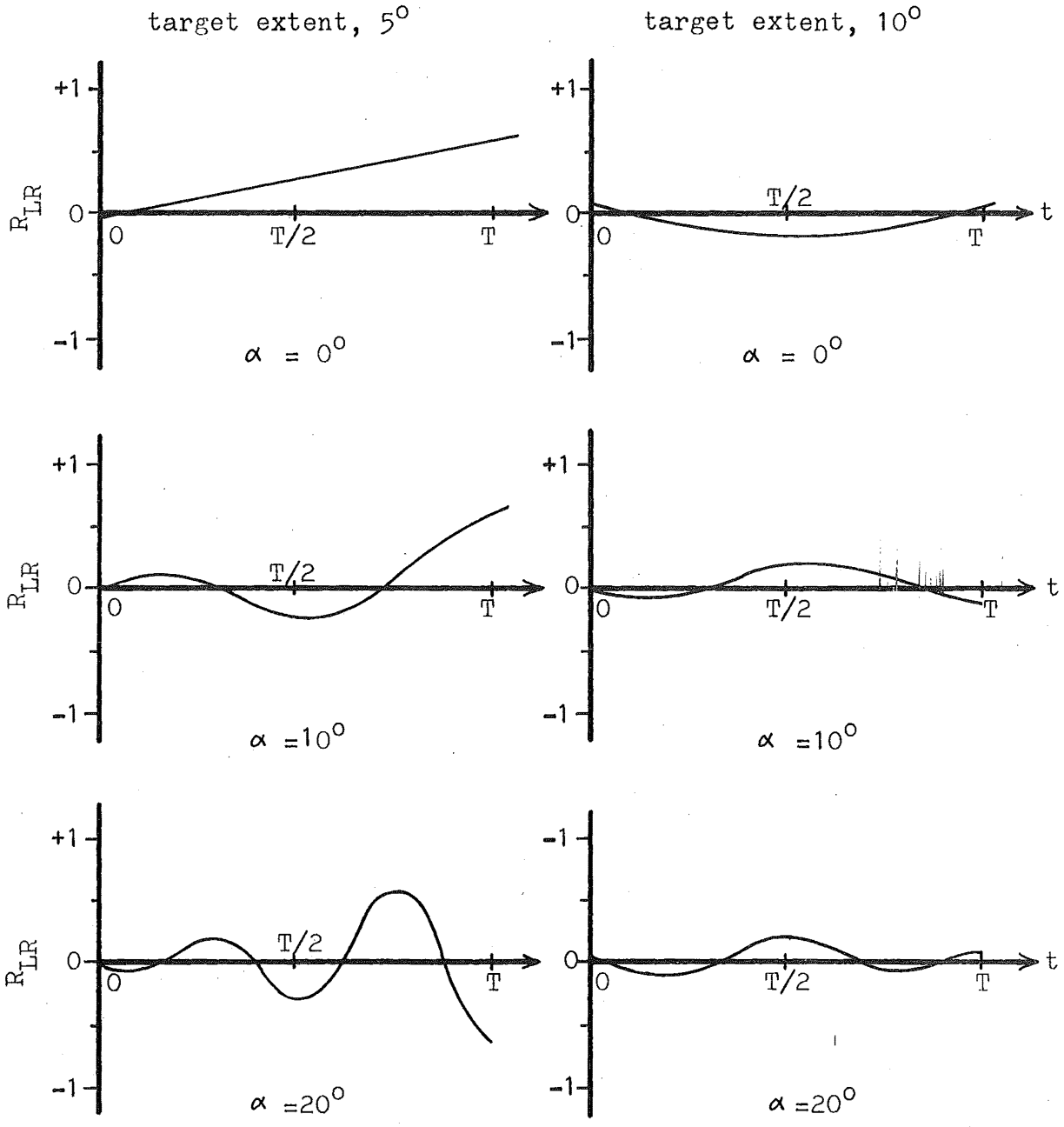

Figure 6.10. Variation of R_{LR} with time, t, for various target azimuth angles, and target extents of 5^o and 10^1. (Diffuse target.)

The rather surprising result indicated by Fig. 6.10 is that even when the angular extent of the target is only 5^{o}, the value of R_{LR} never exceeds 0.65, and for a target extent of 10^{o}, R_{LR} never exceeds 0.23. The reduction in interaural correlation with increasing target extent is due solely to the spatial separation of the two receiving arrays since no account of amplitude variation across the width of the target has been taken. The reason for the substantial reduction in cross correlation for a comparatively small array separation ($\approx 9\lambda$) is that the arrays are well within the near field of the scattered energy. For instance if the target range is 100 m and its extent is 5^{o}, the far field distance is approximately 6.1 km. Clearly, at a distance of only 100 m from the target, rapid reduction in cross correlation is to be expected for small receiver separation.

The stimulus condition for signal in this case is rather complex. For a target at near zero azimuth, there exist effectively three signal components: one binaural, a, one monaural at the left ear, b, and one monaural at the right ear, c. (a, b and c rms pressure levels). Here, 'a' is the portion of signal which is perfectly correlated when the interaural phase shift for 'a' is zero. Since the interaural phase difference for this component varies with t, 'a' contributes a component whose cross correlation coefficient varies between -1 and +1. b anc c are completely uncorrelated components. For $R_{LR}(max) = 0.65$, $a = 0.78$, $b = c = 0.57$ (see section 6.2). For the target with an angular extent of 5^{o} then, binaural detection is more likely than monaural detection if the target azimuth is near zero. The stimulus for the binaural component will be S_{θ}. For $R_{LR}(max) = 0.23$, $a = 0.48$, $b = c = 0.88$ so for

the target of 10^{o} angular extent, detection will almost certainly be monaural, Sm. If the target azimuth angle is appreciable, monaural detection will result due to the large intensity difference, regardless of the target extent.

6.4 Detection of Targets

In the preceding section, it was shown that the background noise due to reverberation, has effectively zero interaural correlation. For all signal conditions, then the noise stimulus is Nu. As was discussed in section 6.2, under some circumstances, a release from masking is possible for signals presented against a background of uncorrelated noise. From the delay line model of the binaural masking process, and from the results shown in Fig. 6.3(a), it is apparent that interaural phase difference for signal is unimportant for background Nu. The only quantities which affect the threshold S/N ratios for the detection of targets are thus: signal frequency, interaural amplitude differences, and the interaural correlation coefficient.

For the case of a specular target detected at near zero azimuth and at the maximum audio frequency of the system (3 kHz) it seems unlikely that there will be any release from masking and detection would be expected at a threshold S/N of about 17 dB. (See section 6.2.) If, however, first detection occurs at a frequency of 1 kHz or lower, a masking release of approximately 3 dB may be expected (see Fig. 6.3(a) and Fig. 6.14). The detection threshold will then be approximately 14 dB. If the target azimuth angle is sufficiently large to produce a large interaural amplitude difference (Nu-Sm) the MLD will be zero.

For the case of a target comprising a large number of scatterers and detected at near zero azimuth a release from masking of up to 3 dB may be expected under the same circumstances as for the specular target provided also the angular extent of the target is less than about 5^{o}. For target extents much greater than 5^{o}, detection will be effectively monaural and a S/N ratio of approximately 17 dB will be required for detection. If the extent of the target in range is greater than $R\Delta f_s/f_s$, i.e. if the signal returns occupy a bandwidth greater than the critical bandwidth, the detection threshold will be raised since only signal energy within the critical bandwidth contributes to detection. In practice, this is unimportant since (a) such an extent is unlikely at threshold range and (b) an increase in extent probably implies an increase in scattering strength so the range at which first detection occurs would not necessarily be reduced.

The question now arises: Can we consider a fish shoal to be representable as a very large number of scatterers? Clearly the number of individual scatterers present in a shoal of fish will be far from large in the statistical sense. However, if we assume that the individual members of the shoal are in continuous independent motion with respect to the shoal and consider the statistics of the target over a period large in comparison with the redistribution time of shoal, then the effective number of scatterers <u>is</u> very large. If this assumption is justifiable, then the preceding analysis for the large number of scatterers will be equally applicable to fish shoals. There appear to be no published results on the spatial distribution of fish in a shoal, but this appears to be a reasonable approach, at least to the problem of fish shoal

detection.

As was mentioned in section 6.2, the detection threshold for signals in noise is dependent on signal duration since the ear is capable of integrating energy over periods of 0.2 sec. or more. Since in the present application, the signal duration is at least 1 sec. at realistic operating ranges, we may assume that the S/N ratio required for detection will be minimal.

6.5 Recognition of Fish Shoal Targets

In this section, the characteristics of fish shoals and individual fish, which may provide cues for the recognition of fish shoals in the presence of weed, rocks, etc., are examined.

Haslett[29,30] and others [31,32] have shown that the effective target cross-section of individual fish of many species is significantly dependent on (a) signal frequency, and (b) aspect angle. At frequencies at which the length, L. of the fish is less than about 7λ all major scattering portions of the fish are within the region of Rayleigh scattering and the effective target cross section of the fish varies uniformly as the fourth power of frequency. The most predominant scattering portion at these frequencies is the fleshy body of the fish. As the frequency is increased, the body signal passes into the geometrical scattering region where its cross section is independent of the frequency. At still higher frequencies, other portions of the fish such as the swim bladder and the backbone also pass into the geometrical region, and since they are essentially cylindrical, their contribution varies in proportion to frequency. The signals from swim bladder and

backbone eventually predominate. In the transition region from L = 10λ to 40λ approximately, strong interaction among the reflections from various parts of the fish cause pronounced dips in the overall cross section (15 dB or more). Typical characteristics, predicted from scaled high frequency measurements[29] are shown in Fig. 6.11.

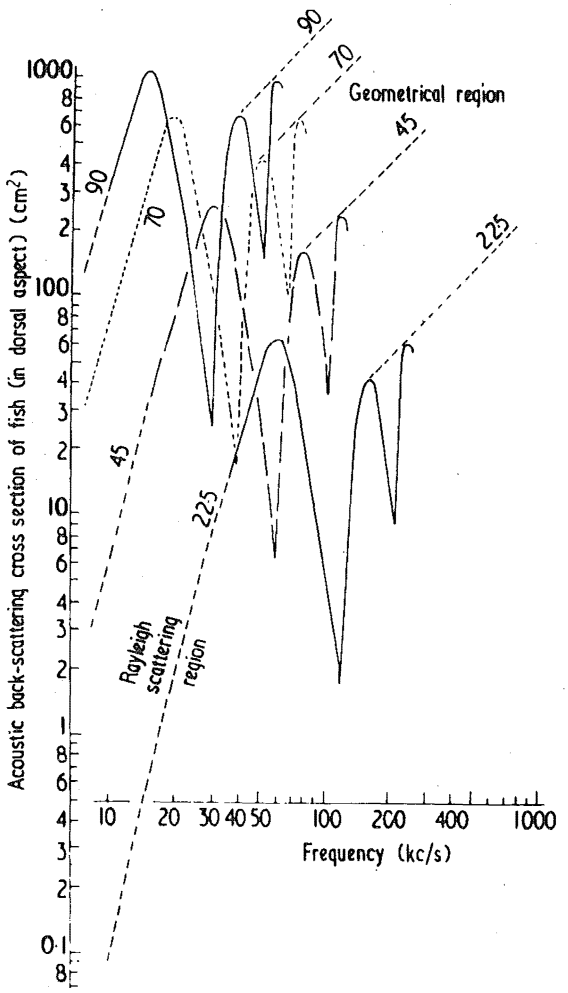

Approximate variations of back-scattering cross sections of fresh-water fish with frequency. Four examples are given for fish of overall lengths 90, 70, 45 and 22·5 cm. (In the geometrical region at high frequencies there are many maxima and minima, so that the general trend of the maxima is shown as a dotted line in each case.)

Figure 6.11. Variation of back scattering cross sections of single fish as a function of frequency for various lengths (after Haslett[29]).

Although these curves are based on measurements with the fish in dorsal aspect, similar characteristics are observed for side aspects, which presumably are most important for horizontal looking sonars.

Back scattering polar diagrams of fish have been determined for various acoustic dimensions and various aspects. Fig. 6.12 shows typical patterns obtained by Haslett for two planes of rotation. These diagrams show that at lengths of interest, the scattering patterns are complex and that as the acoustic length increases, the number of lobes in the patterns increases. The scatter patterns for the horizontal plane (diagrams on the left) which are relevant to the present application show that the width of major lobes does not vary greatly with the acoustic dimension. This confirms the hypothesis that different portions of the fish structure predominate at different frequencies. At $L = 4.4\lambda$, the body must be the most significant contributor since an acoustic dimension of at least 4λ is required to produce the observed lobe widths. At $L = 30.4\lambda$, probably the swim bladder predominates since the width of the main lobe again corresponds to an acoustic dimension of the order of 4λ.

It has been suggested[31] that for quantitative sonar measurements, (measurement of shoal size, density, etc.) the transitional region ($L = 10\lambda$ to 40λ or more) should be avoided since anomalous results are likely. In the present application, quantitative results in the strict sense are not required, although it is desirable to be able to distinguish a large shoal from a small shoal when both are present in the beam. Since the bandwidth is large, it seems unlikely that anomalous results due to the transitional region will affect evaluations of this nature.

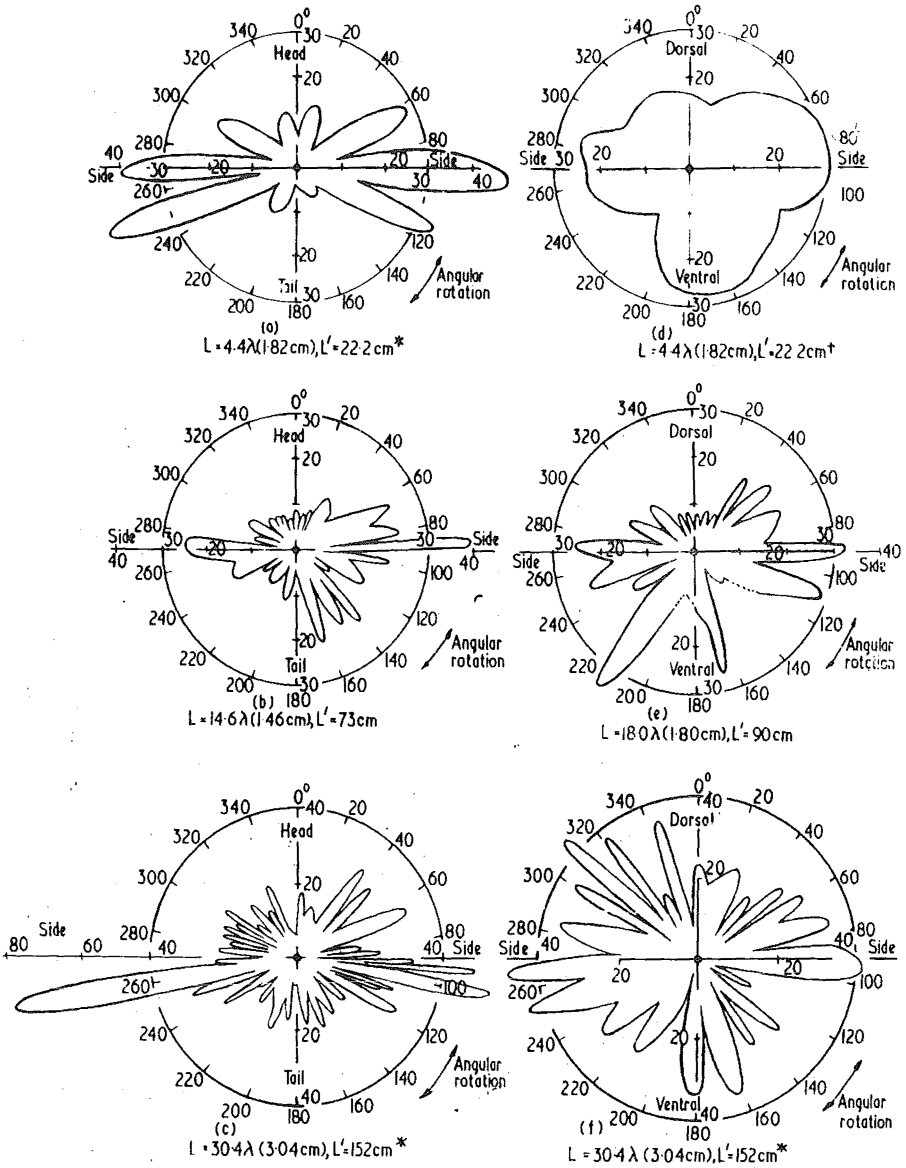

Back-scattering polar diagrams of fish (sticklebacks). The readings were taken under the following conditions:

Plane of observation: (*a*), (*b*) and (*c*), horizontal plane; (*d*), (*e*) and (*f*), vertical plane (perpendicular to longitudinal axis of fish).
Frequency: (*a*) and (*d*), 360 kc/s; (*b*), (*c*), (*e*) and (*f*), 1·48 Mc/s.
Radial scale: amplitude (mv): 20 mv in (*a*) and (*d*) is equivalent to an acoustic cross section of $1·5 \cdot 10^{-2}$ cm² at 360 kc/s (or $8·8 \cdot 10^{-4}$ cm² at 1·48 Mc/s); 20 mv in (*b*), (*c*), (*e*) and (*f*) is equivalent to an acoustic cross section of $1·73 \cdot 10^{-1}$ cm² at 1·48 Mc/s.
L = actual length of fish, L' = equivalent full-size length of fish at 30 kc/s, λ = wavelength in water.

* Mean of two sets of readings. Range = 80 cm.

† Mean of four sets of readings.

Figure 6.12. Backscattering polar diagrams of various acoustic lengths in two planes of rotation. (From Haslett[29]).

Sea trials, discussed in Ch.9, tend to confirm this. Fig. 6.11 shows that the frequency band from 40 kHz to 80 kHz certainly lies in the transitional region for most fish of commercial size.

In view of the wide system bandwidth, the possibility of distinguishing between fish shoals and other similar targets on the basis of differences in scattering cross section/ frequency characteristics presents itself. It is well known that the fish of a particular shoal tend to be of a very similar size, so we would expect similar variations of cross sections with frequency, among members of the shoal. Whether or not such characteristics would be detectable in the audible display of the FM sonar probably depends mainly on the behaviour of individuals in the shoal and the effect of this behaviour on the aspect of individuals, as seen by the sonar. Fig. 6.12 shows that the scattering cross section is very sensitive to small changes in aspect. If the individuals exhibit comparatively small perturbations about some predominant aspect, which seems likely if the shoal is to stay together, then it is likely that a frequency dependence of cross section would be detectable provided (i) the signal to noise ratio is good, and (ii) the cross sectional variation is sufficiently large. It is pure conjecture at this stage as to whether any or all of these conditions would be fulfilled in practice. If the conditions are fulfilled, an amplitude modulation would be superimposed on the complex signals at left and right ears. This modulation would be of very low frequency and may contain only a single dip. Such modulation would, however, be highly correlated at the two ears which would greatly aid its detection. The ability of human

operators to detect amplitude modulations is discussed in section 6.6.

Extensive studies into the locomotion of individual fish have been conducted by Bainbridge[33]. He has shown that for a wide variety of fish species, the number of tail beats per second necessary to maintain a given speed, depends only on the length of the fish. He expresses the relationship in the form:

$$V = \frac{L(3f - 4)}{4}$$

where V is the velocity of the fish (cm/sec), L is the length of the fish (cm) and f is the number of tail beats per second. For fish of commercial size and at commonly observed velocities, Hester[34] has shown that frequency deviations of the order of 200 Hz due to the Doppler effect, may be expected, at 70 kHz. In the present sonar, since frequency shift due to Doppler is preserved with unchanged deviation, the swimming motion of fish in a shoal will have a considerable effect on the audio signals produced by the shoal. If the number of individuals in the shoal is small, it seems likely that the modulation of the signal due to the swimming motion will be recognizable. Experiments with the model sonar operating in air (see Ch. 7 for description) have shown that independent oscillation of up to 20 scatterers is detectable in the audio display when scaled amplitudes and frequencies comparable with those expected for swimming fish are used. When the number of members is very large, it seems unlikely that recognizable patterns will be formed.

Two characteristics of fish, which may in some cases produce recognizable modulations on the audio signals derived from fish shoals, have been briefly reviewed. There is no

evidence, at this stage, to suppose that either effect will be beneficial to the task of recognizing targets. It may be, in fact, that the Doppler spread due to swimming motion will have only the effect of reducing the signal detectability, due to the wider signal bandwidth. In any event, the ability of an operator to distinguish between various narrow band signals, which may or may not originate from a fish shoal target, will depend to a large extent on his ability to detect modulations present on the signal. In order to obtain some quantitative measure of the ability of the human auditory system to detect modulations on a narrow band signal under various noise conditions, the experiment described below was conducted.

6.6 The Detection of Amplitude Modulation on a Tonal Signal under Various Noise Conditions

Amplitude modulation was studied since this appears to be the most likely characteristic of a narrow band signal to be recognizable. In situations where the signal comprises a large number of frequency modulated components, if recognition is possible, it will probably be on the basis of envelope fluctuations (AM) produced as a consequence of the complex FM.

The simplest possible signal: sinusoidally modulated tone burst, was chosen since this limits the number of variables to manageable proportions, and allows comparison of results with results of other workers. In all experiments, the signal was presented in the So condition via matched earphones (Telephonics TDH-39). The carrier frequency used was 1 kHz and the modulating frequency, 4 Hz. The duration of the tone burst was 1 second. The modulation depth (as specified by the

modulation index, m) was the independent variable.

White noise (from a GR random noise generator 1390-B) was employed as masker and interaural correlations of +1 (No) and 0 (Nu) were used in each test. The output of the noise generator was recorded consecutively on the two channels of a stereo tape recorder (Uher 4400 Report Stereo). The No masker was then derived from a single channel of the recorder during playback. The Nu masker was obtained by feeding left and right ears of the subject from the two channel outputs, during playback.

Two listeners, AV, and MC were employed in the experiments and since the results were found to be consistent, no additional subjects were considered necessary. Both subjects had normal hearing and had had no previous experience in psychoacoustic tests of this nature.

Procedure

Thresholds for the detection of pure tone bursts in noise (at the noise level to be used in later tests) were first determined for each subject. This was necessary in order to relate subsequently measured modulation depth thresholds to the level of S/N above threshold value.

For this test and all subsequent tests employing a masker, the noise was continuous and at a spectrum pressure level (SPL) of 42 dB, as measured with a Breul and Kjaer artificial ear (type 4152) and spectrometer (type 2112). A 6 cc coupler was used. The signal for this test was a pure tone burst at 1 kHz, of duration 1 second. To eliminate transients, rise and fall times of 50 msec were employed. The signal level was measured in the same way as for the noise.

The sequence of presentation to the subjects was as follows: A lamp was lit at the commencement of the observation period, and remained lit for 3 seconds. In any observation period there was a 50% probability of the tone being presented, and if presented, it occupied the center 1 sec. period of the observation period. (Tables of random permutations[38] were used to decide whether or not to present the tone.) After the lamp was extinguished, the subject responded by pressing either a Yes or No button to indicate whether or not he had heard the tone.

The psychometric functions relating probability of detection, p(D) to signal level, were determined in the following manner.

1) A preliminary test to determine the approximate region of the threshold was conducted.

2) Eight signal levels in the vicinity of the threshold were then chosen.

3) The eight signal levels were then arranged in random sequence and at least 20 trials were conducted at each level. For the three levels nearest the 50% threshold, a further 20 trials were conducted. If results at these three points were not consistent, a further complete test was conducted at a later date and results were pooled. Each psychometric function, then, involved at least 220 trials. Each complete test occupied approximately 25 minutes.

In this 'free choice' testing procedure[39] there are clearly four possible response conditions, namely, (i) Hit, H ('Yes' when the signal is presented), (ii) 'Miss' ('No' when the signal is presented), (iii) Correct dismissal ('No' when the signal is not presented) and (iv) False alarm, F ('Yes'

when the signal is not presented). The probability of detection, p(D) is then given by,

$$p(D) = p(H) - p(F).$$

This psycho-acoustic method has an advantage over two interval, forced-choice procedures[36] in that the subject is not obliged to make decisions at random, and thus fewer trials are necessary. Although slower than 'threshold seeking' methods[37], it has the advantage that the shape of the psychometric function is obtained, so there is a form of check on changes in operator performance.

The results obtained for the two subjects are shown in Fig. 6.13 for both correlated and uncorrelated maskers. There is a clear separation between the psychometric functions for the two types of masker, for both subjects. The MLD's obtained here are not significantly less than those obtained at 500 Hz by Robinson and Jeffress[15]. The shape and position of the psychometric functions agree closely with results obtained by other workers[40,41].

Next, the thresholds for the detection of amplitude modulation in the quiet (Noise SPL less than -6 dB) were determined for each subject. The sound pressure level (SL) of the modulated tone burst used was 79 dB.

In this and subsequent tests, a 'two-interval, free-choice' procedure was adopted, the sequence of presentation being as follows:

i) A lamp, labelled 'reference' was lit for a total duration of three seconds.

ii) 1 sec. after the above lamp was lit, a 1 sec. burst of pure tone was presented.

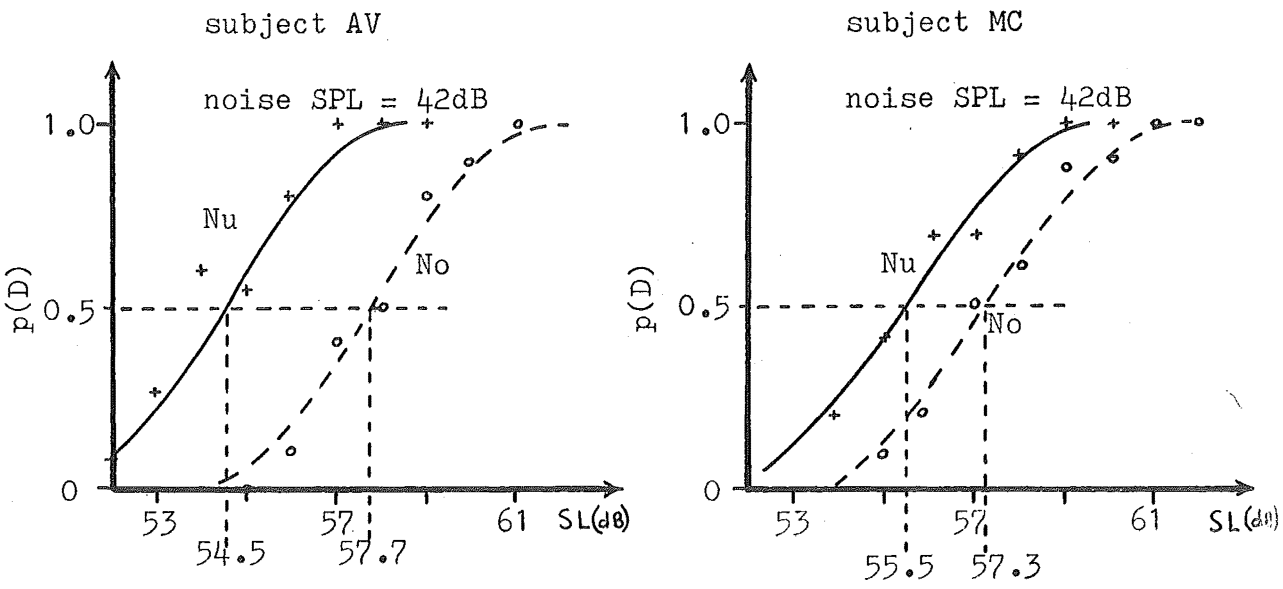

Figure 6.13. Psychometric functions for the detection of a 1 kHz tone burst (So) in correlated (No) and uncorrelated (Nu) noise.

iii) Immediately after the 'reference' lamp was extinguished, a lamp labelled, 'test' was lit.

iv) 1 sec. after the 'test' lamp was lit, a 1 sec. burst of tone, which was either modulated or unmodulated, was presented.

v) After the 'test' lamp was extinguished, the subject responded by pressing either a button labelled 'same' or a button labelled 'different', depending on whether he considered the second tone to differ from the first.

In the test interval there was a 50% probability of the tone burst being modulated. Seven values of m in the vicinity of threshold (as estimated in a preliminary test) were employed. The number of trials taken at each point was the same for the previous experiment. The sequence of

presentation of the seven levels of modulation was random.

It was found that results were inconsistent unless the subject had some idea of the depth of modulation he was expected to detect in each batch. For instance, if a batch with clearly discernable modulation was followed by one with modulation at near threshold level, the subject responded, 'same' for the first five or six trials of the second batch, then, as he began to suspect that the modulation depth was now significantly smaller, he lowered his acceptance criterion and began to score correctly, or at least above chance level. This problem was solved by providing two sample presentations at the commencement of each batch of 20 trials. The subject was informed that the tone sounded during the 'test' period of these two presentations would be modulated to the extent to be employed in the forthcoming batch. With this knowledge, the subject immediately adjusted his acceptance criterion to suit the stimulus conditions.

In any recognition test of this nature, shift of the acceptance criterion of a subject is unavoidable, but provided there is no significant criterion change within a given batch consistent results may be obtained.

The results for this test are shown in Fig. 6.14. It is seen that the positions and shapes of the psychometric functions are very similar for the two subjects. The 50% thresholds are comparable with results of other workers for similar conditions[42,43].

Next, tests were conducted using correlated and uncorrelated noise maskers at a spectrum pressure level of 42 dB, and at two signal levels: 64 and 79 dB.

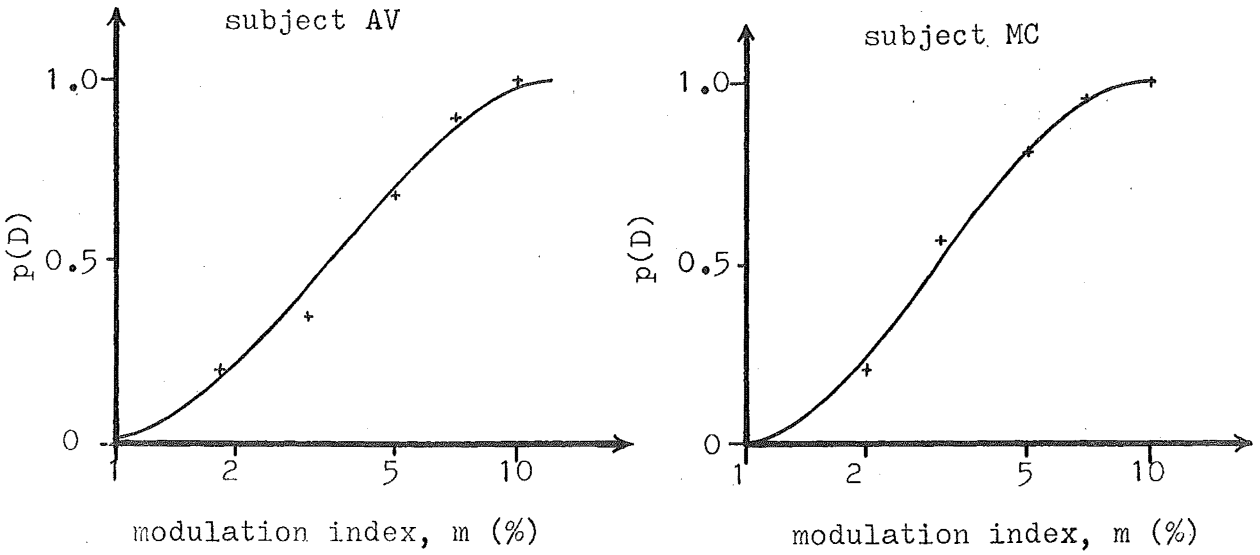

Figure 6.14. Psychometric functions for the detection of AM of variable m at 4 Hz (1 sec. modulated tone burst at a carrier frequency of 1 kHz).

The same psychoacoustic method as for the preceding test was employed. The psychometric functions obtained are shown in Fig. 6.15. The curves obtained under quiet conditions (Fig. 6.14) are also shown for comparison.

The results show that as the S/N conditions are degraded, the threshold modulation depth rises rapidly. Under poor S/N conditions, there is a significant improvement in the detectability of modulation when the masker is uncorrelated, rather than correlated. When the S/N is good (SL 79 dB) there is no noticeable difference between the two masking conditions. Presumably the mechanism for the reduction of threshold for poor S/N, with noise Nu, is an improvement in S/N for this condition, over the No condition. The S/N conditions are not

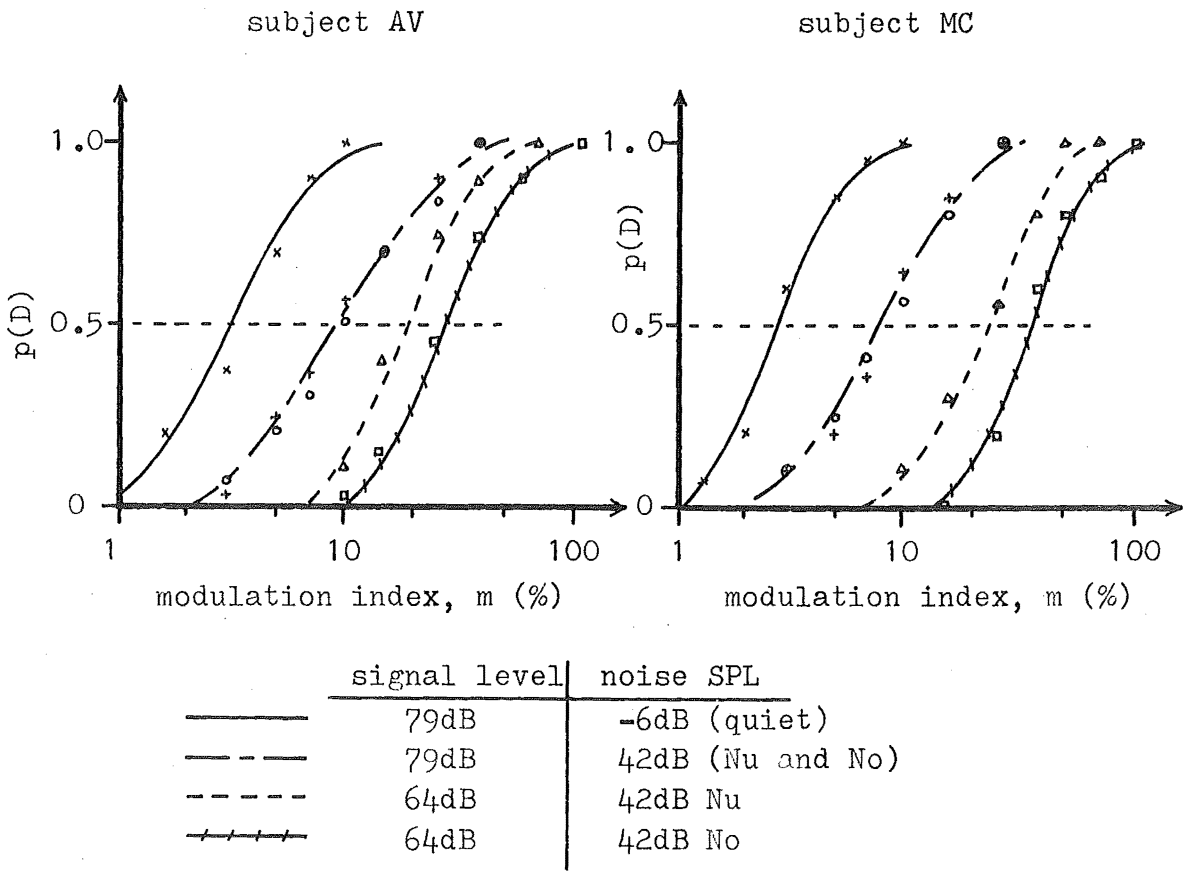

Figure 6.15. Psychometric functions for the detection of amplitude modulation under various signal and noise conditions.

significantly altered between these conditions when the S/N is already high.

At the high S/N conditions (SL, 79 dB) the slope of the psychometric functions are significantly less than for the other conditions, for both subjects. This implies that the subject shifts his acceptance criterion considerably more under conditions of good S/N, than he does either in the quiet or under poor S/N conditions. There appears to be no simple explanation for this phenomena.

Figure 6.16 summarizes the effect of S/N ratio on the detectability of amplitude modulation. 50% p(D) thresholds are plotted here as a function of the extent by which the S/N ratio for a particular test exceeds the detection threshold for the appropriate masking condition; i.e. the 79 dB signal level is considered to be 21.5 dB above threshold for subject AV, when the noise is correlated and 24 dB above threshold when the noise is uncorrelated, etc.

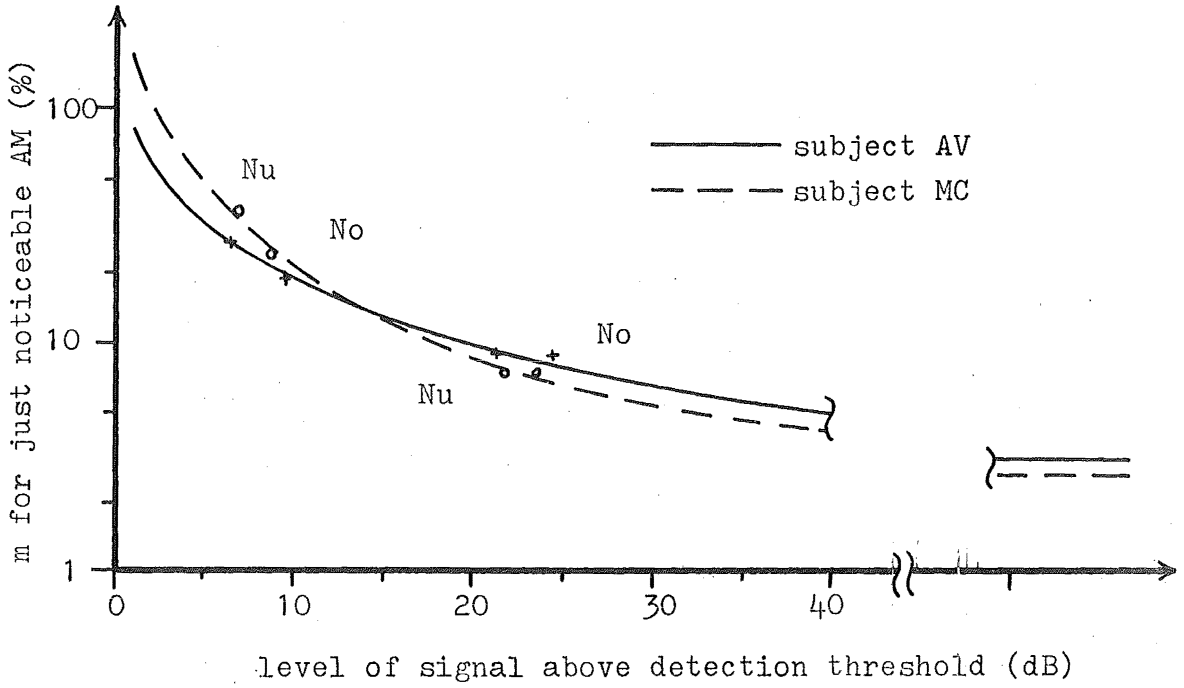

Figure 6.16. The detectability of amplitude modulation as a function of the level of S/N above threshold level.

The results are seen to lie on a smooth curve which becomes very steep as the detection threshold is approached. Even at a S/N ratio of 20 dB the level of modulation necessary for detection is significantly higher than that necessary under quiet conditions.

6.7 Conclusions

Some aspects of signals and noise at the audio display have been considered in the context of the problems of signals detection and recognition. It has been shown that with the particular array configuration used, AF noise signals at the two ears are uncorrelated. Also, if a target comprises a large number of scattering centers, and occupies an angular sector much in excess of 5^{o}, the binaural signals due to the target will have low cross correlation. This latter consideration may, in some cases, affect the detection threshold for such a target, and significantly change the mechanism by which an operator lateralizes the target. (Although the target tracking performance may not necessarily suffer. See chapter 7.)

It is, perhaps, desirable to consider at this stage whether or not some other array configuration would be preferable to the present one with regard to display effectiveness. Concerning the task of detection, the loss of correlation of the binaural signals from a target can raise the detection threshold by as much as 3 dB. If the receiving arrays were coincident, (i.e. the two patterns derived from a single array using a beam steering technique, such as is described in chapter 8), these signals would be highly correlated until the angular extent became comparable with the array beamwidths. It is doubtful, however, whether in a practical situation, this would materially improve the detection performance, since it is likely that targets of large lateral extent will be detected at greater ranges due to their greater scattering strength. i.e. initial detection is likely when the angular extent of the target is comparatively small, regardless of target size. Also, unless the target lies almost directly forward of the

vessel, initial detection will be monaural and interaural correlation will play no part.

The ability to recognize a target may in some cases be improved by an increase in interaural correlation, depending on the manner in which envelope modulation on the resulting narrow band signal is produced. If the envelope modulation is due to a common variation of scattering strength of individual scatterers, (as is the case for frequency dependent cross sections - see section 6.5) this modulation will be highly correlated at the two receivers, even if their separation is considerable. If however, a recognizable modulation is produced by the superposition of the individual scattered signals due to their differing frequencies, such modulation will be uncorrelated at the two arrays in the present configuration. If the arrays were coincident, this modulation also would be highly correlated. The detectability of such modulation would undoubtedly be improved in this case. If the number of individual scatterers is small, modulation due to this cause may well be detectable, but for a very large number of scatterers, it seems unlikely that any recognizable pattern of envelope fluctuations would be formed. At this stage, there is no reason to suspect that any other array configuration would significantly improve the system performance.

It has been shown that the ability of a subject to detect amplitude modulation reduces rapidly as the S/N ratio is reduced towards the threshold level for detection. Even at a S/N ratio of 20 dB above threshold, the required modulation depth for detection is substantially higher than that necessary under quiet conditions.

When the S/N ratio is poor, a significant improvement in the ability to detect AM is observed when the masking noise is uncorrelated (Nu), rather than perfectly correlated (No). The minimum modulation index for detection is approximately 30% less when the noise is uncorrelated. This reduction is consistent with the effective improvement in S/N ratio due to the MLD obtained for the Nu-So stimulus.

6.8 References

1. J.C.R. Licklider, "The Influence of Interaural Phase Relations upon the Masking of Speech and White Noise", J. Acoust. Soc. Am., 20 : 150 (1948).
2. I.J. Hirsh, "The Influence of Interaural Phase on Interaural Summation and Inhibition", J. Acoust. Soc. Am. 20 : 563 (1948).
3. L.A. Jeffress, H.C. Blodgett, T.T. Sandel, and C.L. Wood, "Masking of Tonal Signals", J. Acoust. Soc. Am., 28 : 416 (1956).
4. H.C. Blodgett, L.A. Jeffress and R.W. Taylor, "Relation of the Masked Threshold to Signal Duration for Various Interaural Phase Combinations", Am. J. Psychol. 71 : 283 (1958).
5. L.A. Jeffress, H.C. Blodgett and B.H. Deatherage, "The Masking of Tones by White Noise as a Function of the Interaural Phases of Both Components, I. 500 cycles", J. Acoust. Soc. Am., 24 : 523 (1952).
6. L.A. Jeffress, "A Place Theory of Sound Localization", J. Comp. Physiol. Psychol. 41 : 35 (1948).
7. L.A. Jeffress and D.E. Robinson, "Formulas for the Coefficient of Interaural Correlation for Noise", J.

Acoust. Soc. Am., 34 : 1658(A) (1962).

8. see ref. 3, p420.

9. R.G. Klump and H.R. Eady, "Some Measurements of Interaural Time Difference Thresholds", J. Acoust. Soc. Am., 28 : 859 (1956).

10. H. Fletcher, "Auditory Patterns", Rev. Mod. Phys., 12 : 47 (1940).

11. J.A. Swets, D.M. Green, and W.P. Tanner, "On the Width of the Critical Bands", J. Acoust. Soc. Am., 34 : 108 (1962).

13. S.O. Rice, "Mathematical Analysis of Random Noise", in Noise and Stochastic Processes, ed. N. Wax, Dover Publications, N.Y. (1954).

14. J.P. Egan, "Masking Level Differences as a Function of Interaural Disparities in Intensity of Signal and Noise", J. Acoust. Soc. Am., 38 : 1043 (1965).

15. D.E. Robinson and L.A. Jeffress, "The Effect of Varying the Interaural Noise Correlation on the Detectability of Tonal Signals", J. Acoust. Soc. Am., 35 : 1947 (1963).

16. L.A. Jeffress, H.C. Blodgett and B.H. Deatherage, "Masking and Interaural Phase. II. 167 Cycles" J. Acoust. Soc. Am., 34 : 1124 (1962).

17. T.L. Langford and L.A. Jeffress, "Effect of Noise Cross-correlation on Binaural Signal Detection", 36 : 1455 (1964).

18. N.I. Durlach, "Note on Binaural Masking-Level Differences as a Function of Interaural Correlation of the Masking Noise", J. Acoust. Soc. Am., 36 : 1613 (1964).

19. H.C. Blodgett, L.A. Jeffress and R.H. Whitworth, "Effect of Noise at One Ear on the Masked Threshold for Tone at

the Other", J. Acoust. Soc. Am., 34 : 979 (1962).

20. L.A. Jeffress, "Mathematical and Electrical Models of Auditory Detection", J. Acoust. Soc. Am., 44 : 187 (1968).

21. C.W. Sherwin, F. Kodman, J.J. Kovaly, W.C. Prote, and J. Melrose, "Detection of Signals in Noise : A Comparison between the Human Detector and an Electronic Detector", J. Acoust. Soc. Am., 28 : 617 (1956).

22. J.J. Zwislocki, "Theory of Temporal Auditory Summation", J. Acoust. Soc. Am., 32 : 1046 (1960).

23. W.R. Garner, "The Effect of Frequency Spectrum on Temporal Integration of Energy in the Ear", J. Acoust. Soc. Am., 19 : 808 (1947).

24. W.A. Wilbanks and J.K. Whitmore, "Detection of Monaural Signals as a Function of Interaural Noise Correlation and Signal Frequency", J. Acoust. Soc. Am., 43 : 785 (1968).

25. F.A. Webster, "Influence of Interaural Phase on Masked Thresholds", J. Acoust. Soc. Am., 23 : 452 (1951).

26. M.E. Rilling and L.A. Jeffress, "Narrow-Band Noise and Tones as Signals in Binaural Detection", 38 : 202 (1965).

27. C.D. Creelman, "Detection of Complex Signals as a Function of Signal Bandwidth and Duration", J. Acoust. Soc. Am., 33 : 89 (1961).

28. V.V. Olshevskii, Characteristics of Sea Reverberation, Consultants Bureau Special Research Report, 1967.

29. R.W.G. Haslett, "Determination of the Acoustic Back-scattering Patterns and Cross sections of Fish", Brit. J. Appl. Phys., 13 : 349 (1962).

30. R.W.G. Haslett, "The Target Strengths of Fish", J. Sound Vib. 9(2) : 181 (1969).

31. D.H. Cushing, F.R. Harden Jones, R.B. Mitson, G.H. Ellis and G. Pearce, "Measurements of the Target Strength of Fish", J. Brit. I.R.E. April (1963) p.299.

32. F.R.H. Jones and G. Pearce, "Acoustic Reflexion with Perch to Determine the Proportion of the Echo Returned by the Swim Bladder", J. Exp. Biol. 35 : 437 (1958).

33. Bainbridge, R., "The Swimming Speed of Fish", J. Expt. Biol., 35 (1) : 109 (1958).

34. F.J. Hester, "Identification of Biological Sonar Targets from Body-motion Doppler Shifts", in Marine Bio-Acoustics vol. 2, Pergamon Press, New York, 1967.

36. J.A. Swets, "Is there a Sensory Threshold", Science, 134 : 168 (1961).

37. R.A. Campbell and E.Z. Lasky, "Adaptive Threshold Procedures:, J. Acoust. Soc. Am., 44 : 537 (1968).

38. J.W. Green, "Tables of Random Permutations", Forest and Timber Bureau, Canberra, Australia, 1968.

39. A.E. Brown, "Measurement of Auditory Thresholds", J. Acoust. Soc. Am., 38 : 86 (1965).

40. J.P. Egan, "Masking-Level Difference as a Function of Interaural Disparities in Intensity of Signal and of Noise", J. Acoust. Soc. Am., 38 : 1043 (1965).

41. D. McFadden, "Lateralization and Detection of a Tonal Signal in Noise", J. Acoust. Soc. Am., 45 : 1505 (1969).

42. J. Rutschmann and Leo Rubinstein, "Binaural Beats and Binaural Amplitude-Modulated Tones : Successive Comparison of Loudness Fluctuations", J. Acoust. Soc. Am., 38 : 759 (1965).

43. von D. Maiwald, "A Functional Model of the Ear for Explaining the Detectability of Small Changes in Frequency and Amplitude", (in German) Acustica, 18 : 81 (1967).

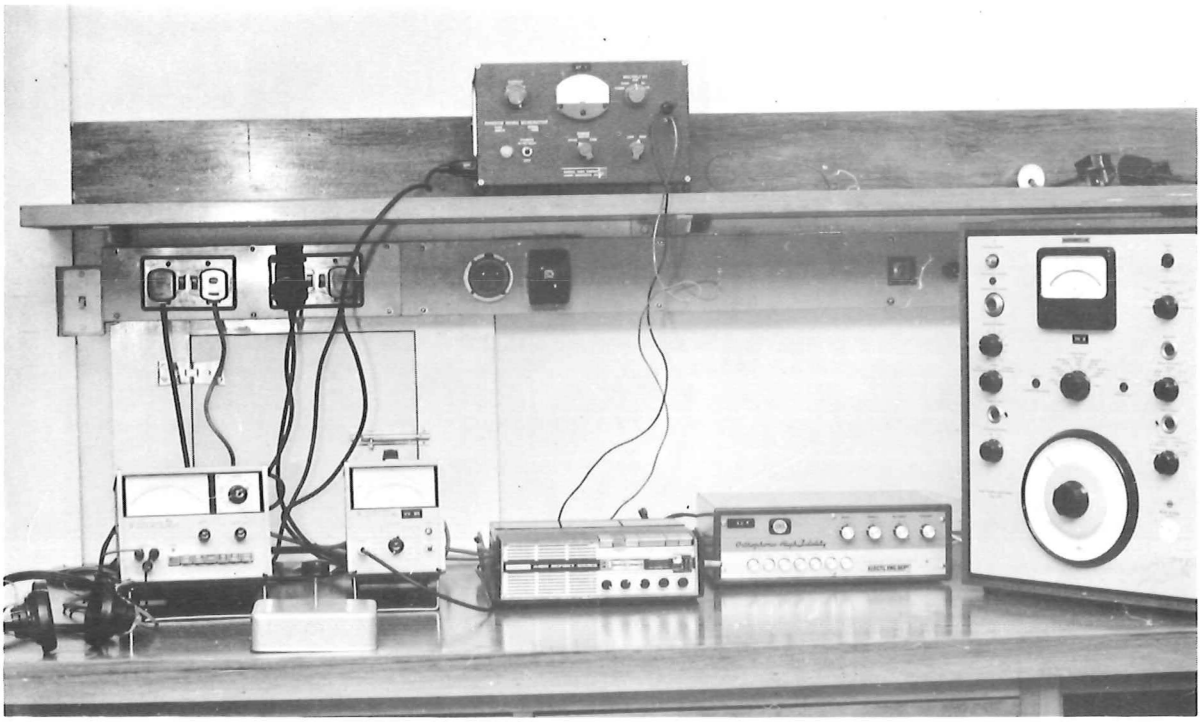

CHAPTER 7

LATERALIZATION OF SIGNALS AND THE TRACKING OF TARGETS

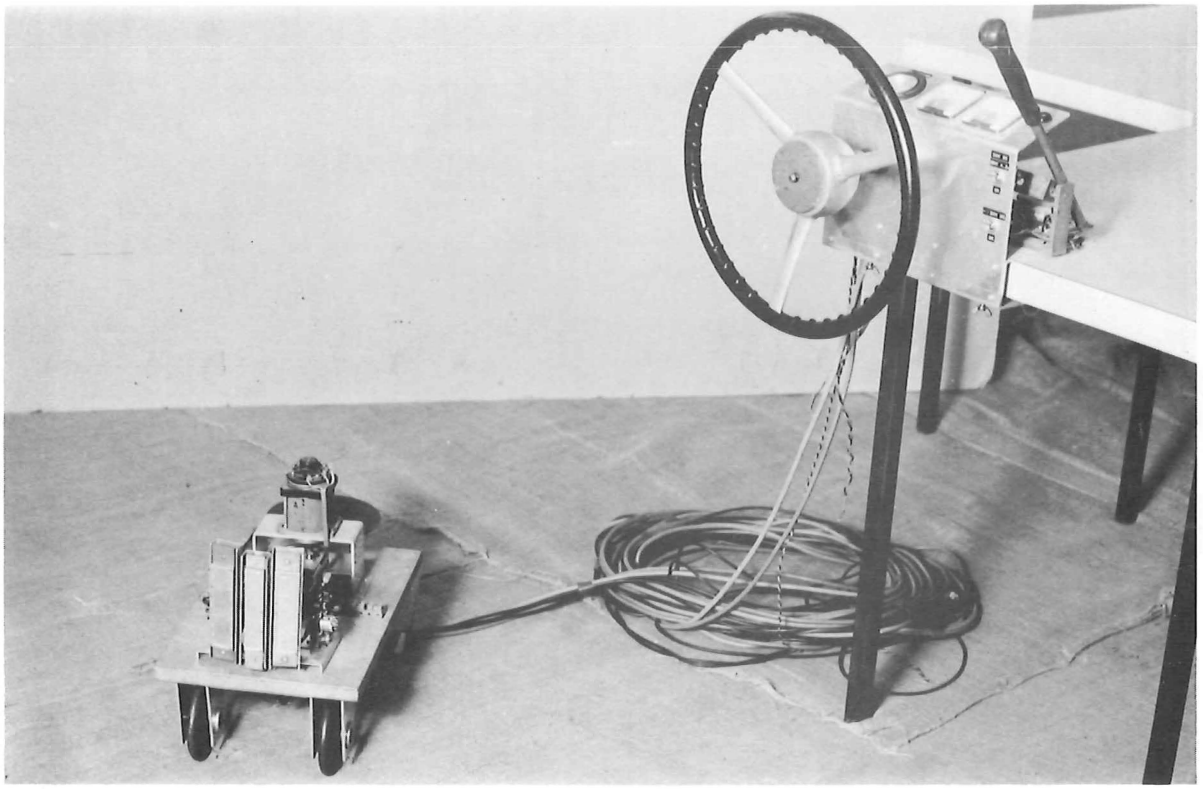

CHAPTER 7

LATERALIZATION OF SIGNALS AND THE TRACKING OF TARGETS

7.1 Introduction

In normal hearing, the process of perceiving the position of a sound source in space by the mechanism of binaural hearing is known as localization. When binaural signals are presented via earphones, the image produced, generally appears to be within the head, occupying an intracranial position which is dependent on interaural differences between the two signals. Only in very rare circumstances[1,2] does the image appear to be remote from the listener. The process of judging the intracranial position of a dichotic image is known as lateralization, and it is this process with which we are primarily concerned in the present sonar display.

Since the prime objective of a fishfinding sonar is to track targets, rather than to estimate their position in azimuth, it is not essential that there should be a unique relationship between the azimuth angle and the perceived image position. It is more important that the manner in which the binaural signals are produced should best suit the role of target tracking.

In the tracking task, the binaural display is used by the operator as an error indicating device. He determines from this display an estimate of the difference between the course of the vessel and the true course to the target, and attempts to minimize the difference. Any remaining error in course will gradually increase as the vessel proceeds in the general direction of the target, so a continuous process of updating

the vessel's course is necessary. If the display could function for all ranges, however small, the final error in position would be negligible. i.e. vessel and target would coincide exactly, providing the target was not evasive. The performance of the display in this case would be reflected in the departures of the path of the vessel during the approach, from an optimum path for which some quantity such as approach time or path length would be minimum.

In practice the target does not move in the plane containing the array axes so it will be lost at a finite horizontal range dependent on its depth and the directivity pattern of the arrays in the vertical plane. In this case there will, in general, be a significant final error in position, so that both the path travelled and the positional error when the vessel is closest to the target, are important measures of the tracking performance.

Interaural amplitude difference (IAD) is the cue provided at the binaural display, to enable the operator to estimate the error in course. Fig. 7.1 shows a simplified block diagram of the control system involved in the tracking task.

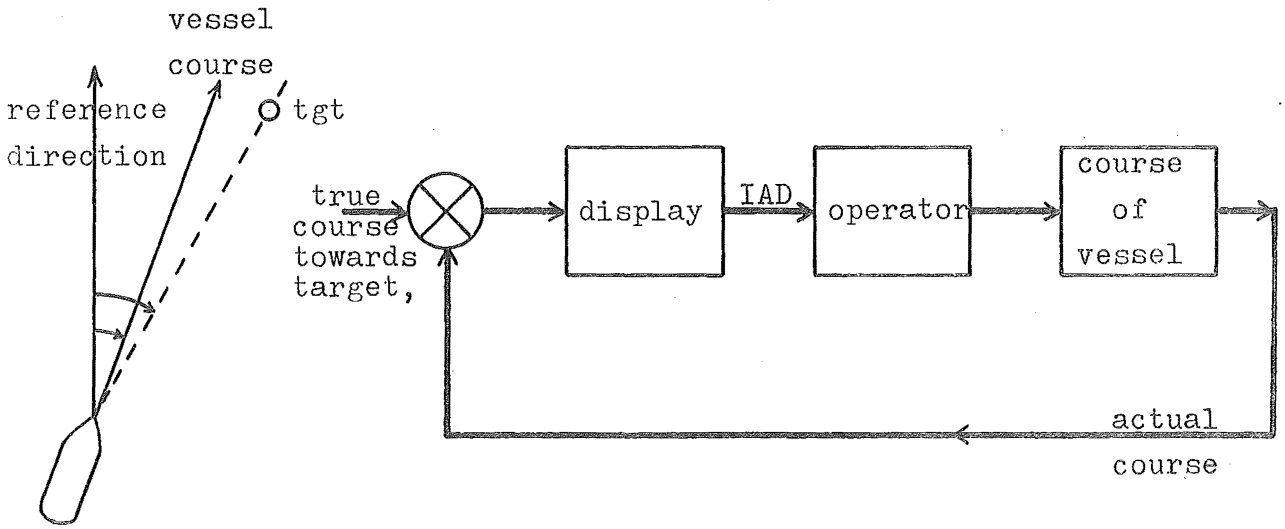

Figure 7.1. Block diagram of the control system involved in target tracking.

Clearly the transfer function of the binaural display which relates the IAD to target azimuth angle, α, will determine the performance of the sonar/operator combination in a tracking task. This chapter is primarily concerned with the design of this transfer characteristic and with predictions of tracking performance.

Certain important results in the field of signal lateralization phenomena are reviewed since they provide the basis for performance predictions. A psychoacoustic experiment to determine the effects of a low, or zero, interaural correlation between the binaural signals on the tracking performance, is described. This study is necessary since the results of Ch. 6 indicate that binaural signals from fish shoal targets are likely to be poorly correlated.

The results of a tracking experiment using a model of the underwater sonar, operating in air, are presented.

7.2 Signal Lateralization Phenomena

It has been repeatedly shown [3,4] that, in normal hearing, the binaural auditory system utilizes interaural time differences (ITD's) and interaural amplitude differences (IAD's) between the signals arriving at the inner ears, to localize a source of sound. It is also agreed (2) that when the signals are presented dichotically, the same cues (if present) are used in the same manner, in order to lateralize the resulting sound image. The subject's impression of the dichotically produced image is, however, quite different from that produced in normal hearing since it appears to be within the head, rather than external. Since it is much simpler to produce known ITD's and IAD's with earphone presentation,much of the

experimentation in localization phenomena has used this form of presentation. Some of the most significant features of the process of signal lateralization (or localization) will be reviewed here, briefly.

Studies with dichotic tonal signals have shown that if ITD is the only cue provided, lateralization is not possible at frequencies above about 1300 Hz[5,6]. Although the auditory system is not insensitive to phase at frequencies above 1300 Hz[7], it appears unable to utilize it as an aid to lateralization of tones. When the stimulus is narrow band noise, however, ITD allows lateralization for center frequencies in excess of 3 kHz[6] (no frequency components below 2 kHz present). This suggests that when the time difference cue is presented unambiguously, as in the case of noise signals, lateralization using ITD alone is possible over a wider frequency range. In normal hearing, the predominant cue for the localization of a sound source whose frequency components lie below 1300 Hz appears to be ITD, whereas above this frequency, IAD dominates. This conclusion has been confirmed by Mills[10] who has shown that below about 1500 Hz the just noticeable phase shift for dichotic signals is commensurate with the actual phase shift which occurs at the ears when a sound source is just noticeably shifted from the median position, whereas the amplitude difference which occurs is well below the dichotic threshold. Above about 1500 Hz, the converse holds.

Many workers have investigated the magnitude of the IAD or ITD necessary to produce a just noticeable shift in image position[6,8,4]. Klump and Eady[6] show that for tonal signals

the just noticeable shift (jns) in image position from the median plane occurs at an ITD of 11 μsec at 1000 Hz, 17 μsec at 500 Hz, and 27 μsec at 250 Hz. At 1300 Hz (the highest frequency at which a shift could be detected) the ITD was 24 μsec. Other experimenters[8] report similar results. When the initial position of the image is offset, the ITD necessary for jns is found to increase[6]. The threshold increases by about 1 μsec for each 20 μsec of initial ITD. Signal intensity is also found to affect the magnitude of the threshold[8], lower intensities requiring a greater ITD for jns of the image.

Measurement of the jns of image position under IAD alone, is complicated by the fact that monaural phenomena are also present. i.e. the intensity change at one ear due to a small IAD may be detected on a purely monaural basis. Although it is clear that a shift in the position of the perceived image does occur given sufficient IAD, near threshold the situation is confused. Elfner and Perrott[9] show that for a 1000 Hz tone, the jns (if that is really what they are measuring) is about 2 dB at high signal level (60 dB) increasing to about 6 dB for quiet signals (20 dB). Although they used initial IAD's of -12 dB, 0 dB and +12 dB, differences in the total intensity for these stimuli make it difficult to draw any conclusions as to the effect of these offsets on the magnitude of the jns. They do show however, that the auditory system is more sensitive to jns's due to intensity changes at the ear receiving the greater intensity, than to changes at the other ear. There does appear to be some reduction in sensitivity to IAD changes for the offset images. Mills[10] gives a value of about 1 dB for the jns from the median plane for tonal

signals at 1000 Hz and shows that near this frequency the ear is least sensitive to IAD. AT lower and higher frequencies the threshold IAD reduces to about 0.6 dB.

Various workers have conducted experiments in which IAD is traded against ITD, i.e. the image is offset by ITD say, and the subject attempts to center it by manipulating an opposed IAD. Early results[11,12] were inconsistent since it was not recognized that more than one image may be formed. Whitworth and Jeffress[13] show that two images are generally formed, one whose position depends mainly on ITD and another whose position is determined by the relative magnitudes of ITD and IAD. Once this is realised (particularly by the subject) consistent results in trading experiments using this latter image may be obtained[14,15]. There does, however, appear to be a basic difference in the nature of the image perceived under IAD and that perceived under ITD. Whereas the position of the image displaced by ITD appears well defined, in the case of IAD it becomes much more diffuse[16]. This restricts the accuracy of trading experiments. The most consistently obtained values for the trading ratio appear to be in the range, 20-35 μsec/dB[13,15], i.e. an image offset by 20-35 μsec of ITD requires an IAD of 1 dB to be recentered. Taking a value of 25 μsec/dB for the trading ratio, and from the fact that in normal hearing, a 1 degree displacement in azimuth (from the median plane) of a sound source, produces an ITD of approximately 9 μsec, we would expect an IAD of 1 dB to displace an image by 25/9 = 2.8 degrees. This value of 2.8 deg./dB for the localization constant for IAD is comparable to values obtained by Rowell[17], although he shows that considerable variation among subjects is common. Although, in

his extensive study of the localization of tonal signals, Rowell used dichotic signals and varied IAD only, he maintained that subjects could associate a direction with the perceived sound image, and was thus able to obtain the localization constant from direct subjective measurements. Image projection from dichotic signals, even to this limited extent, is rarely reported in the literature. Rowell also reports that the value of the localization constant is not greatly dependent on frequency and is not systematically dependent on signal intensity, signal duration, or on the azimuthal position of the perceived image.

Several studies on the requirements for the formation of a 'fused' image (necessary for lateralization or localization under ITD) in cases when the stimuli presented to the two ears have different waveforms have been reported. Deatherage[18], using stimuli in the form of clicks, shows that considerable differences in the frequency content of the clicks presented to the two ears are possible before fusion is lost and the images are perceived separately. David, Guttman and van Bereijk[19] show that lateralization of incoherent high frequency noise bursts is possible if the envelopes are similar. Leakey, Sayers and Cherry[20] also show the importance of the envelope in the lateralization of high frequency sounds, and propose that for signals whose frequency components are above 1500 Hz, the auditory system performs a short term running cross correlation of the envelopes at the two ears in order to lateralize the source. Toole and Sayers[21], using signals in the form of multiple tones and repetitive transients, show that even without interaural differences multiple images may be formed under ITD. In particular, for

repetitive transient signals, tonal images at harmonics of the repetition frequency are formed in addition to the transient image.

Even if fusion does not occur, the presence of a signal at one ear can affect lateralization of a signal at the other ear. Thurlow and Elfner[22] show that if a tonal signal is presented at one ear, a second tonal signal presented to the other ear whose frequency is within about 10% of the first will tend to pull the perceived position of first tone inwards from the extreme lateral position. Rowell[23] has shown similar effects using two dichotic tonal signals of differing frequency and IAD. He found that when the frequencies of the two tones are within about half an octave of each other, lateralization of either image is impossible.

When small differences between the frequencies of tonal signals presented to the two ears exist, several effects are observed. At very small frequency differences (less than 2 Hz) a cyclic shift in image position ('rotating tone'[24]) is observed, presumably because the auditory system tracks the phase variation. At difference frequencies between about 3 and 6 Hz, the image maintains a constant position, but fluctuates in loudness ('binaural beat')[25]. Further increase in frequency difference gives a roughness sensation similar to that observed in monaural beats, and when the difference is sufficient (about 50 Hz), the two tones are perceived separately.

The effect of noise on the lateralization of signals has been investigated under conditions of ITD and IAD. Houtgast and Plomp[26] used octave noise bands for both signal and masker. They introduced a 400 μsec time delay to one ear for

the masker, in order to shift the masking image from the median position. They then examined the effect of S/N on the variance of the perceived position of the signal for the median position, using ITD. They found that below a certain S/N value, (dependent on signal duration) the variance increased uniformly with reducing S/N. They claim that the increase in variance is not attributable to a vagueness in the perceived signal position, but rather to the increasing effect of chance interaction between signal and masker. Egan and Benson[27] used correlated and uncorrelated noise sources as maskers and presented tonal signals, monaurally stimulating either the left or the right ear. They examined the effect of S/N on the subject's ability to lateralize the tone. With uncorrelated noise, the threshold S/N for lateralization was only about 1 dB above that for detection, but with correlated noise (for which there is a considerable release from masking; see section 6.2) the lateralization threshold is considerably higher than the detection threshold. It appears that conditions which produce a considerable MLD do not necessarily produce a significant improvement in ability to lateralize. McFadden[28] used correlated noise as masker and examined the effect of S/N on lateralization under various conditions of IAD for signal. His results show that an increase in IAD produces a reduction in S/N threshold for lateralization, as one might expect. Typical results for the No-So stimulus are shown below (first two columns only).

IAD	Threshold for Lateralization	Estimated Threshold for symmetrical IAD
3 dB	11 dB	9.5 dB
6 dB	9 dB	6 dB
12 dB	7 dB	1 dB

Presumably if Mc Fadden had used symmetrical changes, in IAD, rather than unilateral reductions, the values shown in column three would have been obtained. These values are obtained by taking the mean interaural signal level instead of the level at the more intensely stimulated ear.

7.3 Design of Horizontal Beam Configuration

As was indicated in the block diagram of Fig. 7.1, the display produces binaural signals at its output, which posses an IAD which is some function of the azimuthal position of the target. The transfer characteristic which relates target azimuth angle to IAD must be designed to yield a satisfactory tracking performance. This transfer characteristic is dependent only on the receiver directivity patterns and the angle of splay between their normal axes. It is not feasible to choose a suitable transfer characteristic, then design the arrays to produce it, since such a characteristic will not, in general, be realizable in hardware. One must instead examine the effects of varying splay angles and beamwidths of realizable arrays.

The constant beamwidth receiving arrays discussed in Ch. 4, section 4.3 have directivity patterns which are essentially of the sinx/x shape, at least for the main lobe.

To simplify the analysis below, sinx/x patterns are assumed.

The effects of varying the splay angle, on the shape of the IAD vs azimuth characteristic, may be examined without reference to the magnitudes of the beamwidths by expressing both splay angle and azimuth angle as fractions of the main lobe width, W, (measured between zero points).

Fig. 7.2 shows a sequence of three IAD characteristics for splay angles of 0.25W, 0.5W, 0.75W. Combined sensitivity characteristics for these three cases are also shown.

The principle effects of varying the splay angle, as indicated in Fig. 7.2, may be summarized as follows:

(i) The width of the region over which an unambiguous relationship between splay angle and IAD exists (i.e. the central region between the innermost poles of the characteristics) increases as splay angle reduces.

(ii) The slope of the IAD characteristic at the origin increases as splay angle increases.

(iii) The width of the region over which a correct indication is obtained as to whether the target is left or right, (i.e. the central region between the innermost zeros of the characteristics - excluding the origin) increases as splay angle increases.

(iv) The overall width of the combined sensitivity characteristic increases as splay angle increases, but a pronounced dip begins to appear at wide splay angles.

The intermediate value of splay angle, 0.5W, would appear to offer the best compromise choice. It gives an approximately uniform combined sensitivity over a wide region without a dip in the center of the pattern.

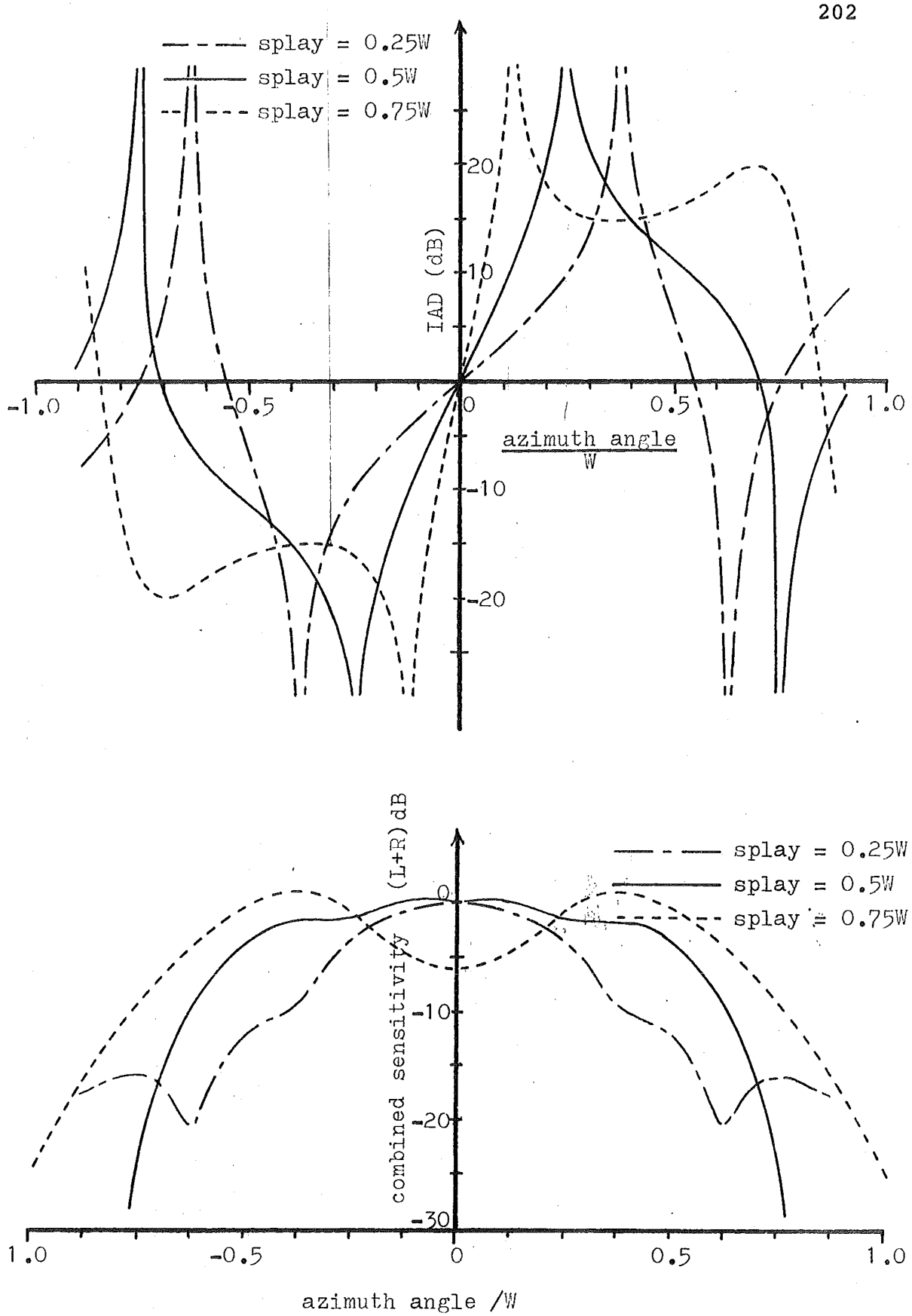

Figure 7.2. Variation of IAD Characteristic and Combined Sensitivity Characteristic with Splay Angle.

The wider splay angle (0.75W) gives a 6 dB reduction in the central region which would degrade the S/N ratio by at least 6 dB in this most important region. This is clearly undesirable. The smaller splay angle gives a substantial reduction in overall beamwidth.

Also with a splay angle of 0.5W, the unambiguous central region has a width of 0.5W, twice as wide as that achieved with the wider splay angle. The width of the region over which correct left/right indication is available, is 1.4W, or approximately 30% greater than that achieved with the smaller splay angle.

Having chosen the splay angle in terms of the receiver beamwidth, it now remains to select a value of beamwidth. The choice of beamwidth determines the scale of the horizontal axes of Fig. 7.2 in degrees. Clearly, the narrower the beams, the steeper will be the IAD characteristic at the origin, and the narrower will be the unambiguous region.

A minimum limit on the choice of receiver beamwidth is imposed by one or both of the following factors:

(i) The beamwidths must not be so small that the width of the combined sensitivity characteristic becomes less than the required overall horizontal beamwidth of 60^{o} (see Ch.2, section 2.2). From Fig. 7.2 this implies a minimum receiver beamwidth (total main lobe width), W, of $\approx 60^{o}$, or a minimum 3 dB beamwidth of $\approx 30^{o}$.

(ii) The beamwidths must not be so small that the slope of the IAD characteristic at the origin is steep enough to cause instability in the tracking system (see Fig. 7.1). If this slope is too steep the binaural image of the target will switch rapidly from left to right causing an oscillatory

approach path.

A maximum limit on the choice of beamwidth is imposed by one or both of the following considerations:

(i) The effective level of sea noise increases as the beamwidth increases, while no corresponding increase in signal level occurs. A greater transmitted power level is thus required for wider beamwidths, to produce a reverberation limited mode of operation.

(ii) The slope of the IAD characteristic reduces with increasing beamwidth. If this slope becomes too shallow tracking accuracy may become unacceptably low. The minimum possible value for beamwidth (3 dB beamwidth of $\approx 30^{o}$) was chosen. This yields the maximum possible IAD slope at the origin. It was felt that the IAD slope which this gives (1.43 dB/deg.) would not be high enough to cause tracking instability. This was confirmed in model experiments (see Section 7.7) and subsequent sea trials (see Ch. 9).

The actual 3 dB beamwidths measured for the constant beamwidth receiving arrays (see Ch. 4) was 27^{o} (rather than the design figure of 30^{o}). In view of this, a splay angle of 27^{o} was specified.

7.4 Lateralization Cues in the FM Sonar Display

Consider a single specular target lying in the field of the sonar arrays. With the present array configuration, signals at left and right ears due to the presence of this target will have different amplitudes (due to the splay of the receiving array directivity patterns) and slightly different frequencies (due to the slight difference in path length from the target to each array). The difference in frequency will be

less than 2 Hz for any realistic sweep rate and any target azimuth angle within the main beam. We have, then, the conditions for the production of a 'rotating tone' rather than a 'binaural beat' due to the effective time varying ITD for the tone. In addition to the intended cue for signal lateralization, IAD, then we also have, in general, the spurious cue due to ITD. At frequencies below about 1300 Hz this spurious cue may confuse the lateralization process to some extent. Above 1500 Hz it will have no effect.

When the target comprises a large number of scatterers occupying a small angular sector, the IAD of the audio signals produced by each scatterer will be essentially the same. The ITD for each scatterer, however, will vary significantly. This is in fact the mechanism which reduces the interaural correlation for signals from an extended target. As the extended target approaches the arrays, the interaural correlation of the audio signals produced by the target will progressively reduce since the target will occupy an increasing angular width. Jeffress et al.[29] have shown that the effectiveness of the ITD cue for lateralization diminishes slowly as the interaural correlation is reduced since only the fused portion of an image may be lateralized with this cue. It is shown in section 7.6 that the process of lateralization under IAD, however, is not necessarily degraded at all by loss of correlation. This is fortunate since as the extended target is approached, the spurious cue (ITD) becomes less and less significant whereas the intended cue (IAD) does not suffer. Confusion of lateralization for the case of a fish shoal target then, is only likely under the following conditions:

i) when the range is small enough for the center frequency of the audio signals produced by the shoal to be below 1300 Hz, and

ii) when the range is large enough for the interaural correlation to be high.

The extent of confusion when both these conditions are fulfilled depends on the variation of the cue magnitudes with azimuth angle. This is duscussed in section 7.5.

For the case of a specular target, the signals are perfectly correlated interaurally in the sense that their waveforms are identical, but are in general displaced by a time varying phase angle, so confusion of lateralization is likely at all ranges for which the signal frequency is less than 1300 Hz. This problem is discussed further in section 7.5.

7.5 The Magnitudes of Intended (IAD) and Spurious (ITD) Lateralization Cues

As was discussed in section 7.2, the beam configuration of the three arrays was designed to produce a rapid variation of IAD with azimuth angle in the center region of the beam to yield a high tracking accuracy. Although such an arrangement has the disadvantage that the angular resolution is effectively zero in the outer regions of the beam it is felt that the improvement in tracking capability outweighs this disadvantage. For the case of a single target only, in the beam, no resolution is required for the outer regions of the beam. It is sufficient to know whether the target is to the left or to the right so that the course of the vessel may be changed in order to bring the target into the central (high angular resolution) portion of the beam. This information is,

of course, available with the present array configuration. The situation which is not catered for is the case when there are two or more targets towards the extremity of the beam. No information is available to resolve these targets in angle. However, even if the arrays were designed so as to produce a smoothly varying IAD characteristic over the entire beam angle, it seems unlikely in the light of work by Thurlow and Elfner[22] and Rowell[23], that the auditory system could cope with this multiple target situation unless the targets produced signals which were clearly separated in frequency.

The IAD vs azimuth angle characteristic for the receiving arrays with a 27^{o} splay angle (used in all trials) is shown in Fig. 7.3. The 'best case' and 'worst case' characteristics correspond to frequencies at which the side lobes of the receiver directivity patterns are minimum and maximum, respectively. The overall sensitivity pattern for the three arrays, derived on the assumption of incoherent addition of signals from left and right channels is also shown. Since the beamwidth and mainlobe shape of the receiver directivity patterns is maintained constant over the entire frequency band, both the IAD characteristic and the sensitivity characteristic in the central 25^{o} sector of the beam are also invariant with frequency.

The slope of the IAD characteristic near zero azimuth is 1.43 dB/deg., which is approximately four times that which is produced in the localization of high frequency sounds in normal hearing (see section 7.2). i.e. the displacement of a target by 5^{o} from the median position produces approximately the same IAD as the displacement of a high frequency sound source by 20^{o} in normal hearing.

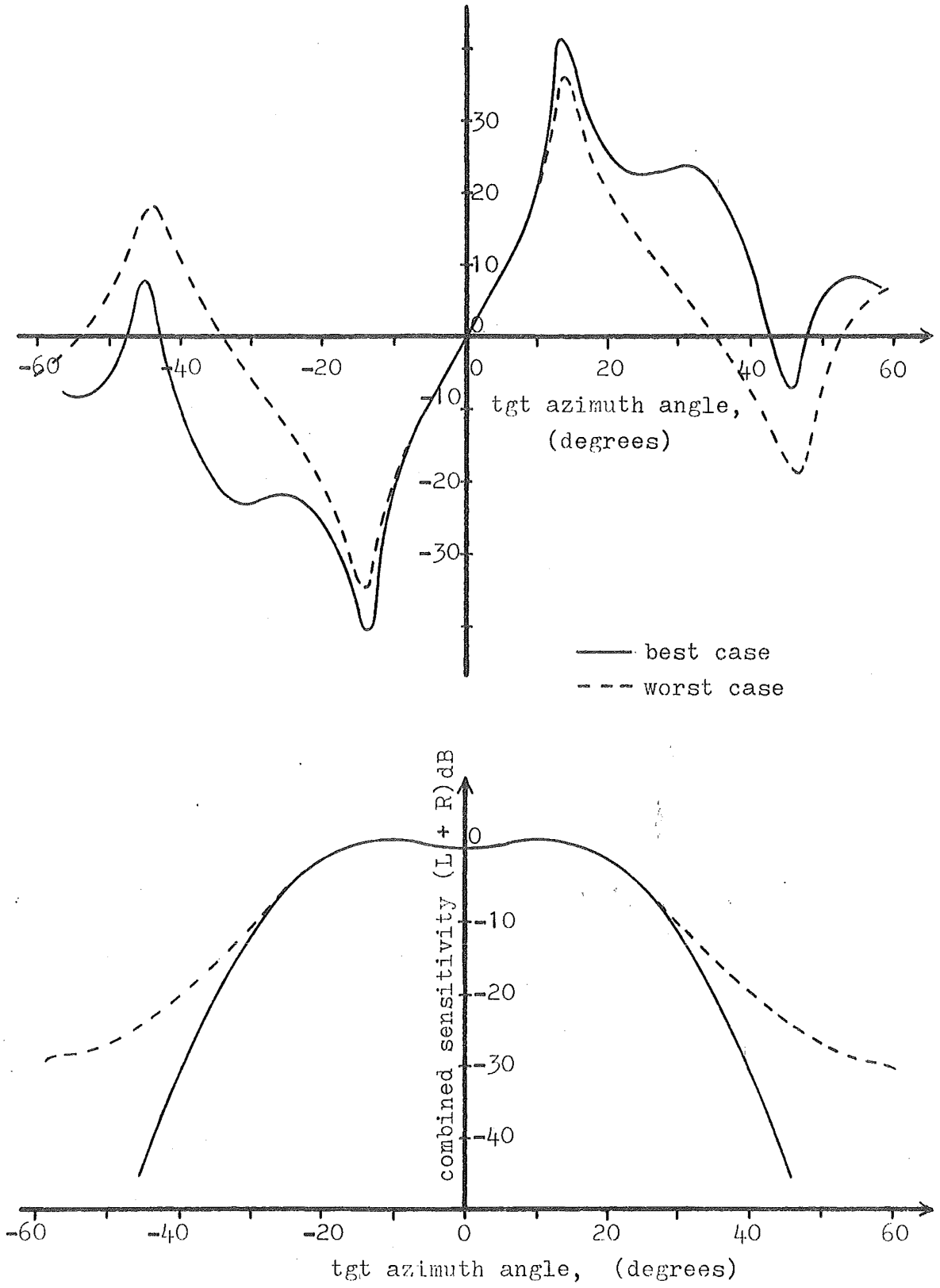

Figure 7.3. Variation of IAD and overall sensitivity as a function of target azimuth angle.

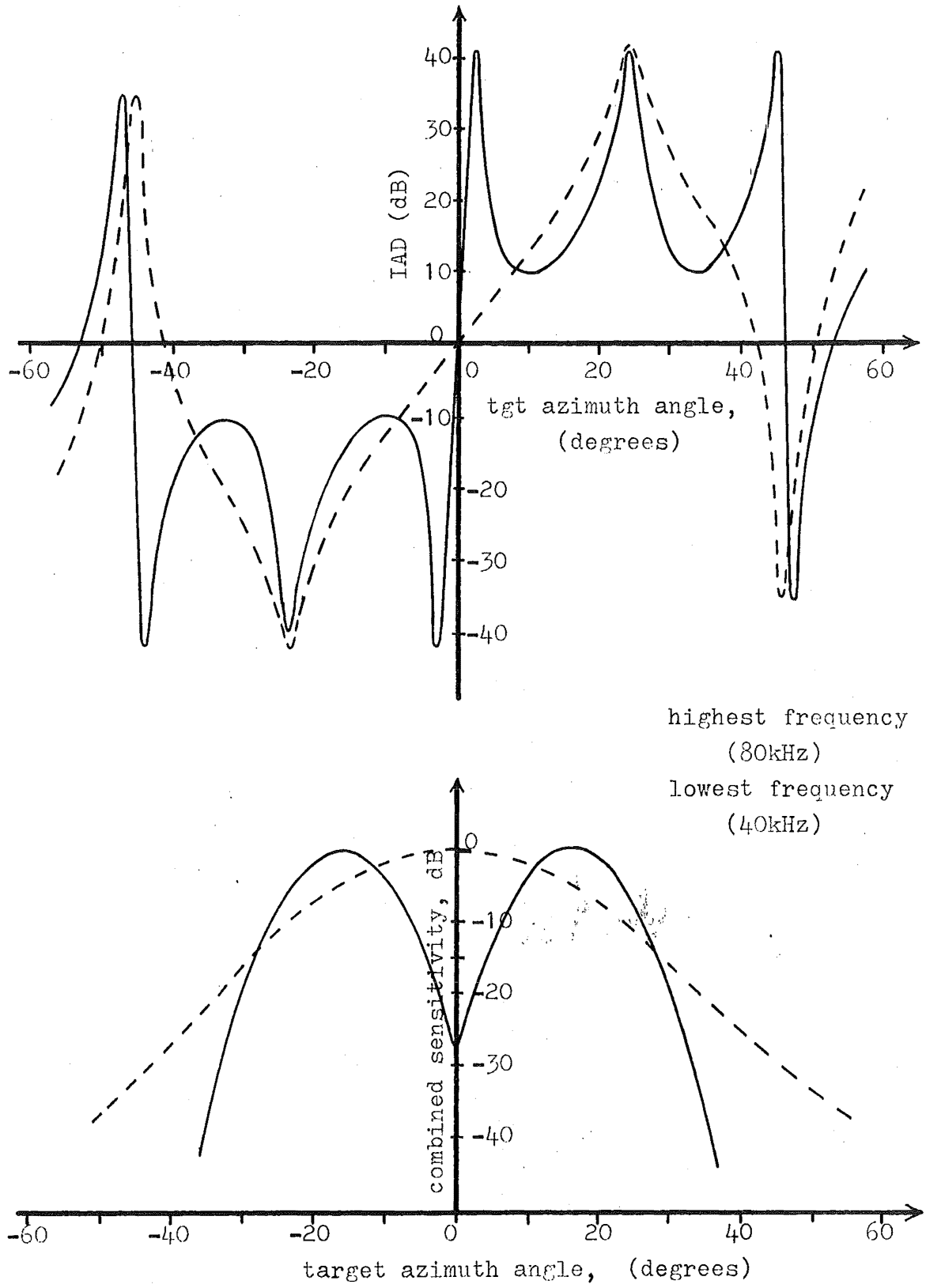

Figure 7.4. Sensitivity and IAD as a function of azimuth angle for uncontrolled receiving array directivity patterns.

Figure 7.4 shows sensitivity and IAD characteristics which would result if the receiver beam patterns were not controlled (sin (x)/x patterns assumed).

It is seen from Fig. 7.3 that the IAD becomes very large at $\alpha = 13.5^{o}$, then falls rapidly, reaching 0 dB at an angle of 35^{o}. This suggests that if a target is initially detected at an azimuth angle greater than 13.5^{o}, contradictory cues for centering the target are likely. There are several factors which help to overcome this situation. Firstly, if the target azimuth is in the range, 13.5^{o} to 25^{o}, the IAD will be at least 13 dB in the correct direction for the entire sweep duration. The <u>average</u> IAD over the sweep duration will be approximately 18 dB. Although the IAD will increase, rather than decrease when a correct course change is made, confusion is unlikely, since the image will remain well to the side until the target enters the center region of the beam.

If the target is initially detected at an azimuth angle greater than 25^{o}, there is an additional cue available, which will immediately indicate whether or not an incorrect course change has been made. This cue is the variation of total signal level with α. For $\alpha > 25^{o}$, the signal level due to the presence of target falls at a rate of at least 1.7 dB per degree increase in α. If an incorrect course change is made, then the rapid reduction in signal level will immediately indicate it.

Target tracking studies with a model sonar operating in air (see section 7.7) and with the underwater sonar (see chapter 9) show that incorrect course changes are rare, and that loss of a target due to this cause is unlikely.

We next consider the effect of spurious ITD cues on decision making during the tracking of a target. Sayers[16]

has shown that when an IAD of 12 dB or more exists, no amount of ITD can return the perceived image to the median plane. We thus need only consider the central portion of the beam where $\alpha < 7.5^{o}$. For a specular target, even in this comparatively narrow sector, considerable interaural phase differences are possible, as indicated by the variation of the cross correlation coefficient for the binaural signals (see chapter 6, Fig. 6.9). The interaural phase difference (which is equivalent to an ITD for tonal signals) may assume any value between 0 and 2π and within a single sweep may vary by as much as 270^{o} depending on the azimuth angle. Due to the complex interaction between IAD and ITD cues, it is difficult to assess the error in a particular situation. In the worst case, however, the error can be no larger than 7.5^{o}. This is not particularly serious since the absolute positional error when the vessel passes closest to the target will be at most:

$$R_{min} \tan 7.5^{o}$$

where R_{min} is the minimum range at which the target may be detected. For a target depth of 100 ft, R_{min} is of the order of 150 ft, depending on the target cross section, so a maximum positional error of about 20 ft would be expected.

For a fish shoal target of considerable extent in angle, the situation will be improved due to the reduction in interaural correlation of the audio signals which will greatly reduce the significance of ITD cues, but will not adversely affect IAD cues (see section 7.6). The final positional error will be mainly dependent on the ability of the operator to equalize the loudness of the binaural signals.

7.6 Image Centering vs Loudness Balancing in the Binaural Display

It was shown in section 6.3 that a diffuse target whose angular extent is much greater than 5^{o} will produce signals at the left and right ears which have low interaural correlation. In the tracking of a target such as a fish shoal then, we may presume that the interaural correlation of signals will be high at considerable ranges, but as the range becomes small (at which time course accuracy is most important) the interaural correlation will become negligible. Initially, tracking of the target will be on the basis of controlling the course of the vessel to center the fused image of the target. At short ranges, the course must be controlled to equalize the loudness of the uncorrelated signals at the two ears.

It is of interest then to know the comparative performance of an operator in these two tasks. An experiment was designed to quantitatively measure these capabilities and rather interesting results were obtained.

White noise signals, either perfectly correlated (No) or uncorrelated (Nu) were presented dichotically to three subjects with normal hearing. The noise was generated in the same manner as for the recognition experiment of chapter 6, and was presented at an SPL of 60 dB. The interaural amplitude difference of the noise signals was varied by the experimenter in random fashion, IAD's in the range -12 dB to +12 dB (2 dB increments) being equally likely in any one trial. The subject (blindfolded) was asked to center the image or equalize the loudness, whichever was appropriate, by adjusting a potentiometer. The subject had no way of knowing the position of the potentiometer at any time. No time limit was imposed but judgements were generally made in less than ten seconds.

After the subject was satisfied with his choice, the noise was presented for 5 secs with zero IAD. This gave him an estimate of the correctness of his previous decision, and also provided him with a reference on which to base his next decision.

Results were obtained by comparing the magnitudes of the rms noise voltages (one second averaging time) at the two earphones when the subject had completed his adjustment. The IAD thus obtained was recorded for each trial. Four sessions were conducted for each subject, two in which correlated noise was used, two with uncorrelated noise. The duration of a session was about 15 minutes and 36 trials were conducted in each session. No significant differences in either means or standard deviations for the pairs of sessions of a given type were observed and results were combined.

Fig. 7.5 shows histograms of the results for each subject and each noise condition. Means and standard deviations determined from the raw data are indicated on each histogram. Each histogram represents the results of 72 trials for a particular subject.

It is seen from Fig. 7.5 that, although significant differences in performance among subjects is apparent (possibly due to different techniques employed in balancing), there is no significant difference for a given subject between the two noise conditions. This rather surprising result indicates that the binaural auditory system is equally capable of balancing the loudness of uncorrelated noise sources as it is of centering a fused image due to correlated noise sources. Although all subjects reported that there was no concise image formed for Nu as is the case for No, their performance in the two tasks was very similar.

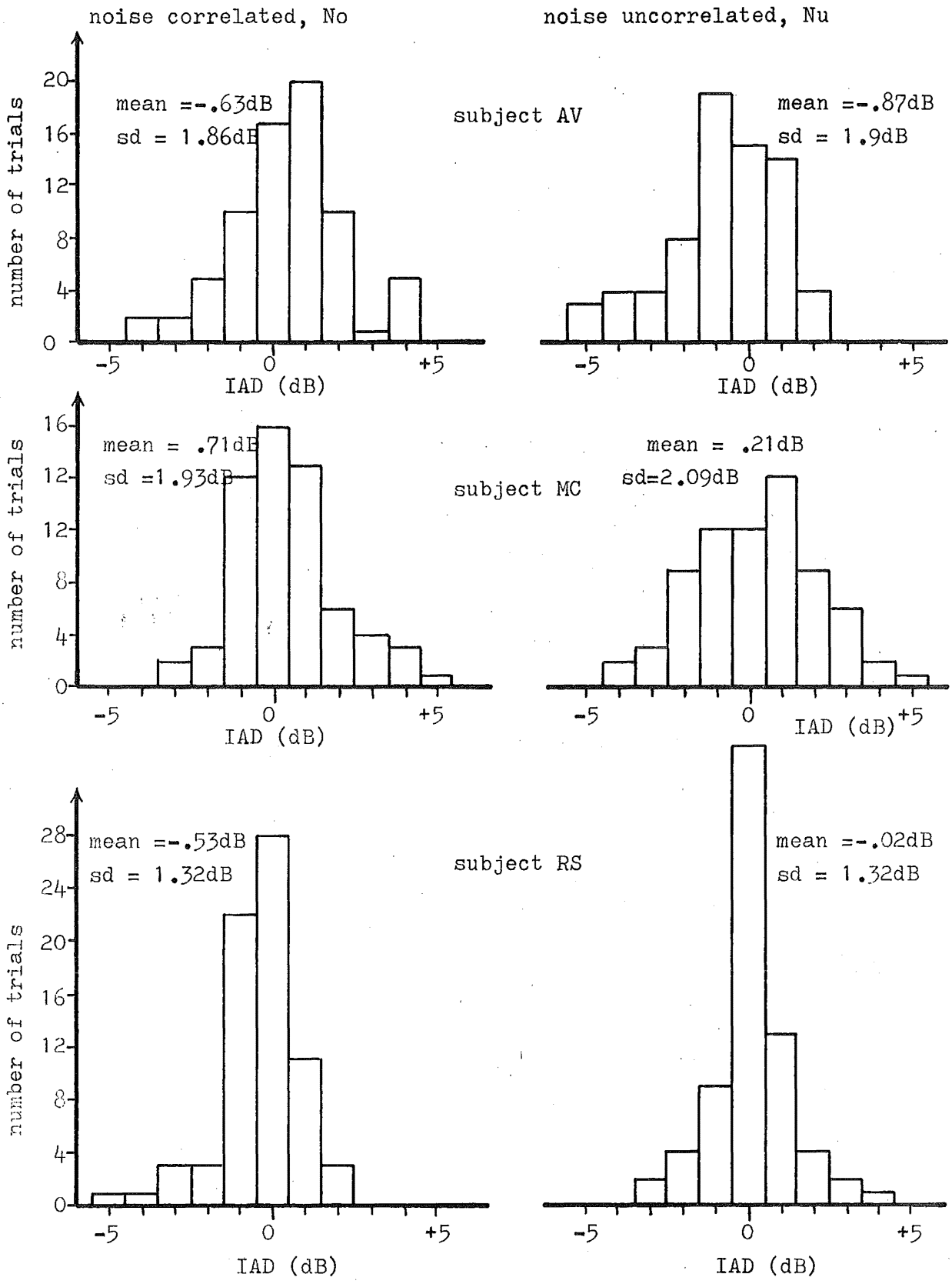

Figure 7.5. Histograms of the results of centering a noise image (No) and balancing the loudness of uncorrelated noise signals (Nu).

This strongly suggests that the mechanism by which the binaural auditory system lateralizes or localizes a sound source under IAD is by level comparison at the outputs of the detector-integrators, (see section 6.2) and that no coherent comparison is involved. This, in turn, implies an essential difference between the processes of lateralization (or localization) under IAD and that under ITD. When ITD is the only cue provided, clearly the comparison of binaural signals must take place prior to detection since no differences exist at the detector outputs. A model such as that of Jeffress[30] is apparently necessary to explain the localization mechanism in this case (see section 6.2). When IAD is the only cue provided, comparison may, and apparently does, take place at the detector outputs.

If these conclusions are justified, several results of psychoacoustic studies of lateralization phenomena may be explained. The difficulty of conducting experiments in which IAD and ITD are traded against each other is clearly explicable since the cues act in different neural regions. Also, the difficult in resolving more than one image under IAD when the frequencies are close[22,23] is understandable since under these conditions both signals would presumably be present at the detector outputs. No such difficulty arises when the predominant directional cue is ITD (viz. 'the cocktail party effect'[31]).

A further consequence of this result is that when IAD cues are involved, monaural phenomena are inseparable from binaural phenomena. For instance, in an experiment involving the detection of jns of image position under IAD, monitoring intensity changes at one ear would be almost as good as

attempting to detect the image 'shift' since both processes involve comparisons at the detector outputs.

In the audio display, it is fortunate that the auditory system functions in this way. If it did not, diffuse target tracking would be severely restricted. It is interesting to note that if the system had been designed with ITD as the lateralization cue (if this is possible), the tracking of large diffuse targets would not have been possible.

7.7 Experiments in Target Tracking Using a Model System Operating in Air

Although a large number of fish shoals have been tracked at sea, (see chapter 9) it was not possible to quantitatively evaluate the operator performance in the tracking task, under these circumstances, since there was no means available to record either the path of the vessel from the point of initial detection to the closest passing point, or the magnitude of the passing distance. This information is required to evaluate the effectiveness of the binaural display for target tracking.

To enable these measurements to be made, a model system was constructed for operation in air. It comprised a remotely controlled trolley (see lower photograph of title page of this chapter) upon which were mounted three electrostatic transducers having beam patterns in the horizontal plane which closely resemble those of the underwater sonar. The constant beamwidth technique developed in chapter 4 was applied to the two receiving transducers by sectioning the back plates, thus obtaining three independently controllable elements (see description in appendix VI). The vertical dimension of each

transducer was large in order to obtain very narrow beams in the vertical plane and thus extend the working range in air.

The trolley, which was free to move in a large room, was controlled by an operator who was unable to view its position or that of the target. The operator was provided with essentially the same information and controls as would be available when tracking a target at sea, namely,

i) speed indication and control

ii) rudder position indication and control

iii) true absolute course indication

iv) binaural auditory display derived from the arrays on the trolley.

A diplane 3 ft high and with 6" side was employed as target. This was just detectable at a range of approximately 35 ft (at zero azimuth). It was intended to employ also a diffuse target comprising a large number of small diplanes but the range attainable with such a target is prohibitively small for a realistic tracking situation.

A range scaling factor of 10 : 1 was assumed so that the air system effectively models a tracking situation at sea in which a target is detected at a maximum range of 350 ft. The range of speeds available was chosen to give approach times similar to those which were attainable with the vessel used in the sea trials discussed in chapter 9. The rudder control was designed to give rotation rates comparable with those obtainable with the above vessel.

Since the ratio of propagation velocities (seawater to air) is 5 : 1 sweep rates of twice those used at sea were necessary to give the same frequency to scaled range coding. This change does not significantly affect the tracking task.

The experiment was conducted in the following manner:

i) The trolley was placed at a range greater than the maximum detectable range, from the target, and the initial course of the trolley was chosen so that at the point of first detection the azimuth angle of the target would be in the range -30° to $+30^{\circ}$. The initial azimuth angle was chosen at random in this range for each trial.

ii) The operator was asked to start the trolley and leave the rudder position at 0° until the target was detected.

iii) When the target was first detected, the operator would indicate this and proceed to track the target using the binaural display and the controls in any manner he saw fit.

iv) The path of the trolley from the point of initial detection until the range was approximately two feet was recorded by the experimenter.

Three subjects, two of whom had had experience in tracking targets with the underwater sonar, were employed in the experiment. Several practice runs were conducted before results were recorded. No systematic differences in performance among subjects were noticed and typical results obtained are shown in Fig. 7.6.

It is seen from Fig. 7.6 that in the region from the range at which first detection occurs (R_{max}) until about half this range, significant errors are likely in the course of the vessel, presumably due to the poor S/N conditions. When the range is less than about $R_{max}/3$, however, the course remains close to the ideal course and course changes are very small when they occur. The circle drawn about the target has a radius of 6" and represents the standard deviation of the

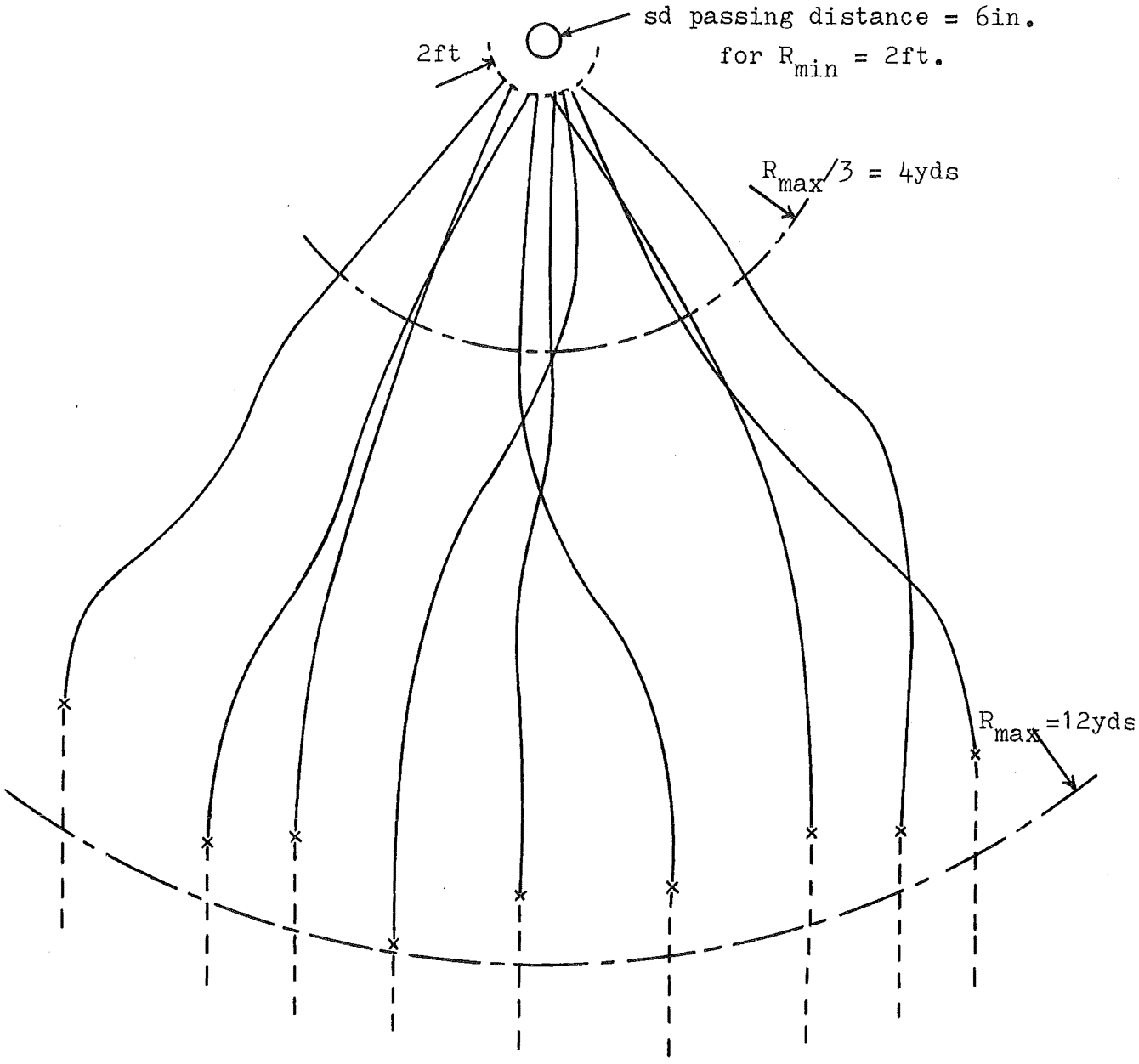

Figure 7.6. Typical approach paths for the model system tracking a specular static target.

passing distances obtained by extrapolating the course from the minimum range of 2 feet. (This figure was obtained from the results of 40 trials). If the minimum range was assumed to be 10 ft, rather than 2 ft, the standard deviation passing distance would not be greatly increased, due to the approximately constant course in the region $R < R_{max}/3$. The value of the s.d. for this case was determined as 10.5". This implies that in the corresponding tracking situation at sea, the s.d. passing distance for a target whose minimum range for detection is 100 ft, will only be approximately 9 ft.

The approach paths recorded in the model study indicate that the tracking performance with the present binaural audio display is excellent. Departures of the actual approach path from an ideal straight line path are comparatively small in terms of path length differences. This conclusion is confirmed by the tracking accuracy which was achieved in the tracking of targets at sea, at least to the extent to which this could be evaluated (see chapter 9).

7.8 Conclusions

It has been shown that the cues provided in the binaural auditory display of the FM sonar are well suited to the task of tracking a target.

When the target is a specular reflector, confusing cues due to ITD may result due to the spatial separation of the receiving arrays, but the tracking performance should not be seriously impaired by this cause. Results described in section 7.6 indicate that accurate tracking is possible for a target of this type. When the target is diffuse and has considerable extent in angle, signals produced at the two ears

will have low cross correlation, and the process of centering the target in front of the vessel will involve loudness balancing, rather than image centering. Experiments described in section 7.5 indicate that the binaural auditory system is equally capable of these two tasks.

Experiments with a model system in a tracking situation show that at poor S/N conditions, appreciable errors in course may exist, but in no case during these tests was a target lost due to this cause. The degradation of lateralization ability with reducing S/N suggests a similar trend to that reported by McFadden[28] who showed effectively that the lower the S/N ratio, the greater must be the IAD for lateralization. In the tracking of a target, failure of the operator to correctly lateralize the target will in general result in an increasing IAD, so the system is self-protective to this extent.

Although results to date are encouraging, further studies of tracking performance would appear warranted. Possibly an analogue computer simulation of the audio display similar to that used by Rowell[32] would be preferable to further studies with the air model. Although the implementation would be much more complex, the environmental conditions could be more closely specified and operator performance could be more easily monitored. An extensive study of this type would enable the elements of the block diagram of Fig. 7.1 to be determined, at least for some situations.

7.8 References

1. H. Fletcher, Speech and Hearing in Communication, Ch. 13 Van Nostrand, New Jersey, 1953.
2. L.A. Jeffress and R.W. Taylor, "Lateralization vs Localization", J. Acoust. Soc. Am., 33 : 482 (1961).
3. T.T. Sandel, D.C. Teas, W.E. Fedderson and L.A. Jeffress, "Localization of Sound from Single and Paired Sources", J. Acoust. Soc. Am., 27 : 842 (1955).
4. L.F. Elfner and R.T. Tomsic, "Temporal and Intensive Factors in Binaural Lateralization of Auditory Transients", J. Acoust. Soc. Am., 43 : 746 (1968).
5. O.C. Trimble, "Intensity-Difference and Phase-Difference as Conditions of Stimulation in Binaural Sound Localization", Am. J. Psychol. 47 : 264 (1953).
6. R.G. Klump and H.R. Eady, "Some measurements of interaural time difference thresholds", J. Acoust. Soc. Am., 28 : 859 (1956).
7. J.H. Craig and L.A. Jeffress, "Effect of Phase on the Quality of a Two-Component Tone", J. Acoust. Soc. Am., 34 : 1752 (1965).
8. J. Zwislocki and R.S. Feldman, "Just Noticeable Differences in Dichotic Phase", J. Acoust. Soc. Am., 28 : 860 (1956).
9. L.F. Elfner and D.R. Perrot, "Lateralization and Intensity Discrimination", J. Acoust. Soc. Am., 42 : 441 (1967).
10. A.W. Mills, "Lateralization of High Frequency Tones", J. Acoust. Soc. Am., 32 : 132 (1960).
11. G.G. Harris, "Binaural Interaction of Impulsive Stimuli and Pure Tones", J. Acoust. Soc. Am., 32 : 685 (1960).

12. E.E. David, N. Guttman and W.A. van Bergeijk, "Binaural Interaction of High Frequency Stimuli", J. Acoust. Soc. Am., 31 : 774 (1959).

13. R.H. Whitworth and L.A. Jeffress, "Time vs Intensity in the Localization of Tones", J. Acoust. Soc. Am., 33 : 925 (1961).

14. L.R. Hafter and L.A. Jeffress, "Two Image Lateralization of Tones and Clicks", J. Acoust. Soc. Am., 44 : 563 (1968).

15. B. McA. Sayers and P.A. Lynn, "Interaural Amplitude Effects in Binaural Hearing", J. Acoust. Soc. Am., 44 : 973 (1968).

16. B. McA. Sayers, "Acoustic Image Lateralization Judgements with Binaural Tones", J. Acoust. Soc. Am., 36 : 923 (1964).

17. D. Rowell, "Auditory Display of Spatial Information", Ph.D. Thesis, University of Canterbury (unpublished), Ch. 4.

18. B.H. Deatherage, "Binaural Interaction of Clicks of Different Frequency Content", J. Acoust. Soc. Am., 33 : 138 (1961).

19. E.E. David, N. Guttman and W.A. van Bergeijk, "On the Mechanism of Binaural Fusion", J. Acoust. Soc. Am., 30 : 801 (1958).

20. D.M. Leakey, B.McA. Sayers and E.C. Cherry, "Binaural Fusion of Low- and High-Frequency Sounds", J. Acoust. Soc. Am., 30 : 222 (1958).

21. F.E. Toole and B.McA. Sayers, "Lateralization Judgements and the Nature of Binaural Acoustic Images", J. Acoust. Soc. Am., 37 : 319 (1965).

22. W.R. Thurlow and L.F. Elfner, "Pure Tone Cross-Ear Localization Effects", J. Acoust. Soc. Am., 31 : 1606 (1959).

23. D. Rowell, op. cit., Ch. 7.

24. J. Rutschmann and L. Rubinstein, "Binaural Beats and Binaural Amplitude Modulated Tones: Successive Comparison of Loudness Fluctuations", J. Acoust. Soc. Am., 38 : 759 (1965).

25. C.E. Lane, "Binaural Beats", Phys. Rev. 26 : 401 (1925).

26. T. Houtgast and R. Plomp, "Lateralization Threshold of a Signal in Noise", J. Acoust. Soc. Am., 44 : 807 (1968).

27. J.P. Egan and W. Benson, "Lateralization of a Weak Signal Presented with Correlated and Uncorrelated Noise", J. Acoust. Soc. Am., 40 : 20 (1966).

28. D. McFadden, "Lateralization and Detection of a Tonal Signal in Noise", J. Acoust. Soc. Am., 1505 (1962).

29. L.A. Jeffress, H.C. Blodgett and B.H. Deatherage, "Effect of Interaural Correlation on the Precision of Centering a Noise", J. Acoust. Soc. Am., 34 : 1122 (1962).

30. L.A. Jeffress, "A Place Theory of Sound Localization", J. Comp. Physiol. Psychol. 41 : 35 (1948).

31. E.C. Cherry, "Some Experiments on the Recognition of Speech with One and with Two Ears", J. Acoust. Soc. Am., 25 : 975 (1953).

32. D. Rowell, op. cit., Ch. 8.

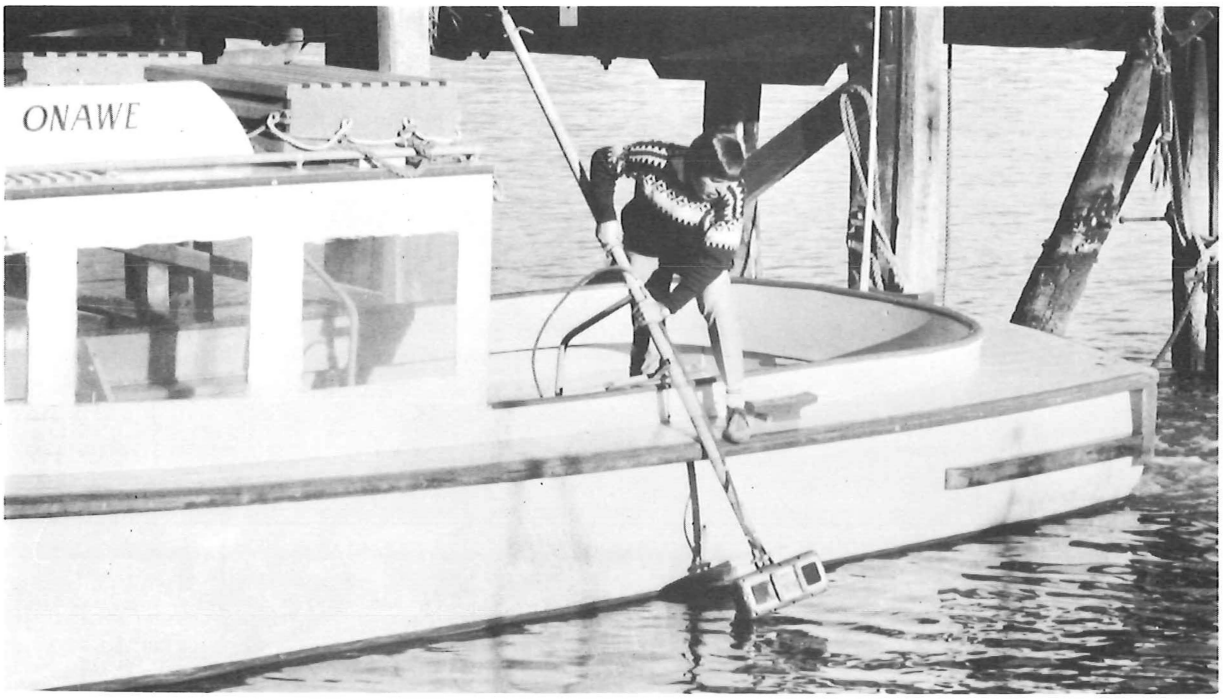

CHAPTER 8

PRELIMINARY ANALYSIS OF SYSTEM PERFORMANCE

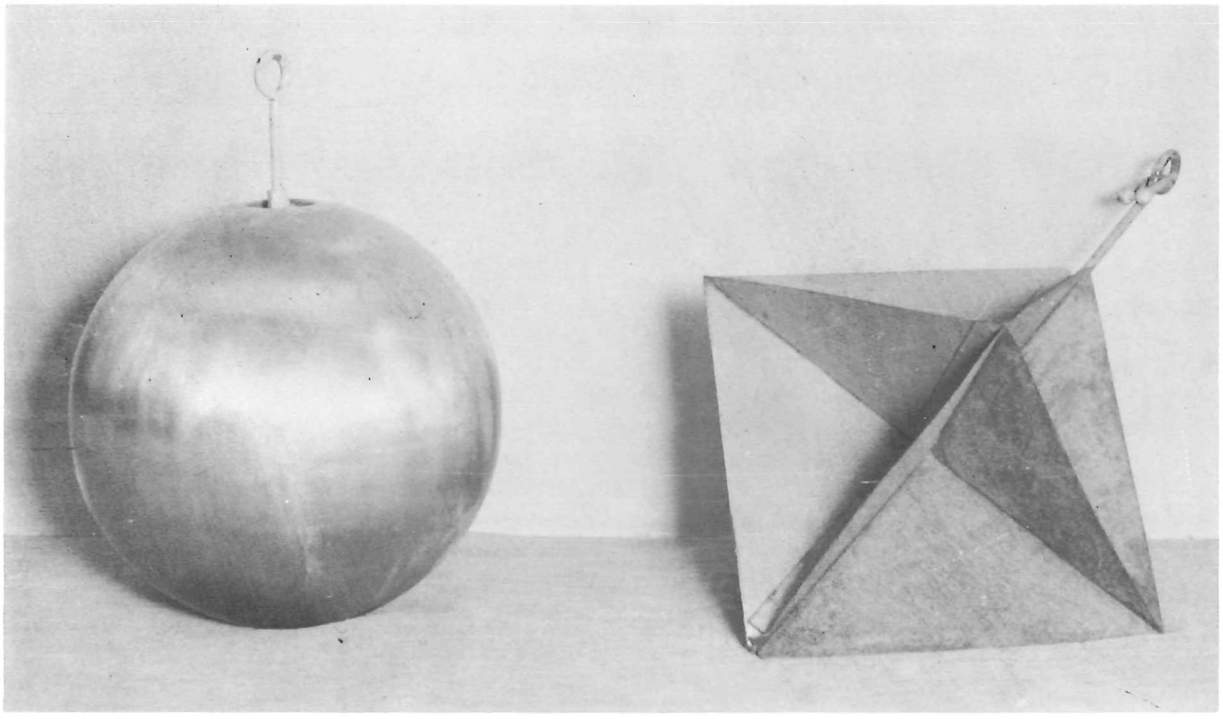

CHAPTER 8

PRELIMINARY ANALYSIS OF SYSTEM PERFORMANCE

8.1 Introduction

In this chapter, the results of preliminary tests with the sonar in shallow water are discussed. These tests in no way indicate the effectiveness of the sonar in a fishfinding role, but serve as a rough performance check.

Certain problems that first became apparent in these shallow water tests are discussed together with solutions which have been investigated.

8.2 Shallow Water Tests

With the exception of the sea trials discussed in Ch. 9, all experimentation with the sonar, to this date, has been conducted in Lyttelton Harbour. The water depth in this area is typically 30 feet and the bottom is predominantly sand and mud. Although this testing area is far from ideal due to the shallow depth, its close proximity and ease of access made the cost of experimentation there quite low.

Targets used in experimentation with the sonar were as follows:

i) 20 in. diam. hollow sphere,

ii) Tri-plane of 18 in. edge, of 0.022 in. thick steel plates,

iii) Vertical wooden pole, 15 in. diam., extending from surface to bottom,

iv) Sides of ships.

Maximum ranges for detection of the above targets are difficult to predict, due to the fact that real targets depart considerably from rigid perfect geometrical forms for which the theory is available. Using certain approximations, estimates are made of the target strengths of these targets and comparisons are made between predicted and observed maximum ranges.

8.2.1 Prediction of Maximum Detectable Ranges

The auditory detection threshold of a tonal signal against an interaurally uncorrelated noise background corresponds typically to a signal/noise ratio (sound pressure level of signal to spectrum pressure level of noise) of 14 dB (see Ch. 6, Fig. 6.12 and refs 40, 41 of Ch. 6).

Taking 100 Hz as a typical width of the critical band, a noise SPL of -14 dB with respect to the signal corresponds to a total noise level in the critical band of $-14 + 10 \log 100 = +6$ dB. It thus appears reasonable to assume that a target will be just detectable at the range at which the target strength is equal to the reverberation strength produced by that region of the sea bottom defined by the critical band centered on the audio frequency produced by the target. This assumption is made in the prediction of maximum ranges.

For a sand/mud bottom, the backscattering strength for shallow grazing angles, referred to unit area of the bottom is typically -35 dB[1]. The maximum detectable range is thus defined by the equation,

$$TS = RS$$

$$= -35 + 10 \log \frac{\pi R_{max}^2}{6.20} \qquad 8.1$$

where TS is the target strength, RS is the reverberation strength in the critical band containing the target signal,

R_{max} is the maximum detectable range, $\pi/6$ being the nominal beamwidth of one receiving array in the horizontal plane and $R_{max}/20$ is the extent of the relevant backscattering region of the bottom, in range, corresponding to an assumed critical bandwidth of 5% of the center frequency.

Eqn 8.1 simplifies to:

$$TS = -50.8 + 20 \log R_{max} \qquad 8.2$$

i) Sphere

The target strength of a thin-walled hollow sphere is difficult to predict due to the excitation of flexural waves round its surface. Diercks and Hickling[2] and Hickling and Means[3] have shown that this effect can produce variation of target strength with frequency of 40 dB or more. Even solid spheres exhibit wide variation of scattering cross section with frequency[4] due to penetration of acoustic energy into the material of the sphere.

It will be assumed for the present purposes that the frequency averaged target strength of the sphere will be that of a rigid sphere, i.e. that flexural waves will merely cause an oscillation of target strength with frequency about this mean value.

The target strength is thus given by[4]

$TS = 10 \log a^2/4$, a = radius.

For the 20 in. diam. sphere used, this gives a strength of TS = -17 dB. From eqn 8.2 then, the maximum detectable range is given by:

$$-17 = -50.8 + 20 \log R_{max}$$

Thus

$$\underline{R_{max} = 49 \text{ yds.}}$$

ii) Tri-plane

The target strength of a tri-plane is even more difficult to predict than that of the sphere since it varies greatly with both frequency (due to the excitation of transverse vibrational modes[5]) and aspect.

Gross approximations are made here to estimate at least the order of magnitude of the target strength. Consider the aspect of the triplane to be such that the direction of incident energy is equally inclined to the three planes. The quadrant returning sound energy in the direction of incidence in this case has an area of 0.054 yd^2, intercepting incident energy.

A flat rigid plate with the same intercepting area and oriented normal to the direction of incidence would have a target strength of 5.8 dB. Since the plates of the tri-plane are approximately $\lambda/50$ in thickness, a reflectivity of about 64% would obtain for a normally incident plane wave. Taking this value to be representative also for slant incidence, a loss of 3.9 dB per reflection would result, and since three reflections are involved in general, a target strength of $5.8 - 11.7 = \underline{-5.9 \text{ dB}}$ is indicated.

This value is assumed for the determination of maximum detectable range, although the average over all expected aspects would probably be somewhat smaller.

From eqn 8.2, we have:

$$-5.9 = -50.8 + 20 \log R_{max}$$

Thus,

$$\underline{R_{max} = 175 \text{ yds}}$$

iii) Wooden Pole

Exact analytical solution of the target strength of a long pole is difficult to predict even if one assumes a perfect rigid cylinder. This is because deeper sections of the pole lie at increasing angles to the direction of incidence, i.e. the sonar is inevitably within the near field of the scattered signal.

The assumption is made here that the most significant contribution to the received signal will come from the portion of the pole from the surface down to the point where the path difference is $\lambda/4$.

From the geometry, this gives an effective length, L, defined by:

$$L^2 \doteq 2\, R_{max} . \lambda/4 \qquad 8.3$$

The reflectivity of wood is typically 22%, indicating a 14 dB loss with respect to a rigid pole.

Thus we have[6]

$$TS = 10 \log \frac{a\, L^2}{2} - 14 \qquad 8.4$$

and from eqns 8.2, 8.3, 8.4, this yields a maximum range of,

$$\underline{R_{max} = 480 \text{ yds}}.$$

8.2.2 Experimental Determination of Maximum Ranges

Maximum detectable ranges strongly depend on ambient conditions, and results are presented for three sea conditions, namely,

1) Flat calm - surface virtually unrippled, allowing a

shallow tilt angle to be set on the transducer arrays without significant surface reverberation being received. The use of a shallow tilt angle gives greater illumination of the target than of the region of the bottom contributing masking reverberation. Since wedge shaped beams are assumed in the above calculations, greater ranges would be expected under flat calm conditions.

2) Calm - surface slightly rippled due to light breeze. No significant motion of the sonar-carrying vessel. A greater tilt angle is necessary under such conditions due to a significant reverberation contribution from the surface.

3) Choppy - wave height 6 in. to 18 in. Same tilt angle used as for calm conditions, but much stronger surface reverberation level causing a significant reduction in achieved ranges.

The average results obtained from a large number of trials over a period of two years are summarized in the table of Table 8.1.

Conditions / Target	1. Flat Calm	2. Calm	3. Choppy	Theoretical values
Sphere	60 yds	46 yds	40 yds	49 yds
Triplane	100 yds	65 yds	50 yds	170 yds
Pole	*	*	300 yds	480 yds

*No values obtained

Table 8.1. Table summarizing observed and predicted maximum ranges for three target types under various sea conditions.

Results of Table 8.1 show reasonably good agreement between predicted and observed maximum ranges, in view of the large number of approximations involved in the theoretical calculations.

The maximum ranges were determined by slowly backing off from the target and noting the range at which the target was just lost. The transducers were scanned manually to achieve maximum signal strength at all times. Maximum ranges typically 25% smaller than those quoted are observed if measurements are made while the vessel is approaching the target, the reduction being presumably due to the uncertainty of the frequency of the signal to be detected.

Time/frequency analysis of tape recorded audio signals produced by some of the above targets was performed with the aid of a type 6061B Kay Sonagraph. This device effectively comprises a bank of band-pass filters, each of 45 Hz 3 dB bandwidth, covering the range from 85 Hz to 8 kHz. The output level of these filters intensity modulates a graphic display, resulting in a plot of filter frequency (y axis) versus time for the duration of a single sweep (x axis), with level at a particular frequency-time point being represented by intensity. Although the band-pass filter bandwidth is half the typical critical bandwidth of the auditory system, targets could be detected by listening, at greater ranges than they could be observed on the sonagraph charts.

Fig. 8.1(a) shows a sonagraph of a signal from the sphere at a range of 46 yds. The sphere echo appears as a dark stripe which is interrupted at several points within the sweep, presumably due to variations in scattering cross

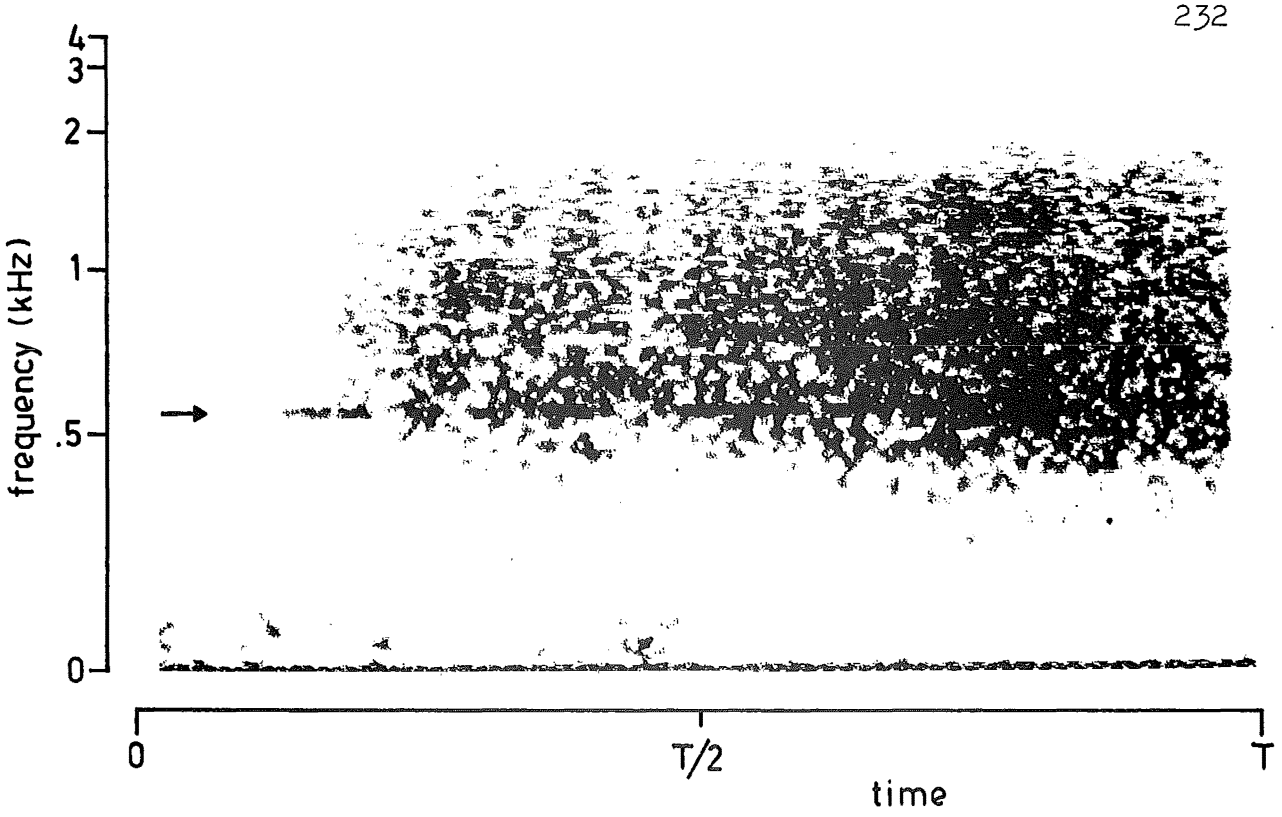

Figure 8.1.(a) Sonagraph from sphere (arrow) at range of 46yds.

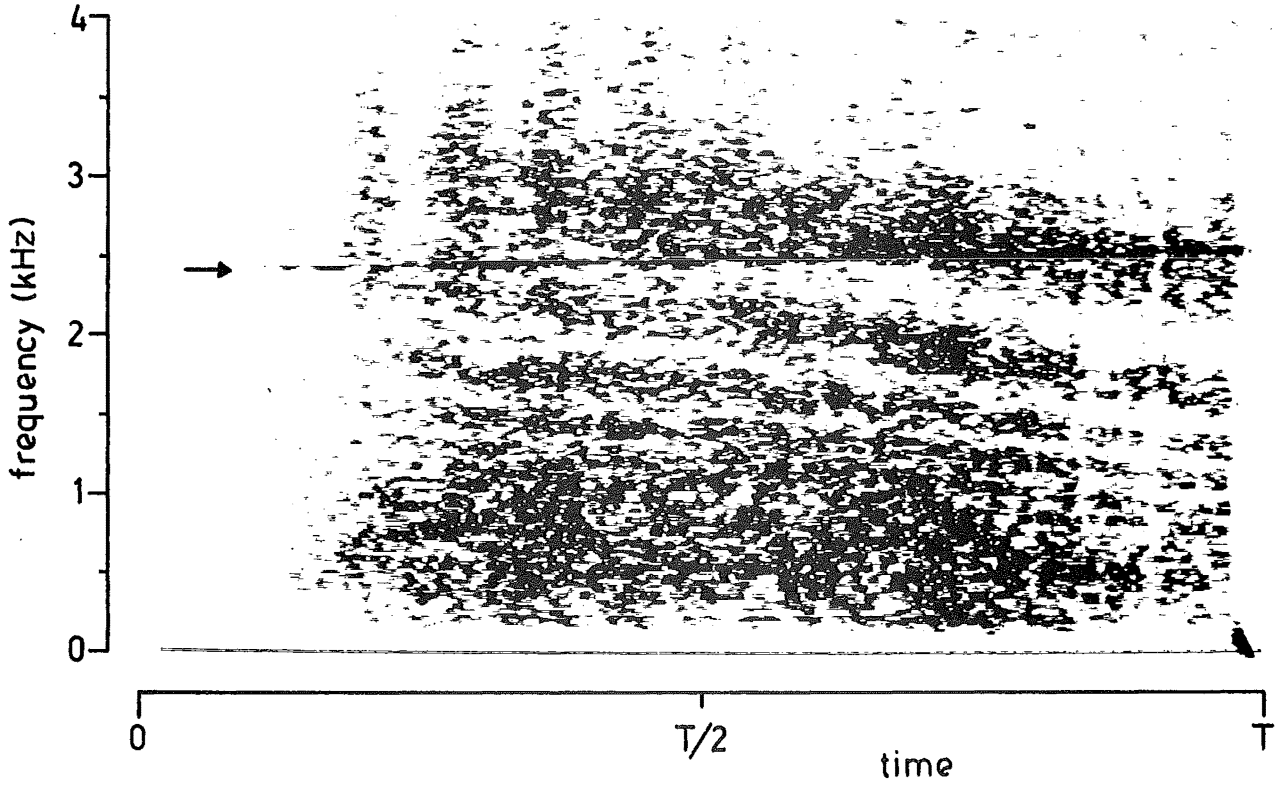

Figure 8.1.(b) Sonagraph from wooden pole (arrow) at range of 225yds. (range increasing)

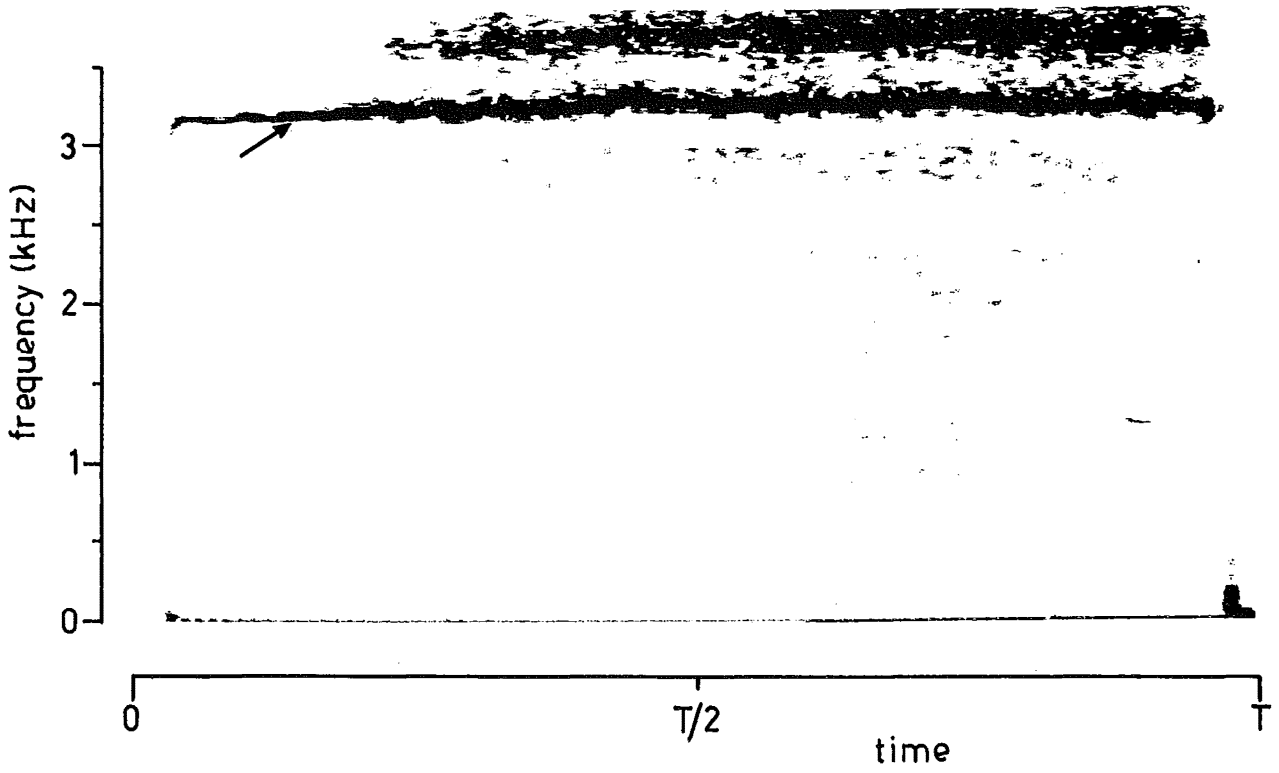

Figure 8.1.(c) Sonagraph from ship (arrow) at 270yds in broadside aspect. Sonar and target stationary.

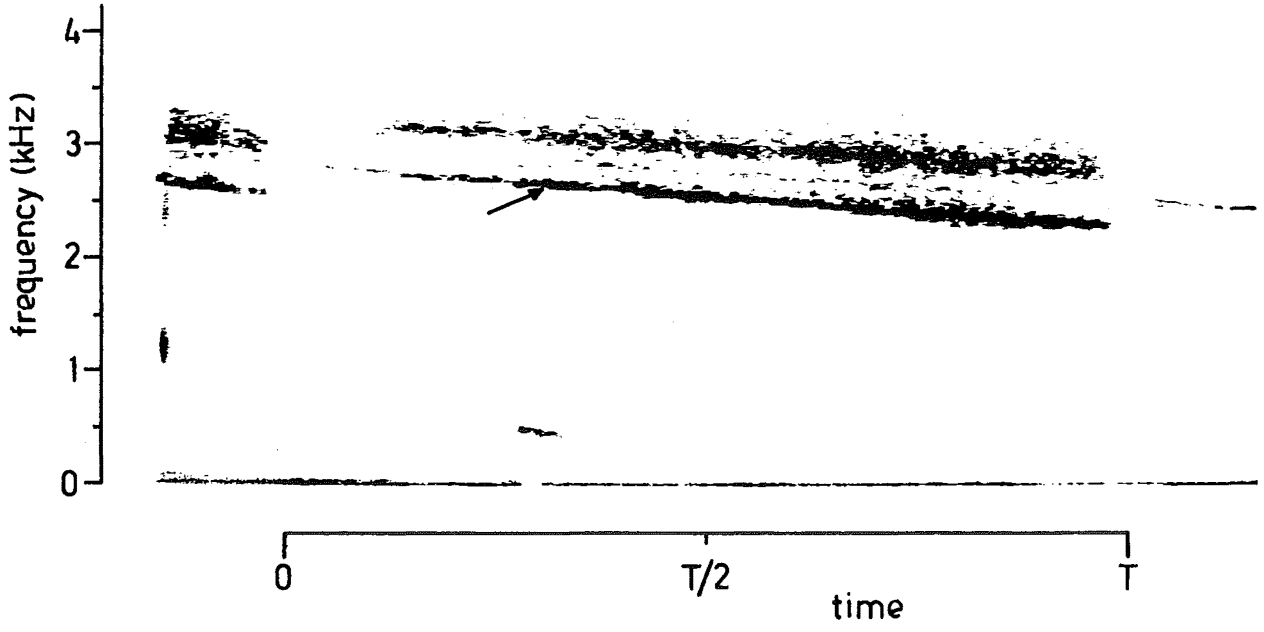

Figure 8.1.(d) Sonagraph made during approach to ship (arrow) at approximately 6 knots.

section with incident frequency.

Fig. 8.1(b) shows a sonagraph of a signal from the wooden pole at a range of 225 yds. The tape recording from which this sonagraph was made, was taken while the vessel was receding from the pole, as indicated by the upward frequency modulation of the audio signal produced by the combined effects of Doppler and increasing range.

Fig. 8.1(c) shows a sonagraph of a signal from a ship in broadside aspect at a range of 270 yds (ship and sonar-carrying vessel both stationary).

Fig. 8.1(d) shows a sonagraph of a signal from the same ship at approximately the same range but with the sonar-carrying vessel approaching at about 6 knots. The last portion of the previous sweep and the first portion of the following sweep are also shown to indicate the separate frequency modulating effects of closing range and Doppler. The step in frequency between the end of one sweep and the beginning of the next is due solely to the differing Doppler shifts at the upper and lower frequency limits. The reduction in frequency from the commencement of one sweep to the commencement of the next indicates the reduction in range.

8.3 Cross-talk and Methods of Suppression

In any continuous transmission sonar, the direct acoustic feed-through from transmitting array to receiving array imposes restraints on the front end electronic design, and may limit the system performance. With the present sonar, no real estimate of the magnitude of cross-talk signals could be made until the arrays had been built and tank tests had been conducted. Early experiments showed that a cross-talk signal

of pressure magnitude -40 dB with respect to the transmitter source strength could exist. The effect showed considerable frequency dependence with a general tendency to become higher at higher frequencies. This magnitude is such that under almost all operating conditions, the cross-talk signal is greater by 40 dB or more than signals from targets of interest.

The principal effect of the presence of a large cross-talk signal is a reduction of the effective dynamic range of the RF amplifier stages. If intermodulation distortion is to be avoided, the RF stages and demodulator must have small enough gain to pass the cross talk signal without distortion. For a given transmitter level then a maximum gain is defined. A minimum gain condition is also imposed by amplifier noise considerations. This may be demonstrated by the following analysis.

Consider the simplified schematic of one receiver channel shown in Fig. 8.2. Let ρ_1 be the noise power spectral density referred to the input of the RF stages due to noise generated within these stages. Also, let G_1 be the overall gain, and W_1 be the bandwidth of the RF stages. The effective noise source at the input, due to RF amplifier noise thus has a power, $\rho_1 W_1$. At the demodulator input, this noise level becomes, $\rho_1 W_1 G_1$. At the low pass filter output, this gives rise to noise power,

$$\frac{2\rho_1 W_1 G_1}{m}$$

where m is the ratio of RF bandwidth to audio bandwidth and the factor 2 accounts for the two side bands involved.

If ρ_2 is the power spectral density of noise generated within the audio amplifier and referred to its input, then the noise power introduced by audio amplifier noise at this point is

$$\rho_2 W_2$$

where W_2 is the audio bandwidth.

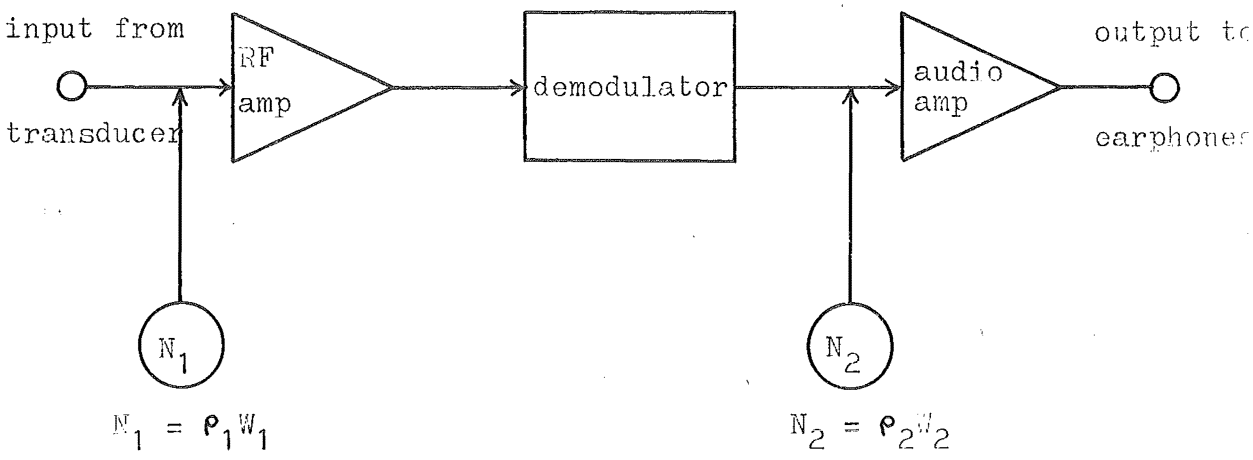

Figure 8.2. Schematic showing noise sources within the receiver electronics.

To achieve best noise performance it is clearly desirable that noise introduced by the audio stages should be of negligible magnitude compared with that due to the RF input stage, i.e. that the ratio,

$$\frac{2\rho_1 W_1 G_1}{m\rho_2 W_2}$$

should be 20 dB or more. Since $W_1/W_2 = m$, this implies,

$$\frac{2\rho_1 G_1}{\rho_2} > 100$$

ρ_2 will normally be greater than ρ_1 even if both audio and RF stages are designed for low noise performance since 1/f noise will contribute to ρ_2. A minimum voltage gain of 10 is thus required.

It was found that at the highest required transmitting levels, the two limiting gain conditions could not be met simultaneously. Thus, with an RF gain of 10, considerable intermodulation distortion was noticed at high transmitter levels. The principle effect of this distortion was an apparent amplitude modulation of all audio signals at a low frequency corresponding to the propagation delay from transmitting array to receiving array. At high frequency sweep rates, the effect could hardly be noticed since the 'modulating' frequency becomes high. However, at more normal sweep rates (repetition period greater than one second), the effect proved extremely distracting and detection performance would, most certainly, suffer.

Two methods of overcoming this problem were investigated, one which treated the problem (the use of absorbent baffles to suppress the cross-talk signal) and the other which treated the symptoms (the use of a cross-talk derived carrier to suppress intermodulation distortion). These methods are discussed below.

i) The use of absorbent baffles

Considerable suppression of cross-talk signal magnitude may be achieved by the use of baffles mounted between the arrays and projecting outwards from the housing by 1 or 2 in. (see lower right hand photograph of the title page of Ch. 4).

A number of possible materials were considered for the fabrication of baffles. Measurements were made on sample

specimens of these to determine their absorptive and reflective properties. Ideally, the baffle material should have a high absorption coefficient and a low reflection coefficient so as to produce maximum cross-talk suppression with minimal disturbance to the directivity patterns of the arrays. Table 8.2 shows data from transmission and reflection measurements made on samples of a fixed size and shape.

Material	Thickness (in)	Transmitted Level (dB)	Reflected Level (dB)
Hairlock	1	-12	-20
Foam Chip Rubber	1	-20	-19
Neoprene	¼	0	-52
Sponge rubber	$\frac{3}{4}$	-20	-18
Asbestos	½	-23	- 5
Rope (immediately after immersion)	$\frac{3}{4}$	-26	-11
Rope (several hours after immersion)	$\frac{3}{4}$	-35	-18
Loaded Rubber	$\frac{3}{4}$	-30	-20

Table 8.2. Reflected and transmitted signal levels re incident signal level for various materials.

The best materials tested were loaded rubber compositions and a series of experiments using baffles of this material of varying thickness were conducted. As the thickness (dimension measured outwards from the array faces) was increased, the cross-talk level progressively reduced, reaching negligible proportions at a thickness of approximately 2.5 in.

A compromise is necessary, however, in choosing the baffle thickness since the baffles (a) create turbulence in the flow around the housing and (b) degrade the directivity patterns of the arrays. A baffle thickness of approximately 1.5 in. appears to be an adequate compromise. This produces a reduction in cross-talk signal magnitude of approximately 15 dB at the frequency at which it is a maximum. Fig. 8.3 shows cross-talk signal magnitude as a function of frequency both with and without baffles.

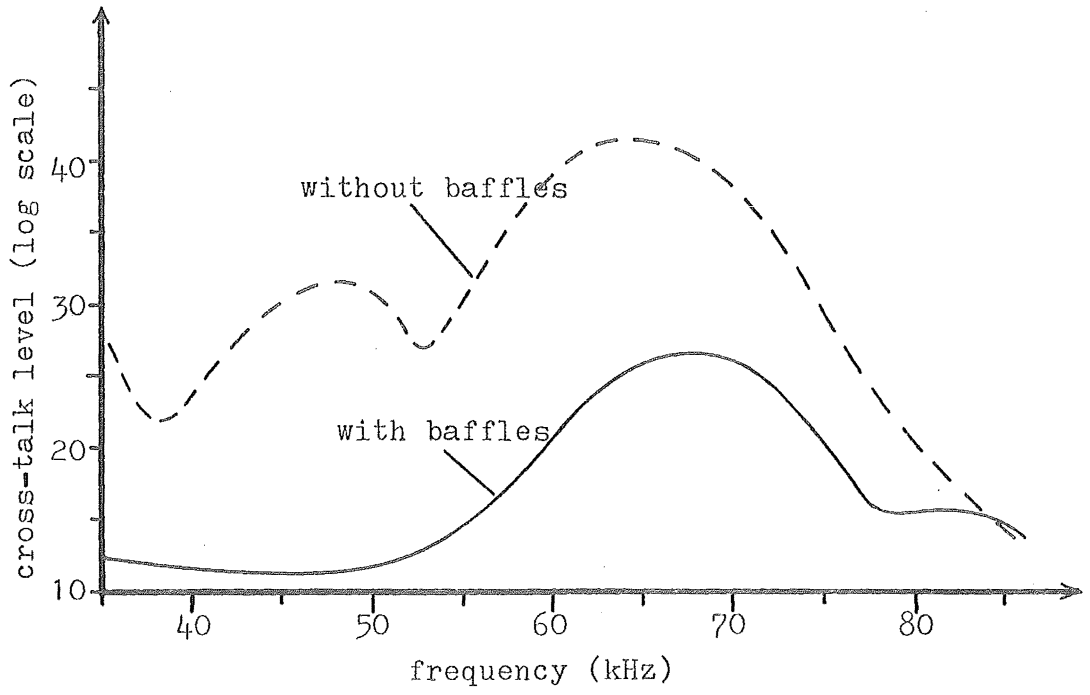

Figure 8.3. Frequency variation of cross-talk signal magnitude with and without baffles.

The considerable variation of cross-talk level with frequency evidenced by Fig. 8.3 is to be expected since the receiving array is within the near field of the transmitting array. Considerable temporal variation of cross-talk level has been noticed during operation at sea. This is presumably due to the motion of water across the arrays causing irregular phase shifts of the cross coupled signals.

Considerable reduction in intermodulation distortion is achieved by the use of baffles as described above. At the maximum transmitting level, however, distortion is still just noticeable. It is doubtful whether any performance degradation would be produced by this residual level.

ii) Cross-talk carrier derivation

An alternative method of overcoming the deleterious effects of cross-talk without actually reducing its magnitude was also investigated. This involved the derivation of the carrier signal (for injection into the demodulators) from the cross-talk signal itself, when the latter exceeded a certain predetermined level.

When the cross-talk signal is large enough to cause intermodulation distortion, it is of the order of 40 dB above the level of signals of interest. Thus, by amplifying the received signal and detecting zero crossings, a switching signal at cross-talk frequency may be derived. If this switching signal is used for demodulation, there is then no frequency difference between carrier and cross-talk so no intermodulation products are formed.

There is, however, a difficulty in implementing this technique due to fluctuating level of the cross-talk signal due to frequency variation and water motion. Fig. 8.4 shows a

schematic diagram of the method used to test the feasibility of this scheme. An envelope detector is used to determine whether the cross-talk signal is large enough to successfully derive the carrier from it. If it is not large enough, the normal carrier (derived from the transmitting waveform) is used.

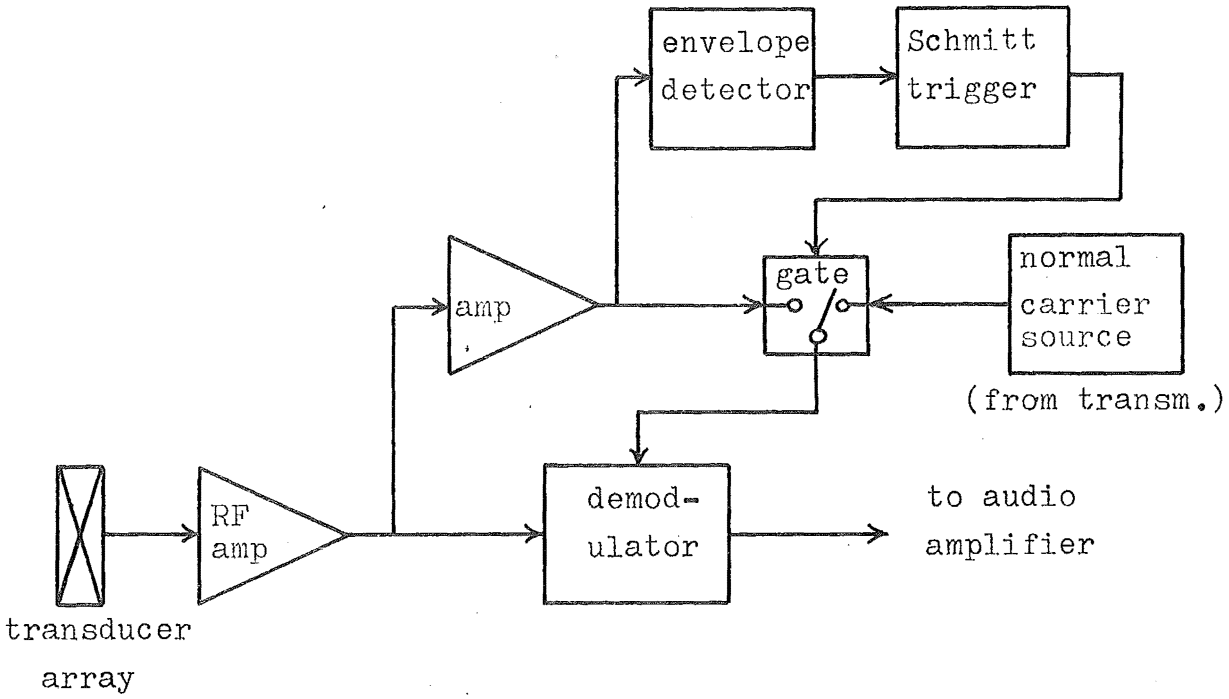

Figure 8.4. Schematic showing the method of implementing the cross-talk derived carrier method.

This technique completely eliminates intermodulation distortion but suffers from the disadvantage that a transient is generally introduced due to the step phase change produced by changing from one carrier source to the other. The audio signal suffers a phase change equal to the phase change of the fundamental component of the carrier waveform so a click is produced unless the two carrier signals happen to be in phase at the moment of switching. Due to this characteristic, the method was abandoned.

8.4 Surface Reverberation and Methods of Reduction

Early experience with the sonar showed that in some sea conditions, even without breaking waves (which give rise to air bubbles, see section 8.5) very large signals could be returned from the sea surface, immediately in front of the vessel. Like most acoustic phenomena of the sea, the effect was extremely variable, the scattered signal level sometimes fluctuating rapidly by up to 40 dB, sometimes remaining very low for several minutes, then rising to consistently high levels for similar periods.

In general the effect showed a high correlation with sea state. In calm conditions the effect was rarely noticed. In choppy seas, strong signals were generally produced and the magnitude showed no significant dependence on the direction the sonar array was trained with respect to the wind. In rolling seas, the effect was sometimes negligible, but when present showed a pronounced dependence on the direction of the sonar beam with respect to the waves.

The problem which arises due to surface reverberation of this nature is, as with the cross-talk problem (see section 8.3), that the RF amplification stages may become overloaded, producing considerable distortion of signals from all ranges. The audio signals produced by the surface scattered signals pose no problem in themselves since the largest signals are at sub-audible frequencies or at least at very low audible frequencies and are at worst distracting. They produce no masking of signals of interest since they are well removed in frequency (see Ch. 6, section 6.2). The harmonic and inter-modulation distortion of the signals of interest, however, will in general degrade the performance of the sonar with

regard to the detection and recognition of targets.

The main factor responsible for the appreciable signal returns from the surface is the comparatively wide beamwidth in the vertical plane, which means that significant side lobes exist in directions at considerable angles to the array normal. Since the sea surface is only a few feet above the array, these side lobes may give rise to the reception of large signals from the surface.

Two specific methods for reducing the effects of surface scattered signals were investigated. These were:

(i) The use of an asymmetrical beam in the vertical plane to reduce side lobes in the direction of the surface,

(ii) The use of a zig-zag array to increase the effective number of array elements in the vertical direction. Amplitude tapering was used in conjunction with the above approaches to minimize the remaining side lobes.

It will be recalled that the size of the faces of the elements used in the arrays is 17 mm diameter. This dimension was chosen to keep the number of elements for each array reasonably small to simplify construction. At the time of this choice, a realistic estimation of the magnitude of surface scattering could not be made. Thus, when it was found that surface scattering presented a problem, solutions investigated had to be based on this element size as no others were available.

With the rectangular array format, the separation between the adjacent rows of elements must be at least 17 mm assuming negligible separation between elements. The acoustic separation between rows is thus approximately one half wavelength at 40 kHz, whereas at 80 kHz, the separation is about

one wavelength. At 80 kHz then, the directivity pattern will contain a repetition of the major lobe at an angle of 90^{o} to the normal to the array. This second major lobe is, of course, considerably smaller than the central major lobe due to the appreciable directivity of the individual elements (see directivity patterns of Ch. 4, Fig. 4.14 and 4.15).

The magnitude of the second major lobe is dependent on the element directivity and to some extent by the housing and window[7]. Its magnitude cannot, however, be affected by sensitivity shading as any change in element sensitivity affects all major lobes in an identical fashion. This is true, regardless of the number of elements in the array, provided they are uniformly spaced. The angular position of the second major lobe, θ_2, with respect to the central lobe is given by:

$$\theta_2 = \text{arc sin } \lambda/d$$

so that reduction of the element spacing is one method by which this lobe may be shifted out of the range of real angles. Another method by which the effect of one of the two secondary major lobes may be reduced is to shift the entire pattern in angle, with respect to the normal direction, thus eliminating the second major lobe on one side. Both these methods were investigated using the receiving arrays.

8.4.1 Asymmetrical Beam Method

If the beam of the array is deflected to one side by introducing time delay sections between rows of the array, the second major lobe on the side towards which the beam is deflected may be shifted out of the range of real angles. The second major lobe on the other side, of course, shifts inwards and becomes more pronounced. This is not a severe

disadvantage since the sea bottom is far further removed than is the surface so there is no fear of overloading by bottom returns.

Since the bandwidth is wide, true time delay sections, rather than phase shift networks must be used to produce the deflection. Fig. 8.5 shows a schematic diagram of the electronics employed.

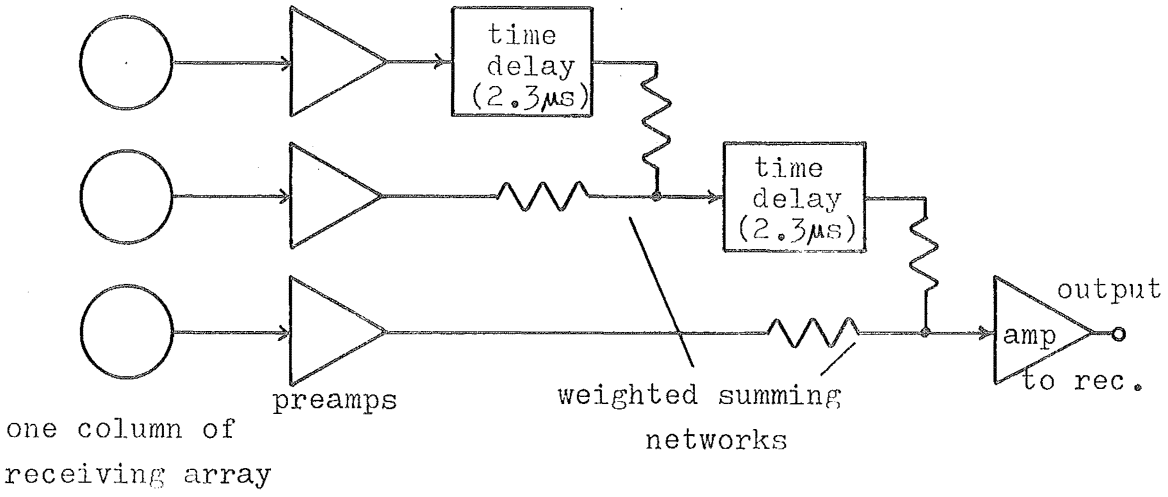

Figure 8.5. Schematic diagram of the electronics used to deflect the beams of the receiving arrays in the vertical plane.

The chosen time delays of 2.3 μsecs cause shifts of approximately 18° for the secondary major lobes and approximately 11° for the central major lobe. The 'weighted summing networks' shown in Fig. 8.5 minimize the magnitude of the minor lobes. Fig. 8.6 shows directivity patterns measured in the vertical plane for this array. Horizontal patterns were unaltered apart from the 11° shift of the 'horizontal' plane from the normal to the face of the array.

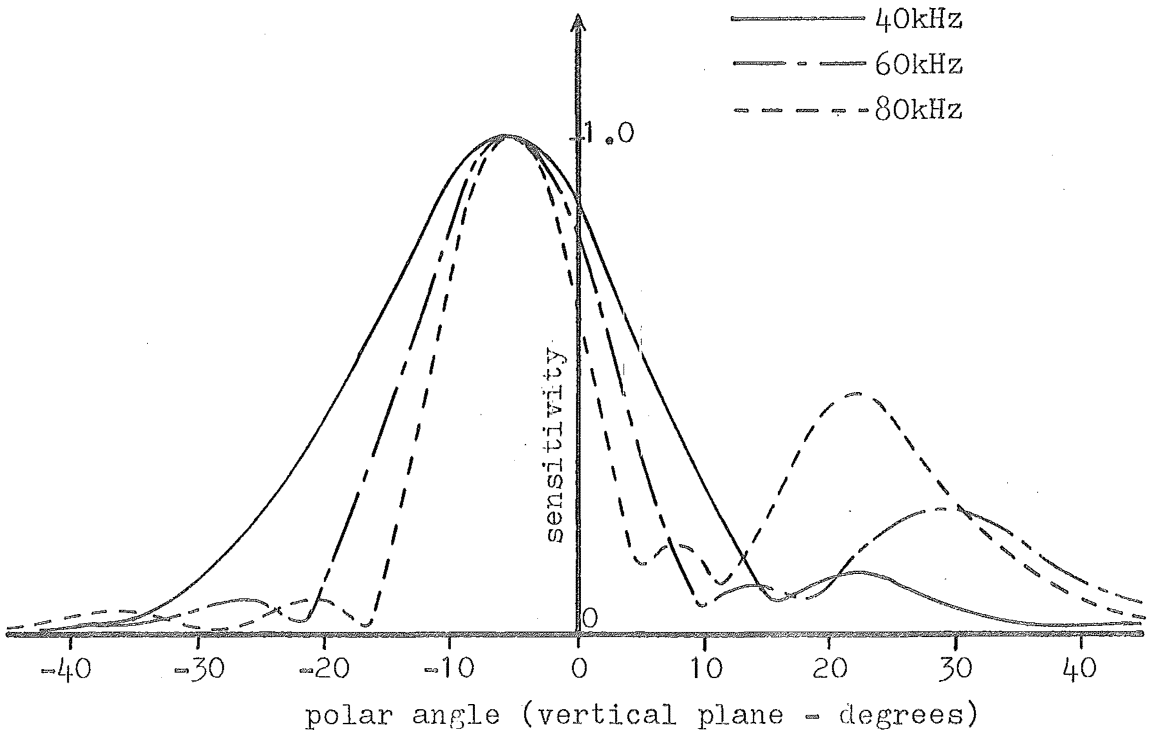

Figure 8.6. Directivity patterns measured in the vertical plane for the beam-deflected array.

A significant reduction in side lobe levels on one side is apparent from Fig. 8.6. The side lobe suppression, including the second major lobe produced by this configuration is approximately 15 dB better than that for the normal array.

A significant reduction in the effects of surface scattering was noted in experiments in which one array was left in the original configuration and the other had the beam deflected. In some circumstances overloading still occurred although the incidence was very much less for the beam-deflected array.

It was found to be prohibitively expensive to apply this technique to the transmitting array since active circuitry for

producing time delays cannot be used efficiently with high level signals. Three separate power amplifiers would be required to implement the technique. Unless all three beams are deflected it becomes extremely difficult mechanically to house all three arrays in a single enclosure due to the different orientations required for the three array surfaces. In view of this, the beam-deflection method was abandoned for the second version of the arrays which used a single housing (see lower right hand photograph on the title page of Ch. 4).

8.4.2 Zig-zag Array Method

An alternative method to eliminate the second major lobes in the vertical directivity pattern is to increase the effective number of rows of elements in the array, and reduce their separation accordingly to maintain the same overall array dimension. If smaller elements were available, this would be a comparatively simple task. However, even with the original large elements, an improvement may be effected by displacing two of the four columns of elements vertically with respect to the other two (see sketch of Fig. 8.7).

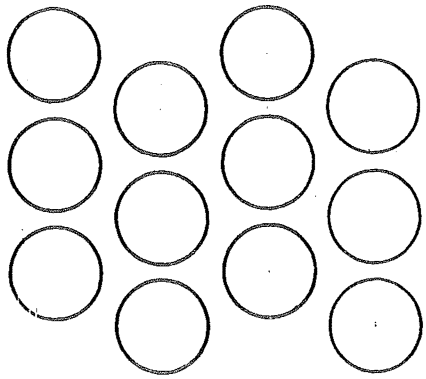

Figure 8.7. Zig-zag array configuration.

This arrangement gives effectively six rows of elements at a separation of half that achieved with the rectangular array. The second major lobe is then well outside the range of real angles.

Three sensitivity levels may be used with this array to suppress side lobe levels. Fig. 8.8 shows measured directivity patterns obtained using Dolph-Chebychev shading.

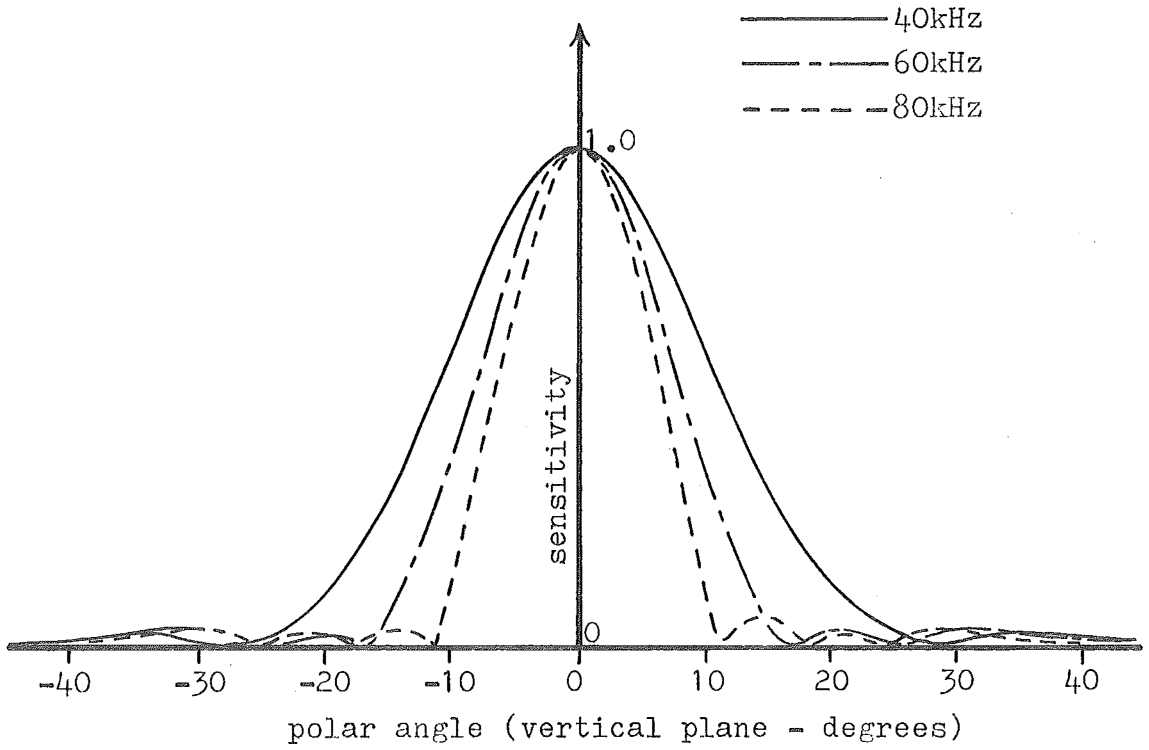

Figure 8.8. Directivity patterns in the vertical plane for the 'zig-zag' receiving array.

It is clear that considerable side lobe suppression may be achieved with this configuration. The suppression is, in fact, 14 dB better than that for the normal rectangular array.

This type of element configuration was employed in the receiving arrays when the single housing was incorporated.

8.5 Effects of Air Bubbles in the Water

A problem which was not anticipated was encountered when air bubbles, in significant concentration, were present in front of the arrays. This condition, if present in turbulent water was found to produce strong noise signals of considerable bandwidth at the audio display.

The two most prominent sources of air bubbles near the sea surface appear to be:

i) wave action, and

ii) ship wakes.

In choppy sea conditions, air bubbles are frequently produced and the smaller bubbles may remain within a few feet of the surface for several minutes. If the concentration is high and the bubbles are close to the arrays, overloading of the RF amplifier stages may occur due to the strong scattered signals. As with the cross-talk problem (see section 8.3) this causes intermodulation distortion of signals from more distant targets. However, the problem with this type of aeration is not too severe since it arises in only some sea conditions and is never present for more than about 5% of the time due to the local nature of the effect.

Very much more severe degradation of the performance of the sonar results when wakes of ships are encountered. Air bubbles produced by this means are accompanied by severe turbulence in the water and both the turbulence and the aeration may last for several minutes.

It was found that when a wake is close to, and in front of, the arrays audio noise at high level and with frequency components of significant magnitude up to at least 3 kHz is produced. Initially, it was thought that these wide band

signals were in some way generated by RF amplifier distortion, but subsequent experiments at low transmitter level showed that this was not the case. Further experiments using a constant frequency CW transmission showed exactly the same effects, indicating that the wide band noise was not produced by the normal frequency modulation process. Fig. 8.9 shows a typical audio spectrum obtained in the presence of a wake, and for comparison, a spectrum recorded shortly before the wake was encountered. Spectral analysis was performed with a Kay Sonagraph. A CW transmission at the fixed frequency of 60 kHz was used in both cases.

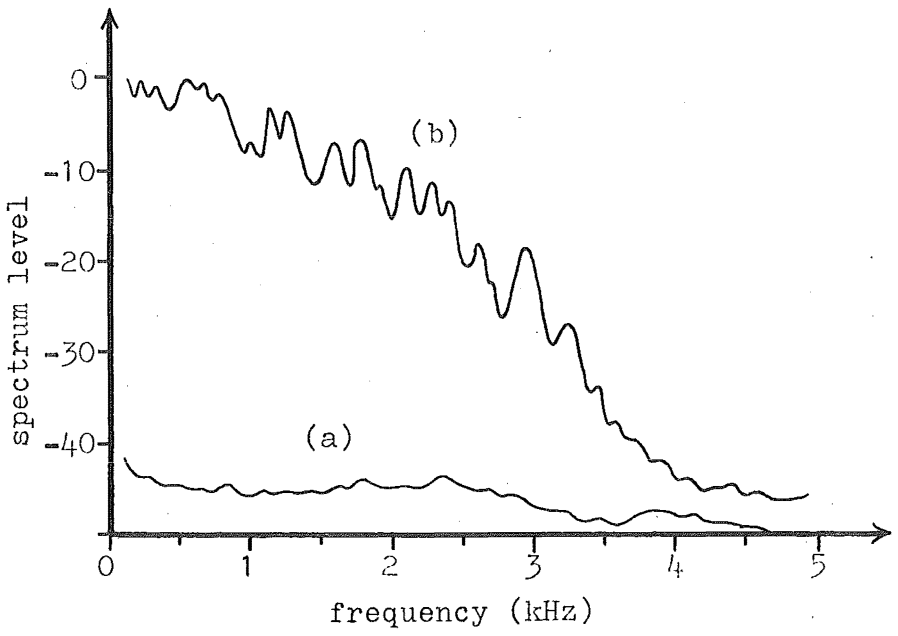

Figure 8.9. Audio spectrums measured (a) before encountering a wake and (b) in the presence of a wake.

Spectrum (b) shows that strong spectral components up to approximately 3 kHz are produced. (An audio amplifier with flat frequency response was used.)

The possibility of bubble motion producing direct Doppler shifts of this order was rejected since velocities in excess of 100 ft/sec. would be required. Also, if this was the mechanism, a rapid reduction of the spectrum level with increasing frequency would be expected.

At this time, no rigorous investigation into the effect has been conducted but a possible mechanism is proposed here.

Several workers[8,9,10] have shown that the propagation velocity of sound in water containing bubbles may depart considerably from that measured in pure water. Fig. 8.10, which is reproduced from Fox et al.[8] shows that over a comparatively small frequency range near the resonant frequency of the bubbles, the velocity may vary from 0.5c to 1.5c. (c is the velocity in bubble-free water.) This variation is produced with bubbles of average diameter 1.1 mm and with a total air concentration by volume of only two parts in 10,000. At fixed frequency, variation of bubble size or air concentration can produce a similar variation in propagation velocity. It is hypothesized that this is the basic mechanism which gives rise to the wide bandwidth of the scattered signals.

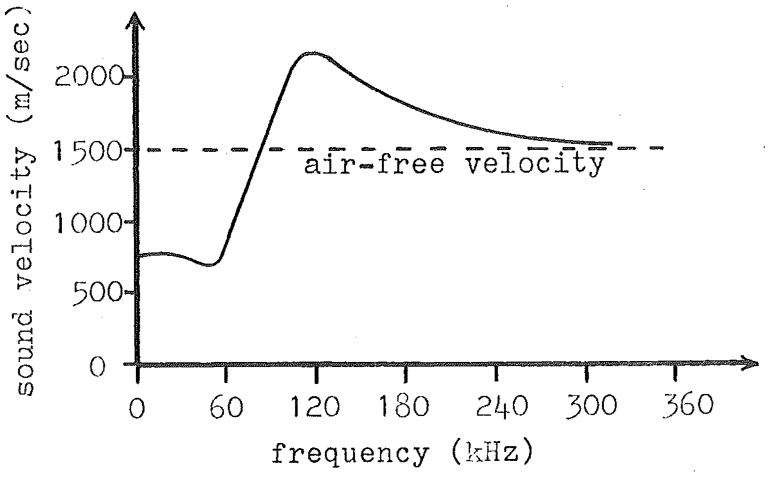

Figure 8.10. Variation of sound propagation velocity with frequency in a bubbly water mixture (after Fox et al.[8]).

To test the feasibility of this proposal, let the Doppler spread produced directly by the motion of individual bubbles be neglected, and consider a volume of turbulent bubbly water in front of the arrays. Consider, specifically, signals scattered from region A, 30 ft distant from the arrays and within a large volume of wake, encompassing the arrays (see Fig. 8.11).

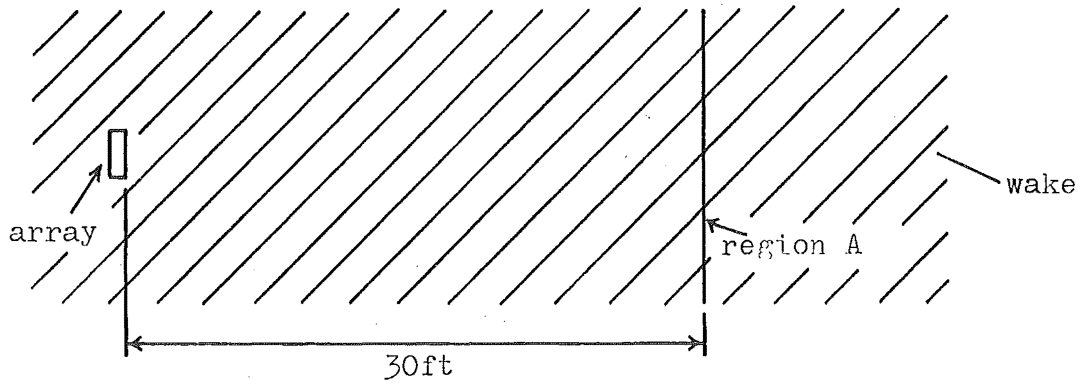

Figure 8.11. Arrays and scattering region lying within the wake.

Assume that the transmission frequency is below the average resonant frequency of the bubbles, so that the propagation velocity in the mixture is given by[10]:

$$v = c \left\{ \frac{1}{1 + 2.5\beta.10^4} \right\}^{\frac{1}{2}}$$

where β is the volume concentration of air.

Let the concentration, β, in the region along which sound travels between the arrays and region A by 10^{-4} initially, reducing to $0.5.\ 10^{-4}$ over a period of say 100 msec. Such a variation would presumably be possible in extremely turbulent conditions.

Assume that the transmission frequency is 60 kHz and that for simplicity, the concentration variation is uniform. Then the signals scattered from region A will (on reception) have a

frequency:

$$f = 60 \cdot \left(1 + \frac{2 \cdot 30(1/v_1 - 1/v_2)}{0.1}\right) \text{ kHz}$$

where v_1 is the initial velocity and v_2 is final velocity determined from the previous equation.

Substitution of values gives a received frequency of approximately 63 kHz. Thus, to produce a frequency shift of 3 kHz for signals from a range of 30 ft requires an air concentration variation at the rate of approximately 2:1 per 100 msec. In extremely turbulent conditions, such as would be expected in a wake, concentration fluctuations at rates of this order would appear feasible.

The presence of a wake in front of the sonar arrays renders the sonar completely ineffective since the scattered signals produce a high noise level over the entire audio bandwidth of the system. In practice, the problem is not too severe since wakes would be rarely encountered in normal fishing situations. It could definitely pose a problem if the sonar carrying vessel turns back on its own wake, or in convoy situations.

The effect is a direct consequence of the nature of the range/Doppler ambiguity characteristic of the FM transmission (see Ch.1). Since the FM sweep rate must be small to suit the characteristics of the human auditory system, Doppler sensitivity is heightened at the expense of range resolution. If an electronic processor with wider bandwidth was used, a faster sweep rate could be employed and improved performance would be expected in the presence of wakes.

8.6 Conclusions

It has been shown that the detection performance of the sonar, as measured with artificial targets in shallow water follows reasonably closely the performance as predicted from scattering data and the geometry of the beams.

The problems which arise when the receivers are overloaded by either surface scattering or transmitter/receiver acoustic cross-talk have been investigated and satisfactory solutions described.

An interesting but apparently insoluble problem arises when turbulent bubbly water (as produced in the wake of a ship) is present in front of and close to the arrays. A plausible mechanism for the formation of wide bandwidth returns from such a mixture is proposed. The high Doppler sensitivity of the present sonar means that such broad band signals cover the entire audio bandwidth rendering the sonar completely ineffective under these conditions. Fortunately the situation is rarely met in normal operating conditions.

8.7 References

1. C.M. McKinney and C.D. Anderson, "Measurements of Back-scattering of Sound from the Ocean Bottom", J. Acoust. Soc. Am., 36 : 158 (1964).

2. K.J. Diercks and R. Hickling, "Echoes from Hollow Aluminium Spheres in Water", J. Acoust. Soc. Am., 41 : 380 (1967).

3. R. Hickling and R.W. Means, "Scattering of Frequency-Modulated Pulses by Spherical Elastic Shells in Water", J. Acoust. Soc. Am., 44 : 1246 (1968).

4. R.J. Urick, Principles of Underwater Sound for Engineers, McGraw-Hill, N.Y., 1967, Ch.9.

5. W.J. Finney, "Reflection of Sound from Submerged Plates", J. Acoust. Soc. Am., 20 : 626 (1948).

6. D.E. Kerr (ed.), Propagation of Short Radio Waves, M.I.T. Radiation Laboratory Series, Vol.13 : 445, McGraw-Hill, N.Y., 1951.

7. V.M. Albers, Underwater Acoustics Handbook, Pennsylvania State University Press, 1960, Ch. 11.

8. F.E. Fox, S.R. Curley, and G.S. Larson, "Phase Velocity and Absorption Measurement in Water containing Bubbles", J. Acoust. Soc. Am., 27 : 534 (1955).

9. L.L. Foldy, "The Multiple Scattering of Waves: 1 - General Theory of Isotropic Scattering by Randomly Distributed Scatterers", Phys. Rev., Feb., 1945, p. 107.

10. R.J. Urick, "A Sound Velocity Method for Determining the Compressibility of Finely Divided Substances", J. Appl. Phys., 18 : 983 (1947).

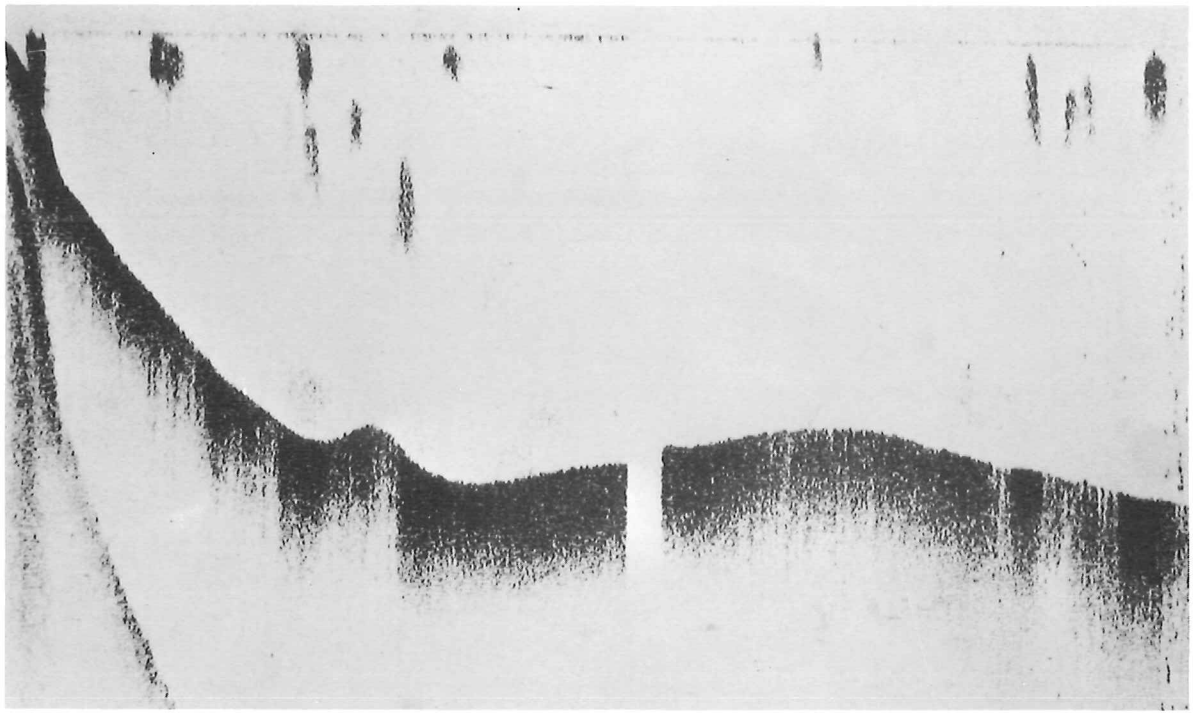

CHAPTER 9
SYSTEM TRIALS AT SEA

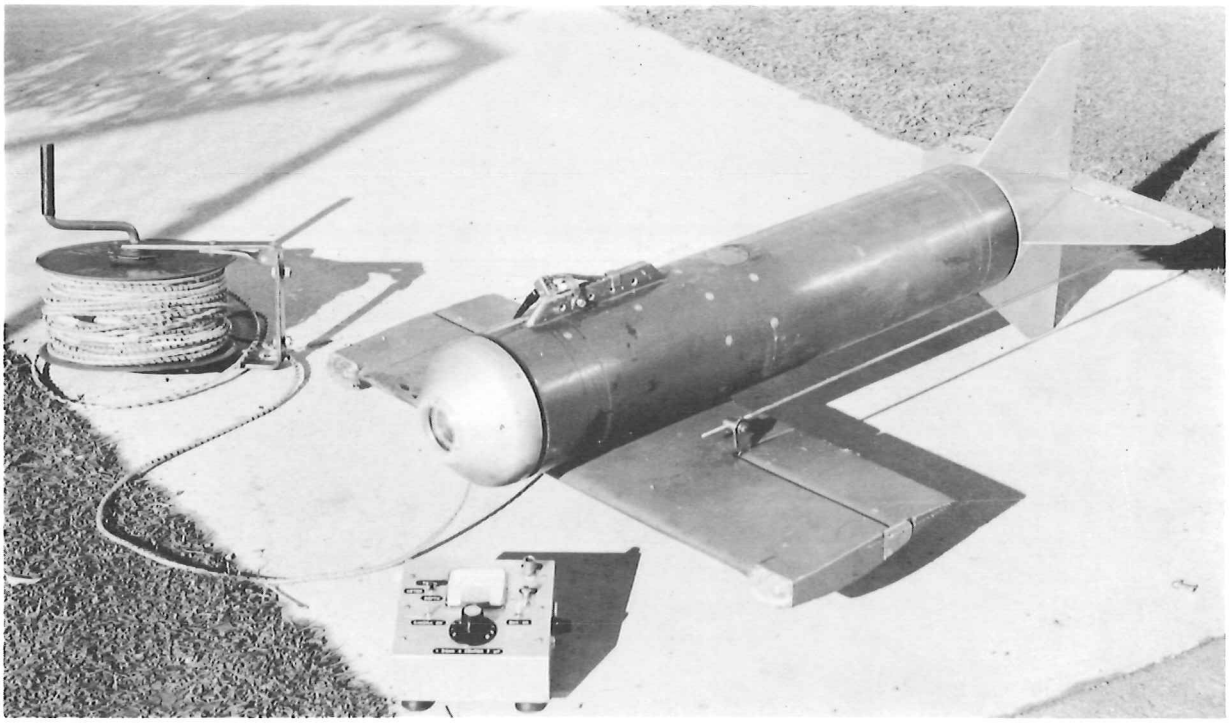

CHAPTER 9

SYSTEM TRIALS AT SEA

9.1 Introduction

In this chapter, the results of two sea trials, each of five days duration, are discussed. The aim of these trials was to obtain a measure of the detection capability of the sonar and to determine the effectiveness of the binaural display for the tracking of targets.

Major difficulties arise in determining, quantitatively, the detection performance of a sonar for fishfinding. The specification of a range is, of course, meaningless unless both the target strength and the reverberation conditions are also specified quantitatively. If the target is a shoal of fish, the target strength will depend on such quantities as the size, aspect, and swimming motion of the individual fish, as well as the density and dimensions of the shoal (see Ch. 6, section 6.5). Such characteristics are virtually impossible to determine in any realistic situation. Similarly, the reverberation level will depend on the nature of the material of the bottom, the macroscopic irregularities of the bottom, and the sea state (which affects the surface reverberation level). Even though these problems exist, it was considered desirable to obtain some estimation of the size and nature of targets detected. Two vastly different methods of target identification were employed in the two trials, the first involving divers and the second, an underwater towed photographic body.

Both sea trials were conducted in Queen Charlotte Sound, an inlet of comparatively deep water in the South Island of New Zealand. Launches about 45 ft in length were used in each case.

The transducer housing was mounted on the end of a double concentric pipe arrangement which permitted the active faces to be rotated to any direction. It was quickly found, however, that there was little to be gained by rotating the arrays since the illuminated field is of very wide angle. This was of course the intention behind the wide beam design.

Although the results described in this chapter are encouraging, they are inconclusive in the sense that the experimental conditions and the targets encountered were not truly representative of a commercial fishing situation. This was because weather conditions and the temporary nature of the housing support prevented operation in the open sea, where most commercial fishing is done. It is intended to install the sonar on a fishing vessel, in the very near future, to achieve a more realistic evaluation of its commercial potential.

9.2 Methods of Search and Target Identification

The intention behind each of the trials was to search for fish shoals and to guide the vessel to a position vertically above the shoal, then, if possible to determine the depth, size and nature of the shoal.

The sonar operator also steered the vessel, thus enabling rapid response in the event of a target detection. A twin channel tape recorder was available to allow subsequent laboratory analysis of the received signals. A depth sounder performed the dual roles of indicating the accuracy of the

target tracking and indicating the depth of the targets which were tracked sufficiently accurately.

During the first trial two divers were employed to attempt to identify the targets detected. As soon as each target was registered on the depth sounder (indicating that the target was directly beneath the vessel), the divers were informed of the depth, then promptly leapt over the side. It was found that when the shoal depth was less than about 70 feet, the divers could sight the shoals with a reasonable success rate. For deeper shoals, however, the time taken to descend, and the effects of underwater currents made the likelihood of detection very small. Of a total of approximately 50 shoals detected during the first trial, only six were positively identified.

During the second trial, a towed photographic body was employed for target identification. This vessel (described in appendix VII) was towed on a cable of up to 250 feet in length and the depth at which it followed could be rapidly controlled from the towing vessel. It contained flash tubes for illumination and a remotely controlled camera. Once activated, the camera would take photographs at the rate of one every two seconds until switched off.

Unfortunately, a number of technical problems with the camera and with the towed body prevented the successful use of the device for much of the trial. The method was, however, shown to be feasible and three shoals were successfully photographed. The total number of shoals detected during the second trial would be about 200.

9.3 Summary of Results

The sonar system was essentially the same for the two trials, although certain hardware differences were made. These were as follows:

i) The transducer arrays were built into a single housing for the second trial,

ii) Zig-zag arrays (see Ch. 8) were employed with the new housing, and

iii) The electronics was redesigned to some extent and re-packaged in a single splash-proof unit (see title page of Ch. 5).

Since the system was essentially unchanged, the results of the two trials are combined below:

9.3.1 Detection of Targets

In all approximately 250 shoals (or what are presumed to have been shoals) were detected. A target was considered to be a fish shoal if it proved to be well clear of the bottom when recorded on the depth sounder. The targets positively identified were all shoals of small herrings, the individual fish estimated to be of the order of 3" to 6" in length. It is considered probable that the majority of the shoals detected were of similar type since all were detected in the same general area. The range at which first detection occurred was generally within the limits, 80 yds to 120 yds, although a few shoals were detected at ranges of the order of 160 yds. Ranges were estimated by timing from the point of first detection to the point at which first indication was available on the depth sounder, and relating this to the speed of the vessel. Ranges were confirmed by subsequent analysis of recorded audio signals.

Measurements of the target strengths of fish in dorsal aspect by Cushing et al.[1] indicate that fish of this size would have target strengths of the order of -40 dB. In the present application, clearly side aspect target strengths should be employed, since the sonar is horizontal looking. However, the wide variation of target strength with varying horizontal aspect angle (see Ch. 6, Fig. 6.11) means that an average value must be taken, and it would appear that the dorsal aspect value would be a fair estimate of the mean horizontal target strength.

Using the above value, and applying the method described in section 8.2.1 to relate target strength to maximum range for detection, an estimate of the number of fish in a shoal detected at a certain range may be made. Consider 100 yds to be a representative range, and assume that the scattered energy increases in direct proportion to the number of fish within the shoal. (This implies that the fish are not so closely distributed as to be obscured by one another.) Then,

$$TS + 10 \log n = S_b + 10 \log \frac{\pi R_{max}^2}{6.20}$$

where TS is the target strength assumed for an individual fish (taken as -40 dB in this case), S_b is the bottom scattering coefficient, and n is the number of fish in the shoal. Taking -35 dB for S_b (this is probably the lowest figure which would be encountered for a sand/silt bottom[2]) and substituting the above mentioned values for TS and R_{max}, we obtain,

$$n \doteq 2500.$$

In view of the number of approximations involved in the derivation of this figure, little accuracy can be associated with it. It does, however, seem to be of a feasible order of magnitude, and is in general agreement with equally vague estimates of shoal size made by divers. They estimated two of the shoals sighted to be approximately 15 ft long (in the direction of motion) and about 10 ft in diameter. This would give a density of slightly more than two individuals per cubic foot, which seems reasonable.

A comparative estimation of target strength was possible from the audible signals when the reverberation conditions were approximately constant. A first impression was possible from the range (frequency) at which first detection occurred and a further estimate was possible from the apparent signal/background ratio when the target reached a certain familiar range.

In many instances during the pursuit of one shoal, a second would be detected. In most cases it was immediately apparent that one or other shoal was larger, even though the audio signal/background ratios were quite different due to the differing ranges. No such estimation could be made in situations where the water depth was changing continuously.

Some estimation of shoal depth was also possible with practice. After encountering a large number of shoals at various depths, the operator became familiar with the relationship between the range (frequency) at which a target was lost by it moving out of the beam, and the subsequently recorded depth. With considerable experience, an operator could probably recognize 4 or 5 depth increments for a given water depth.

The question of whether or not it will be possible to distinguish between shoals of different sized fish or perhaps even different species remains largely unresolved, since only one type of shoal is known positively to have been encountered. During the first trial, several quite deep (greater than 120 ft) shoals were encountered, which appeared to produce a much more tonal signal than other shoals encountered. No firm conclusion can be drawn from this, however, due to the lack of identification.

A large number of individual fish (presumably) were detected during the trials. Although these were detected at very short ranges, the audio signals produced were distinctly tonal and quite different from the signals produced by shoals. The signals from the latter were apparently similar to narrow band noise signals.

9.3.2 Tracking of Targets

Once detected, targets could be approached with comparative ease using the binaural lateralization process. Target tracking was, in fact, sufficiently accurate that more than 80% of the targets detected were subsequently recorded on the depth sounder, indicating that they passed approximately vertically below the vessel.

After very little practice, an operator could approach a target along a path at least as good as those recorded in experiments with the model system (see Ch. 7, Fig. 7.7). After considerable practice, approach paths became even more direct without reversal of curvature.

No problems were observed due to the potential lateralization ambiguity at large azimuth angles (see Ch. 7, Fig. 7.3), presumably since targets were not detected at these large

angles.

As was mentioned in the previous section, on many occasions during the tracking of one target, another would be detected at a different range and azimuth. It was found that this situation was in no way confusing, and either target could be selected and approached. Confusion would be expected if the two targets were at closely similar ranges, but such a situation did not arise.

The subjective impression of centering the audio image of the targets (or balancing the apparent loudness) was similar to the wide band noise centering experiments described in Ch. 7. The centering task became significantly easier as the range reduced and the signal/background ratio correspondingly improved. Even at the detection threshold, however, it was possible to decide reliably, which side the target was on, and to steer the vessel accordingly.

The targets which were not successfully tracked (i.e. not registered on the depth sounder) were lost soon after detection due to the fact that they were deep shoals or small shoals and passed out of the detectable region before an accurate approach path could be established.

During the searching process, vessel speeds of from 6 to 8 knots were generally employed. Once a detection occurred, the engine speed was reduced slightly and the vessel speed reduced continuously during the approach giving a final speed of 4 or 5 knots. Using this method, it was found that even for targets detected at ranges as small as 60 yds, the audible image could be accurately centered, and an appropriate bearing chosen before the target became too close to the vessel to be detectable.

9.3.3 Performance in Choppy Conditions

Comparatively rough sea conditions produce two main effects on the system performance. Firstly, the wave action produces aeration of the water to some extent, near the surface. Secondly, the pitching and rolling of the vessel produces periodic increases and decreases in the reverberation level. The problem of air bubbles in the water (discussed in Ch. 8, section 8.5) has no solution short of lowering the arrays more than 10 feet below the surface (a rather hazardous solution). However, it was found that the effect on the overall performance was not too severe since the effect is very local and present for only a small fraction of the time. Its effect as an annoyance is probably greater than the direct masking effect, since it causes considerable fluctuations in 'noise' level. Pitching and rolling of the vessel can produce large increases in surface reverberation and alternately bottom reverberation, since no stabilization of the transducer arrays is employed. Target detection and tracking was found to be not seriously impaired by this effect, due to the almost continuous nature of the received signals. The increase in audio background could be immediately related to the attitude of the vessel and although a target would often be masked by this increase, it could be readily detected again as the vessel became level again.

Narrow beam scanning sonars with unstabilized transducers are adversely affected by this situation generally as they rely on integration of several traces on the recording instrument. Recordings of targets of interest may be completely masked by the periodic increases in reverberation level.

9.4 Analysis of Recorded Signals

Tape recordings were made of the majority of shoals detected during the two trials. Many of these recordings were subsequently analysed using the Kay Sonagraph. (This instrument is briefly described in Ch. 8, section 8.2.)

Fig. 9.1 shows sonagraph records of three shoals detected at ranges of 85, 95 and 100 yds respectively. The area below the mark of the shoal is clear in all three cases indicating that at the time that the recordings were made, the shoals were close enough to the sonar to be clear of bottom reverberation. Bottom reverberation shows up as the speckled dark areas above the shoals. The width of the marks of the shoals in the vertical direction is comparable with the analyser bandwidth, so all that can be concluded about the extent of the shoals in the range dimension is that they are less than about 15 ft.

Fig. 9.2 shows a sonagraph record of two shoals detected in quick succession. Both shoals are clearly detectable simultaneously by listening to the tape, and distinctly different azimuthal positions are apparent. Both shoals have significantly greater extent in the range dimension than those of Fig. 9.1 and from the sonagraph this extent is estimated at approximately 60 ft. The more distant shoal produced a noticeably larger audio response at all ranges than did the closer shoal (lower mark on the diagram). This is confirmed by a darker mark. The respective ranges at the time the recording for this sonagraph was made are 62 yds and 100 yds.

Figs 9.3(a) and (b) show sonagraph records of two consecutive received pulses following the detection of a shoal.

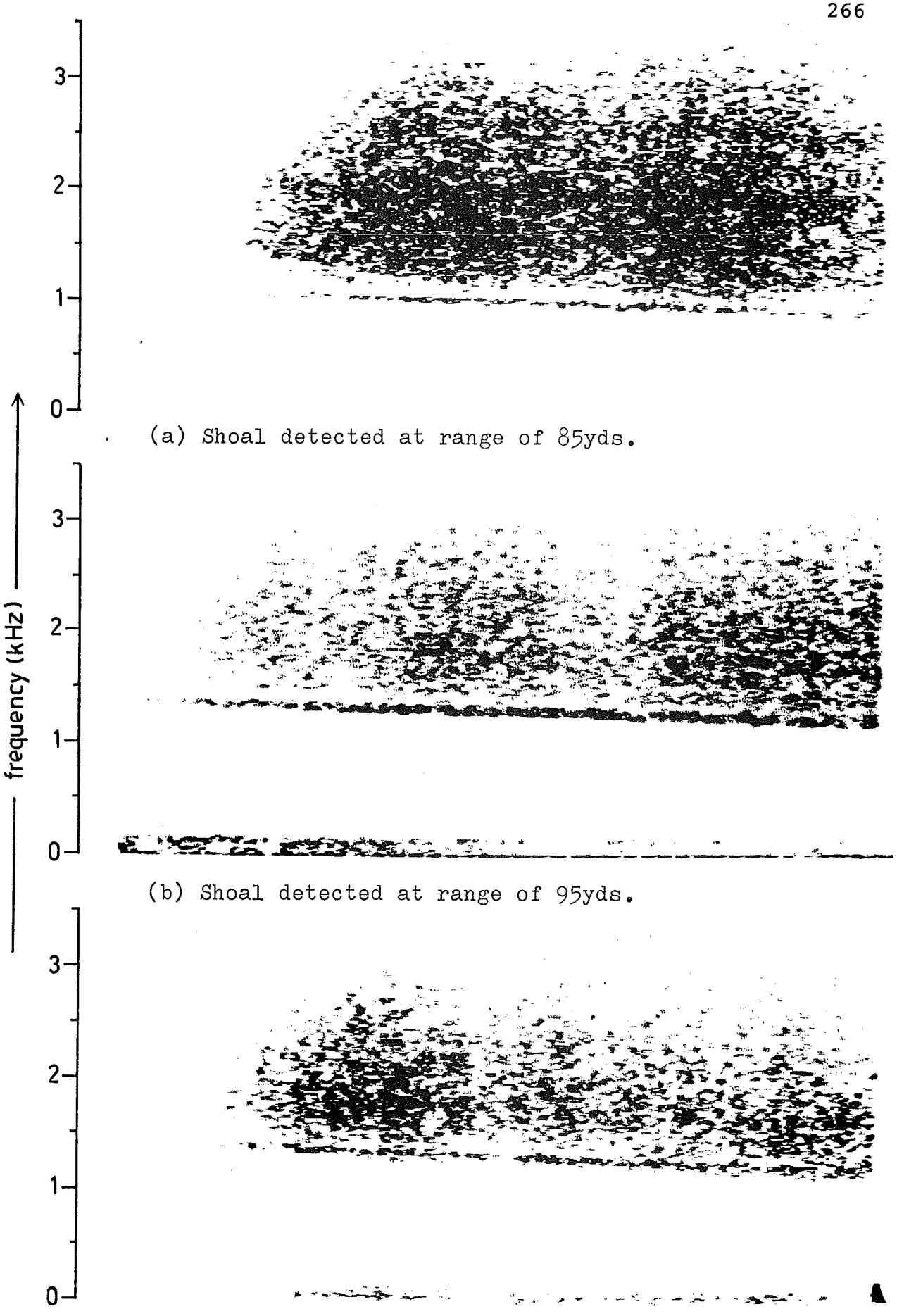

Figure 9.1. Sonagraphs from three fish shoals detected at ranges of 85yds, 95yds, and 100yds.

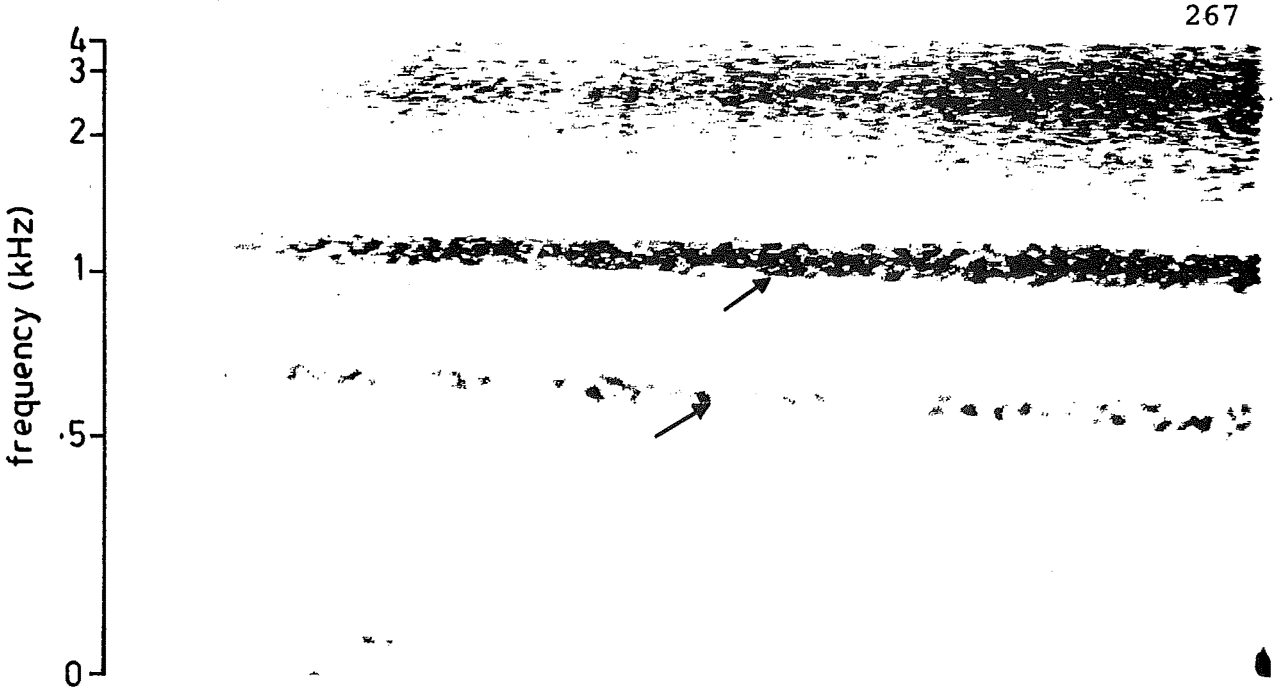

Figure 9.2. Sonagraph showing two shoals (arrows) present simultaneously in the beam, at ranges of 62yds and 100yds.

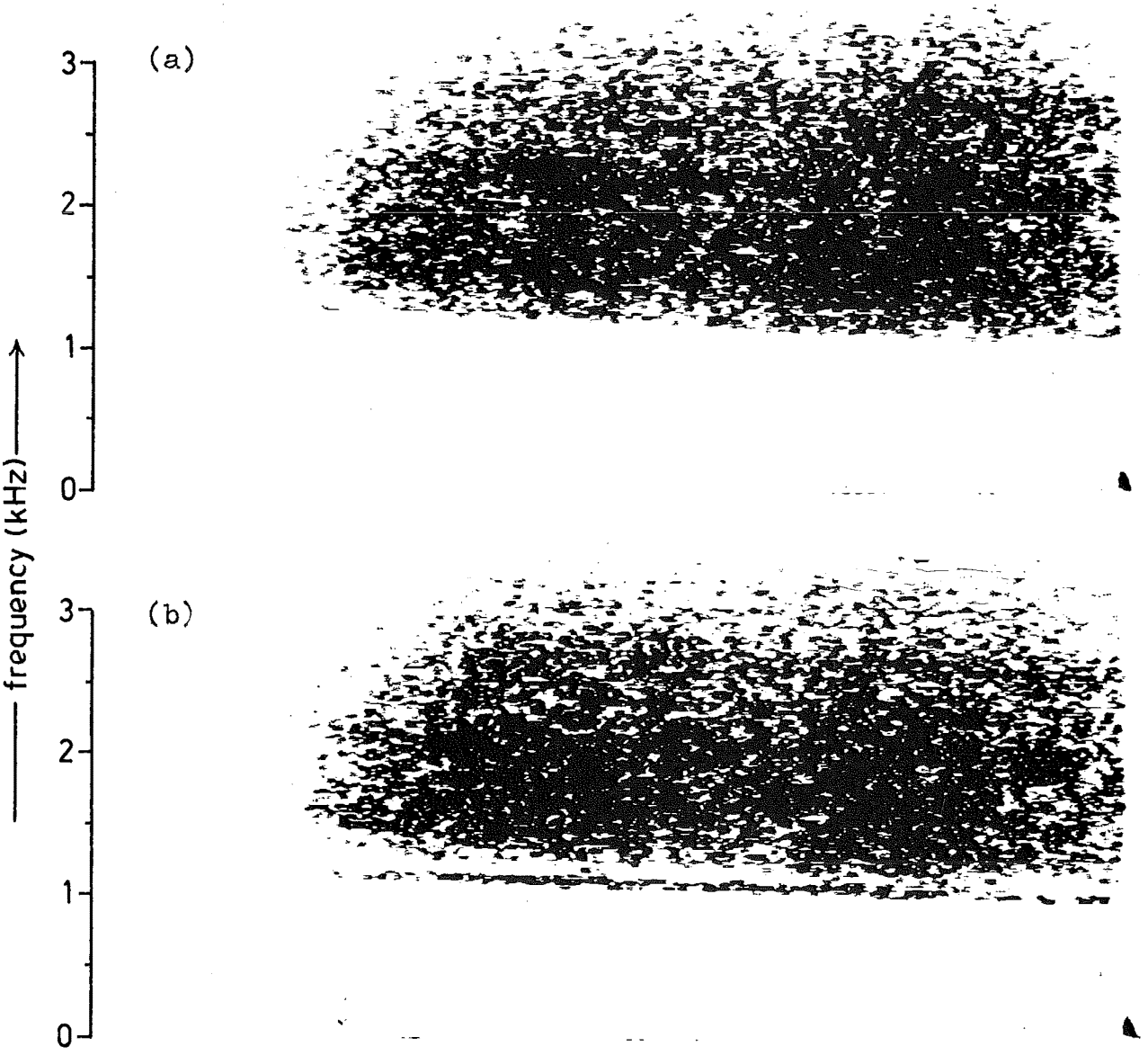

Figure 9.3. Sonagraphs from two consecutive received pulses following the detection of a shoal.

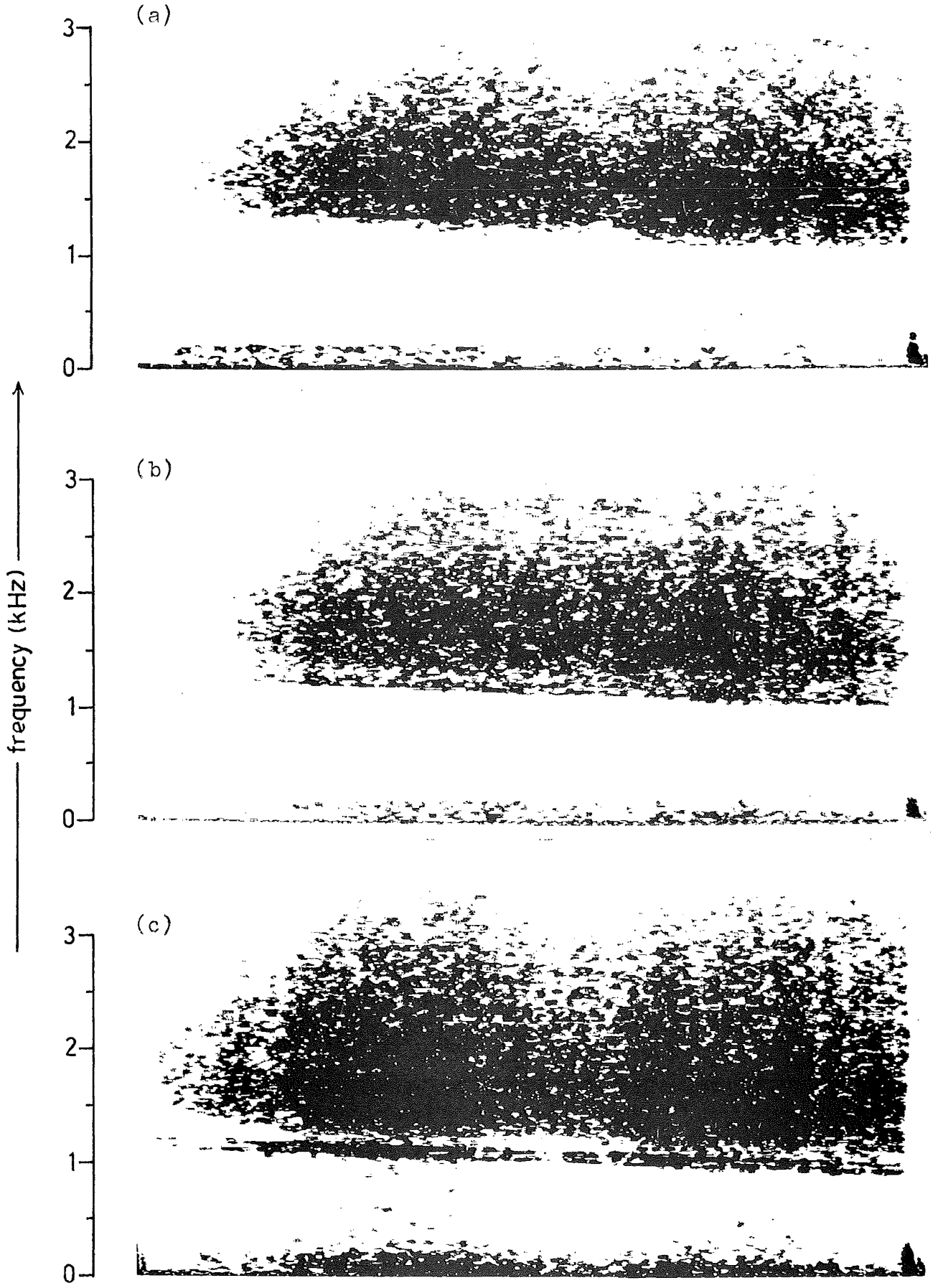

Figure 9.4. Sequence of three sonagraphs from three consecutive received pulses following the detection of a shoal.

This shoal was first detected audibly during the received pulse immediately prior to that of Fig. 9.3(a), but the signal is not noticeable in this sonagraph. It first becomes apparent in the sonagraph of Fig. 9.3(b), which was taken more than six seconds after first audible detection. It appears that visual detection from this type of record is inferior to auditory detection even though the analyser bandwidth is approximately half that of the critical band of the auditory system.

Fig. 9.4, parts (a), (b) and (c) shows a similar sequence following the detection of another shoal. These sonagraphs were taken from three consecutive received pulses following auditory detection, but the signal from the shoal becomes clearly apparent in the third sonagraph only.

It is also interesting to note from Fig. 9.4(c) that a double line is produced by this shoal, presumably indicating two distinct centers at differing ranges.

9.5 Discussion of Results

At first glance, the detection ranges quoted in section 9.3 appear unimpressive. It must be remembered, however, that all information relating to target identification suggests that most or all of the shoals detected were of very small fish, 3 in. to 6 in. in length.

The target strength of individual fish increases typically as the cube of length[3] so that a shoal comprising a similar number of fish of say 18 in. in length would have a target strength about 14 dB greater than those detected. This would increase the maximum detectable range by a factor of four times under similar conditions. A shoal of 2500 fish of 18 in. length is not large by commercial standards, so that the

ranges to be expected for the detection of shoals of commercial interest could be from 300 to 500 yds.

In view of the above the device appears quite suitable for the detection of pelagic fish shoals. For demersal species, all factors are against detection from the surface. The fish are generally sparsely distributed so the target strength within a given resolution cell width is small and since the fish are very close to the sea bottom, they will be no more strongly illuminated than will the region of the bottom which is masking them. A possible solution to this problem, utilizing an alternative version of the present sonar is described in Ch. 10, section 10.4.

The sea trials have clearly indicated the feasibility of tracking targets using a binaural monopulse type of system. The method, besides being extremely effective, is immediate in indication and simple to interpret. It is felt that this direction finding technique, suitably adapted, would be invaluable in such situations as purse seining, where immediate information as to the position of the shoal is vital just prior to shooting the net.

9.6 References

1. D.H. Cushing, F.R. Harden Jones, R.B. Mitson, G.H. Ellis and G. Pearce, "Measurements of the Target Strength of Fish", J. Brit. I.R.E. 25 : 299 (1963).

2. R.J. Urick, Principles of Underwater Sound for Engineers, McGraw-Hill, N.Y., 1967, Ch. 8.

3. R.J. Urick, Principles of Underwater Sound for Engineers, McGraw-Hill, N.Y., 1967, Ch. 9.

CHAPTER 10
CONCLUSIONS

CHAPTER 10

CONCLUSIONS

10.1 General

Conclusions relating the specific areas of research and development have been discussed within the thesis. In this chapter, conclusions relating to the system as a whole are given, and recommendations for future work and other methods of application of the system are discussed.

10.2 The System Performance

It has been shown that a forward looking sonar system utilizing a purely audible display can be used very effectively for the tracking of underwater targets. Several significant advantages of audible presentation for a system configuration such as that described are apparent. These are:

i) The display equipment is of negligible cost compared to more conventional visual display devices;

ii) A wide arc of illumination may be used, while retaining an accurate tracking capability. This allows the use of transducers which are fixed in relation to the tracking vessel, thus significantly reducing the installation and maintenance cost of the system;

iii) Due to the almost continuous nature of the audible signals from a target derived from the heterodyne correlator receiver, and the immediacy of the audible display, the system may be used effectively in comparatively rough seas without stabilized transducers;

iv) With a purely audible display, the full display output of

the sonar may be presented to an operator without distracting his vision. This means that the sonar operator may also act as helmsman, an ideal situation for target tracking.

The use of a linear FM transmission in conjunction with a direct heterodyne correlator receiver gives rise to an effective and easily interpreted audible display. In view of the bandwidth and filter characteristics of the human auditory system, it is necessary to use a transmission waveform of comparatively wide bandwidth, certainly wider than would be necessary to achieve comparable resolution with an electronic detector.

The use of interaural intensity difference as a cue to the centering of targets gives sufficient information in a suitable form to allow the accurate tracking of targets whether the targets give rise to a 'fused' auditory image or not (see Ch. 7). When the auditory image due to the presence of a target is not fused (due to the lack of correlation of signals at the two receiving arrays), the process of centering the 'image' or balancing the loudness is an unnatural process in the sense that it has no counterpart in normal hearing. It is fortunate (but curious) that the auditory system can cope so well with this situation, since fish shoal targets of significant size give rise to unfused images (see Ch. 6, section 6.3).

10.3 Alternative System Configurations

Although it has been shown conclusively that information derived from an underwater sonar can be displayed effectively to the human auditory system and interpreted effectively by that system, no attempt has been made to determine to what extent the system could be degraded without degradation at the display. This area of study is a very important stage if the system is to be used commercially.

The wide bandwidth of the system poses the most severe restraints on the hardware implementation since it demands special transducer element techniques and array beamwidth control. For this reason, this would be the most important area for study.

If the fractional bandwidth of the system could be reduced three or four times, the cost of the arrays would be at least equally reduced. Such a reduction would eliminate the possibility of determining something of the nature of the target from a variation of the target strength with frequency, but this may not be possible, or may be of little use in a practical situation.

The fractional bandwidth could be reduced by either i) retaining the same absolute bandwidth but raising the center frequency or, ii) reducing the bandwidth for the same center frequency. Experiments during the sea trials involving up to a four times reduction in bandwidth did not appear to significantly affect the detection performance, although under such variable search conditions, this could not be firmly established. Reducing the bandwidth did increase the fatiguing effect of the signals due to the shorter repetition period required to give the same range/frequency coding. This could

be a significant disadvantage to such an approach. Raising the center frequency would have the added advantage that the complete array housing could be scaled down in size accordingly.

10.4 Future Applications of the System for Fish Detection

The use of a wide beamwidth in the horizontal plane and the obtaining of directional information without either electronically or mechanically scanning a beam is a new and promising possibility for fishfinding devices.

Although it was considered convenient for experimental purposes to mount the device on the hull of the searching vessel, such an arrangement may not be the most effective in practice. The principle disadvantage of mounting any horizontal looking sonar on the hull is that one is inevitably attempting to detect targets against a strong background, produced by the sea bottom. The problem is particularly severe when the target is very close to the bottom so that it is no more strongly illuminated than the background. Since demersal species of fish form the major part of the fish landed in New Zealand and many other countries this difficult situation is the most common.

A possible solution to this problem is offered by the use of the techniques developed in this thesis in a slightly different configuration. If the beamwidth of the arrays in the vertical plane is reduced to the order of 5^{o} or less and the entire array housing is attached to and towed with the bottom trawl the problem of bottom reverberation masking targets just above the bottom, is significantly reduced. The targets are then much more strongly illuminated than is the sea bottom in

the near vicinity and considerable improvement in target detectability would result.

By retaining the wide beamwidth in the horizontal plane, a wide search beam ahead of the net would be achieved and since no scanning of the arrays is required, the housing could be of comparatively simple aerodynamic design. More conventional scanning sonars have seen little application under tow due to the added complication of towing a device which must be scanned. Providing it was suitably designed, the array housing would be well stabilized by the water motion so there would be little problem in maintaining the beam accurately horizontal. This would be important due to the necessarily narrow vertical beamwidth.

It is strongly recommended that a new array configuration be designed in a form which could be towed, to evaluate the feasibility of this approach.

In its ship mounted form, the present sonar would be most effective for the detection of surface or midwater shoals. For the detection of demersal species it would be somewhat less effective than sonars which use a narrow forward looking scanned beam due to the larger area of the bottom illuminated by the wide horizontal beam. It may offer distinct advantages in rolling seas, however, over other sonars without stabilized beams.

10.5 Other Applications

The advantages of a wide arc of illumination, tracking or directional determination, and purely auditory presentation are not offered by any other sonar system to the author's knowledge.

Two other applications where these characteristics may be desirable are as follows:

i) In small deep diving submersibles, where scanning arrays pose severe problems due to the pressure and where space for electronics and display devices is strictly limited, the present type of system would appear well suited, and

ii) As an aid to divers working in poor visibility conditions, or searching for objects on the sea floor, this system has advantages in that the display is purely audible, leaving the divers' vision free, and if mounted on the head, would also leave his hands free.

The wide beam concept would give the diver an awareness of a large part of his environment without need for scanning.

A feasibility study of some aspects of this application is at present being conducted at the University of Canterbury.

APPENDICES

APPENDIX I

SPECIFICATION OF ELECTROSTRICTIVE RINGS USED IN MATCHED TRANSDUCER ELEMENTS

Material: P2T-4 (a lead zirconate - lead titanate composition from the Clevite Corporation)

Dimensions: Ring of O.D. 15 mm

I.D. 6 mm

Thickness 2 mm

Polarization: Axial

Electrodes: Flat surfaces silvered

Natural Free Resonant Frequency (thickness mode): 1.15 MHz

Velocity of Propagation (axial direction, constant D),

$v_t^D = 4600$ m/s

Dielectric Impermeability, $\beta_{33}^S = 0.178.10^9 m/F$

Elastic Stiffness Constant, $C_{33}^D = 15.9.10^{10} N/m^2$

Piezoelectric Stress Constant, $h_{33} = 26.8.10^8 V/m$

Effective Coupling Factor, $k_t = 0.52$

Clamped Capacitance, $C_0 = 417$ pF

Density, $\rho = 7500$ kg/m^3

APPENDIX II

CHARACTERISTICS AND DIMENSIONS OF SECTIONS OF MATCHED ELEMENTS

Single Match Element

Matching Section: Material: Araldite (Ciba Co. Pty Ltd) resin D(CY230) with hardener (HY951) loaded with 82% by weight powdered Garnet

Diameter:	17 mm
Thickness:	5.1 mm
Prop. Velocity:	1240 m/sec.
Density:	5370 kg/m^3

Active Section: See Appendix I

Backing Section:

Material:	brass
Diameter:	16.5 mm
Thickness:	14.6 mm
Prop. Velocity:	3500 m/sec.
Density:	8200 kg/m^3

Double Match Element

Outer Matching Section: Material: Araldite (as above) loaded with 35% by weight powdered garnet.

Diameter:	17 mm
Thickness:	6.8 mm ($\lambda/4$ at 60 kHz)
Prop. Velocity:	1630 m/sec
Density:	1810 kg/m^3

Inner Matching Section:	Material:	Aluminium
	Diameter:	16.5 mm
	Thickness:	21.4 mm
	Prop. Velocity:	5240 m/sec.
	Density:	2700 kg/m^3
Active Section:	See Appendix I	
Backing Section:	Material:	Brass
	Diameter:	16.5 mm
	Thickness:	14.6 mm
	Prop. Velocity:	3500 m/sec
	Density:	8200 kg/m^3

APPENDIX III

"FREE-FIELD" TESTING OF TRANSDUCER ELEMENTS AND ARRAYS IN A WATER TANK OF FINITE SIZE

A cylindrical concrete water tank, 11 ft in diameter and 8 ft 6 in. high was employed for these measurements. This gives a water depth of 8 ft.

It can be simply shown that if the transmitting and receiving units are placed diametrically opposite each other at mid-depth and at a distance of 3.8 ft from the center of the tank (see dgm) the greatest delay between a direct transmission and a reflected signal from bottom, surface or walls is achieved.

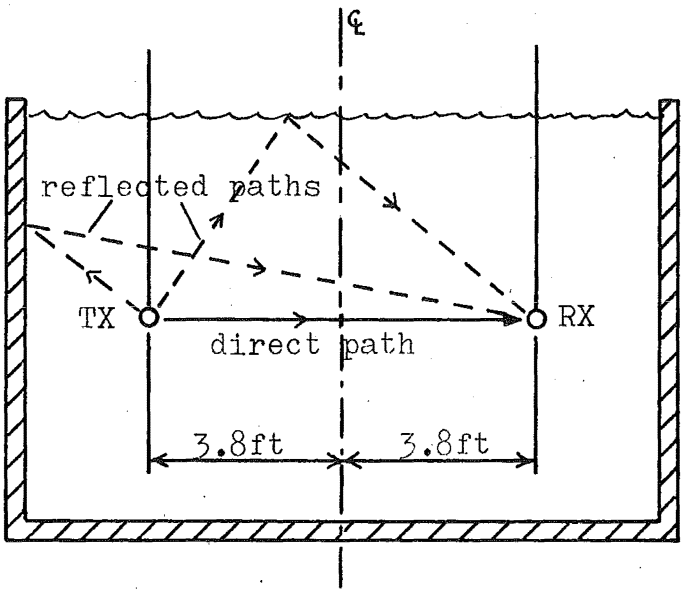

Optimum Arrangement of Transmitting and Receiving Units

With this configuration, the first reflected signal arrives 0.7 msec. after the arrival of the direct transmission signal.

In practice then, if a short pulse is transmitted, the response it provokes at the receiving unit may be examined for a period of 0.7 msec. in true 'free-field' conditions. This implies, of course, that transducers and arrays being tested must have a response time which is shorter than 0.7 msec. (i.e. a bandwidth greater than ≈ 1.5 kHz). The transducers and arrays considered in this thesis have bandwidths approximately 40 times wider than this minimum limit and in fact most high frequency underwater sonar transducers also have bandwidths somewhat larger than 1.5 kHz. This tank may thus be used for a wide range of transducer measurements.

The procedure for directly plotting polar responses or frequency responses of transducers or arrays in this tank is illustrated diagrammatically on the following page.

The transmitting unit is pulsed about 10 times per second (this allows sufficient time for reverberation to reduce to negligible proportions) and a delayed gate extracts that part of the received pulse which comprises the direct path signal only. The peak amplitude of this pulse is stored in the sample and hold unit until a new value is available. The output thus comprises a dc level proportional to the most recent sample of the direct path pulse. With a new sample every 100 msec, polar patterns over a 180° arc may be plotted to an accuracy of 5% or better in less than 1 minute.

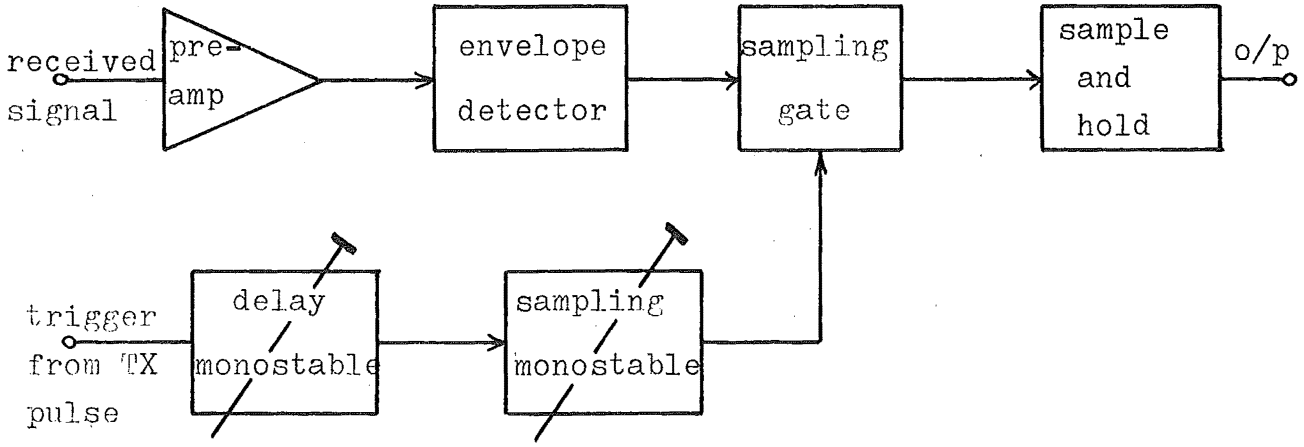

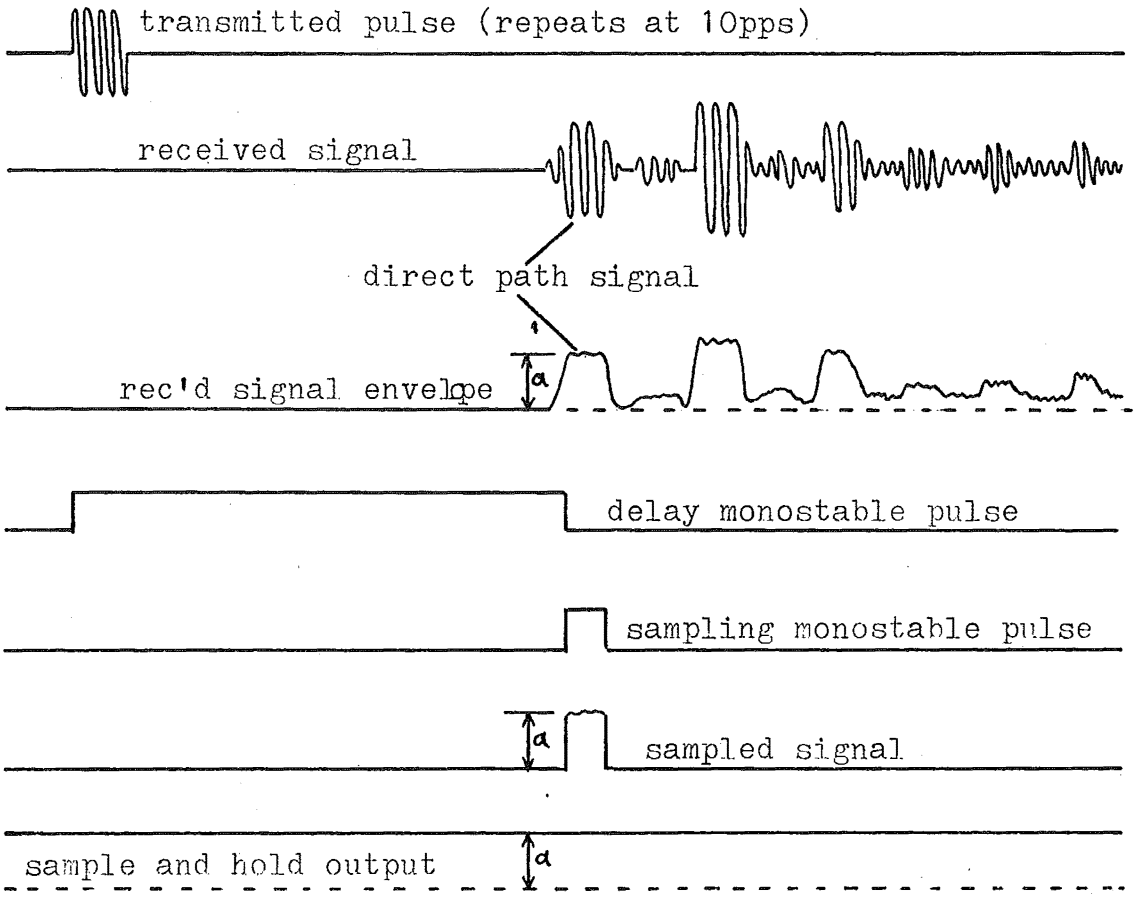

Block diagram and waveforms for the direct plotting of frequency responses or polar patterns.

Pages 283 - 288

APPENDIX IV

ACUSTICA
S. HIRZEL VERLAG · STUTTGART
Vol. 23 1970 Heft 1

Constant Beamwidth Receiving Arrays for Broad Band Sonar Systems

by R. P. Smith

Department of Electrical Engineering, University of Canterbury, New Zealand

Summary

A simple and inexpensive technique for maintaining the beamwidth of a transducer constant, over frequency bands up to an octave in width, is described. Theoretical and experimental results are presented. With the aid of a simple passive network, the half-power beamwidth of an array may be held constant to within 2% over an octave band, with negligible variation of beam shape. This latter characteristic allows virtually undistorted reception of broad band acoustic pulses over the entire angle of the main lobe of the directional pattern. A compensation network designed for a particular frequency band may be used, without modification, for linear arrays of any length, and thus any beamwidth, within that band. The constant beamwidth technique is applicable to arrays with as few as four independent sections, as is demonstrated by the experimental results reported herein. Compensation for beamwidth variation in both horizontal and vertical planes is possible with a single network.

Empfängerzeilen mit konstanter Peilschärfe für breitbandige Sonarsysteme

Title: Constant Beamwidth Receiving Arrays for Broad Band Sonar Systems
Author: Smith, R. P.
Source: Acta Acustica united with Acustica, Volume 23, Number 1, 1970, pp. 21-26(6)
Publisher: S. Hirzel Verlag
https://www.ingentaconnect.com/content/dav/aaua/1970/00000023/00000001/art00006?crawler=true

APPENDIX V

ELECTRONIC CIRCUITS

(i) Ramp Generator and Voltage Controlled Oscillator

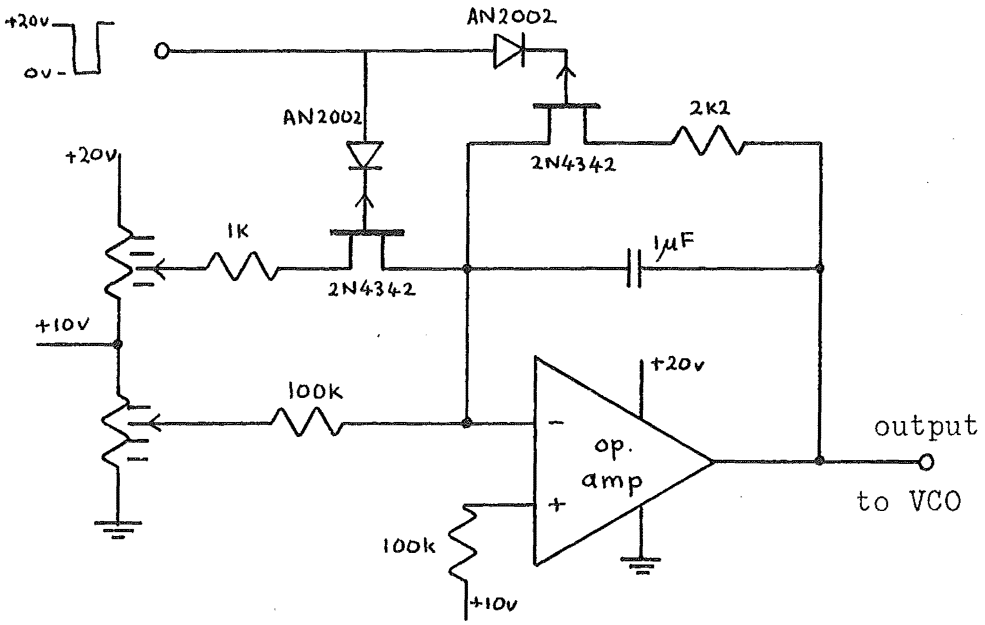

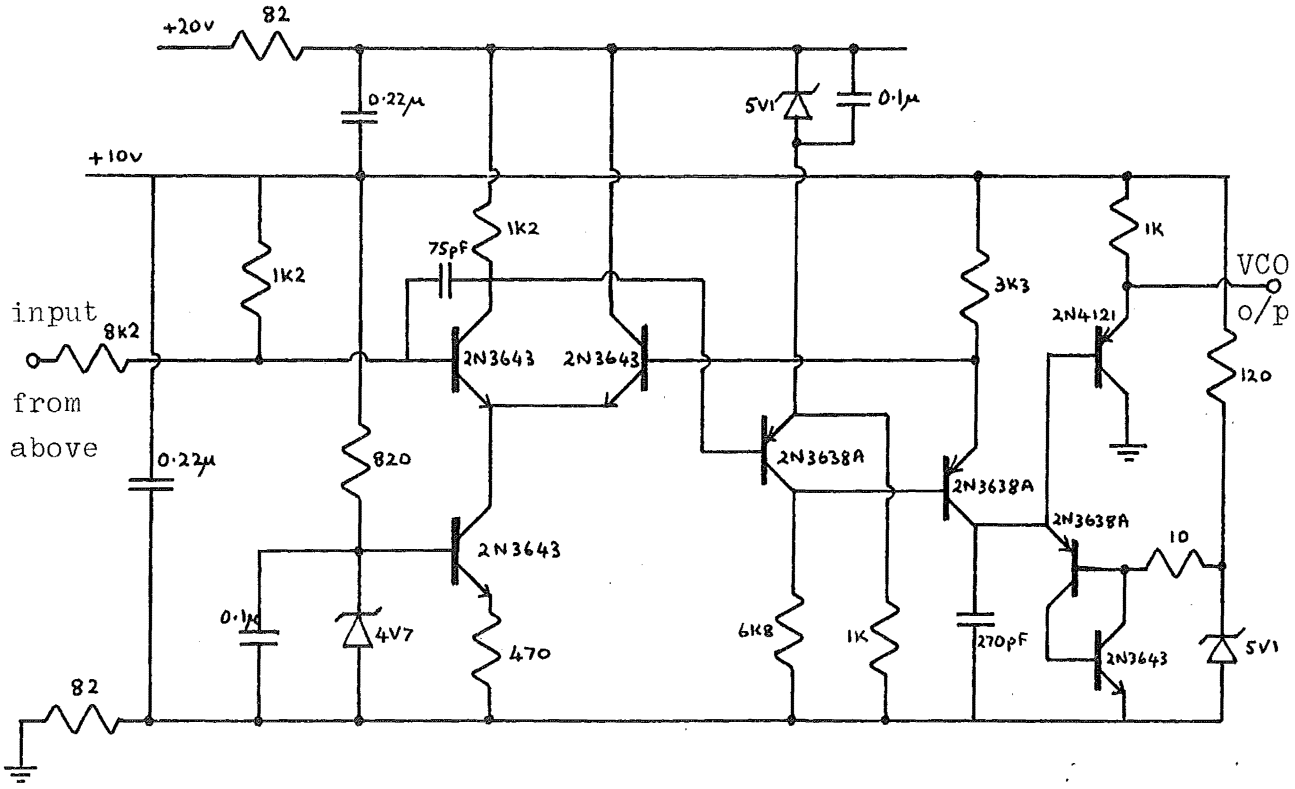

(ii) Transmitter and Receiver Filters

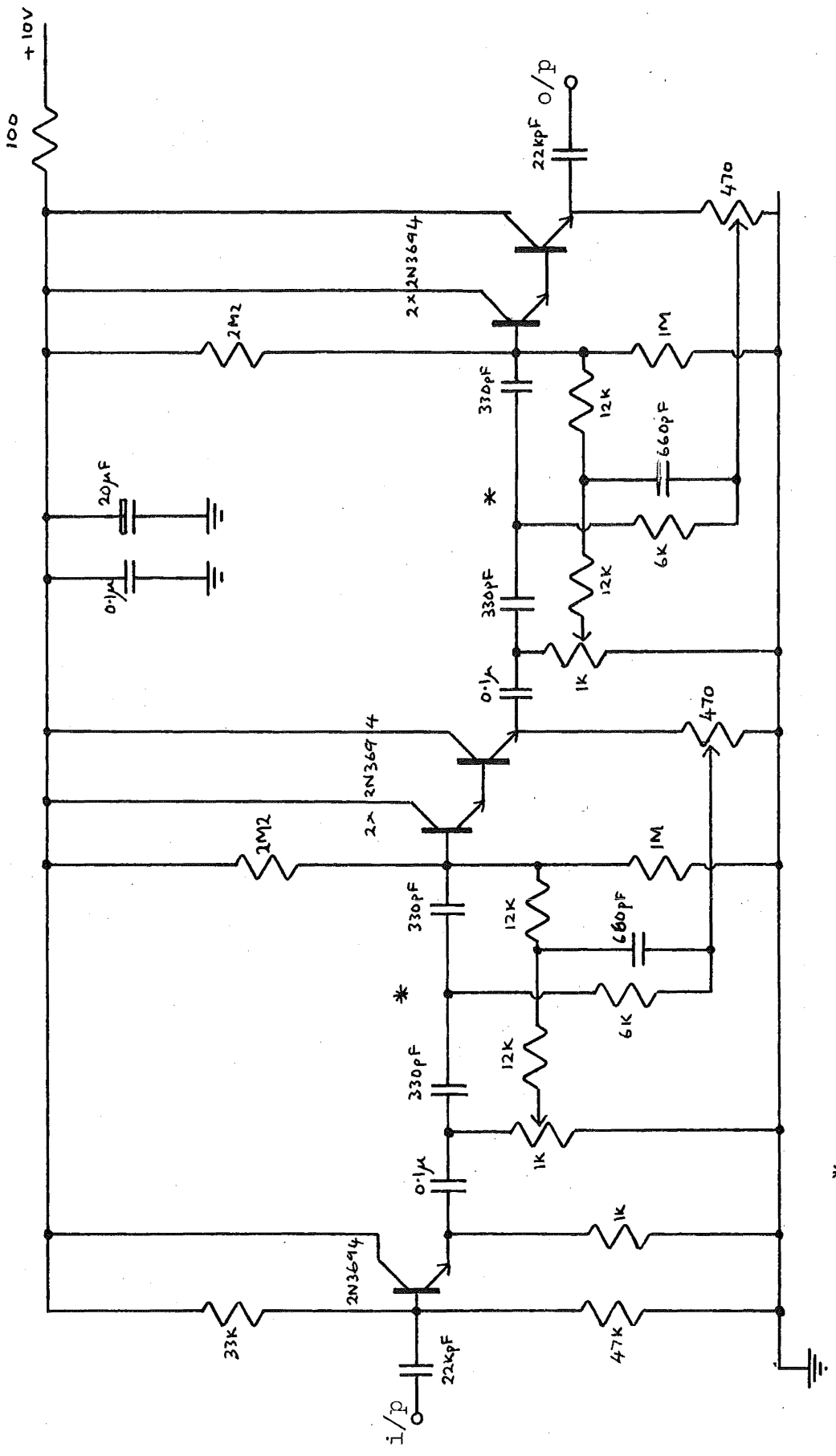

* Receiver high-pass filter only shown. Transmitter low pass filter is identical apart from transposition of resistors and capacitors in twin-T's

(iii) Transmitter and Receiver Gates

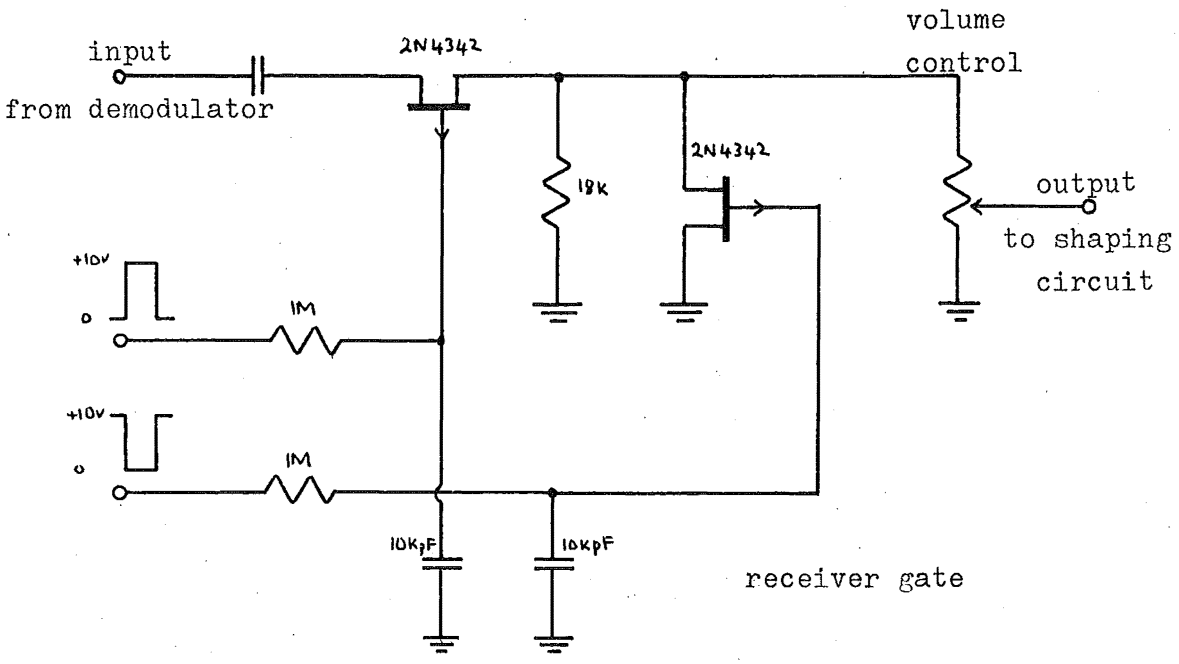

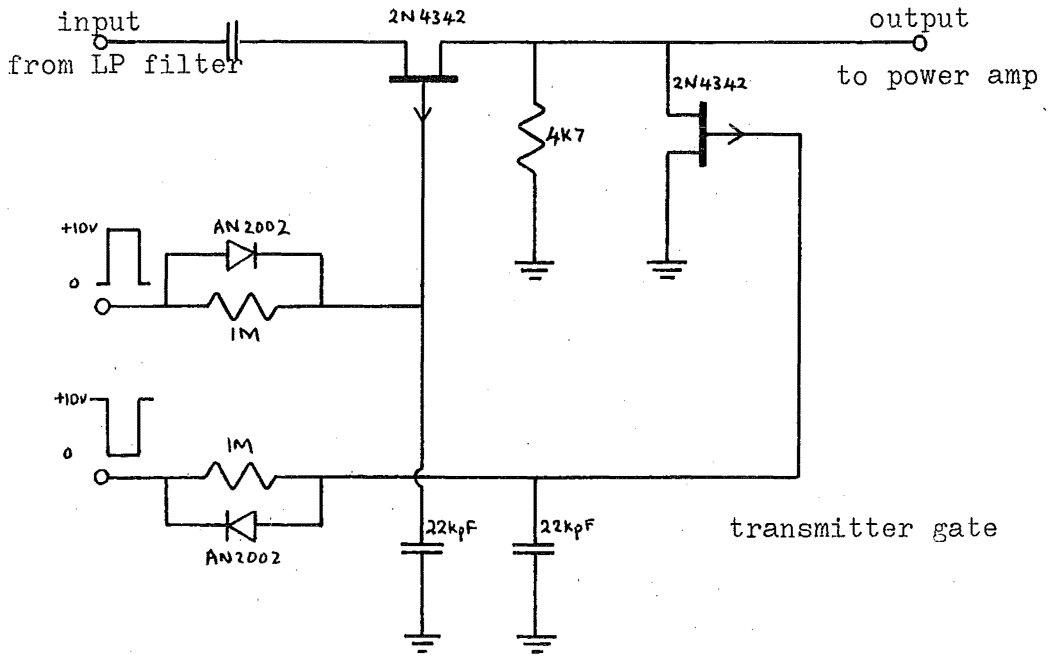

(iv) Demodulators

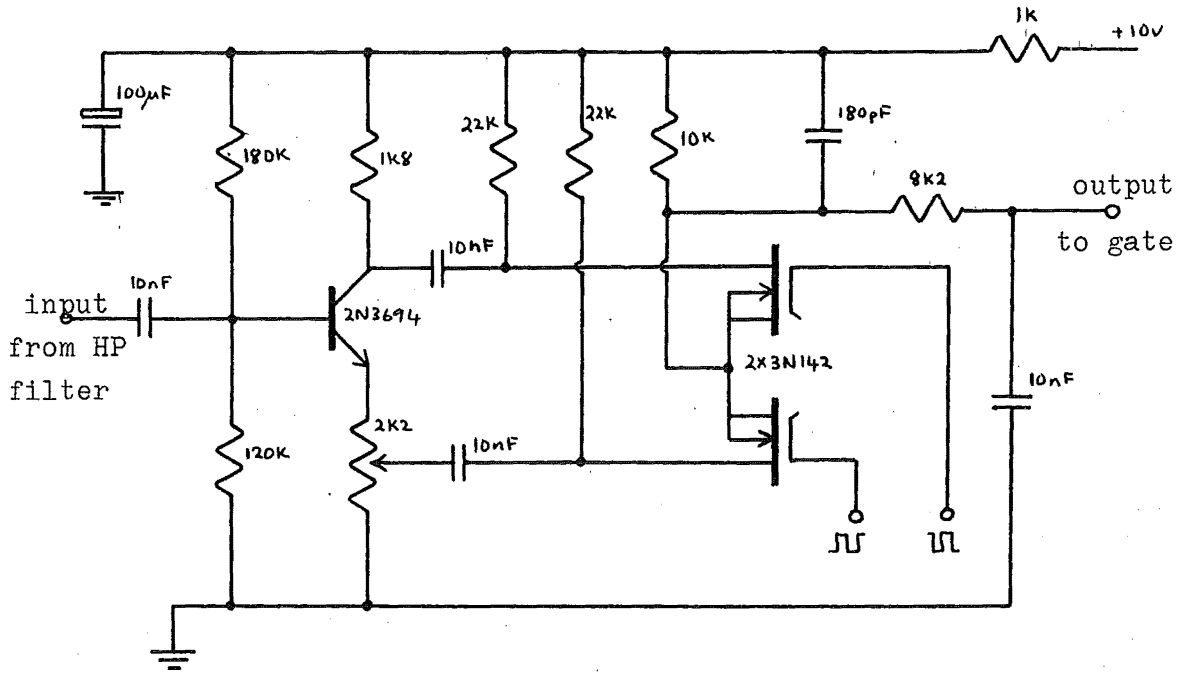

(v) Audio Shaping Circuits

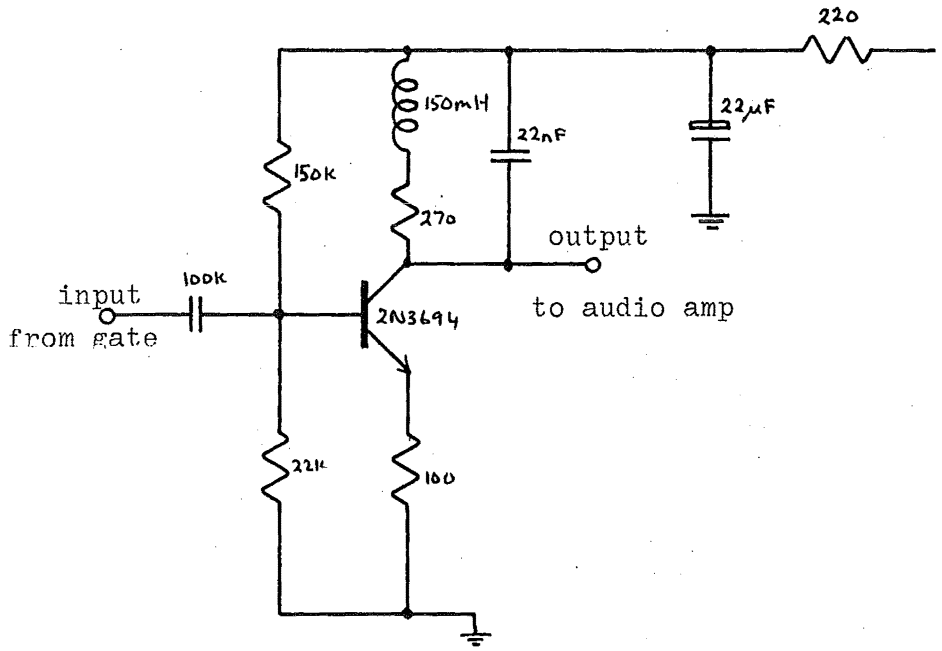

(vi) Transmitter Power Amplifier

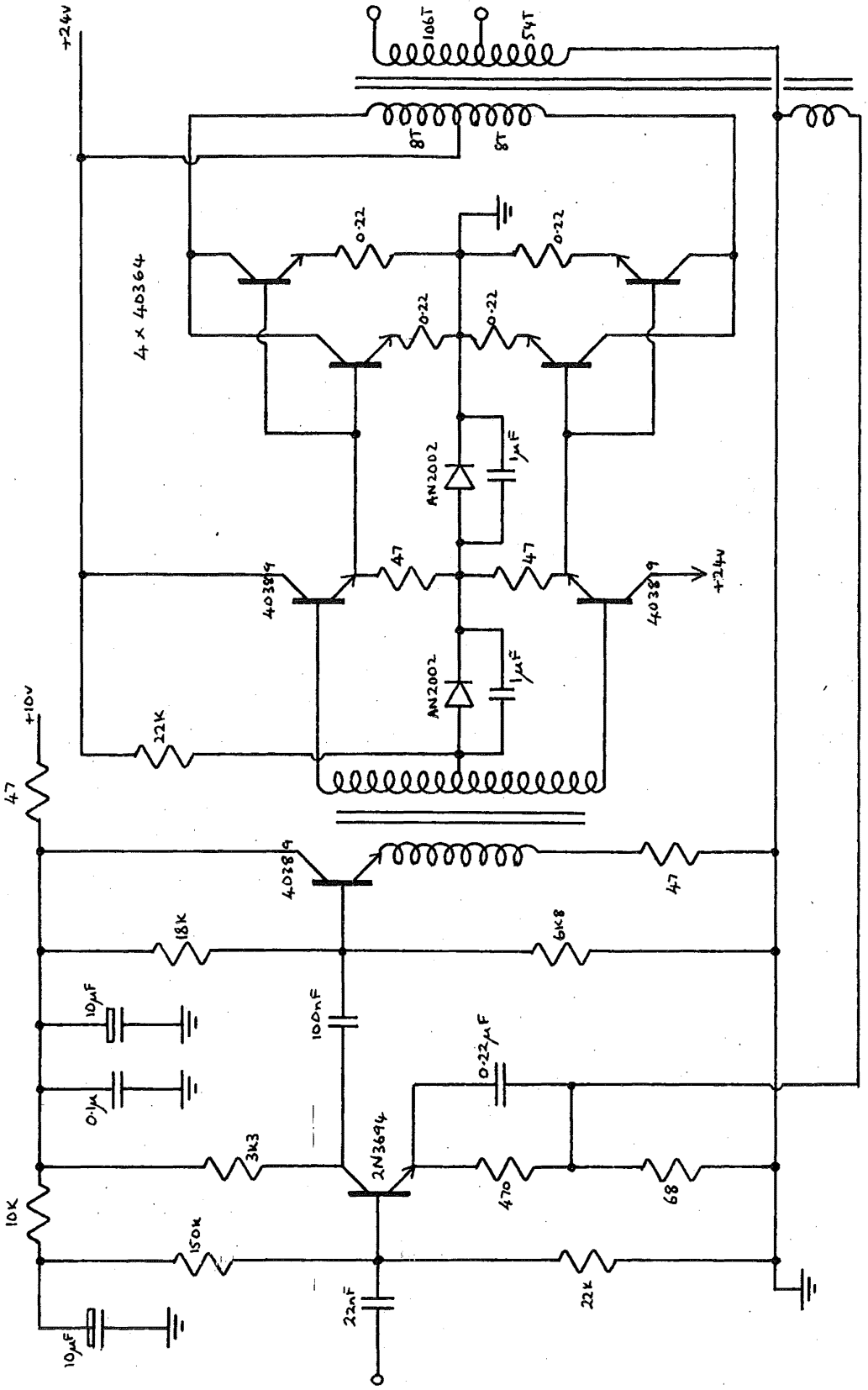

(vii) Timing Unit

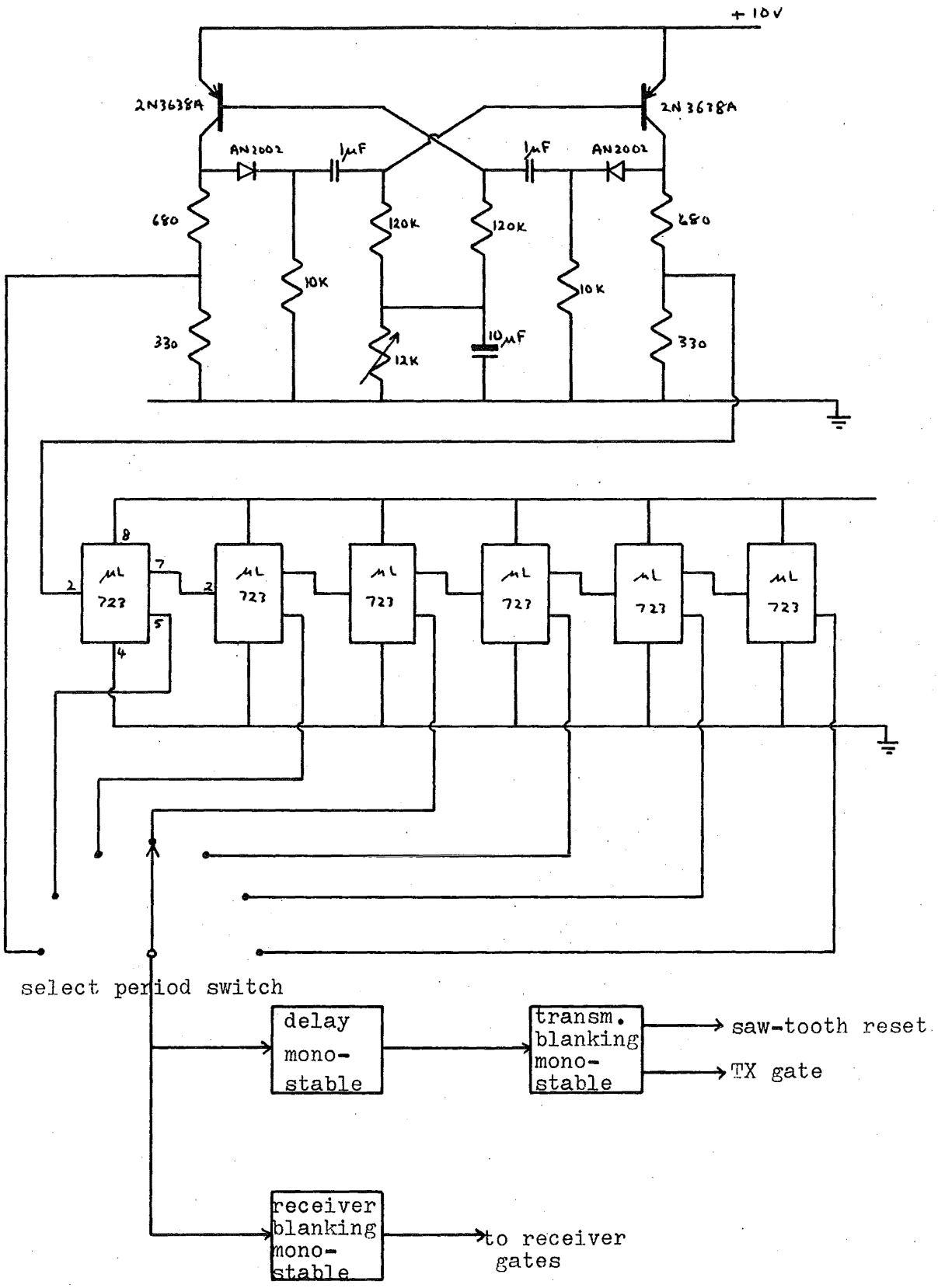

(viii) Receiver RF and Audio Amplifiers

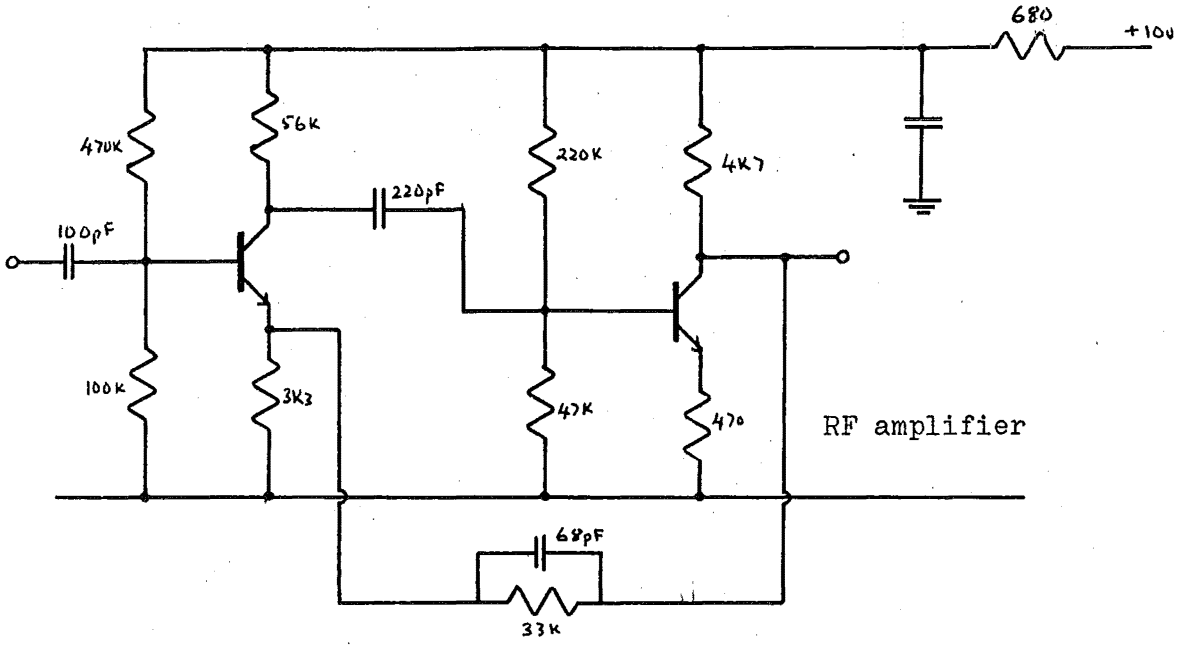

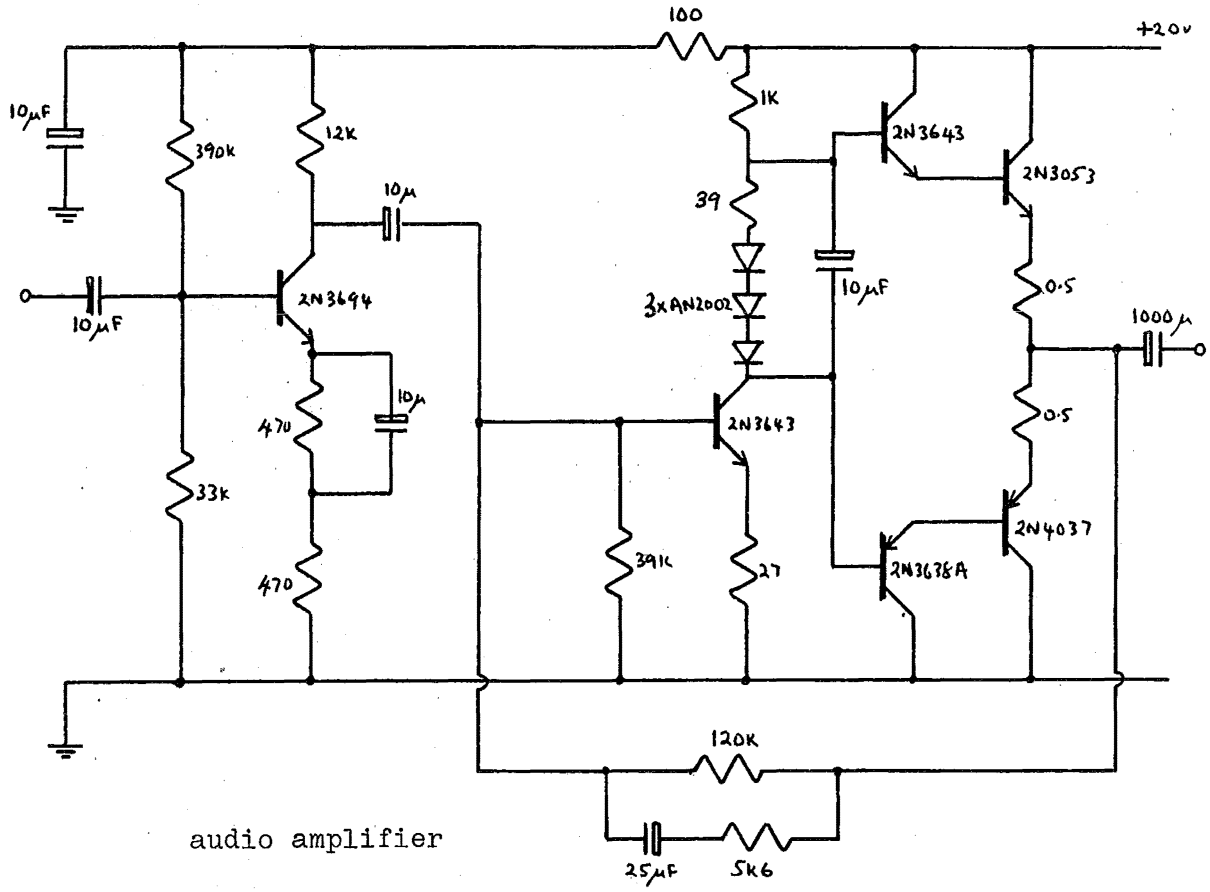

(ix) Beam Control Networks

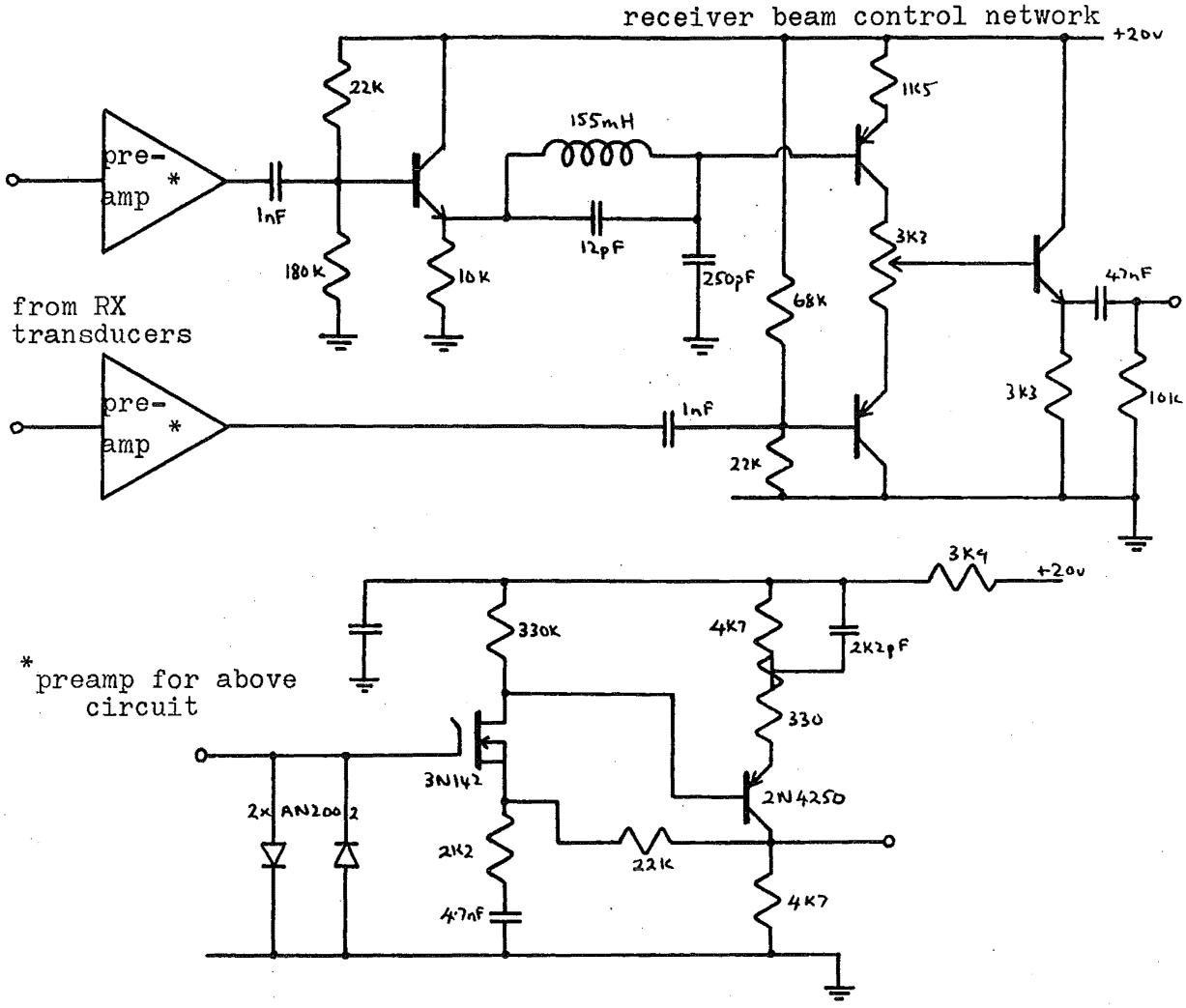

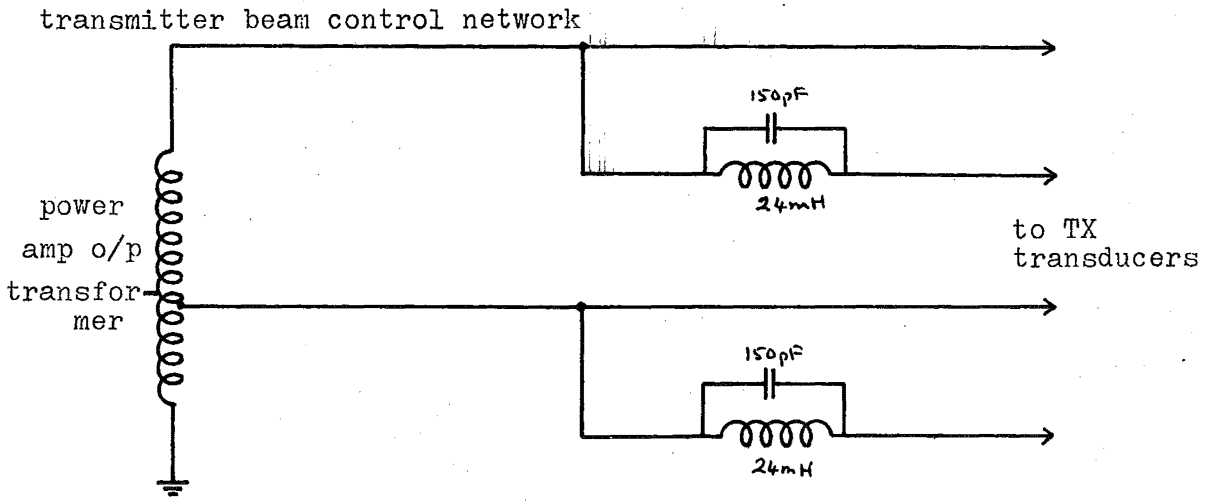

APPENDIX VI

Remotely Controlled Trolley for Target Tracking Studies

The construction of the trolley is indicated in the lower photograph on the title page of Ch. 7. Essentially, it comprises a small platform mounted on three wheels, two at the front, one at the rear. The rear wheel is both driven and steerable, control signals and power being transmitted along a 45 ft long cable.

Controls are provided at the operators panel to set speed and 'rudder' angle. Speed is varied by armature current control of a small dc motor and rudder angle is controlled by two synchros, one geared to a steering wheel at the control panel and the other geared to a swivel support on the rear wheel of the trolley.

Three meters are provided at the control panel giving indications of speed, rudder angle and true direction (relative to a fixed reference direction). Speed indication is derived from the motor shaft by a photocell/rotating-vane sensor coupled to an analogue frequency meter. Rudder angle indication is derived from a potentiometer rotated by the swivelling action of the rear wheel. True direction indication is obtained by pulse-height-modulating the constant width pulses generated by the analogue frequency meter, and integrating the resulting waveform.

This third indication was considered necessary in view of strategies evolved for tracking targets at sea. It was found during sea trials that most successful tracking was achieved by reducing the rate of rotation of the vessel as the target

approached the straight-ahead position. Such 'angular velocity feedback' is only possible if a true direction indication is available since angular velocity is a function of both speed and rudder angle.

The available ranges of speed and rudder angle were chosen to give similar approach times and manoeuvrability to those achieved at sea.

Rectangular solid-dielectric type capacitor microphone transducers were developed to model the underwater arrays in the horizontal plane (see lower photo on the title page of Ch. 7). Very narrow beamwidths (less than 5^{o}) were employed in the vertical plane to extend the operating range of the system to a realistic magnitude for model studies. A range of 40 ft could be achieved on a vertical diplane of 6" side. Since the velocity of sound in air is five times smaller than that in water, this is equivalent to a 200 ft range in water.

The constant beamwidth techniques developed in Ch. 4 were employed with the air transducers, to achieve closely similar directivity patterns to those of the underwater arrays. The method used to obtain independently controlled transducer sections (necessary for the constant beamwidth design) is indicated diagrammatically below.

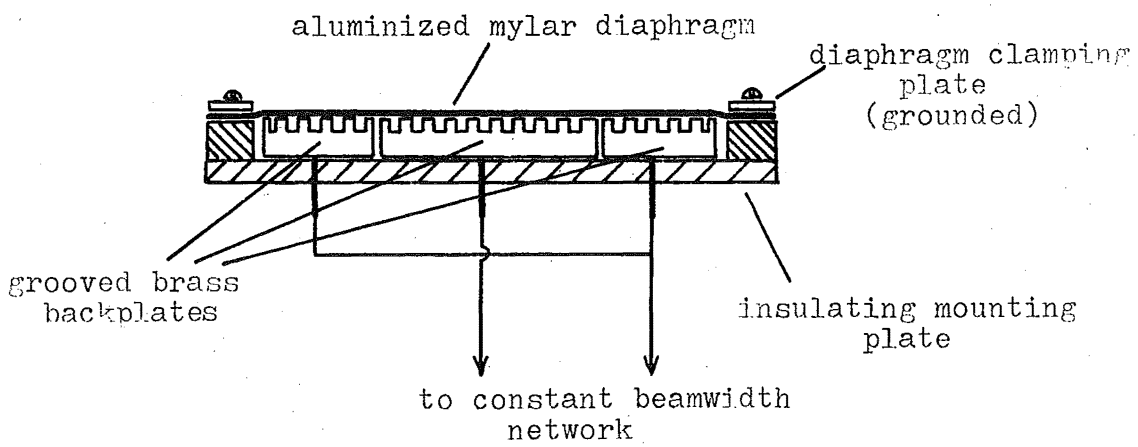

Cross-section of solid-dielectric constant beamwidth transducer

Preamplifiers for the receiving array sections were mounted on the trolley, the resultant output signals being transmitted up the cable to the receiver electronics.

APPENDIX VII

Towed Photographic Body for Target Identification

The lower photograph on the title page of Ch. 9 shows the basic design of the towed body. It comprises, essentially, a cylindrical tube, six inches in diameter, fitted to a cast aluminium-alloy wing with controllable flaps. Vertical and horizontal tail fins are provided at the rear for stability, and a conical nose with a perspex window is fitted to the front of the tube, to allow photographing of objects forward of the body.

The body is towed on a multiple conductor cable with a stainless steel wire core. This cable includes four separate conductors for the transmission and reception of control and monitored signals. A total cable length of 250 feet is attached to the unit.

The wing was designed so that with the flaps in the neutral position, a downwards thrust of approximately 50 lbs would be generated at a towing speed of approximately 4 knots. The total drag force on the body with this flap configuration and at this speed, is approximately 5 lbs. This high "lift" to drag ratio largely determines the greatest towing depth for a given cable length. It is clearly desirable to have the cable as short as possible.

The depth at which the body follows the towing vessel is varied by controlling the flap positions, with a servo mechanism operating from signals transmitted down the cable.

A depth sensor on the body transmits an FM signal up the cable providing a true depth indication to an accuracy of ±5

feet. Two flash tubes at the extremities of the wing provide illumination for photography. A total flash energy of 60 joules is employed. The camera fitted to the unit is a Super-8 millimetre movie camera with shutter removed (exposure being controlled by the flash illumination).

Upon initiation of a command signal from the towing vessel, the camera and flash tubes commence a repetitive sequence photographing at the rate of one frame every 1.8 seconds. The procedure for use of the towed photographic body, then, is as follows:

Once a suitable search area is established, the photographic body is towed behind the towing vessel at a depth of approximately 50 feet until a target is detected with the sonar. Following detection, the target is tracked in the normal manner (see Ch. 9) and as soon as it passes vertically beneath the vessel, its depth is noted from the depth sounder. At this time the towing depth of the photographic body is adjusted to equal the target depth. (The total time required to reach any depth between 0 and 170 feet is less than 20 seconds.) The distance from the towed body to the shoal may be estimated from vessel speed and cable length, depth etc. and the camera is activated shortly before the estimated time of contact. Photographs are then taken at the rate of one every 1.8 seconds until the towed body is obviously well clear of the shoal.

Initial experiments with the towed body were conducted in a water tank intended for the testing of river flow-velocity meters. This tank enabled measurements of lift, drag, stability etc. to be made under all towing speeds and flap configurations.

From these measurements, and measurements of the drag characteristics of the cable, the cable shape could be predicted for any particular speed or flap position. The predicted characteristics are shown in the diagram below.

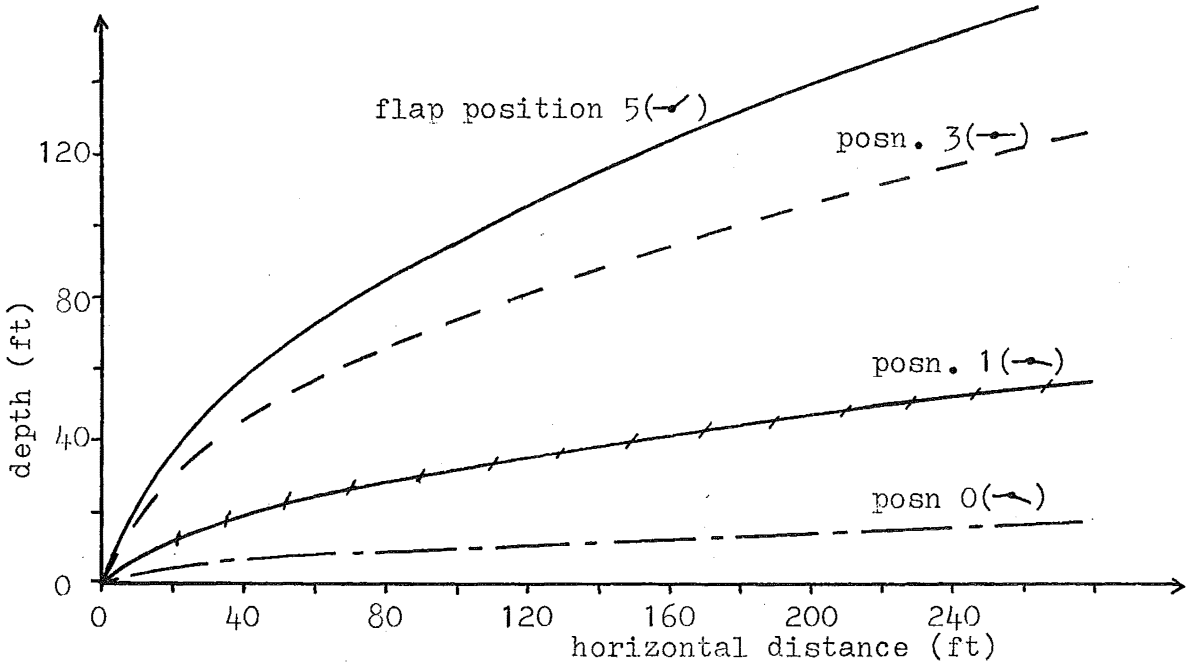

These results were proved in trials to be very accurate, and the dynamic performance of the vessel at sea was found to be very satisfactory.

A sequence of three consecutive photographs taken as the towed body entered one particular shoal is shown on the following page.

The effective range of the flash illumination in this instance is approximately 15 ft. Although the fish are too small to be resolved in detail, it is clear that the shoal comprises a very large number of individuals (approximately 50 are visible in the center photo). Photographs taken immediately prior to and after this sequence show no fish at all, so it may be presumed that the extent of the shoal in the forward direction is less than the distance travelled by the photographic body during this sequence. This provides an estimate of <24 ft for this dimension of the shoal.

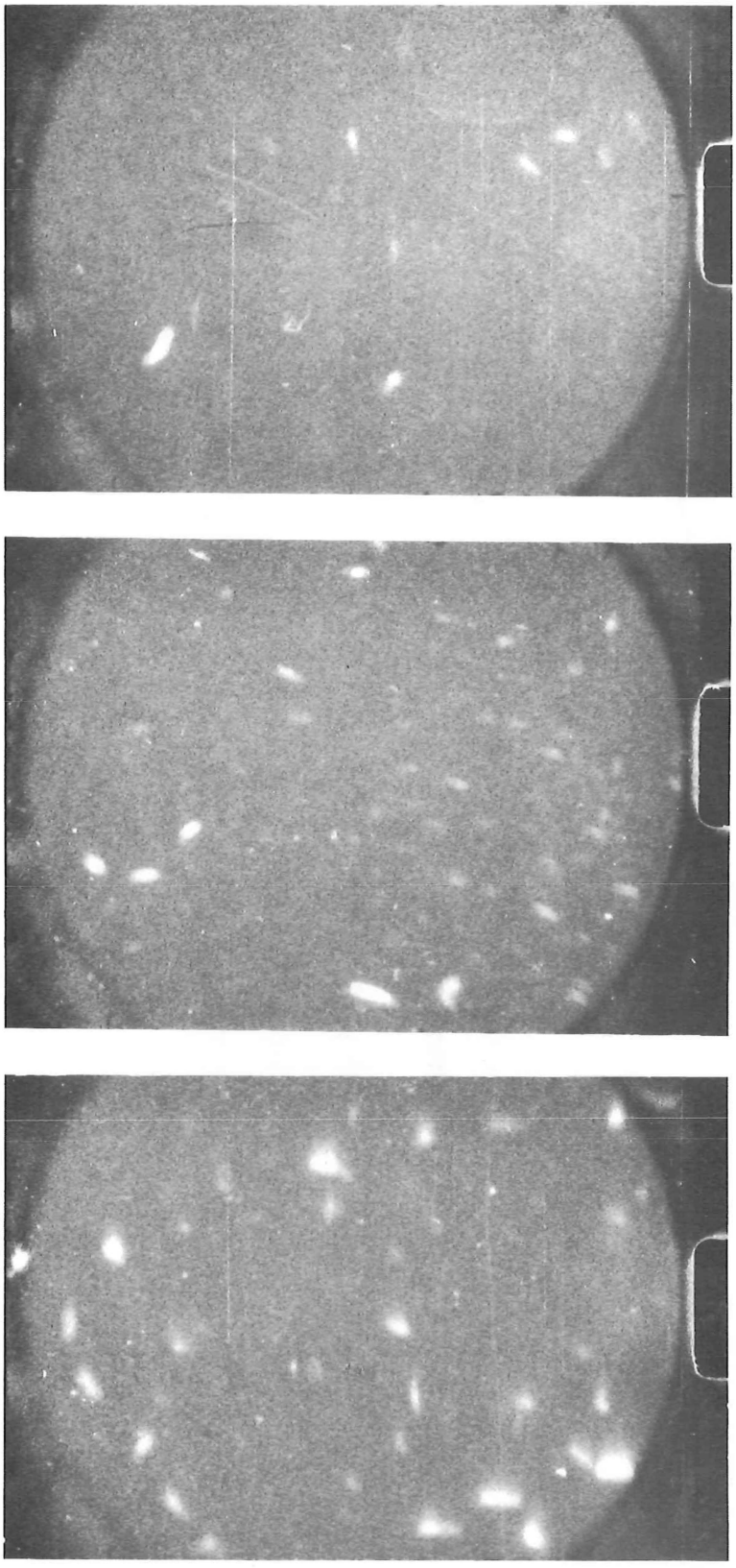

Sequence of three photographs taken at intervals of 1.8secs during passage through a shoal.